Visual Attention along the Visual Field's Meridians

Computational Modeling of Neural and Behavioral Dynamics

Inauguraldissertation
zur Erlangung des Doktorgrades
der Humanwissenschaftlichen Fakultät
der Universität zu Köln
nach der Promotionsordnung vom 18.12.2018
vorgelegt von

Simon R. Steinkamp

aus
Bayreuth
Dezember 2020

Diese Dissertation wurde von der Humanwissenschaftlichen Fakultät der Universität zu Köln im April, 2021 angenommen.

Visual Attention along the Visual Field's Meridians

Computational Modeling of Neural and Behavioral Dynamics

Simon R. Steinkamp

Abstract

The ability to orient attention towards things we consider important, but also to reorient it towards new, salient, and unexpected stimuli, is key to navigate life. To investigate these two aspects of attention, Posner's spatial cuing task has been used for decades and has been influential as hemispatial neglect provides a good lesion model about the underlying brain regions (Posner et al., 1984). As hemispatial neglect most often extends along the visual field's horizontal meridian, less is known about attentional (re)orienting along the vertical meridian. To fully understand neglect, however, it is important to study attentional (re)orienting along the whole visual field.

In my first project, I investigated differences in vertical and horizontal (re)orienting on a behavioral and neural level, using statistical, machine learning, and dynamic causal modeling (DCM) analyses. Results suggest, that attentional (re)orienting along the two meridians is very similar in terms of reaction times and fMRI data. This indicates that attentional resources are distributed evenly across the visual field.

Statistical analysis, however, can only provide indirect associations between neural and behavioral processes; for a direct link, the simultaneous modeling of brain and behavior is required. Rigoux and Daunizeau (2015) have shown that this can be done with behavioral DCM for binary measures. Continuous data, however, often contains more information, especially in Posner's task. Hence, I extended and validated bDCM for continuous measures, making it available for more tasks. Furthermore, bDCM parameters could be used to classify vertical and horizontal runs, which was not possible with other data, showing that bDCM is sensitive to small variations in task design.

Acknowledgments

This thesis is the result of a four-year-long journey, which has only been possible with the help and support of many others, for which I am incredibly grateful.

My deepest gratitude goes to my wonderful "doctoral parents", without whom all of this would not have been possible: PD Dr. Ralph Weidner who trusted me and gave me the confidence to explore new paths, for his guidance and advice along the way, for all his support and help throughout these years. And Jun.-Prof. Dr. Simone Vossel for her support, for sharing her knowledge, for her invaluable feedback and advice.

I also want to thank Prof. Dr. Gereon R. Fink for his advice and for giving me the opportunity to do this work at the Forschungszentrum Jülich.

Furthermore, I want to thank the past and present members of the INM-3 who made the time there so much more pleasant. I am especially glad for Dr. Eva Nießen, Dr. Paola Mengotti, Dr. Alexander Geiger, and Dr. Nils Rosjat, who picked me up on the first days, for all the playful, sunny, wintry, but also the bumpy times. My thanks goes to Dr. Shivakumar Viswanathan and Max Hommelsen for pleasant conversations and heated discussions. I further want to thank Dr. Zoe (Hang) Zeng and Anne-Sophie Käsbauer for being the company you wish to have on such a journey.

Moreover, I am thankful for the unconditional support, help, and warmth of my parents Thomas and Petra, especially in the dark times. I also want to thank my late grandmother Erika Wedeking, who always had an open ear, for her love and trust.

Finally, I am eternally grateful for having Anna Plachti by my side, who paved the way and provided me with all the help, support, strength, and love to stick through it to the end.

Contents

List of Figures

List of Tables

Abbreviatons and Acronyms

bDCM behavioral dynamic causal modeling

BF Bayes factor

BOLD blood oxygen level-dependent

DCM dynamic causal modeling

EEG electroencephalography

FEF frontal eye-fields

fMRI functional magnetic resonance imaging

GLM general linear model

HRF hemodynamic response function

HVA horizontal-vertical anisotropy

IFG inferior frontal gyrus

IPS intraparietal sulcus

LIP lateral intraparietal area

MFG middle frontal gyrus

SC superior colliculus

SLF superior longitudinal fasciculus

TE echo time

TMS transcranial magnetic stimulation

TPJ temporoparietal junction

TR repetition time

TVA Theory of visual attention

VLSM voxel-based lesion-symptom mapping

VOI volume of interest

1 | Overview

1.1 Introduction

Imagine the car in front of you signals right to leave the highway. As it was driving slowly before, you prepare to overtake it. Instead of paying attention to the car in front, you begin looking ahead, monitoring the lane on your left, and checking the rear-mirror. Suddenly, you realize that the car in front now signals to the left. Instead of speeding up and overtaking the car, you now need to reconsider your actions.

This might be a real-life example of an experiment by Micheal Posner commonly used to investigate visual spatial attention (Posner, 1980). In his spatial cuing paradigm, a pre-cue (like the turning signal) indicates the location where a target is about to appear (valid trial). Although this cue is mostly correct, some cues indicate the wrong location (invalid trial). In some cases, the experiment also includes trials with a neutral cue, as a baseline condition. When comparing behavioral data of valid against neutral cue conditions, participants perform better in valid trials. Invalid trials, however, lead to a significant reduction in performance (Posner et al., 1978). Because this kind of task requires participants to both voluntarily direct their attention (valid cue → orienting) and to react reflexively to targets in unexpected locations (invalid cue → reorienting), it is tapping elegantly into these two crucial aspects of attention.

1.2 Motivation

One reasons why Posner's cuing task has been influential for the investigation of visual spatial attention, is that unilateral brain lesions can impair the reorienting of attention to the contralesional side of the visual field, providing unique insights into the underlying brain networks. This condition is called hemispatial neglect. Most neuroimaging studies, studying the neural representation of the task, however, only investigate (re)orienting along the horizontal meridian, which is most often affected by neglect. But to obtain a full image of how and which brain lesions cause neglect, it is important to study attentional (re)orienting in other directions, especially along the vertical meridian.

To investigate whether there are different neural representations of vertical and horizontal attentional (re)orienting, I recorded behavioral and fMRI data of participants who performed Posner's cuing task along the two meridians of the visual field. The objective of this first project being that differences between the meridians might indicate why horizontal reorienting is especially vulnerable.

To fully understand how neural and behavioral observations are linked, it is necessary to model them simultaneously. This kind of modeling analysis, however, is very difficult as it requires to determine the underlying (hidden) processes causing both. Rigoux and Daunizeau (2015) have proposed a framework greatly facilitating simultaneous modeling of brain and behavior, which also allows manipulations of the model, to simulate how brain lesions affect behavior. But bDCM has so far only been used with binary responses (like button presses).

For a thorough description of cognitive processes behind Posner's cuing task, however, it is necessary to describe behavior in terms of reaction times (continuous responses). The objective of my second project was thus, to test and validate bDCM with

reaction times in Posner's cuing task, in order to better understand which connections and brain regions are especially implicated in hemispatial neglect and to open this method up for a larger community.

1.3   Structure

1.3.1   Horizontal and vertical orienting of attention

As introduced, I used Posner's cuing task in my first project, to investigate attentional orienting along the visual field's horizontal and vertical meridians. Although asymmetries along and within these two major axes are well known in vision research (Abrams et al., 2012; Brederoo et al., 2019; Carrasco et al., 2001), most studies using Posner's cuing task only display stimuli along the horizontal axis. The prevalence of horizontal stimulus layouts, might be due to hemispatial neglect which describes the inability of patients to respond to stimuli in either the left or right visual field. As neglect is commonly caused by unilateral brain lesions, it is thus providing critical insights into the brain areas involved in attentional reorienting (Posner et al., 1984). Neglect, however, is most often reported along the horizontal axis, although there are cases of upper and lower visual field neglect (Morris et al., 2020; Shelton et al., 1990). But neglect is not only a clinical phenomenon, healthy participants also tend to have a slightly biased representation of visual space. For example, healthy participants tend to bisect a line slightly to the left, hence ignoring the right side, a phenomenon called pseudo-neglect (Jewell & McCourt, 2000). Because vertical and horizontal (pseudo-)neglects appear to be independent of each other (Nicholls et al., 2004), horizontal attentional (re)orienting might be distinct of vertical orienting in terms of the underlying brain networks. Only a few neuroimaging studies have investigated this question and reported mixed results (Fink et al., 2001; Macaluso & Patria, 2007; Mao et al., 2007). Thus, I contrasted horizontal and vertical attentional (re) orienting in Posner's cuing task, to clarify the neural underpinnings and possibly better understand the causes of hemispatial neglect.

To introduce my publication on this topic, I will provide an overview of attention as a concept, detailing the choices one has to make when conducting a spatial cuing experiment. This general introduction is followed by a detailed review about what we know in terms of visual field asymmetries and their connection to spatial attention.

A second chapter will then introduce in broad terms, how we can investigate the brain networks related to attentional orienting using fMRI, what the strengths of Bayesian inference are, and how machine learning can be used to strengthen statistical conclusions.

We will then shift to computational modeling, the main aspect of my second project.

1.3.2   Simultaneous modeling of brain and behavior

Translating research questions into mathematical models, helps researchers formulating clear and testable hypotheses (Smaldino, 2020). They are also a crucial step towards building theories (Navarro, 2020), which are sometimes insufficiently described in psychological research (Fried, 2020).

One exception is mathematical psychology. For example, Rescorla and Wagner (1972) used a reinforcement learning algorithm to model how rats learn stimulus-response mappings in classical conditioning. Their model can also describe how participants learn the pre-cue's validity in Posner's cuing task (Mengotti et al., 2017). Computational modeling also plays a major role in neuroscience (Kriegeskorte & Douglas, 2018). For example, DCM (Friston et al., 2003) can be used to investigate how experimental manipulations influence dynamics of brain signals. Unfortunately, there has been little interaction between the psychological and neuroscientific modeling communities in the past, although

combined models of brain and behavior are key to understand how the brain generates behavior (B. M. Turner et al., 2017).

Rigoux and Daunizeau (2015) provide such a simultaneous modeling approach, termed bDCM, which my second project is all about. Here I investigated how bDCM can be extended to reaction time data and applied this new approach to Posner's cuing task. This project, although using the same data, is very different from the first, so I decided to provide a separate introduction consisting of two chapters.

In Chapter 4, I will shortly introduce computational modeling and describe example models of visual attention in detail. Chapter 5 then provides a description of the key concepts involved in DCM and bDCM.

1.3.3 Publications

With the introductory chapters providing motivation and reasoning for key questions of my work, I include my publication *"Attentional reorientation along the meridians of the visual field: Are there different neural mechanisms at play?"* in Chapter 6 and preprint *"Simultaneous Modeling of Reaction Times and Brain Dynamics in a Spatial Cuing Task"* in Chapter 7. A few additional analyses, that I found necessary to better understand the second study's results, but did not fit into the preprint, are included in Chapter 8.

Finally, Chapters 9 and 10 summarize and thoroughly discuss the implications of my work presented here, leading to the conclusion in Chapter 11.

1.4 Notation

Although research is a highly collaborative process, I will use "I" throughout this dissertation. Still, most of the work presented here would not have been possible without my coauthors and supervisors, for whom I am incredibly thankful!

Throughout my dissertation I will also use "(re)orientation" or "(re)orienting" as a short hand for "orienting and reorienting" to refer to both cognitive processes at the same time.

> **Box 1.1: Boxes**
>
> Instead of footnotes, I will use gray boxes to provide additional background information and context to the main texts. Furthermore, there will be blue boxes for future directions and orange boxes for limitations in the discussion chapter.

1.4.1 Mathematical notation

I will use the following notation for most equations. Still, there might be a few exceptions, especially, when I cite formulas from other contexts.

x	A cursive lowercase letter is used for scalars.
$\mathbf{x}$	Lowercase letters in bold are used for (column) vectors.
A	Uppercase letters indicate matrices.
$D_r, x_t, \mathbf{x}_{t-1}$	Subscripts in most formulas are used to describe the variable's identity, for example D_r to distinguish behavioral parameters from neural parameters D in bDCM. Time is also seen as a form of identity.
D^j, x^i	Superscripts are used to indicate the index of a vector or matrix (e.g. x^i is the ith entry in $\mathbf{x}$).
α, κ, θ	Greek letters will often refer to single parameters or sets of parameters.

$\mu, \sigma, \hat{y}$ In some formulas I will use commonly used notations, such as μ
                                        for the mean, or $\hat{y}$ for predicted values.

2 | Attentional (Re)Orienting

Introductions of visual attention studies often start by stressing how *"our senses are constantly bombarded with information"* and that *"we need to select the most relevant information"*, because of the *"limited processing capacities of our brain"* (e.g. Steinkamp, Vossel, et al., 2020).

In others, you might find William James' famous quote

> *"Every one knows what attention is. It is the taking possession by the mind, in clear and vivid form, of one out of what seem several simultaneously possible objects or trains of thought. Focalization, concentration, of consciousness are of its essence. It implies withdrawal from some things in order to deal effectively with others […]."* (James, 1890)

And sometimes authors might quote famous poets.

> *"Choice of attention — to pay attention to this and ignore that — is to the inner life what choice of action is to the outer. In both cases, a man is responsible for his choice and must accept the consequences, whatever they may be."* (W.H. Auden, *from Konnikova, 2020*)

These quotes describe attention as a mostly *voluntary* process, where the selection of relevant and unimportant information, is crucial for our daily lives.

Paying attention, allows us to have a conversation with another person at a party, despite many other conversations around us and loud music (Cherry, 1953). We might be so focused that we do not even realize when somebody in a gorilla costume passes between us (Simons & Chabris, 1999). Not noticing the gorilla means missing out on a great story or if the gorilla was real, immediate danger. Fortunately, attention can also be grabbed *involuntarily*, so that we hear through all the noise, how an old friend calls out our name (Moray, 1959).

2.1 What is attention?

The literature on attention is massive and — unfortunately — scattered. There is a plethora of different theories, tasks, and sub-fields, all committed to study the same phenomenon. To make it more complicated attention is often both the object of investigation, and in the same turn the explanation of observed phenomena (*"No one knows what attention is"*, Hommel et al., 2019).

To make sense of such a complex concept researchers have used different metaphors to describe and guide their research of attention (Fernandez-Duque & Johnson, 1999), which I will describe in the following short and incomplete history of attentional theories. Before we dive into the specifics, let us have a look at what most researchers can agree upon, summarized by Fernandez-Duque and Johnson (1999).

- *"Attention improves performance on a wide range of tasks, such as perception, various motor activities and many kinds of cognitive operations.*
- *Correspondingly, attention minimizes distraction.*
- *Attention enhances processes in the area one is attending to.*

- *Attention involves some form of stimulus selection.*

- *Attention facilitates access to awareness, that is, attention is necessary for focused awareness."*

(Fernandez-Duque and Johnson, 1999)

Let us being in the 1950s, when signal processing metaphors were dominant. Inspired by the ("Cocktail"-)party scenario described above, researchers were using dichotic listening tasks, to understand how humans can separate the sheer amount of information constantly picked up by their sense. In dichotic listening participants actively repeated one of two narrators presented to them via headphones (Cherry, 1953). Typically, participants had no troubles following the attended speaker, but could only report basic physical properties (e.g. pitch) of the unattended speaker. This observation was described in terms of filters: As only a limited amount of the presented sensory-information is perceived, it has been concluded that there has to be an information bottleneck. Broadbent (1958) presumed the information bottleneck to be at an early processing stage, so that irrelevant information is filtered out on the basis of physical properties.

But modifications to dichotic listening experiments, were indicating that more information reaches conscious awareness. People would often respond to their own name when it was presented in the unattended stream (Moray, 1959). Furthermore, participants would continue to follow a story that was initially told by the attended speaker and would later be continued by the unattended speaker (Treisman, 1960). Thus, information selection was assumed to take place at a later state, so that information would for example be selected based on semantics (Deutsch & Deutsch, 1963). As an alternative to static late and early selection models, an attenuation model was proposed, arguing that filters are not blocking information from consciousness completely, but rather attenuate the amount of information that arrives in consciousness at multiple stages (Treisman, 1960).

As attention research moved from auditory experiments to the visual domain, especially with such iconic experimental designs like Posner's cuing task (Posner, 1980) or the Eriksen flanker task (Eriksen & Eriksen, 1974), the attention metaphors shifted. Attention was now seen as a spotlight, that would rapidly scan the visual field for points of interested and could also be voluntarily directed (Fernandez-Duque & Johnson, 1999). Experimental data supported this idea initially, as not only the awareness of stimuli, but also visual acuity was enhanced by the spotlight (Carrasco & Barbot, 2014). Importantly, the attentional spotlight does not rely on eye-movements. Which gave rise to the pre-motor theory of attention, in which the "spotlight" was seen as a planning step for upcoming eye-movements (Rizzolatti et al., 1987).

Visual search experiments have been playing another important role. In these experiments participants had to select a target stimulus from many based on one or more features. If the task is relatively easy visual search can sometimes be done rapidly and in parallel. If the target shares multiple features with distractor stimuli, then each stimulus in the scene has to be processed serially, slowing down performance (Treisman & Gelade, 1980). Jeremy Wolfe expanded Anne Treisman's feature integration theory in his model of guided search. Here, the serial stage is guided by features registered in the parallel early stage. Features of interest "guide" attention towards possible targets, successively narrowing down the search (Wolfe, 1994; Wolfe, 2007).

More modern theories of attention try to reconcile observations of different domains. Load-theory assumes that information selection is driven by external and internal factors. High perceptual load moves information filtering to early stages, so that distractors have less impact on information processing in general. Whereas under low perceptual load, almost all stimuli reach conscious awareness. Task difficulty has the opposite effect, so that more information reaches consciousness in difficult tasks (Lavie & Tsal, 1994; Murphy

et al., 2016). In biased-competition, sensory information competes to reach awareness. If information is relevant to our current goals, it is enhanced, otherwise it is suppressed. But non-relevant information can be so salient that it arrives in our awareness regardless (Kastner & Ungerleider, 2001). Recently, a rhythmic theory of attention has been proposed. Periods of voluntary engagement and suppression of sensory perception are followed by a release of attention, allowing us to perceive salient and non-relevant information (Fiebelkorn & Kastner, 2019, 2020).

2.2 Attentional Orienting

In the previous sections, it became clear, that there are two different selection processes involved in attention. A *voluntary* direction of attention, following internal goals and strategies, and an *involuntary* redirection of attention to salient stimuli from the outside. Both processes are of key interest in my thesis.
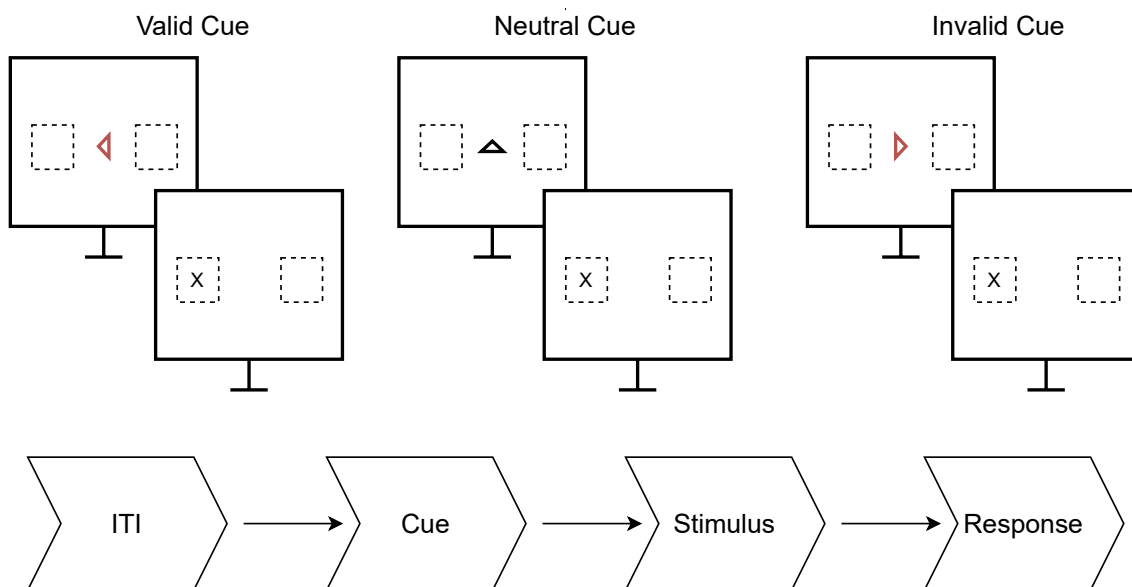
Figure 2.1: Posner's cuing task in its original form (Posner, 1980). Participants had to detect a brief flash of light and indicate where it appeared. In valid trials a pre-cue indicates the correct location of the flash 80% of the time, invalid cues indicate the side opposite of the flash 20% of the time. Neutral cues leave the participant guessing i.e., being 50% accurate. *ITI - inter trial interval*

To study the processes behind attentional orienting, Michael Posner devised his influential spatial cuing paradigm (see Figure 2.1). Participants are asked to indicate and detect the location of a very brief flash of light. Before the light flash, however, a probabilistic pre-cue was presented. In 80 % of the trials the cue indicated the correct location, in the other 20 % the cue was incorrect. Using this manipulation, participants voluntarily engaged their attention to the cued location, but had to reorient attention after invalid cues. Neutral cues served as a control condition (Posner, 1980; Posner, 2016).

The positive effect of attention has been shown in lower reaction times to valid trials compared to neutral and invalid trials (Figure 2.2, A). But it has been shown that the disengagement and reorientation of attention leads to increased reaction times when comparing invalid trials against valid and neutral trials (Posner et al., 1978).

In the last decades, spatial-cuing paradigms, inspired by Posner's work, have been adapted to study attentional orienting in a variety of situations. Some used symbolic, oth-
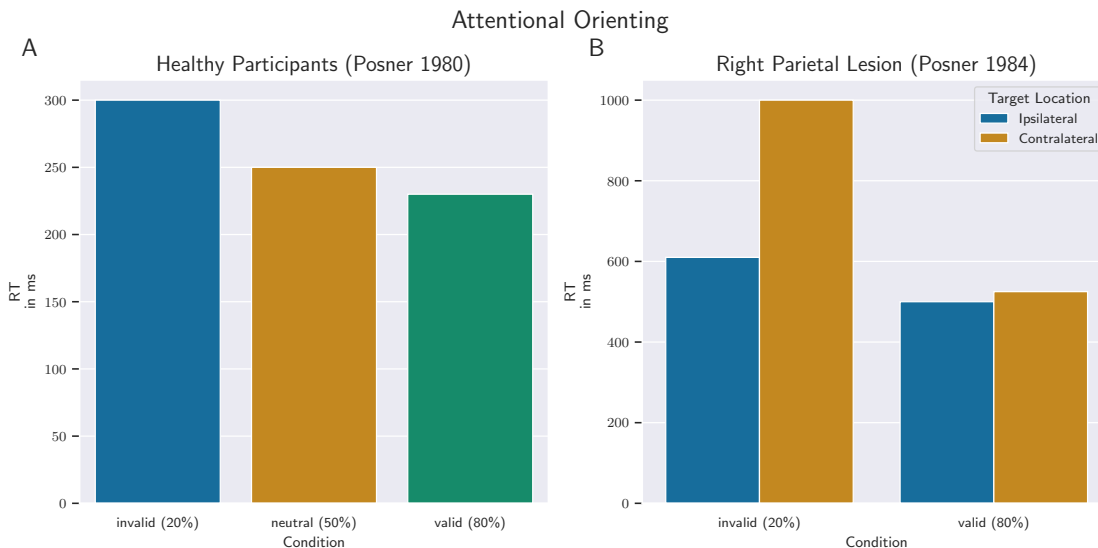
Figure 2.2: Idealized reaction time distributions typically observed in Posner's cuing task (Posner, 1980), see Figure 2.1. A) Reaction times for valid (80 %), neutral (50 %), and invalid (20 %) trials. One sees the large reaction time costs due to invalid cues, and the smaller benefit of valid cuing. B) Reaction time distributions of neglect patients as observed in Posner et al. (1984). Showing the increase in reaction times towards invalid trials in the contralateral hemifield. The other conditions, however, appear to be largely unaffected.

ers used explicit cuing, or even investigated the effect of attentional cuing across different sensory modalities (Chambers et al., 2004; Mengotti et al., 2018). Meaning, that there are many experimental choices the researcher has to take (Chica et al., 2014).

2.2.1 Experimental design

In his original experiments Posner studied the effects of different cuing conditions. Symbolic cues — like arrows on the screen's center — evoke different reaction time patterns than cues at the target's location. Symbolic cues are known as *endogenous cues*, as they require the controlled (voluntary) orienting of attention. Cues at the target position, on the other hand, are typically known as *exogenous cues*, as attentional orienting is reflexive or transient (Chica et al., 2014). To observe the attentional benefit of endogenous cues, orienting requires about ~200 ms and can be sustained for several seconds. Exogenous cues, however, lead to an attentional benefit after a very short time (~50 ms), however, after around ~250 ms the so-called inhibition of return occurs, resulting in additional costs when responding to targets in the cued location (Corbetta et al., 2000; Klein, 2000).

Another choice the experimenter faces is whether to allow eye-movements or not (Chica et al., 2014). In spatial cuing tasks using covert orienting, participants fix theirs eyes on a point on the screen, in overt orienting they are allowed to freely move their eyes (see Figure 2.3, B). There is some debate about whether there is a necessity for fixation (Carrasco, 2011). Covert orienting might be seen as a "pure" measure of attention, as oculomotor processes are not interfering with the response. As mentioned earlier, the pre-motor theory of attention considers covert orienting as a planning stage for the next saccade (i.e., overt orienting) (Rizzolatti et al., 1987): Inhibiting automatically planned eye-movements, might therefore be confound in covert attention experiments. This view hold true for a while, as in covert orienting the frontal eye-fields (FEF) were less activated as in overt orienting, indicating a preparatory phase in attention (Corbetta et al., 1998).
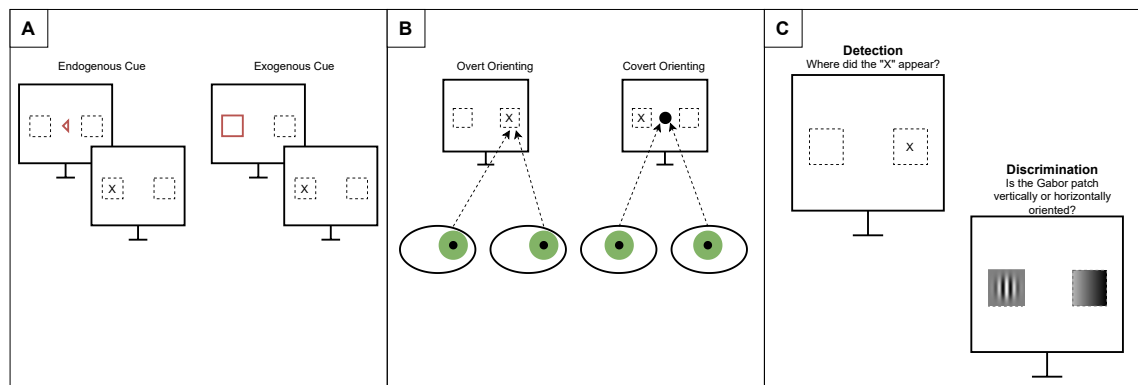
Figure 2.3: Decisions to make in designing a spatial-cuing paradigm. A) should the cue be exogenous or endogenous, B) should orienting be overt or covert? C) Are participants performing a detection or discrimination task?

However, attentional orienting and eye-movements occur in neighboring, but distinct brain regions (Thompson, 2005). As methods like fMRI do not necessarily have a high enough spatial resolution, the common practice is to control for eye-movements and use covert orienting.

Another point of consideration is the participant's task. In Posner's (1980) original experiment, participants had to indicate by a single button press whether a flash of light occurred on the screen (a *detection* task). But to ensure that participants are paying attention requires a more complex task design, including catch trials without a target stimulus. By increasing the task complexity slightly, for example by replacing the detection task with a *discrimination* task, removes the requirement for catch trials (see Figure 2.3, C). A further advantage of using a discrimination over a detection task is that participants have to actively spend attention on the target stimulus and do not react reflexively (Chica et al., 2014).

Finally, one has to choose whether to use informative or non-informative cues. By adding a degree of uncertainty, the experimenter can access the benefit of paying attention. However, task difficulty might also increase (see Figure 2.2 A, and Posner, 1980).

Anecdotally, this became obvious in piloting my experimental design, as I was considering modeling error specifics aspects in the task, I had to ensure that participant's made a considerable amount of errors in the task. Therefore, I tried to calibrate the discrimination task's perceptual difficulty, so that participants would be 80 % accurate. To keep the calibration session as short as possible only valid cues were used. With 100 % valid cues, participants were incredibly good at discriminating just the smallest of differences between target stimuli. Accuracy, however, degraded to chance level as soon as invalidly cued trials were introduced. One also has to consider the validity of the pre-cue. The more predictive a cue is, the larger is the cost of invalid trials. But with more predictive cues, also the overall number of trials in the experiment has to be increased, to have a reasonable estimate of the reaction time in invalid trials (Chica et al., 2014; Dombert et al., 2016).

Box 2.1: Neglect

Patients with lesions to the right posterior parietal cortex are often unable to voluntarily attend to or react to stimuli in the left visual field. A syndrome termed hemispatial neglect, often caused by stroke. A key component of hemispatial neglect is that the visual pathways are unaffected, making it an attentional or intentional disorder

(Heilman et al., 2000). Neglect, however, does not only affect the contralesional hemifield (left or right) but can also extend to different frames of reference. For example, altitudinal neglect affects the upper or lower visual field, but also object and self-perception can be affected (Halligan et al., 2003; Heilman et al., 2000; Karnath, 2015).

Neglect is often diagnosed by using line-bisection (see Figure 2.6) or cancellation tasks. But as described in the main text and in Figure 2.2, other aspects of attention, like performance in Posner's cuing task seems to be severely affected as well (Heilman et al., 2000; Posner et al., 1984).

Until now, the mechanisms of neglect are not very well understood, due to the sometimes unclear expression of the disorder and to very large brain lesions affecting many cognitive functions (see Box 2.2) (Karnath et al., 2011). However, there are several theories — which are more discussed in the main text — explaining the neural origin of neglect.

Because neglect is more prolonged and severe after right than left hemispheric damage (Beume et al., 2017; Karnath et al., 2011), a right hemispheric specialization for attentional processes is presumed (Duecker & Sack, 2015). Next to more dorsal parietal brain areas, damage to right temporoparietal junction (TPJ) (Corbetta et al., 2008) and right frontal areas (Verdon et al., 2010), was implicated in severe impairments of attentional reorienting, supporting the idea of strong right hemispheric lateralization of attentional orienting (Corbetta & Shulman, 2011). However, studies indicating that focal damage to the dorsal attention network can also cause hemispatial neglect challenged these conclusions (Gillebert et al., 2011).

Attributing widespread behavioral impairments to cortical brain regions, however, might not reveal the whole picture. Brain lesions after stroke often extend to the underlying white-matter tracts, thus leading to widespread disconnections of distant brain areas. For example damage to the superior longitudinal fasciculus (SLF)II and SLFIII can lead to disconnections of dorsal and ventral attention networks, that might go unnoticed if one focuses on cortical areas alone (Thiebaut de Schotten et al., 2014; Thiebaut de Schotten et al., 2020). Furthermore, damage to white-matter bundles is also providing good indications about the severity and progression of neglect. Especially, damage to inter-hemispheric connections seems to severely affecting compensation strategies, therefore prolonging or even preventing recovery in patients (Lunven & Bartolomeo, 2017; Lunven et al., 2015).
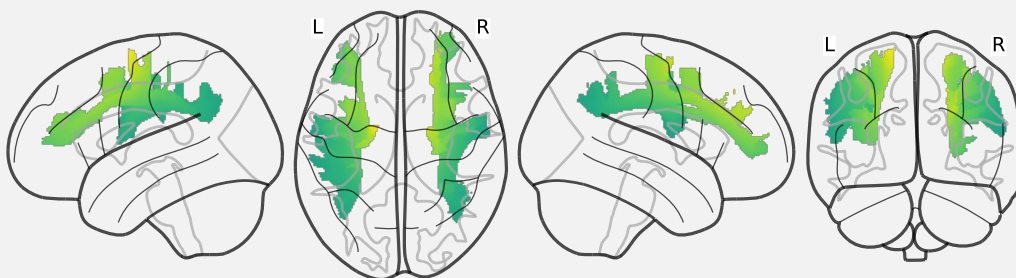

Figure 2.4: Graphic of the superior longitudinal fasiculus. Created from a binary mask. Color gradients were included for better visualization. Retrieved from https://zenodo.org/record/3627772/files/, see also Yeh et al. (2018)
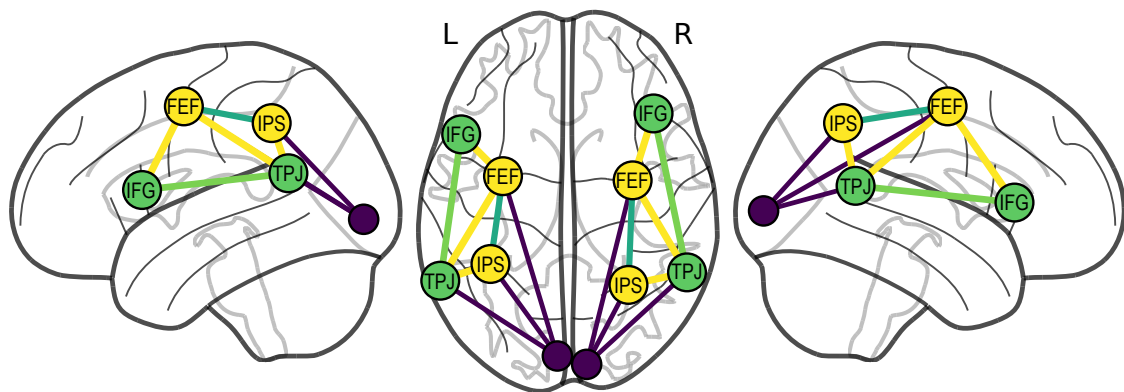
2.3 Attentional Orienting in the Brain

Figure 2.5: Dorsal and ventral attention networks and their proposed connectivity. Inspired by Vossel, Geng, et al. (2014)

Posner's spatial cuing task has been hugely influential, as it could be used to link brain regions to specific behaviors. Posner et al. (1984) could show that participants with unilateral damage to the posterior parietal cortex were strongly impaired in responding to invalidly cued targets in the contralesional visual field (see Box 2.1 for an introduction to neglect). Lesions, however, did not have an effect on the other task conditions, apart from generally longer response times, when compared to healthy controls (see Figure 2.2, B), which provided convincing evidence that parietal cortex plays a crucial role in attentional orienting.

Since then, the advancement of neuroimaging methods and lesion studies lead to further insights of how attention is represented in the brain. Multiple brain networks have been related to attentional processing: alertness, execution, self-regulation, orienting, and reorienting. The latter two being of special interest for our cuing paradigm (Petersen & Posner, 2012).

Attentional orienting has been associated with a dorsal fronto-parietal network, which is distinct from, but interacting with a ventral fronto-parietal network which is activated during attentional reorienting (Corbetta et al., 2008; Vossel et al., 2012).

2.3.1 Dorsal attention network

The dorsal attention network includes bilateral intraparietal sulci (IPS) and frontal eyefields (FEF). As alluded to there is lesion evidence for the posterior parietal cortex (including IPS) (Posner et al., 1984), but also evidence from multiple functional magnetic resonance imaging (fMRI) studies. For example, both regions already respond to the pre-cue in a spatial cuing task, indicating their importance for the orientating of attention (Corbetta et al., 2000). Furthermore, transcranial magnetic stimulation (TMS) studies (see Box 2.2) have provided clear evidence that both IPS and FEF directly modulate early visual cortices, indicating their role in deploying attention to specific regions of the visual field (Duecker & Sack, 2015; Ruff et al., 2008). Additional evidence comes from invasive recording in monkeys, where neurons in both FEF and lateral intraparietal area (LIP) (the monkey homolog of the IPS) show detailed time courses of the orienting process (Noudoost et al., 2010). And from TMS evidence where both FEF and IPS have been shown to assert top-down influence on the visual cortex (Ruff et al., 2009). Although the two regions appear to be very similar, they have distinct roles.

A major difference between IPS and FEF appears to be the spatial reference frames they are operating in. The IPS closely represents space as it is represented on the retina, while the FEF acts in a real world (i.e., absolute) spatial reference frame (Golomb & Kanwisher, 2012). This spatiotopic frame of reference is necessary to plan and execute to plan and execute eye-movements, which appears to be one of the FEF's primary functions (Golomb & Kanwisher, 2012). As FEF are activated more during overt than covert attentional orienting (Corbetta et al., 1998), it was seen as evidence for the pre-motor theory of attention (Rizzolatti et al., 1987). However, cell recordings later that neighboring but distinct neural populations are either involved in preparing saccades or covertly orienting attention (Thompson, 2005).

Most studies of attentional orienting — like this one — focus on IPS and FEF as the main nodes of the dorsal attention network. But several studies have shown that subcortical areas like the superior colliculus (SC) and the pulvinar nucleus of the thalamus are also involved in attentional orienting (Bisley, 2011). Where the SC is involved in saccade planing and target selection (Krauzlis et al., 2013; Noudoost et al., 2010) and the pulvinar appears to suppress unwanted information (Green et al., 2017).

> **Box 2.2: TMS and lesion studies**
>
> Patients living with specific or extensive brain lesions, like Phineas Gage and many others, often known by their initials (H.M., D.F.) have been crucial in connecting behavior with brain function (Milner, 2017; Thiebaut de Schotten et al., 2015). Spatial attention research with its insights from hemispatial neglect is no exception (c.f. Posner et al., 1984). Although, lesion studies provide some of the best causal evidence of how brain regions are connected to specific behaviors, interpreting lesion data can be difficult (Thiebaut de Schotten et al., 2015). One difficulty is due to the lesion's size, which often extents to multiple areas of the brain. Although it is possible to average lesion areas across patients with similar symptoms, to pinpoint the underlying brain region, patients might experience a wide range of behavioral impairments and differ remarkably in neuropsychological assessments (Verdon et al., 2010). One successful solution to this problem has been voxel-based lesion-symptom mapping (VLSM), which is used to estimate how likely each voxel is related to a symptom or test score (Mirman et al., 2018).
>
> One issue with current lesion studies is that their results are often combined with task fMRI studies of healthy participants, to describe the function of cortical brain areas. This approach, however, does not consider how brain areas might be part of a physical network, i.e., ignoring the underlying white matter tracts (Thiebaut de Schotten et al., 2015; Thiebaut de Schotten et al., 2020).
>
> Relying on brain lesions, however, is not the only way to obtain causal evidence between brain regions and behavior. Using brain stimulation methods like TMS it is possible to investigate how brain areas interact and to inflict temporal brain lesions and investigate how behavior changes afterwards. This application is very powerful not only in combination with other brain imaging methods, but especially because the same participant can be tested multiple times with different protocols (Valero-Cabré et al., 2017).

2.3.2 Ventral attention network

Compared to the dorsal attention network, the brain areas belonging to the ventral attention network are less clearly defined by anatomical boundaries. In functional studies, however, TPJ and ventral frontal cortex (middle frontal gyrus (MFG) and inferior frontal gyrus
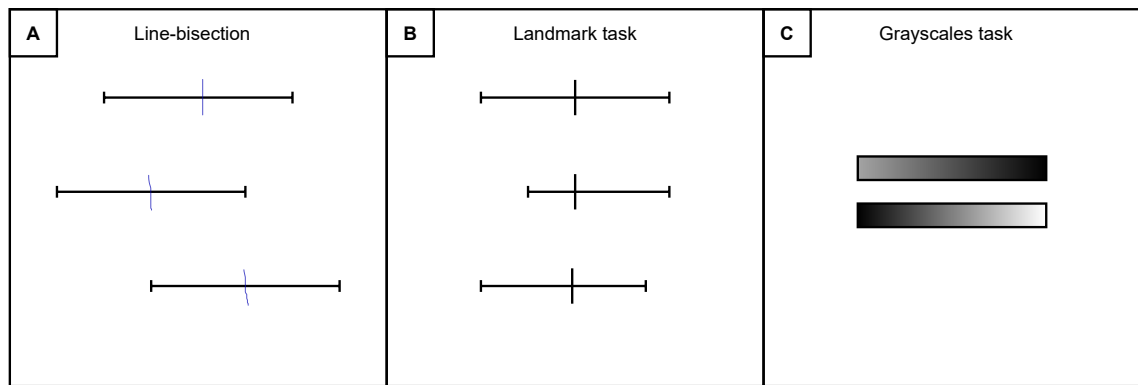
Figure 2.6: Tasks used for the assessment of neglect and pseudo-neglect. A) a typical line-bisection task (with marks by me), where participants are asked to manually indicate the line's center (Jewell & McCourt, 2000). B) a landmark task where participants have to judge whether the line is correctly pre-bisected or not (Fink et al., 2001). C) Stylized example of the "grayscales" task used by Nicholls et al. (2004), here participants have to judge which of the two bars is darker (here the upper bar). Response bias was associated with stimulus's darker side. This example, would therefore be categorized as a "right" response.

(IFG)) are reliably activated during attentional reorienting (Vossel, Geng, et al., 2014). Additionally, the ventral attention system has been described as strictly right lateralized (Corbetta et al., 2008), serving as a non-spatial novelty detector or "circuit-breaker", which signals when it is necessary to shift attention (Corbetta et al., 2008; Vossel, Geng, et al., 2014). More recent studies, however, also consider homologous regions in the left hemisphere as parts of the ventral attention network (Beume et al., 2017; Malherbe et al., 2018). Still, it is very likely that the ventral attention is right dominant (but not strictly lateralized), as left and right TPJ play different roles in attentional reorienting (Mengotti et al., 2020; Silvetti et al., 2016).

Although the ventral attention network appears to be involved in higher cognitive processing, that is not related to visual spatial influence, retinotopically organized subregions in left and right TPJ have been found (Dugué et al., 2018). Furthermore, TMS studies could show that disruption of right TPJ can lead to neglect like extinctions, that are usually expected after stimulation of the posterior parietal cortex (Meister et al., 2006). It is thus still possible that TPJ is also involved in spatial processing.

Furthermore, there are many questions about the interaction of dorsal and ventral attention networks (Vossel, Geng, et al., 2014). So far studies have shown that increased activity in right IFG leads to suppression of activity in right IPS (Weissman & Prado, 2012). Additionally, it has been shown that connections of right TPJ to right IPS are modulated by cue-validity, further showing that the ventral attention network provides feedback about the relative surprise of new stimuli to the dorsal attention network (Vossel et al., 2012). Similarly, higher activity in the ventral attention network, when compared to the dorsal attention networks, is correlated to worse behavioral performance in valid trials (Wen et al., 2012), also indicating the ventral attention network's role in loosening the grip on the dorsal attention network.

2.4 Meridians of the Visual Field

In the anatomical discussion of spatial cuing tasks, I introduced the concept of hemispheric asymmetries and dominance. Depending on the task, these hemispheric asymmetries

can have a direct influence on behavioral performances. Distinguishing facial emotions for example is faster for stimuli in the right visual field than for stimuli in the left visual field, indicating a preference for processing of emotions in the left hemisphere (Brederoo et al., 2019). Landmark tasks (Figure 2.6, C), however, are preferably processed by the right hemisphere, leading to an overestimation of the stimulus' left side. As this bias has also been observed in healthy participants performing line-bisection tasks, which is a clinical instrument in the diagnosis of hemispatial neglect, this slight "neglect" of the right visual field has been named pseudo-neglect (Figure 2.6, A) (Jewell & McCourt, 2000).

Hemispheric asymmetries and the readily available lesion model for spatial attention along the visual field's horizontal meridian, are possibly explanations for the larger number of studies using horizontal, rather than vertical stimulus layouts. Even though, asymmetries are also present along the visual field's vertical meridian (Nicholls et al., 2004). Just like stimulus processing along the horizontal meridian, different kinds of stimuli are preferably processed in the lower or upper visual fields (Levine & McAnany, 2005). But there is also a horizontal-vertical anisotropy (HVA), describing the better stimulus processing along the horizontal meridian when compared to the vertical meridian (Carrasco et al., 2001). Although, the most parsimonious explanation for this HVA might be due to physiological factors, like the distributions of cells in the retina (Carrasco et al., 2001; Jóhannesson et al., 2018), some neuroimaging studies show different brain areas involved in horizontal versus vertical processing (Lemos et al., 2016; Mao et al., 2007). Thus, I was interested in, whether there also is a HVA in spatial orienting and reorienting of attention.

To my knowledge, only a few neuroimaging studies have contrasted stimulus processing along the two meridians. For example, Fink et al. (2001) found no evidence for asymmetries between the meridians in an fMRI study using a landmark task. Mao et al. (2007) on the other hand provided evidence for differential activation along the vertical and horizontal meridian in a cued-attention task (but using only valid trials). Differential effects have also been found between horizontal and vertical saccades and anti-saccades (Lemos et al., 2016, 2017). A study explicitly investigating spatial orienting and reorienting using Posner's cuing task, however, found neither neuroimaging nor behavioral evidence for a HVA (Macaluso & Patria, 2007).

Lesion studies, however, complicate the picture. Nicholls et al. (2004) hypothesized that visual field asymmetries in neglect and pseudo-neglect are additive, not multiplicative, which indicates separate routes of neural processing, possibly indicating a perceptual versus attentional basis for vertical versus horizontal asymmetries (Carrasco et al., 2001). On the other hand, there are case-studies reporting altitudinal neglect after bilateral lesions in the parietal and occipital cortex (Rapcsak et al., 1988), and after bilateral temporal lobe lesions (Shelton et al., 1990), brain regions that are also associated with attention. Neural degenerative diseases affecting bilateral subcortical areas also impair patients' ability to perform saccades along the vertical meridian, however, these impairments might be more related to motor-control (Lemos et al., 2016, 2017).

In contrast to Nicholls et al. (2004), however, other studies have found that lesions of the right parietal cortex can also lead to stronger neglect in the lower left visual field, indicating that there is an interaction between the two meridians (Müri et al., 2009; Pitzalis et al., 1997). The opposite observation has been made in a recent case-study showing neglect of the upper visual field after a lesion to the right temporal lobe (Morris et al., 2020).

Especially these lesion studies let me wonder whether there is a HVA in attentional orienting and how it is represented in neural recordings. Hence the title of my first publication:

Attentional reorientation along the meridians of the visual field: Are there different neural mechanisms at play?

To answer this question, I used a modified version of the Posner cuing task. Participants reported the orientation of a pre-cued (80 % valid) target stimulus, by pressing a button with either the left or right index finger. Boxes in the four cardinalities indicated possible target stimulus positions. With each target stimulus, distractors appeared in all other possible positions. I split the task, however, so that cues and target stimuli appeared either only along the vertical or the horizontal meridian. Further details can be found in Steinkamp, Vossel, et al., 2020.

3 | Methods

In this first methods section I will introduce the main methodologies that I used to study attentional (re)orienting along the vertical and horizontal meridian in my first publication. The exception being dynamic causal modeling (DCM), which gets its own chapter (Chapter 5).

3.1 (Functional) Magnetic Resonance Imaging

Magnetic resonance imaging has been established in the early 1970s as a technique to create anatomical and functional images. In MRI a strong magnet is used to align protons in a magnetic field. Applying a radiofrequency pulse excites these protons, inducing a phaselocked spin, essentially knocking them out of their alignment. In the relaxation phase one can measure how long these protons need to realign with the magnetic field (T_1 recovery) or how long it takes till the phaselocking breaks down due to spin-spin interactions between protons (T_2 decay). As tissues have different properties, T_1 weighted imaging especially highlights fatty tissues, whereas T_2 weighted images highlight water as well as fat. A special case is T_2^* decay which takes next to spin-spin interactions also local field inhomogeneities into account and is used in blood oxygen level-dependent (BOLD) functional magnetic resonance imaging (fMRI).

T_1 and T_2 are constants, which depend on strength of the magnetic field. But one can change the measured images' content, by modifying the parameters of imaging sequences. The two most important parameters here are the repetition time (TR), which is the time between excitations in seconds, and the echo time (TE) typically reported in milliseconds, which reports the time point at which data is acquired. In high resolution imaging (for example for anatomical images) single axial (2D) slices of the brain are recorded per TR, which are later combined to create a 3D image. A special sequence called echo planar imaging (EPI), however, allows the excitation and recording of multiple slices during a single TR, providing faster but spatially less accurate images, and is often used in fMRI (Huettel et al., 2008, chapters 3 to 5).

Imaging based on T_1 or T_2 contrasts, is used for structural measures in clinical diagnostics (for example to locate brain lesions). In 1990, however, Ogawa et al. (1990) were able to measure cerebral blood flow due to the magnetic properties of oxygenized (HbO_2) and deoxygenized (Hb) hemoglobin, the BOLD signal. A discovery that had and still has a major impact on neuroimaging research (Bandettini, 2012). It is important to note that the BOLD signal is only a proxy of neural activity, which measures changes in cerebral bloodflow caused by an increased oxygen demand due to firing neurons (Glover, 2011). However, cell firing does not increase the demand for oxygen significantly, when compared to resting activity. So it is presumed that the driver for cerebral bloodflow is an increased demand for energy (glucose), which in turn also leads to a higher inflow of HbO_2 and less overall Hb (Fox, 2012). One of the most important validations for the use of fMRI has been that increases in local bloodflow are directly related to cell firing in the excited area, and are not due to down-stream cell activity (Logothetis et al., 2001).

To successfully perform statistical analysis of fMRI data, especially on the group level, the raw images have to undergo several preprocessing steps. As described above, MRI's are recorded in slices, so that, depending on the scanner protocol, it is possible that there are several seconds between the acquisition of the first and last scan of the 3D image.

These delays can be removed by a procedure called *slice-time correction*. Because a whole fMRI session can last for a long time, participants do not lie perfectly still in the scanner. Thus, each of the images in a session has to be realigned. This is done by linearly rotating and translating images so that they match an average image or the scanning run's first image. Another possible preprocessing step can include a correction of magnetic fields inhomogeneities (Wang et al., 2017).

As brain anatomy varies a lot between individuals, MR scans are transformed to a common coordinate space and the same voxel-size (MNI or Talairach). Furthermore, these images are often non-linearly morphed to a template image, to ensure anatomical proximity. Finally, to increase the fidelity of statistical analysis, spatial smoothing is often applied as a last step (Soares et al., 2016).

Although fMRI is ubiquitous in cognitive neuroscience research, there is no consensus on a single preprocessing pipeline. For classical fMRI analysis, however, a robust and well maintained pipeline — fMRIPREP — has been developed recently (Esteban et al., 2019), which has also been utilized in this thesis. Conveniently, it also creates a boilerplate methods section, following best practices in reporting of analysis details (Nichols et al., 2017), which can be found in each of my publication's supplemental materials (Chapters 6 and 7).

3.1.1   fMRI analysis

The most common form of fMRI analysis uses statistical parametric mapping (SPM) a mass-univariate analysis technique. For each voxel in the brain a general linear model (GLM) is calculated and contrasts between factors in the GLM are displayed in brain space. Typically this is done in two steps. First, for each participant a GLM is calculated using each voxel's time series as the dependent variable and including independent variables corresponding to task manipulation or physiological noise.

In principle the GLM for each voxel is described by the regression formula:

$$(3.1) \qquad\qquad\qquad Y = X\beta + \epsilon$$

Where Y represents the measured data (for example the time course of one or more voxel), X are the independent variable (or features), β the coefficients, and ϵ the measurement error. Note here, that X is a n by m matrix, with n time points (i.e. volumes measured using fMRI) and m features (see Figure 3.1). To represent the relationship between experimental manipulations in event related designs, the onsets of experimental manipulation are described as delta functions which are then convolved with a hemodynamic response function (HRF) function (Poline & Brett, 2012). While calculation of a classical GLM can be achieved by using least squares optimization, software like SPM (Friston, 2007), FSL, or AFNI (Poline & Brett, 2012) use different estimators for efficient calculation or might use mixed-effects models. Note that one can account for physiological noise and scanner drifts by including nuisance regressors as features (Friston et al., 1996; Liu, 2017).

On the first level basic contrasts are often calculated, for example addressing whether brain activity in one condition higher than in the other, or whether the BOLD amplitude in the condition is higher than the implicit baseline, following the idea of substraction by Donders (Raichle, 1998). In general this means that we get a contrast value for each voxel and participant of the estimated regression weights, which can then be further analyzed across participants.

GLMs can also be used on the group level, for example as a mixed-effects model with participant as random factor, and including different between participant covariates (e.g. sex or age). In my studies, however, this step has been conducted as one sample t-tests
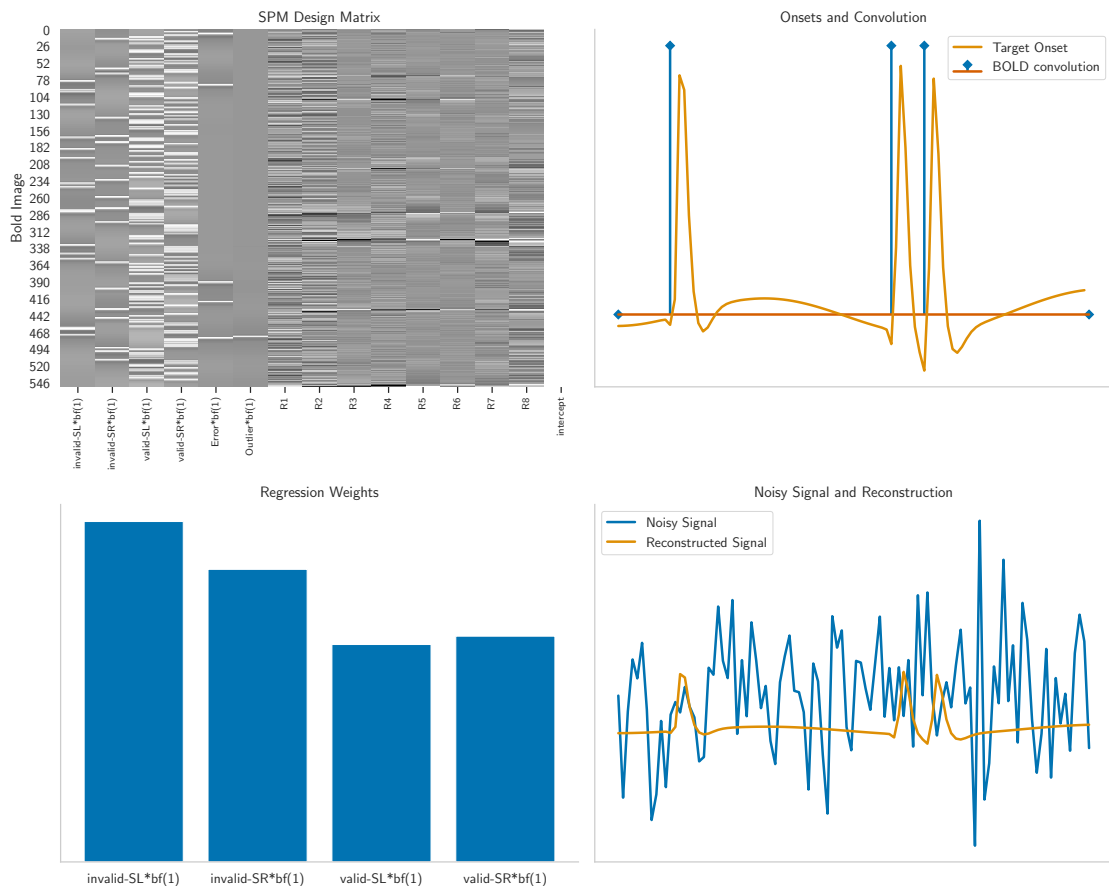
Figure 3.1: Event-related fMRI analysis. **Upper left:** A cut-out of the second project's SPM design matrix. Each column represents a regressor used in the GLM, where the first six regressors correspond to conditions (invalid left, invalid right, valid left, valid right, errors, outliers) and the others are nuisance parameters (like head movements). Each row corresponds to an individual scan. **Upper right:** Truncated example of the design matrix's second column. The blue lines indicate a target stimulus' onset. The orange line is the convolution with a hemodynamic response function, which is used in later regression analysis and included in the design matrix. **Lower right:** Example of the BOLD signal recorded at a single voxel (in blue). The orange line displays the reconstructed signal based on the GLM result. **Lower left:** β weights for the four regressors of interest, estimated for the time series in the lower right panel. This figure exemplifies the analysis performed for each voxel in the brain.

against zero or paired t-tests (Poline & Brett, 2012; Soares et al., 2016).

However, rather than using standard t-statistics to estimate the significance of single voxels, I applied permutation testing, which can lead to more stable and reliable statistical inference (Nichols & Holmes, 2002). In permutation testing an empirical null distribution is created for each voxel, by calculating the t-statistics for (in my case) 10 000 permutations. In each permutation the sign of a participant's voxel value is randomly assigned. The permutation p-value is then given by the proportion of random t-values that are greater than the observed t-value (Ojala & Garriga, 2010). Further steps are then taken to transform the permutation statistics back to t-statistics and to allow the family-wise-error-correction procedures implemented in SPM (Nichols & Holmes, 2002).

3.2   Machine Learning

Next to mass-univariate analyses, there are also multivariate approaches to investigate differences between conditions in fMRI analysis. The small number of samples (participants) and the large number of features (voxels), i.e., the curse of dimensionality, however, can become a problem for multivariate inference, as almost all possible separations between two conditions can be estimated. In classical statistics this can become a issue. Although machine learning, trying to maximize a model's generalizability, is also affected, the approach also provides tools to alleviate the problem (Domingos, 2012; Misaki et al., 2010). First, one has to distinguish between encoding and decoding models in neuroscience. Encoding models (or forward modeling), much like the classical GLM, described above, often act on a single voxel basis, investigating how certain experimental inputs change brain activity (Miyawaki et al., 2008; Poline & Brett, 2012). Decoding models, on the other hand, allow us to classify which state the brain is in at a given time (Misaki et al., 2010; K. A. Norman et al., 2006). I used this approach to decode brain states from the averaged signal of multiple volumes of interest (VOIs) or from parameters of computational models. Other approaches like search-light decoders, or more general multi-voxel pattern analysis, can provide whole-brain maps of classifier weights (i.e., a measure of importance), or maps of classification accuracies, of how well individual voxels can separate different brain states (Grosenick et al., 2013; Misaki et al., 2010).

While machine learning can lead to clinical applications, like informing hearing aids with electroencephalography (EEG) (O'Sullivan et al., 2014), or using age prediction models to search for neural abnormalities (Cole et al., 2019), the different mindset of machine learning can also be useful for statistical inference. Statistics is used to draw inference about a population using a (often small) sample, whereas the goal of machine-learning is to find predictive patterns in data, that generalize to unseen cases (Bzdok et al., 2018). This means, that the same methods can be used for different purposes. For example one can use logistic regression to infer the factors that separate two groups (statistics) or use logistic regression to classify a new instance into one of the two groups. Interestingly, while significant parameters in the first approach might be relevant for the second, these might not be the most important features for the machine learning model (Bzdok et al., 2020).

3.2.1   Prediction and generalization

As alluded to, in machine learning we do not necessarily care about significant parameter estimates, but are interested in a model's predictive performance. Typical performance metrics are accuracy ($\frac{TP+TN}{TP+TN+FP+FN}$, where TN are the true negatives, TP the true positives, FP the false positives, FN the false negatives) for classification tasks and mean absolute error for regression tasks ($\frac{1}{n}\sum_i^n |y_i - \hat{y_i}|$). Importantly, predictive performance estimates how well the algorithm performs on unseen data, which is usually different from the model fit of statistical methods (Domingos, 2012; Efron, 2020).

To access a given model's predictive performance, we therefore have to test it on unseen data. As data collection is often difficult and expensive, especially in neuroscience, collecting a separate data set just for testing purposes is often unfeasible. Typically, data is therefore split into different parts, a training set (about 60 % of the data), a validation set (20% of the data) and a test set (20% of the data). The split into different sets is necessary, as training a machine learning model often requires some tweaking of hyperparamters (like regularization in logistic regression). Thus, the model is only trained on the training set and the best set of hyperparameters is selected based on the model's performance on the validation set. The end result is the performance on the test set, which has not been used up-to that point.
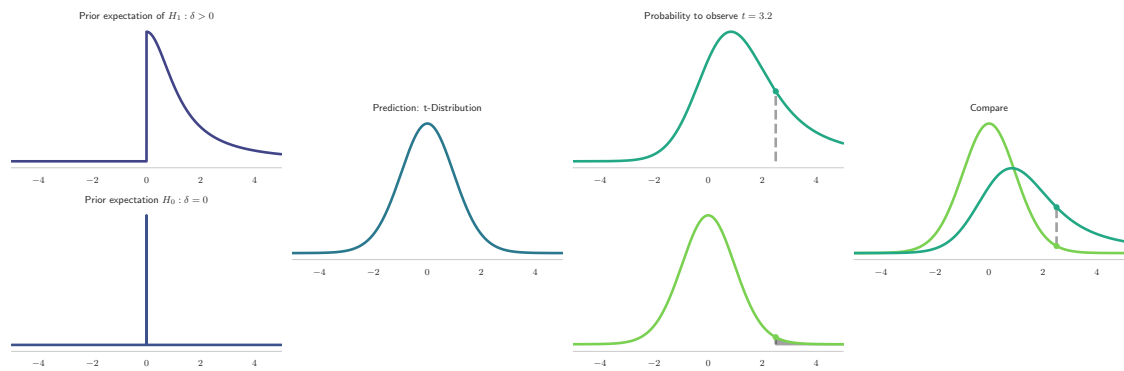
Figure 3.2: Estimating the BF for a one sample t-test. Starting from left to right. We begin with specifying our hypothesis about the expected effect size (i.e., prior distribution). Upper panel, half-cauchy displaying the probability of $H_1 : d > 0$. Lower panel the prior distribution for observing $H_0 : d = 0$. Our prediction for the observed t-value will be the t-distribution with $n_{samples} - 1$ degrees of freedom. We can now estimate the observed t-value's probability by looking at the posterior distributions. Note in the lower panel, that the shaded area indicates the frequentist p-value. Finally, we can compare the probabilities of the observed t-value under H_0 and H_1, and calculated the Bayes Factor.

Again, as data is expensive and researchers want to have an unbiased estimate of predictive performance, cross-validation is often used. Here, the training and validation procedure is repeated for different splits of the data (Varoquaux, 2017). In the first and the second study such procedures came into play using linear models to either show that we can differentiate valid and invalid trials across the horizontal and vertical run, as well as that we can separate the vertical and horizontal run from each other using parameters derived from computational models.

3.3   Bayesian Analysis

Because I reported null-results in my first study, I could not readily apply frequentist statistics, as they can only reject the absence of an effect (but see Lakens, 2017), i.e., the null hypothesis (H_0). Using Bayesian statistics, however, we can estimate the absence or presence of a statistical effect (Keysers et al., 2020). The general concepts (i.e., Bayes rule, and Bayesian belief updating) also play a large role in the estimation of generative models like DCM and my implementation of the Rescorla-Wagner model, described in Chapters 4 and 5 (Friston et al., 2003; Mathys, 2011; B. M. Turner & Van Zandt, 2012).

In recent years, criticisms of null-hypothesis significance testing and the over-reliance on p-values and their cut-offs for statistical significance has grown (Benjamin et al., 2018). One issue, for example is, that p-values are uniformly distributed, thus obtaining $p = 0.01$ is equally likely as getting $p = 0.95$, which means that p-value do not provide information about an effect's strength. Furthermore, p-values can change dramatically as a function of sample size (Keysers et al., 2020).

An alternative consideration to quantify evidence or the absence of evidence is the BF (Jarosz & Wiley, 2014). Bayes factors describe the (odds-)ratio of two models or hypotheses, often by dividing the posterior likelihood. The Bayes Factor, therefore is an assessment of how likely a given observation (H_1) is compared to another (H_0) (Jarosz & Wiley, 2014). This likelihood can be derived from Bayes' rule, following the notation in

Morey et al. (2016):

$$(3.2) \qquad\qquad \pi(H_i|y) = \frac{p(y|H_i)}{p(y)}\pi(H_i)$$

Where π is the prior and the posterior probability and p the probability given the observed data. To compare two hypotheses we divide their posterior probabilities to obtain the Bayes Factor:

$$(3.3) \qquad\qquad \frac{\pi_y(H_i)}{\pi_y(H_j)} = \frac{p(y|H_i)}{p(y|H_j)} \times \frac{\pi(H_i)}{\pi(H_j)}$$

Other formulations of the Bayes Factor and Bayesian updating rules commonly use θ_i instead of H_i, depending on whether one compares hypotheses or model parameters (Keysers et al., 2020)

Using Bayes Factors for null-hypothesis tests, like the t-test is relatively straight forward. The hypotheses are defined in terms of a standardized effect size like Cohen's δ.

$$(3.4) \qquad\qquad \delta = \frac{(\mu_a - \mu_b)}{\sigma}$$

We then define the null hypothesis as $H_0 : \delta = 0$, meaning that no effect is present and the alternative hypothesis as $H_1 : \delta > 0$, meaning that we expect to observe any nonzero effect size. Using a prior distribution like the Cauchy distribution, we also specify what effect sizes we expect to observe for H_1 (for medium effect sizes the shape parameter $r = 0.707$ is used) (Rouder et al., 2009). For H_0 a delta function is used with a single entry at 0. The likelihood distribution is then given by Student's t-distribution with $n-1$ degrees of freedom (see also Figure 3.2). Following Bayes' rule, combining prior and likelihood results in the posterior probability distribution.

Finally, we can calculate the t-value:

$$(3.5) \qquad\qquad t = \frac{\hat{x} - \mu}{\frac{s}{\sqrt{n}}}$$

and look up the t-value's probability in the posterior distribution of H_0 and H_1. The Bayes Factor in favor of H_1 would then be defined as:

$$(3.6) \qquad\qquad B_{10} = \frac{p(t|H_1)}{p(t|H_0)}$$

While the idea behind Bayes Factors is in part to remove arbitrary cut-offs and to consciously evaluate evidence – c.f. the discussion about p-values (Benjamin et al., 2018) – some general rules are followed. A $BF_{10} > 3$ is often seen as positive evidence for H_1, a $\frac{1}{3} < BF_{10} < 3$ as inconclusive evidence and a $BF_{10} < \frac{1}{3}$ as positive evidence for H_0 (Jarosz & Wiley, 2014).

For other statistical models like analyses of variance (ANOVA), we can also use Bayes Factors to calculate which model is more likely and therefore which factors could be deemed as more "*significant*". First, all models here are tested against a null-model, only including an intercept term or random-intercepts (i.e., offsets for individual participants). At this stage we only know how much more likely certain models are against the null-model. Next, we can also include a test of the models against each other, to see for example whether a model including factor "A" is more likely than a model including factors "A" and "B" (Keysers et al., 2020).

Box 3.1: Bayesian updating

Note, that in Bayesian updating, one can step-by step refine the posterior distribution of estimated parameters with new data. This means, if for example in an experiment new data is collected, one can update the Bayes factor (BF) for the effect of interest, not by re-calculating everything from the beginning, but by using the old posterior as the new prior distribution for the observed effect size (Keysers et al., 2020).

4 | Computational Modeling

No substantial part of the universe is so simple that it can be grasped and controlled without abstraction. Abstraction consists in replacing the part of the universe under consideration by a model of similar but simpler structure.

Rosenblueth and Wiener, 1945

Although my first and second project use the same data, they are conceptually very different. This second introduction will thus include a conceptual discussion of computational modeling and a more mathematical introduction to the dynamic causal modeling (DCM) framework.

4.1 Introduction to Computational Modeling

> **Box 4.1: Computational modeling**
>
> The computational modeling community in neursocience might appear to be very homogeneous, but researcher's goals vary. Some might want to have realistic models on the macroscopic, microscopic or behavioral scale, some want their models to be used in a clinical context. Most, however, want to have a "useful" model (Kording et al., 2018). Keeping the diversity in modeling approaches in mind, I think it is useful to introduce two different viewpoints on computational models.
> David Marr (2010, p. 24ff) famously formulated his three levels at which a computational model can be understood, these levels are not hierarchical and do not depend on each other.
>
> **Computational theory** Describing the physical properties of retinal cells, and their respective receptive fields, will not provide us with an understanding of their purpose. Asking questions of what the purpose of different receptive fields is and why they are arranged in such a way, will require understanding of computational properties like filters and differential operators (Marr, 2010, p. 25). In short: What is the system's goal, and why is it its goal?
>
> **Representation and algorithm** Marr (2010, p. 26ff) provides an example from psychophysics, of how participants perceive surface orienting and how different representations can be tested. In short: This level is about the "how" does the system solve computations, and how is information represented in the system.
>
> **Hardware implementation** Picking up the first example again, this is now about the neuroanatomy. What is the structure of the cells? How are different Ganglion cells connected, to perform necessary computations. In short: What are the physical properties the system has to fulfill in order to solve problems on the other levels.

While it is sometimes impossible to describe a system at all three levels, a full description is necessary, to gain a deep understanding of the underlying system. Thus, Marr stresses the need of computational theory to advance our knowledge in neuroscience (Marr, 2010, p. 27).

As I am using the DCM framework heavily in my thesis, and causal analysis is becoming more and more popular across the sciences, it is interesting to look at the three rungs of Judea Pear's 2018 causal ladder. Which will help us in understanding what approaches like behavioral dynamic causal modeling (bDCM) can and cannot do.

1. **Association** Pearl puts most of today's machine learning and statistical models here, which describe an association between multiple observations. His example: at a store, one might ask, how likely are customers to purchase floss when purchasing tooth-paste (Pearl & Mackenzie, 2018, p. 29 ff.).

2. **Intervention** Intervention means becoming active in the environment: What happens if we double the price of tooth-paste? To answer this question fully, one would need to conduct a randomized controlled trial. However, also a few specifically designed computational models can provide an answer to this question (Pearl & Mackenzie, 2018, p. 32).

3. **Counterfactuals** Would a customer (at time x) have bought toothpaste, if we had doubled the price. Counterfactuals are tricky in the sense that they make statements about other worlds or other timelines. Pearl puts many theories in physics here, as they can come to such statements after many rung two experiments (Pearl & Mackenzie, 2018, p. 34).

An interesting note here is that in other formulations of causal inference, there is no distinction between rung two and three, which makes the distinction between the two levels complicated (Pearl, 2018).

The term "model" is nowadays ubiquitous. Conceptual and approximate models help us to make sense of daily life (e.g. how a thermostat works). For everyday life, it often does not matter that these models are incorrect or oversimplifications (D. A. Norman, 2013, chapter 3). Models have an almost similar role in science, as indicated by Rosenblueth and Wiener (1945). Because we are dealing with very large and complex systems, we need to create abstractions and simplifications to make sense of our observations. Furthermore, these models are used to guide research and theory crafting (Guest & Martin, 2020).

For example, a very simple theory for participant's behavior during Posner's cuing task might be: If the cue is valid, participants know where to look, so they react faster than when they do not know where to look (neutral cue). But if they were expecting the target in the wrong location they respond very slowly (invalid cue). Before we run an experiment of our simple theory, i.e., collecting experimental data, we could create a very simple computational model beforehand. In fact, I already described how a basic mathematical model can be formulated in Chapter 3: Instead of saying reactions are faster or slower in the valid or invalid condition, we could define the minimal effect size we would see as proof for our theory, exactly as one would do in a Bayesian t-test with subjective priors (i.e., prior distributions specifically chosen by the researcher). Calculating summary statistics and for example performing a t-tests or a regression analysis is in a narrow sense already a formulation of a computational model (Haines et al., 2020). The same is true for the general linear model (GLM) used in functional magnetic resonance imaging (fMRI)

analyses (Poline & Brett, 2012).

Simple mathematical models, however, will not lead to a real understanding of the system in question. Referring to Box 4.1, classical statistical models neither allow for intervention nor counterfactual questions (Pearl & Mackenzie, 2018) and are restricted to David Marr's second level (Marr, 2010). To move a step further towards understanding, we need to derive assumptions about the data generation process (Haines et al., 2020). To transcend into even more understanding, we need to formulate the computational theory (Marr's first level), describing why the system acts in a way and test the model against real observation. To get there, we can translate our verbal hypothesis and theories (see example above) into mathematical formulas or programs (Guest & Martin, 2020; Smaldino, 2020). By repeated testing, falsification, and refinements of the model, we can derive and adjust our theories of behavior and the brain, constantly advancing our knowledge (Navarro, 2020).

4.2 Bundesen's Theory of Visual Attention

One example for a computational modeling framework, encompassing a large range of visual spatial attention tasks, is Bundesen's Theory of visual attention (TVA) (Bundesen, 1990). Although, the theory is quite complex in its mathematical reasoning (Kyllingsbæk, 2006), TVA's application to Posner's spatial cuing task is considerably simpler (equations 4.2 - 4.4). As we are already familiar with the task, I think it is a good example for the additional insights we get into the underling cognitive processes using a computational model, over t-tests (Bundesen, 1998). According to TVA performance in visual attention tasks is governed by the time a participant needs to accumulate evidence to perform an action. In the application to Posner's cuing task, there are two parameters. The parameter c, which is the processing capacity or processing rate of how fast sensory evidence is accumulated and b is an intercept term. The attentional weight w for one of the two locations in the original experiment is fully described by the cue-validity p.

$$(4.1) \qquad \frac{w}{(1-w)} = \sqrt{\frac{p}{(1-p)}}$$

With a cue-validity of $p = 0.8$, the attentional weight is $w = 0.67$ for valid targets and $w = 0.33$ for invalid trials. Finally, we can calculate the minimal reaction times to expect in the task (Bundesen, 1990):

$$(4.2) \qquad \mathbb{E}(\text{RT}|\text{valid}) = \frac{1}{0.67 * c} + b$$

$$(4.3) \qquad \mathbb{E}(\text{RT}|\text{invalid}) = \frac{1}{0.33 * c} + b$$

$$(4.4) \qquad \mathbb{E}(\text{RT})_{\text{min}} = 0.8\mathbb{E}(\text{RT}|\text{valid}) + 0.2\mathbb{E}(\text{RT}|\text{invalid})$$

The huge strength of formulating a process (like attentional (re)orienting) in such terms, is that it provides us with ideas of how to describe behavior in mathematical terms. And to draw new hypothesis. For example, if we estimate the above model for a group of participants, we might now ask ourselves whether the decision bias c is constant across different task conditions or mainly driven by the stimulus. To test this, we could now run the experiment with the same participants again, but vary the cue-validity.

Furthermore, we can extend these formulas to allow for new settings. For example to model hemispatial neglect using TVA, Bundesen introduced a new bias parameter, showing that the attentional weighting of the contralesional side was significantly reduced in patients (Bundesen, 1998). The different parameters of the TVA also have been related

to information processing in specific brain regions (Bundesen et al., 2005), so that the TVA presumably includes all three of Marr's levels.
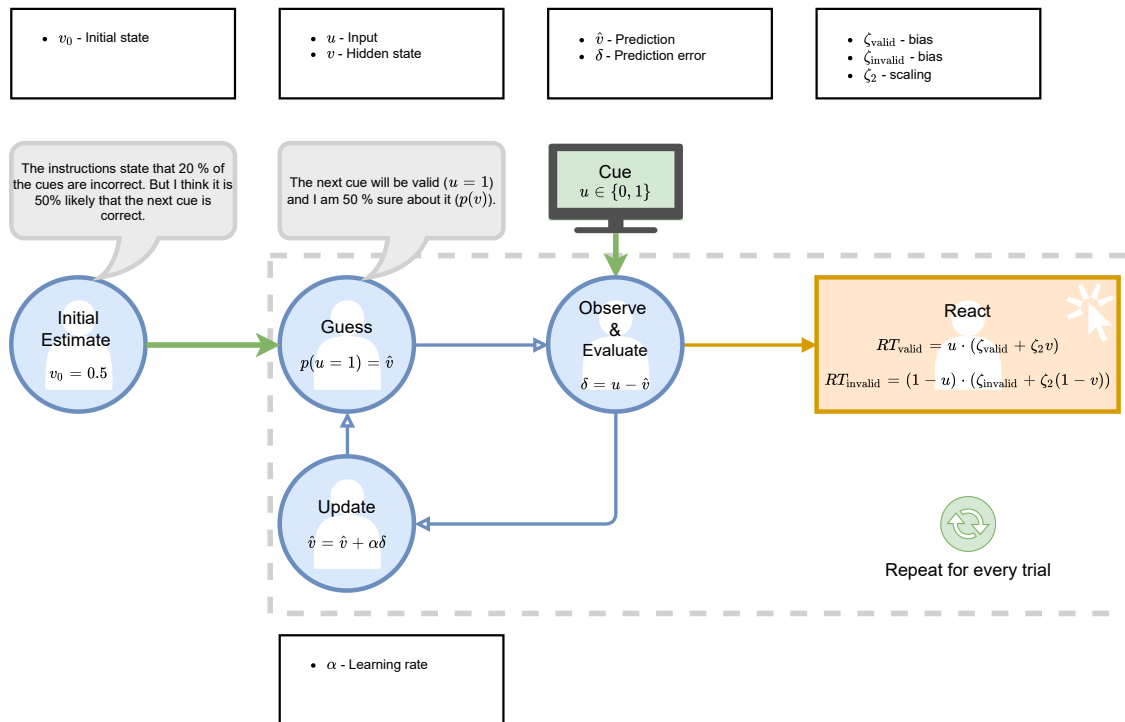
4.3 Rescorla-Wagner Model

Figure 4.1: Visual display of the Rescorla-Wagner model. Starting from an initial probability of the upcoming stimulus' identity, the agent makes a prediction and updates their expectations accordingly. The agent's prediction can also be translated to reaction times. This process is repeated for each trial in the experiment. The meaning of the variables in the formulas are in the white and black boxes above and below.

TVA is not the only computational model of Posner's cuing task. Other models have shown that the main driver of the validity effect is not related to visual acuity but rather the participant's surprise of not observing the target at the cued position (Eckstein et al., 2002). If surprise is an important factor, we might wonder whether previous trials shape our expectation of the future (Vossel, Mathys, et al., 2014). If we want to introduce such information into our model, we need to include temporal dynamics. Luckily, there are previously established models doing so. In 1972, Rescorla and Wagner, published a reinforcement learning model for classical condition in rats. Incidentally, the learning process described in this model, fits well to behavioral observations in Posner's cuing task. Here the cue can be seen as the conditioned stimulus, indicating where the target (or reward) is going to appear. Internally, we build a model of the cue's trustworthiness. If the cue is correct, we will trust it more and use it to predict the next target's location. If it is incorrect, however, trust in the cue will be reduced. Depending on the person, these adjustments of the internal model might be large or small.

As the algorithm of the Rescorla-Wagner describes aspects of DCM very well, I will describe it in more detail (see Figure 4.1 for a visualization). Assume we ask a naive participant to perform Posner's cuing task. The participant received the task instructions and assumes at the start that the cue-probability is $v_0 = 0.8$, i.e., 80 %. After the first cue ($u_1 = 0$, an invalid cue), the participant updates their internal cue-probability by first

assessing how large the prediction error was ($0 - 0.8 = -0.8$, Equation 4.6) and then updating their internal cue-validity ($v_1 = 0.8 + \alpha * -0.8$, Equation 4.5). As we want to model reaction times, not binary decision, the participant's internal cue validity needs to be transformed (Equation 4.7). The hidden state v_t evolves given the parameters over time. Unfortunately, we still need to estimate a number of parameters ($\alpha, v_0, \zeta_{1i}, \zeta_{1v}, \zeta_2$). In a very first step we would try to plug in appropriate values to simulate some data for the task, but we could also test our model against real data and use a solver for ordinary differential equations to derive the parameters. Or we rely on more elaborate Bayesian optimization techniques like Variational Bayesian inference, which we will be shortly introduced in the next chapter.

$$(4.5) \qquad\qquad\qquad\qquad\qquad v_t = v_{t-1} + \alpha\delta$$

$$(4.6) \qquad\qquad\qquad\qquad\qquad \delta = u_t - v_{t-1}$$

$$(4.7) \qquad\qquad g_t = u_t * (\zeta_{1v} + \zeta_2 v_{t-1}) + (1 - u_t)[\zeta_{1i} + \zeta_2(1 - v_{t-1})]$$

4.4 Simultaneous Modeling of Brain and Behavior

So far, I have described psychological models in more detail, but of course there are numerous models to describe neural activity and at the level of neurons to large scale brain networks (Kriegeskorte & Douglas, 2018), ranging from oscillator models of cell-firing to complex deep learning models investigating how physical and neuronal properties shape an organism's ethology (Merel et al., 2019).

Computational modeling has a long history and is well established in both (mathematical) psychology (Navarro, 2020) and neuroscience (Kriegeskorte & Douglas, 2018), but the two disciplines have not interacted that much in the past (B. M. Turner et al., 2017). Still, there have been approaches to bridge the gap between brain and behavior. For example, parameters of the TVA have been associated with functions of certain brain regions (Bundesen et al., 2005). And complex computational models have been derived to explain the exact nature of the computations in a given brain region (Parr & Friston, 2018).

Such claims — while substantiated by the current literature — are often difficult to test with current technology, as they might require invasive imaging methods. A different approach is to inform the analysis of neural or behavioral observations using outputs of computational models. Model based fMRI is such an example: Trial by trial estimates of the internal cue validity are derived using a Bayesian model which are then used as a parametric modulator in a GLM based analysis of fMRI data. This approach can reveal patterns of brain activity that are more informative than using raw measures like reaction times (Dombert et al., 2016; B. M. Turner et al., 2017). But, one could also relate estimates of computational models of both modalities to learn about specific computations in the brain. An example for this is relating effective connectivity parameters of DCM to parameters of the TVA (Vossel et al., 2016).

The challenge — providing us with the most insights — is the simultaneous computational modeling of brain and behavioral responses. This requires us to formulate a computational model, that can represent observed responses of both behavioral and neural measures. Finding such a model is very difficult, both on a conceptual and a computational level (B. M. Turner et al., 2017). One example for such a modeling approach is an extension of the DCM framework to allow a mapping of its hidden-states to observed behavioral responses, called bDCM (Rigoux & Daunizeau, 2015).

4.5   Applying bDCM

Applying bDCM to Posner's cuing paradigm, was the initial goal of my dissertation, for which I took certain design choices in the paradigm. I used methods to maximize the efficiency of the experimental design, described in Daunizeau et al., 2014 and tried to use very long inter-trial intervals. The separation into horizontal and vertical orienting was meant to create an independent test-set of the model. One strength of simultaneous modeling approaches is the use of interventions on the model (see Box 4.1). In bDCM, for example, one can introduce artificial lesions into the network model and simulate their effect on behavior. Because Posner's cuing task has a good lesion model, which can be used to evaluate the validity of simulated responses, we wanted to investigate it with bDCM.

The reaction time difference between reorienting and orienting — the validity effect — is usually the main effect of interest in Posner's cuing task. BDCM, however, has so far only been applied to binary responses (Rigoux & Daunizeau, 2015; Shaw et al., 2019), so that I had to apply some adjustments to the original modeling approach. To evaluate, whether modeling of reaction time and blood oxygen level-dependent (BOLD) data was successful a baseline model was needed for either modality. Because bDCM models BOLD dynamics in the same way DCM does, a standard DCM model served as baseline. For behavioral modeling I decided to use the Rescorla-Wagner model, as it can provide reaction time estimates for each trial in the experiment.

5 | Dynamic Causal Modeling

Dynamic causal modeling (DCM) has been introduced in the previous chapters, but what is it all about? This chapter will introduce DCM and the kinds of analyses it is typically used for, and how it can be extended to behavioral responses.
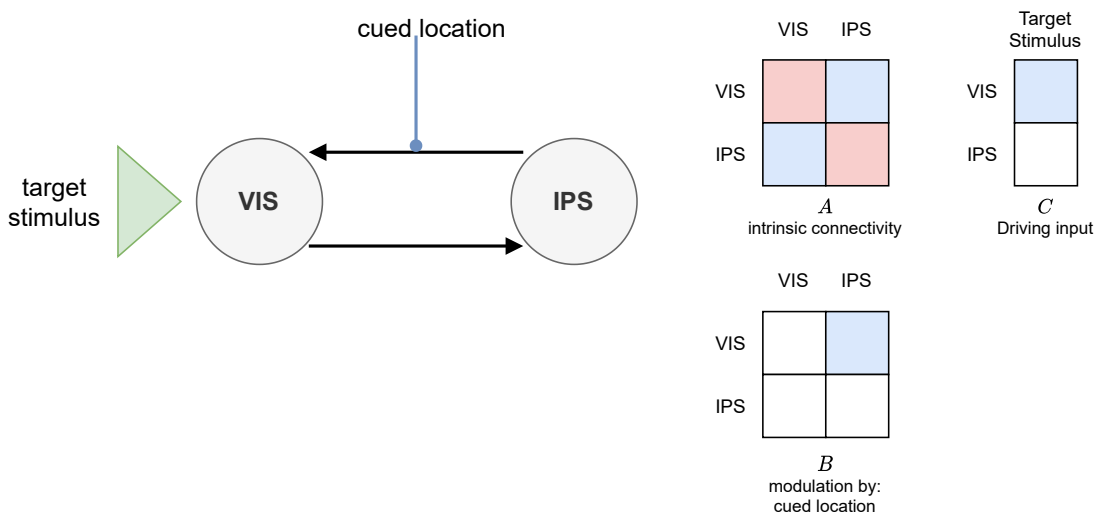
5.1 Conceptual Overview

Figure 5.1: Example of a minimal DCM, that might be used to describe neural dynamics in IPS and visual cortex (VIS) during a spatial cuing task. IPS and visual cortex share a bidirectional connection, i.e., dynamics in both regions influence each other (A matrix). The connection from IPS to visual cortex is modulated by the cued location, for example enhancing the influence of IPS on VIS for cued locations in the contralateral visual field (B matrix). The green triangle on the right indicate the direct increase or decrease of dynamics in visual cortex by a target stimulus (C matrix). On the right the same model is displayed in matrix form. Blue squares indicate the presence of a connection, white the absence, red is indicating the self-inhibition of the A matrix.

The applications of DCM are manifold. Next to other neuroimaging data, it has even been applied to model the population spread of COVID-19 (Friston et al., 2020). The most common application, however, is to functional magnetic resonance imaging (fMRI) data (Friston et al., 2003). In the case of fMRI, DCM is used to describe how neural dynamics between brain regions evolve over time, by modeling interactions between brain regions and external influences (e.g. experimental manipulations).

To do this, one has to define the model first, by deciding which brain regions to include and by defining how these regions are connected to each other and how regions and connections are influenced by external inputs (see Figure 5.1). Because it is often unclear which connections exist (for example in Figure 5.1, "target simulus" might modulate IPS and not VIS), different candidate models (or architectures) have to be defined. One then extracts the blood oxygen level-dependent (BOLD) time series from each volume of in-

terest (VOI)'s voxels for each participant's fMRI data. The DCM architectures are then fit to the data (inverted), and a winning model might be selected.

5.2   Dynamic Causal Modeling

One way to describe DCM is to see it as a generalization of the general linear model (GLM) model implemented in SPM (Friston et al., 2003). In Chapter 3, I described the GLM as a static regression model, however, the same procedure can also be described dynamically, which is similar to the Rescorla-Wagner model.

If we assume, that variations in neural activity are driven by experimental manipulations, we can describe the evolution function at a single voxel or VOI as:

(5.1) $$x_t = x_{t-1} + Ax_{t-1} + Cu_t$$

Here, A describes the influence of the neural dynamics in region x on itself, i.e., the auto-correlation. The experimental manipulation (or rather the onset of a specific trial) is described by u_t, which is also shown by the blue impulse function in the upper right panel of Figure 3.1, where C describes how much the experimental manipulation influences the neural state x_t. Because the repetition time (TR) in a fMRI experiment typically has a very low sampling rate in the order of seconds (e.g., in our study TR = 2.2 s), SPM oversamples the onset of experimental manipulations. Thus, instead of rounding the onset of experimental manipulations to the next TR, they are usually sampled every 0.1 s. If one takes slice-timing into account, as I did, the temporal resolution might be higher. There were 36 slices per BOLD image in my study, thus the sampling rate was $\frac{2.2}{36} = 0.061$). Oversampling is applied to obtain a smoother representation of the hemodynamic response function (HRF). The smooth HRF is then downsampled again, so that it can be used as a regressor in the design matrix (upper right panel in Figure 3.1).

The dynamics of the hidden state x_t described in Equation 5.1 are not enough to model the BOLD signal. While in practice for the GLM a canonical HRF model is convolved with the input vector u_t, we could recreate this process using a dynamical formulation. For this we apply an observation function mimicking the HRF on basis of the Balloon-Windkessel model ($g(x)$) (which in practice has own hidden states, which are dropped here for simplicity):

(5.2) $$z_t = z_{t-1} + g(x_t, \theta)$$

Having now a function f and g to describe hidden dynamics (for example cell firing) and how these relate to measurable BOLD data, we can now model the interactions between multiple brain regions, which is done in DCM. In fact, DCM is described by a set of ordinary differential equations (like Equations 5.1 and 5.2), implemented as a (non-)linear steady state model. Conceptually, however, it is good to keep in mind, that DCM and the Rescorla Wagner model are very similar in their set-up.

DCM in its classic formulation is a bi-linear model (Friston et al., 2003), but has been extended to include non-linear interactions of brain regions and nowadays can also include multiple states for each region or stochastic dynamics (Stephan et al., 2008).

Each brain region has its own hidden state, describing its neural dynamics, which are later translated to the BOLD signal. Depending on the given model architecture, dynamics of the hidden states interact with each other, changing their evolution through time. These temporal dynamics are defined by the evolution function below.

$$(5.3) \qquad \mathbf{z}_t = \mathbf{z}_{t-1} + A\mathbf{z}_{t-1} + \sum_{i=1}^{n_u} u_i B^i \mathbf{z}_{t-1} + \sum_{j=1}^{n_r} z_{t-1}^j D^j \mathbf{z}_{t-1} + C\mathbf{u}_t$$

Here $\mathbf{z}$ is a vector of length n_r (the number of brain regions), that represents the hidden states for each brain region included in the model (I am using the vectorized formulation here). A is a $n_r \times n_r$ matrix, describing how the brain regions are connected, which is called an adjacency matrix. As you can see in the formulation A is only dependent on the previous brain states $\mathbf{z}_{t-1}$, therefore describing brain connectivity in the absence of experimental modulations. Note that the diagonal of the A matrix is typically negative, so that the model will reach an equilibrium at 0 over time. The simplest way how experimental modulations can enter the system is via the matrix C ($n_r \times n_u$), which describes how much each of the brain states increase given each of the n_u inputs. Another possibility is to modulate connections in A via the matrix B (dimension $n_u \times n_r \times n_r$), which describes how connections between two brain regions (described in A) are altered in the presence of input u_i. In the non-linear formulation of DCM each brain state can alter connectivity between other brain states, coded in D (dimension $n_r \times n_r \times n_r$) For example, the activity in region a_1 might influence the connectivity between regions a_2 and a_3. In the model, however, there are next to the n_r neural states, an additional four states for each region, which are part of the Balloon-Windkessel model (Friston et al., 2003), where i signifies a single brain region:

s_i describing how the neural state z_i influences the vasodilatory signal

f_i the inflow corresponding to s_i

v_i the change in blood volume

q_i the change in deoxyhemoglobin content

As these states will play a minor role in the analyses, I refer to Stephan et al. (2007) and Friston et al. (2003) for an in depth treatment of the hemodynamic response function in DCM. Finally, these hidden states are gated through an observation function, that models the measured BOLD signal. I will drop the i index here, but introduce the subscript t to indicate the time.

$$(5.4) \qquad\qquad\qquad y_t = g(q_t, v_t)$$

Again, the general functions are not important here. But I want to stress, that while the function f describes changes in the hidden states, i.e. dynamics over time, the observation function g maps the hidden states back to the observed signal at that time point.

5.3   Model Inversion

Because we often do not know the values for many of the parameters, we have to estimate them from empirical data. In principle, this could be done using a solver for ordinary differential equations, which iteratively minimizes a cost-function (for example the mean-squared error (MSE $= \frac{1}{n} \sum_i^n (y_i - \hat{y}_i)^2$)). DCM, however, relies on a Bayesian inference scheme. This means, that the results of the so-called model inversion are not point estimates for each parameter, but the full posterior-distribution for the parameter (often defined as a Gaussian distribution). Relying on Bayesian inference leads to an

automatic shrinkage in parameter estimates (towards the prior distribution, here a normal distribution), supposedly leading to more stable parameter estimates (Stephan et al., 2008). Furthermore, after model inversion, we could sample from the parameter space to create new models or iteratively update our models — which is done in newer approaches to DCM (Friston et al., 2018).

To do this model inversion, DCM uses Variational Bayesian inference, which iteratively approximates the model evidence and the posterior and is discussed in more detail in Daunizeau et al. (2014). Such an approach is needed, as the exact posterior of generative models ($p(\theta|y, m)$ often cannot be estimated analytical, due to the model's complexities and nonlinearities.

A lower-bound of the model evidence in Variational Bayes is approximated by maximizing the free-energy (F), provided in Equation 4 in Daunizeau et al. (2014):

$$(5.5) \qquad F(q) = < \ln p(\theta|m) + \ln p(y|\theta, m) - \ln q(\theta) >_q, = p(y|m) - D_{\mathsf{KL}}(q(\theta); p(\theta|y, m))$$

This equation describes, that the model evidence F can be maximized with respect to q, by minimizing the Kullback-Leibler divergence (KL) between an approximation of the posterior ($q(\theta)$ and the exact posterior ($p(\theta|y, m)$). If $q(\theta) = p(\theta|y, m)$, then $F(q) = \ln(p(y|m)$ (Daunizeau et al., 2014).

I do not want to discuss more of the details here, but it is important to note that the last equation signifies that $F(q)$ is an approximation to the log-model evidence $\ln(p(y|m)$, which can be used for Bayesian model selection or to calculate the Bayes Factor of two competing models.

5.4   Bayesian Model Selection

The DCM's parameters are often not the only unknown factor in DCM analyses. For example, one wants to test different model architectures, representing competing hypotheses about how brain areas interact. Thus, one has to invert multiple models for each participant and select the winning architecture.

There are various ways to compare models in the DCM framework, which have been discussed in multiple outlets (e.g., Friston et al., 2018; Friston and Penny, 2011; Penny, 2012; Stephan et al., 2008).

The approaches most commonly used, are fixed-effects model selection, in which the model evidence for each model is summed over participants, or mixed-effects model selection which also incorporates model frequencies.

As the number of possible model architectures grows rapidly the more brain regions are included (Lohmann et al., 2012), the above mentioned model selection procedures can become unreliable. To solve this issue it is possible to summarize model evidence's of similar model architectures into families and compare model families instead (Penny et al., 2010). This approach can also be applied to select families hierarchically, which has been done in Steinkamp, Vossel, et al. (2020). Parameter estimates for the winning family are then achieved using Bayesian model averaging, which creates parameter averages, weighted by the model evidence.

Finally, newer approaches proposed in Friston et al., 2018 can be used to estimate the Free-energy of models nested within a full-model, where only the full model needs to be inverted. This approach decreases computational demands dramatically and allows the use of much lager model spaces. Furthermore, by using empirical Bayesian approaches, parameter estimates are further regularized to be closer to the group estimates, leading to a more stable inference.

5.5 Behavioral DCM

An extension to DCM was proposed by Rigoux and Daunizeau (2015), which allows for the additional modeling of behavioral responses. In simple terms, behavioral dynamic causal modeling (bDCM) adds another mapping for the hidden brain states **z** (described above), but instead of modeling brain dynamics, they are used to form a new hidden state **r**, describing "behavioral dynamics". Usually, a single dynamic is used, but multiple (i.e., n_r) are possible. These states change according to the following evolution function:

$$(5.6) \qquad \mathbf{r}_t = \mathbf{r}_{t-1} + A_r \mathbf{z}_{t-1} + \sum_{i=1}^{n_u} u_i B_r^i \mathbf{z}_{t-1} + \sum_{j=1}^{n_r} z_{t-1}^j D_r^j \mathbf{z}_{t-1} + C_r \mathbf{u}_t - \alpha \mathbf{r}_{t-1}$$

This formulation is similar to the evolution function for the neural states, where A_r (dimension $n_b \times n_r$) describes the static influences of the neural states **z** on the behavioral state, which is comparable to the weight vector in a regression model (Rigoux & Daunizeau, 2015), C_r ($n_b \times n_u$) and B_r ($n_u \times n_b \times n_r$) are direct and modulatory influences, and D_r the quadratic influences. Note that there is also a dampening factor α in the formulation, which serves as self inhibition of the behavioral states, similarly to the diagonal of the A matrix in equation 5.3. In Chapter 8 and in Steinkamp, Fink, et al. (2020), I use a different notation. The matrix A_r for example is then referred to as hA.

Next to the evolution function, we also need to include an observation function, to map behavioral dynamics to observed behavior. In the original paper this is done using a sigmoidal function for binary behavioral responses.

$$(5.7) \qquad y_t^r = \frac{1}{1 + e^{\rho - r_t}}$$

I slightly adapted this formulation in my second publication, as a sigmoidal function also describes reaction times in the paradigm very well. The function cannot provide values less than 0, and the experimental design does not allow for reaction times longer than 3 s. Therefore, I used the very slightly modified formulation:

$$(5.8) \qquad y_t^r = \frac{3}{1 + e^{\rho - r_t}}$$

Here ρ is just another scaling parameter. My formulation for continuous data also assumes a Gaussian likelihood function, as opposed to the Bernoulli distribution used in the original implementation (Rigoux & Daunizeau, 2015), modeling choices that were already implemented in the Variational Bayesian Analysis Toolbox (Daunizeau et al., 2014).

5.5.1 Artifical lesions

One approach I investigated, which was proposed in Rigoux and Daunizeau (2015), is the implementation of artificial lesions in the network. This is achieved by removing the incoming connections to the to-be-lesioned brain region.

$$(5.9) \qquad \text{lesion at node } i \iff \begin{cases} A_{i,i'} = 0 \\ B_{i,i'}^j = 0 & \forall i', i'', j \\ C_{i,j'} = 0 \\ D_{i,i'}^{i''} = 0 \end{cases}$$

By removing the incoming connections, the region effectively does not have any dynamics anymore and therefore cannot influence other connected brain areas. I slightly adjusted this approach by successively dampening the incoming signal by a factor κ, which simulates impaired, or strongly reduced activity in the given node. Together with another approach — susceptibility analysis — discussed in Rigoux and Daunizeau (2015), applying such models, could be used in counterfactual (i.e., causal) analysis of a brain region's contribution to behavior.

$$
(5.10) \qquad \text{dampening at node } i \iff
\begin{cases}
A_{i,i'} = \kappa A_{i,i'} \\
B_{i,i'}^{j} = \kappa B_{i,i'}^{j} \\
C_{i,j'} = \kappa C_{i,j'} \\
D_{i,i'}^{i''} = \kappa D_{i,i'}^{i''}
\end{cases}
\quad \forall i', i'', j; \kappa \in [0, 1]
$$

6 | Publication 1

Steinkamp, S. R., Vossel, S., Fink, G. R., & Weidner, R. (2020). Attentional reorientation along the meridians of the visual field: Are there different neural mechanisms at play? *Human Brain Mapping*, *41*(13), 3765–3780. https://doi.org/10.1002/hbm.25086

6.1 Author Contributions

S.R.S, S.V., and R.W. conceptualized and designed the research; S.R.S. and R.W. collected the data; S.R.S. wrote software, analyzed and visualized the data; S.V. and R.W. supervised the research project; S.R.S, S.V., G.R.F., and R.W. wrote the manuscript.

RESEARCH ARTICLE

WILEY

Attentional reorientation along the meridians of the visual field: Are there different neural mechanisms at play?

Simon R. Steinkamp[1] 🄳 | Simone Vossel[1,2] | Gereon R. Fink[1,3] | Ralph Weidner[1]

[1]Cognitive Neuroscience, Institute of Neuroscience & Medicine (INM-3), Research Centre Juelich, Juelich, Germany

[2]Department of Psychology, Faculty of Human Sciences, University of Cologne, Cologne, Germany

[3]Department of Neurology, Faculty of Medicine and University Hospital Cologne, University of Cologne, Cologne, Germany

Correspondence
Simon R. Steinkamp, Cognitive Neuroscience, Institute of Neuroscience and Medicine (INM-3), Forschungszentrum Jülich, Leo-Brand-Str. 5, 52425 Jülich, Germany.
Email: s.steinkamp@fz-juelich.de

Funding information
Bundesministerium für Bildung und Forschung, Grant/Award Number: 01GQ1401

Abstract

Hemispatial neglect, after unilateral lesions to parietal brain areas, is characterized by an inability to respond to unexpected stimuli in contralesional space. As the visual field's horizontal meridian is most severely affected, the brain networks controlling visuospatial processes might be tuned explicitly to this axis. We investigated such a potential directional tuning in the dorsal and ventral frontoparietal attention networks, with a particular focus on attentional reorientation. We used an orientation-discrimination task where a spatial precue indicated the target position with 80% validity. Healthy participants ($n = 29$) performed this task in two runs and were required to (re-)orient attention either only along the horizontal or the vertical meridian, while fMRI and behavioral measures were recorded. By using a general linear model for behavioral and fMRI data, dynamic causal modeling for effective connectivity, and other predictive approaches, we found strong statistical evidence for a reorientation effect for horizontal and vertical runs. However, neither neural nor behavioral measures differed between vertical and horizontal reorienting. Moreover, models from one run successfully predicted the cueing condition in the respective other run. Our results suggest that activations in the dorsal and ventral attention networks represent higher-order cognitive processes related to spatial attentional (re-)orientating that are independent of directional tuning and that unilateral attention deficits after brain damage are based on disrupted interactions between higher-level attention networks and sensory areas.

KEYWORDS
dynamic causal modeling, effective connectivity, fMRI, horizontal vertical reorienting, spatial attention

1 | INTRODUCTION

We are constantly exposed to an almost infinite amount of incoming sensory information. However, our brain's capacities to process new data are limited. An effective selection of important over unimportant information is therefore critical to ensure efficient information processing. This selection process, in which salient features of the sensory environment, as well as our internal goals and preferences, are considered, is commonly referred to as selective attention.

The allocation of attentional resources is controlled by neural structures that are thought to be organized in two distinct but interacting frontoparietal networks (Corbetta, Patel, & Shulman, 2008; Corbetta & Shulman, 2011; Vossel, Geng, & Fink, 2014).

The top-down guided (i.e., voluntary) orienting of attention involves a bilaterally organized dorsal frontoparietal network, encompassing the intraparietal sulcus (IPS) and the frontal eye-fields (FEF). Converging evidence from functional imaging and transcranial magnetic stimulation (TMS) suggests that these regions may modulate the activity in sensory (e.g., visual) cortices to prioritize the processing of stimuli at specific locations in space (e.g., Bressler, Tang, Sylvester, Shulman, & Corbetta, 2008; Hung, Driver, & Walsh, 2011; Ruff et al., 2008; Vossel, Weidner, Driver, Friston, & Fink, 2012).

Unexpected or very salient stimuli may interrupt our current top-down guided focus of attention (Simons, 2000), initiating a redistribution of processing resources. In this case, the allocation of attention is guided in a bottom-up fashion, meaning that it is primarily based on external stimulus features. The ventral frontoparietal attention network supposedly regulates this bottom-up control of attention. A central node within this network is the temporoparietal junction (TPJ), which has been suggested to be the driving force for attentional reorienting (Corbetta et al., 2008). The ventral network further consists of the inferior and the middle frontal gyrus (IFG, MFG) and is typically described as being strongly lateralized to the right hemisphere (Corbetta & Shulman, 2011). Recent studies, however, show that left TPJ is also involved in controlling spatial attention (Beume et al., 2017; Silvetti et al., 2016).

Unilateral lesions following a stroke can lead to an inability to allocate attention to the visual field contralateral to the lesion (Halligan, Fink, Marshall, & Vallar, 2003)—a phenomenon often referred to as hemispatial neglect. Neglect is more frequent and severe following right-hemispheric lesions and causes symptoms predominantly in contralesional space (Karnath, Rennig, Johannsen, & Rorden, 2011). This lateralization suggests a unique role for orienting and reorienting attention along the horizontal meridian and hence motivated research with a focus on that particular spatial dimension. Attentional orienting along the vertical meridian on the other hand seems understudied, despite the fact that there is also evidence for a vertical component in hemispatial neglect (Cappelletti, Freeman, & Cipolotti, 2007) and that cases of vertical neglect of the upper visual field after bilateral lesions to the inferior temporal lobes have been reported (Shelton, Bowers, & Heilman, 1990). Vertical neglect commonly affects the lower left visual field after right hemispheric lesions (Cazzoli, Nyffeler, Hess, & Müri, 2011; Müri, Cazzoli, Nyffeler, & Pflugshaupt, 2009; Pitzalis, Spinelli, & Zoccolotti, 1997). The extent of horizontal and vertical neglect along the meridians seems to be additive, becoming more pronounced at oblique positions (i.e., lower left visual field), which has also been observed for pseudoneglect in healthy participants (Nicholls, Mattingley, Berberovic, Smith, & Bradshaw, 2004). Thus, the allocation of attention along the two meridians may rely on distinct neural mechanisms.

However, it remains unclear if the brain regions controlling shifts of spatial attention are tuned to specific spatial directions or if they constitute a uniform system with no particular spatial preference (i.e., directional tuning). Several attempts have already been made to disentangle the neural mechanisms underlying vertical as compared to horizontal attentional orienting. The evidence coming from different neuroimaging studies, however, is inconclusive about the brain regions involved. On the one hand, orienting attention along a horizontal relative to a vertical axis activated the lingual and right precentral gyrus, whereas orienting attention in a vertical dimension involved more pronounced activation in the precuneus, medial frontal cortex, anterior cingulate, and cerebellum (Mao, Zhou, Zhou, & Han, 2007). Furthermore, ventral medial prefrontal cortex, cuneus, and lingual gyrus have been reported to be more involved in horizontal as compared to vertical antisaccades (Lemos et al., 2017), and left FEF and left superior temporal gyrus are more related to vertical relative to horizontal prosaccades (Lemos et al., 2016). Several other studies could not find any evidence for differences between horizontal and vertical attentional processes (Fink, Marshall, Weiss, & Zilles, 2001; Macaluso & Patria, 2007).

Therefore, the goal of the present fMRI study was to clarify the involvement of attentional control areas in reorienting attention along the vertical and horizontal meridian. To this end, both blood oxygenation level dependent (BOLD) amplitudes and measures of effective connectivity were employed. We used a variant of Posner's spatial cueing paradigm (Posner, 1980) in which participants had to indicate the orientation of a Gabor patch via button presses while ignoring distractor stimuli at other locations. A precue (arrow) indicated the most likely target location. Spatial reorienting of attention was induced by presenting invalid cues in 20% of the trials. The experiment involved two runs that differed about the spatial direction of attentional orienting and reorienting. In these two different runs, cues and targets were presented either along the vertical or the horizontal meridian of the visual field. Potential differences in attentional processing along the vertical or horizontal meridian concerning the BOLD-amplitudes were expected to induce a main effect of direction (horizontal, vertical), or an interaction between direction and cueing (valid, invalid cueing) in the standard general linear model (GLM) analysis of the fMRI data. Furthermore, vertical and horizontal reorienting of attention were expected to generate differential effective connectivity patterns in the activated brain areas in an analysis using dynamic causal modeling (DCM, Friston, Harrison, & Penny, 2003).

2 | METHODS

2.1 | Participants

We recruited 29 right-handed participants (Edinburgh handedness inventory [Oldfield, 1971], M = 0.86, SD = 0.14) with normal or corrected to normal vision, who gave written informed consent. One participant had to be excluded from both behavioral and fMRI analysis due to noncompliance with the task. Another participant was excluded only from further fMRI analysis due to excessive head movements (translation >3 mm); however, the participant's behavioral data were included in further analysis. The remaining 28 participants (15 female) were between 21 to 39 years (M = 25, SD = 3) old. The ethics board of the German Psychological Association had approved the study. Participants were compensated with 15€ per hour.

2.2 | Experiment

Participants performed a spatial cueing paradigm inside a 3 Tesla TRIO MRI scanner (Siemens, Erlangen). Stimuli were displayed on a screen that was mounted at the end of the scanner's bore and could be seen by the participant via a mirror (245 cm distance). The mirror was mounted on top of a 32 channel head coil. Participants' task throughout the experiment was to report the orientation (horizontal 90° or vertical 0° rotation) of a target stimulus (Gabor patch, diameter 1° visual angle) using button presses of their left and right index fingers. Participants were instructed to continually fixate a diamond in the screen's center (0.5° wide). Next to the central diamond, empty boxes (1° wide) were presented in all four cardinalities throughout the experiment with their centers at 4° eccentricity. Each trial began with an alerting signal, a 500 ms brightening of the diamond's center, followed by a spatial cue (duration: 200 ms) after 1,000 ms. Brightening and widening of one of the central diamond's corners served as a symbolic cue (arrowhead), indicating the most likely upcoming target location with 80% probability. We informed the participants about the cue validity during the task instructions. After a variable interval of 400 or 600 ms, the target stimulus appeared (duration: 250 ms) in the cued box (valid trial) or in the box opposite to the cue (invalid trial). Distractor stimuli were presented in the remaining three boxes for the same duration as the stimulus. Distractors were created by superimposing two Gabor patches, which were rotated by 45° and 135°. The resulting pattern matched the target stimulus in intensity and contrast (see Figure 1). The inter-trial interval separating subsequent trials was either 2.0 s, 2.7 s, 3.2 s, 3.9 s, or 4.5 s with equal probability. Trials were presented in two subsequent runs, with a short break in between. In one run, cues pointed only to the left or right, and target stimuli were only presented along the horizontal

meridian. In the other run, cues pointed only upwards or downwards, and the target only appeared in the upper or lower box (i.e., on the vertical meridian). Before each run, participants completed 20 practice trials with immediate feedback regarding accuracy. Each run consisted of 5 blocks, each comprising 32 valid and 8 invalid trials. The 8 possible target properties (position left/right or up/down, left/right response finger, 400/600 ms SOA) were presented with equal probability in each block. Trial order in each block, however, was fully randomized. The order of horizontal and vertical runs and the response mapping (left or right finger for horizontally oriented stimuli) were counterbalanced across participants. Between the different blocks, a 10 to 13 s break period was included. Before the actual spatial cueing paradigm, participants also completed a separate short training to get used to the response mapping between stimulus orientation and response fingers. Here, 60 target stimuli appeared rapidly in the screen's center, and participants had 500 ms time to respond. Immediate feedback was given, and the percentage of correct responses was continuously presented. Recording of responses and stimulus presentation were controlled with PsychoPy (version 1.85.3, Peirce, 2007, 2008; Peirce et al., 2019). Additionally, we recorded eye-movement data during the experiment using an EyeLink® 1000 eye tracker (SR Research). Set-up, analyses, and further descriptions of the methods can be found in the supplementary material (S2).

2.3 | Behavioral analyses

We used a two-step procedure to test for differences in reaction times and error rates between the vertical and horizontal runs and the effects of valid and invalid cueing. The resulting 2 (cueing: valid/invalid
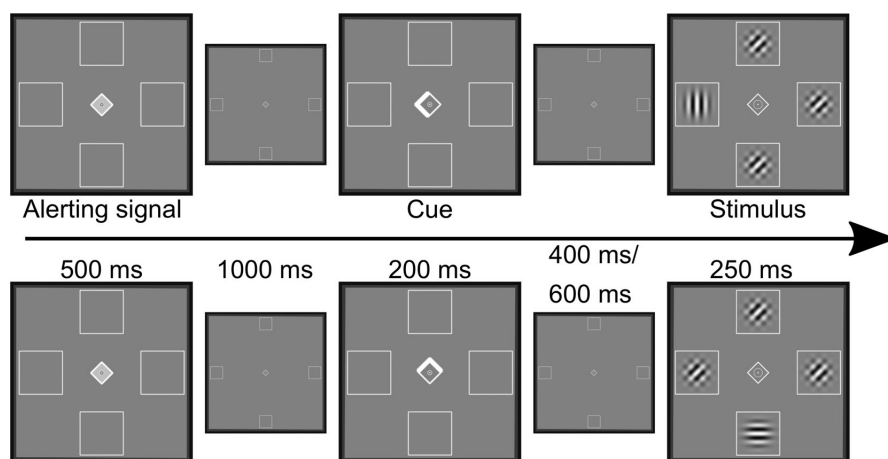

FIGURE 1 One trial for each run of the cued attention task. In the upper row, a valid trial in the horizontal session is displayed, in the lower row, an invalid trial of the vertical session. Displays for the alerting signal, cue, and stimulus presentation were enlarged for better presentation. The smaller displays show the stimulus presentation in the correct proportions. Participants were told to always fixate the center of the screen. Their task was to press a button corresponding to the orientation of the target stimulus (vertical or horizontal Gabor patches)

cues) x 2 (direction: horizontal/vertical) design was subjected to a Bayesian implementation of an analysis of variance (BF_ANOVA), treating participants as random factors (Rouder, Morey, Speckman, & Province, 2012). The Bayes factors (BF) for different models representing the possible combinations of factors were calculated using the BayesFactor package (version 0.9.12–4.2, Morey & Rouder, 2018) implemented in R (version 3.5.1, R Core Team, 2018), using default settings ("medium" scaling factor on the JSZ-prior and 10,000 iterations of the MCMC algorithm). The BF_{10} in favor of the model (H_1) was calculated by dividing the model's posterior probability by the posterior probability of a null model (grand mean plus random factors, H_0). Additionally, we compared the model with the highest BF_{10} against all the other models (main effects and interaction). Following standard conventions, a $BF_{10} > 3$ is regarded as positive evidence and a $BF_{10} > 10$ as strong evidence in favor of H_1. A $BF_{10} < 0.33$ is then seen as positive evidence and a $BF_{10} < 0.1$ as strong evidence in favor of the null hypothesis (Jarosz & Wiley, 2014). The error rates were calculated for each participant by taking the mean of incorrect and missed responses for each direction (horizontal/vertical) and cueing condition (valid/invalid). Reaction times were defined as the median response times for each direction and cueing condition. Before the calculation of the median, we removed the error and post-error trials (to account for post-error slowing), missed responses, trials with response times faster than 200 ms, and response times exceeding the 75% quartile +1.5 * interquartile range (IQR) criterion (number of excluded trials, invalid left M = 2.79, SD = 2.33; invalid right M = 2.43, SD = 2.25, valid left M = 8.14, SD = 5.41; valid right M = 7.64, SD = 5.40; invalid down M = 3.61, SD = 2.25; invalid up M = 3.57, SD = 2.23; valid down M = 8.21, SD = 4.12; valid up M = 7.43, SD = 4.30).

2.4 | FMRI

We obtained 557 T2* weighted images per run using an echo planar imaging (EPI) sequence (time of repetition (TR) 2.2 s; echo time (TE) 30 ms; flip angle 90°). Each image consisted of 36 transverse slices (recorded in an interleaved and ascending manner), with a voxel size of 3.1 mm x 3.1 mm x 3.3 mm and 3 mm slice thickness (field of view 200 mm). We manually discarded the first 5 images of each run to account for T1 equilibrium artifacts. In addition to the BOLD images, we obtained a structural T1 anatomical image for each participant.

The functional and anatomical data were preprocessed using fMRIPrep (version 1.1.1), a standardized and robust preprocessing pipeline (Esteban, Markiewicz, et al., 2019) based on Nipype (Gorgolewski, Burns, et al., 2011) and run as a docker-image. We followed mostly the standard preprocessing steps (details can be found in the supplementary material under MRI-preprocessing, S1). The anatomical images (T1) were corrected for intensity and nonuniformity, skull-stripped, and spatially normalized to the ICBM 152 Nonlinear Asymmetrical template 2009c (Fonov, Evans, McKinstry, Almli, & Collins, 2009). Furthermore, brain-tissue segmentation of cerebrospinal fluid, white-matter, and gray-matter was performed.

The functional data were slice-time and motion-corrected, and an additional "fieldmap-less" distortion correction was applied (Wang et al., 2017). The preprocessed functional images were then co-registered to their anatomical (T1) images and finally warped onto the MNI template. Frame-wise displacement (Power et al., 2014) was calculated for each functional run using the implementation of Nipype.

Additional spatial smoothing of the functional images was performed in SPM12 (version 7,219, Friston, 2007) implemented in MATLAB 2016b (The MathWorks, Inc., Natick, Massachusetts), using an 8 mm FWHM Gaussian kernel.

2.5 | Analyses of imaging data

The first level statistical analysis of the data was performed using SPM12. For group-level analysis, we used the statistical nonparametric mapping (SnPM) toolbox (version 13.1.07, Nichols & Holmes, 2002). At the single-subject level, we modeled both runs in the same design matrix using an event-related design (i.e., a stimulus duration of 0 s), with run-specific intercepts and confounds. As regressors of interest, we used the target onsets of the two cueing-conditions and the four possible target positions. This resulted in eight different regressors for invalid left (iL), invalid right (iR), valid left (vL), valid right (vR), as well as invalid down (iD), invalid up (iU), valid down (vD), and valid up (vU) trials. For each run, up to two additional regressors were added. One regressor was used to account for error and post-error trials and another to account for outlier trials (please, see the behavioral analysis for the definition of outliers). The regressors' onsets were convolved with a canonical hemodynamic response function (HRF). The six movement parameters calculated during realignment and the frame-wise displacement were included in the model as confounds. A cosine set accounting for drifts and high-pass filtering was applied following the SPM12 defaults.

We investigated five planned contrasts: (a) The main effect of all invalid versus valid trials ((iL + iR + iD + iU) – (vL + vR + vD + vU)), (b and c) two contrasts for direction-specific cueing effects: horizontal reorientation (iL + iR) – (vL + vR) and vertical reorientation (iD + iU) – (vD + vU), (d) a contrast for the main effect of direction ((iL + iR + vL + vR) – (iD + iU + vD + vU)), and (e) a contrast for the interaction of cueing and direction ((iL + iR – vL – vR) – (iD + iU – vD – vU)). Additional four tests were performed to show the effects of attentional and perceptual modulation in the visual areas by valid targets. These tests were performed separately for each visual field (vL > vR; vR > vL; vD > vU; vU > vD).

Group level t-maps were then calculated for each contrast using one-sample permutation t-tests (25,000 permutations, no variance smoothing) with a predefined cluster forming threshold of $p < .001$ uncorrected (SnPM: fast option). We report the results of thresholded t-maps, using a significance cut-off of $p < .05$ (FWE corrected at the predefined cluster level). An overview of global and local maxima was created using the function "get_clusters_table" implemented in the Python package Nistats (version 0.0.1b, Abraham et al., 2014).

2.6 | VOI analyses

As we did not find any significant differences in BOLD amplitudes between horizontal and vertical directions, and no significant activations for the interaction of direction and cueing (valid/invalid), we conducted a more sensitive post hoc VOI based analyses. Here, we probed bilateral TPJ, FEF, and IPS, which are key regions of the ventral and dorsal attention networks. While these regions do not include the whole network (see, for example, MFG/IFG), they are the ones we considered to be most likely influenced by the direction of attention reorienting due to their proximity to the visual areas. Furthermore, we limited the regions included in the network, also with regards to the computational complexity that would arise in the following DCM analyses.

The global or local maxima corresponding to the six regions of the condition main effect (Table 1) defined the seed coordinates. These were passed to Nilearn's (version 0.4.2) "NiftiSpheresMasker" function (without standardization and detrending)—implemented in Python 3.7—to extract the mean beta values of the eight regressors of interest using an 8 mm sphere, masked by the thresholded t-map of the main cueing effect (a).

The mean beta values were averaged over visual fields to obtain values for the horizontal and vertical directions. For example, the beta value used for left IPS during invalid horizontal trials consisted of the average extracted beta values from iL and iR. For each VOI, we analyzed whether direction or interaction effects were present using BF_ANOVAs, with the participant as the random factor. We followed the rationale described for the analysis of the behavioral data.

In addition to the BF_ANOVAs, we used logistic regression to test whether brain activity differences between cueing-conditions of one direction were predictive for the cueing effect in the respective other direction. We again used the mean betas of each participant in the six VOIs for each of the eight regressors (iL, iR, iD, iU, vL, vR, vD, vU), this time not collapsing along meridians. Then, we tested whether BOLD amplitude patterns in the six VOIs of the horizontal run (iL, iR, vL, vR) were similar enough to differentiate valid and invalid trials of the vertical run (iD, iU, vD, vU), and vice versa. This was done using logistic regression implemented in scikit-learn (version 0.20.0, Pedregosa et al., 2011). The logistic regression's performance was first estimated on a per run basis using nested cross-validation. Each run's data was split into fives, so that every split served as test-data once. For each round, the remaining splits served as training data and were again subjected to five-fold cross-validation to find the best regularization parameter C in the range $[10^{-4}, 10^{-3} ..., 10^{3}, 10^{4}]$. The regularization parameter that achieved the highest average accuracy in the inner cross-validation loop was used to refit the logistic regression on all of the training data. The run-based model performance was then defined as the average accuracy over the splits. A similar approach was used to estimate generalized performance, where five-fold cross-validation was used on one run to find the best parameter C, and the accuracy was calculated for the predictions made on the other run.

As a performance measure, we used permutation tests by shuffling the class-labels (valid or invalid trials), refitting the logistic regression and then recalculating the accuracies (1,000 permutations). The permutation p-value then represents the proportion of accuracy scores that were higher in the random condition than in the original (Ojala & Garriga, 2010).

2.7 | DCM analyses

In addition to differences in BOLD amplitudes, we were interested in the cueing-dependent effective connectivity patterns in the horizontal and vertical runs. To estimate effective connectivity, we used bilinear DCM (DCM 12, revision 6,755, in MATLAB 2016b). DCM is a state-space model used to infer the cortical dynamics in time between brain regions. The approach leads to a generative model that, once inverted, can be used to simulate neural activity in the network. The state-change equation of neural states in DCM is described by Equation (1) (Friston et al., 2003).

$$\dot{z} = \left(A + \sum_j u_j * B^j \right) * z + C * u \tag{1}$$

The change in the hidden neural states $\dot{z}$ is described by the fixed connectivity matrix A, which represents the coupling between brain regions in the absence of exogenous modulations (u). The coupling can be modulated by the j exogenous inputs (u), which are represented by the parameters in the matrix B (the connections in B are a subset of A). Lastly, the driving input regions, which represent the direct changes of hidden states, is defined by the matrix C. As we were interested in how connection strength differs between invalid trials in the horizontal (u_1) as compared to the vertical run (u_3), we restricted our analysis to the parameters in the matrices B^1 and B^3. Matrices B^2 and B^4 were left empty, which means that connections were not modulated by valid trials (neither in the horizontal nor the vertical run). Since we were interested in investigating potential differences in reorienting of attention (invalid trials), we assumed that connectivity between brain regions in valid trials was the same for both runs (i.e., that all dynamics of valid trials were captured in the baseline connectivity described by the matrix A).

We limited the network analysis to the most representative regions of the classic models of visual spatial attention and extracted the time series in the regions of the VOI analyses. The time series of both runs were concatenated (spm_concat). For the estimation of our DCMs, we defined a new design matrix for each participant. The target onsets of all trials served as driving inputs to the DCM. As in the GLM analysis above, we included the seven motion parameters as nuisance regressors and added run specific intercepts (to center the time series of each run). The VOI coordinates (see Table 1) served as the center of 12 mm spheres in which the participant's nearest local maximum was selected. The new coordinates were then used as the center

of an 8 mm sphere from which the first principle component of the BOLD signal was extracted. The spheres included only task activated voxels (threshold $p < .05$ uncorrected), and the time series were adjusted for the nuisance regressors and mean activity. We used the contrast of valid trials against baseline to select the VOIs for bilateral FEF and IPS, and the contrast invalid trials against baseline for the TPJ VOIs.

The underlying network structure describing the intrinsic coupling during the task (A) was defined by fully connected intra-hemispheric regions and inter-hemispheric connections of homologous regions. All nodes received all driving-inputs because visual input was carefully matched across conditions and visual areas were comparably activated.

Hierarchical family-wise Bayesian model selection (BMS) implemented in the MATLAB VBA-toolbox (version: master/7ac4470b987796cf4ec9bfb275ab049d5aa97931, Daunizeau, Adam, & Rigoux, 2014) and subsequent Bayesian Model Averaging (BMA, implemented in SPM12) were used to find theconnections and parameters in B^1 and B^3 that best describe our data. In the first step, three model families were used to investigate whether modulations by invalid trials occurred only in the left, right, or in both hemispheres. The second class of families was used to decide upon the direction of inter-hemispheric modulations between left and right IPS. The remaining modulations, which can be seen in Figure 2, then describe whether TPJ affects the dorsal attention network or vice versa. The model space was restricted so that at least one modulation between the dorsal and ventral attention network had to be present and that there were no bidirectional modulations. In total, we inverted 72 models per participant. The modulations by invalid trials in horizontal and vertical runs (i.e., in B^1 and B^3) were the same. Hence, while the connectivity parameters could differ, the overall modulation structure by invalid trials stayed the same. Finally, we used BMA on the winning model-family on a participant level, to get more reliable point estimates for the different connections.

The DCMs were created using mostly default settings for bilinear DCM. However, we used 36 instead of the 22 time steps in the discretization of the inversion function to account for slice time correction. Confounds, which were included in the DCM estimation, were manually added, so that temporal drifts, represented by a discrete cosine set, and confounds calculated during the participant's SPM design matrix were included for each run separately.

We tested whether the modulation by invalid trials differed between the vertical and horizontal session by calculating the BF_{10} in favor of any difference between runs using Bayesian paired t-tests for each parameter pair in B^1 and B^3. Testing for differences in effective connectivity strength between runs, however, does not provide us with the full picture. For example, it remains unknown how the parameters interact as a whole within the network. Therefore, using the generative properties of DCM (and the BMA parameter estimates), we simulated the BOLD signal by swapping the inputs (u) between the horizontal and the vertical runs (i.e., iH (u_1) ↔ iV (u_3), vH (u_2) ↔ vV (u_4)). This approach allowed us to evaluate the specificity/generality of the parameters for horizontal and vertical reorienting of attention. If the model performance with the parameters of the

respective other run is comparable to the original data, we can conclude that, regardless of specific parameter values, the neural processes of invalid trials are similar across runs.

The performance of the swapped model was compared against random models in which the onset timings of the impulses in u were kept, but the input streams (u_1, u_2, u_3, u_4) were assigned randomly. We report the proportion of participants with permutation P-values lower than $p < 0.05$ in the original and swapped conditions. The permutation P-values were calculated as the proportion of models where the root mean squared error (RMSE, Equation 2) was larger in the original or swapped data than in 1,000 sets of randomly generated data.

$$RMSE = \sqrt{\frac{1}{n}\sum_{i=1}^{n}(y_i - \bar{y}_i)^2} \qquad (2)$$

3 | RESULTS

3.1 | Behavioral data

Participants' reaction times in invalid trials were higher than reaction times in valid trials, both in the horizontal (invalid M = 718.32 ms, SD = 113.58 ms; valid: M = 674.50 ms, SD = 98.48 ms) and in the vertical run (invalid M = 723.68 ms, SD = 138.74 ms; valid: M = 667.04 ms, SD = 116.52 ms). A similar pattern was observed for error rates (Figure 3). In the horizontal run, error rates were higher for invalid compared to valid trials (invalid M = 4.46%, SD = 5.37; valid: M = 3.44%, SD = 3.41), similarly so in the vertical run (invalid M = 5.54%, SD = 3.56; valid: M = 3.21%, SD = 2.27). The BF_ANOVA for reaction times yielded strong evidence only for the main effect of cueing-condition with a BF_{10} of 17,275.39 against the baseline model. This model was also superior to the other possible combinations of the 2x2 design (evidence in favor of the cueing only model against: direction only BF_{10} = 87,028.43; both main effects BF_{10} = 5.05; main effects plus interaction BF_{10} = 15.7). The analyses of the error rates yielded similar results. The model including only a cueing main effect had the highest BF_{10} against the intercept model (BF_{10} = 16.8), and also stood out against all other possible combinations of factors (evidence in favor of cueing only against: direction only BF_{10} = 64.8; both main effects BF_{10} = 4.13; against main effects plus interaction BF_{10} = 8.32). In sum, these analyses show that the main manipulation of the experiment—the reorientation of attention in invalid trials—induced the expected reaction time costs and increased difficulty, as seen in the error rates. Moreover, they provided positive to strong evidence that neither the overall level of reaction times nor the reorienting costs after invalid cueing differed between the horizontal and vertical runs.

3.2 | GLM

Figure 4 depicts the main effect of cueing (invalid > valid cueing, contrast (a)) for vertical and horizontal runs combined. The automatic

calculation of the cluster-forming threshold at $p < .001$ (cluster corrected FWE $p < .05$) yielded a cluster forming threshold of k ≥ 58 voxels. Cluster size in cubic millimeter, global maxima, up to four local maxima, and their respective t-statistics are provided in Table 1. Reorienting across both runs activated areas of the dorsal and ventral frontoparietal attention networks. The largest cluster stretched along the parietal cortex, with the local maxima located in bilateral IPS and bilateral precuneus. The next cluster included the right FEF and extended into the right insular cortex, as well as into the medial and inferior frontal gyrus. In the right hemisphere, we found a single cluster in the TPJ. Similar activation patterns were observed in the left hemisphere, with separate clusters in the insular cortex, FEF, IFG, and TPJ.

The run-specific activation maps of reorienting-related activity are depicted in Figure 5. In the vertical run, clusters surviving the statistical threshold (k ≥ 57 voxels) were found in bilateral IPS and right TPJ. Additionally, significant activations were observed in the right inferior frontal and middle frontal areas, as well as in the insular cortex. The main effect of cueing in the horizontal run revealed clusters

(k ≥ 47) in bilateral FEF and IPS. Cluster size in cubic millimeter, their global maxima, and the respective t-statistics are provided in Table 2.

Tests for main effects of direction (k ≥ 57) and the interaction of direction and cueing (k ≥ 47) did not yield any significant voxels surviving the cluster-based FWE correction.

Our analysis of the attentional modulation in valid trials in relation to the visual fields (Figure 6) revealed activations (k ≥ 52) in left dorsal and ventral higher-order visual areas (including V4 and V5) for the contrast of right versus left valid targets. The reverse contrast (left versus right valid targets), yielded a cluster (k ≥ 53) of significant activation in ventral parts of right higher-order visual areas. Contrasting trials with lower visual field targets versus upper visual field valid targets resulted in a significant cluster (k ≥ 46) in right and dorsal parts of higher-order visual areas. The reverse contrast did not reveal any significant results.

The statistical t-maps of the GLM analysis can be found on Neurovault in a thresholded and un-thresholded form (https://identifiers.org/neurovault.collection:5622).

TABLE 1   Cluster coordinates for reorienting across horizontal and vertical runs

Global maximum	Local maxima	Side	MNI coordinates			Peak statistic (T)	Cluster size (mm³)
			X	Y	Z		
Precuneus		L	−8	−70	47	7.06	56,750
	Precuneus	R	10	−66	57	6.45	
	Precuneus	L	−8	−60	51	6.44	
	IPS†	R	38	−51	51	6.18	
	IPS†	L	−34	−57	51	6.07	
FEF†		R	29	2	54	6.72	32,967
	Precentral gyrus	R	45	9	31	5.51	
	Precentral gyrus	R	54	12	37	5.36	
	MFG	R	51	24	28	5.35	
SMA		R	10	21	54	6.36	5,994
	SMA	L	−5	24	51	4.83	
Insula		L	−37	21	1	5.72	3,834
FEF†		L	−37	2	57	5.22	16,822
	FEF	L	−27	−1	54	5.12	
	Precentral gyrus	L	−40	2	37	4.87	
	Precentral gyrus	L	−46	6	44	4.82	
STPJ†		L	−58	−60	18	4.92	3,029
	TPJ	L	−65	−63	−2	4.59	
TG		L	−74	−32	−2	4.81	2,126
	MTG	L	−58	−29	−5	4.08	
TPJ†		R	60	−41	1	4.53	2,674
SMG		L	−62	−63	31	3.58	96
Temporal pole		L	−37	21	−22	3.53	96

Note: Global and up to four local maxima's coordinates and peak t-statistics of the thresholded statistical maps. Coordinates annotated with a dagger (†) were included in the further VOI-based and DCM analyses. Rounded MNI coordinates and cluster sizes were estimated using Nistats' get_cluster_table.
Abbreviations: FEF, frontal eye fields; IPS, intraparietal sulcus; MFG, middle frontal gyrus; SMA, supplementary motor area; TPJ, temporoparietal junction; TG, temporal gyrus; MTG, middle temporal gyrus; SMG, supramarginal gyrus.
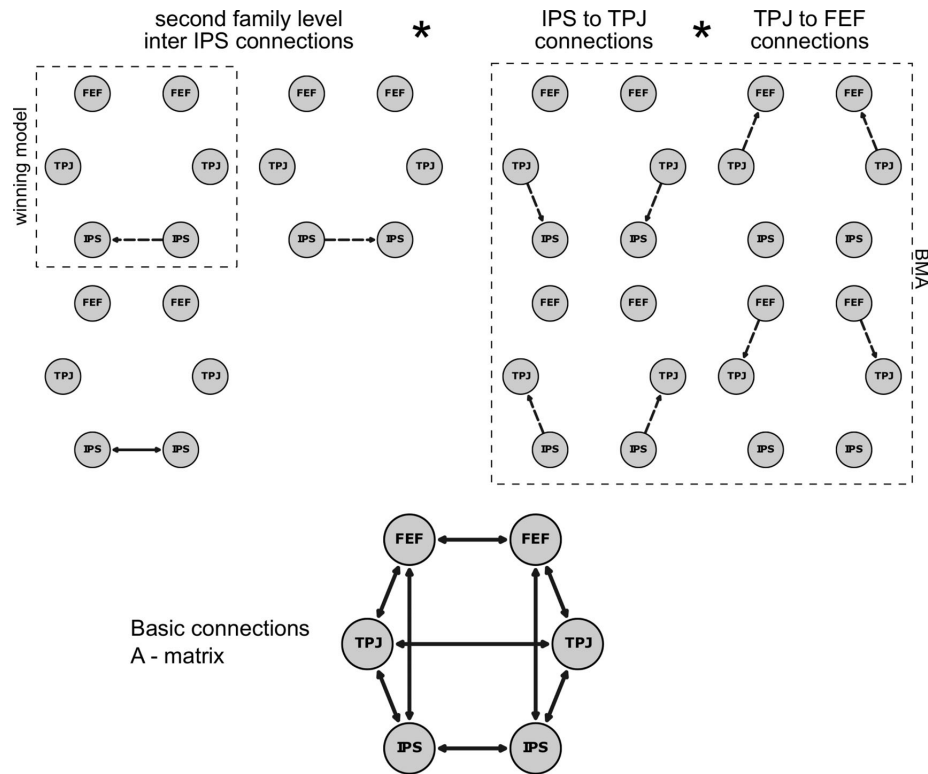
FIGURE 2 A schematic of the model space used in the fMRI analysis. The first model family comparison revealed that modulations between IPS and TPJ and FEF and TPJ were present in both hemispheres (models not shown). Hence, only the models of the bilateral family are shown. Dotted lines are used for unilateral and solid lines for bilateral connections. The second model family comparison favored models with a unidirectional connection from right IPS to left IPS (see left upper panel). The remaining model combinations based on connections between IPS-TPJ and FEF-TPJ were summarized using BMA. The model basis is shown in the lower part of the figure, indicating the fixed connections. BMA, Bayesian model average; FEF, frontal eye-fields; IPS, intraparietal sulcus; TPJ, temporoparietal junction
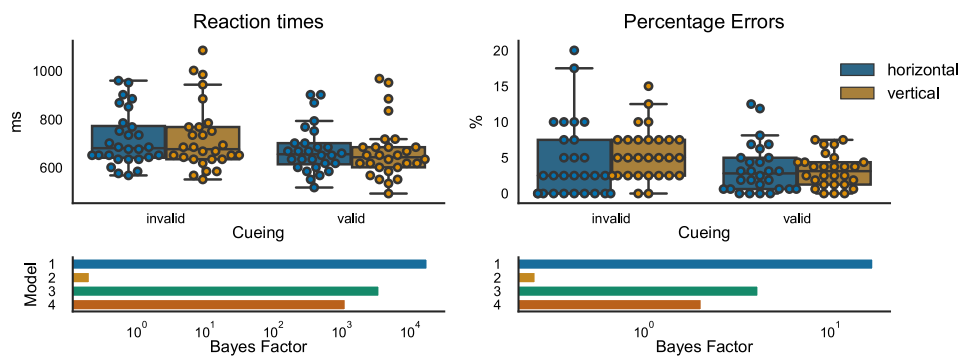
FIGURE 3 Results for the behavioral data. In the upper part of the figure, boxplots show the distribution of the data (the median, 25th, and 75th percentile, whiskers indicate minimum and maximum, outliers are determined using the 1.5 * IQR criterion). Swarm plots were used to indicate individual data points in the sample. The bar graphs in the lower part indicate the Bayes factor (in logarithmic scale) against an intercept model. Model1—cueing only; Model 2—direction only; Model 3—cueing + direction; Model 4—cueing + direction + cueing × direction

3.3 | VOI analyses

As a potentially more sensitive approach, we extracted the regression (beta) weights of the main GLM analysis in six regions that showed significant reorienting related activity (see Table 1). The BF_ANOVA (following the same rationale as in the behavioral analysis, see Figure 7) yielded the highest evidence for the model including only the main effect of cueing in all six regions (BF_{10} for left IPS = 33.13; right IPS BF_{10} = 45.93; left FEF BF_{10} = 10.91; right FEF BF_{10} = 31.44; left TPJ BF_{10} = 5.92; right TPJ BF_{10} = 9.04). Comparing the cueing-only effect against the main effect of direction, both main effects, and main effects plus interaction (Table 3), showed that there was only positive evidence in favor of the cueing main effect ($BF_{10} > 3$) in most of the VOIs. In the right IPS VOI, however, there was only anecdotal evidence (BF_{10} = 1.07) favoring the cueing-only model against the model including both main effects, meaning that we cannot convincingly exclude an additional effect of direction for this region.

Using logistic regression, we tested whether the average beta weights of the eight regressors (valid and invalid trials for all target locations) could predict the cueing-condition (valid/invalid trials) in the respective other run. The prediction was significant for each run with an accuracy of 62.2% (p = .021) for the horizontal and with an accuracy of 62.3% (p = .021) for the vertical run. More importantly, the model trained on the horizontal run generalized to the vertical run with an accuracy of 59.3% (p = .016), and the model trained on the vertical run generalized to the horizontal run with an accuracy of 62.0% (p = .006). These results support the observation that the activation patterns in the six VOIs were highly similar, so that those predictive models generalized well across the two runs.

3.4 | DCM analyses

The DCM analysis was carried out using data from 26 of the remaining 27 participants, as for one participant, the coordinates for the left TPJ VOI could not be established. To select the DCM with the highest evidence of generating the network activity in our data, we

FIGURE 4 Statistical map for the reorienting (invalid > valid) across horizontal and vertical runs. The thresholded map was projected onto the freesurfer inflated surface templates (fsavg5) using nilearn
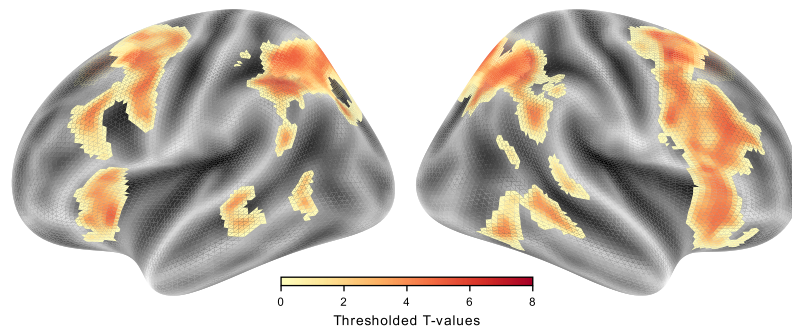
FIGURE 5 Statistical maps of the reorienting (invalid > valid) in each run. The thresholded maps for the two runs were projected onto the freesurfer inflated surface template (fsavg5) using nilearn

Horizontal Run
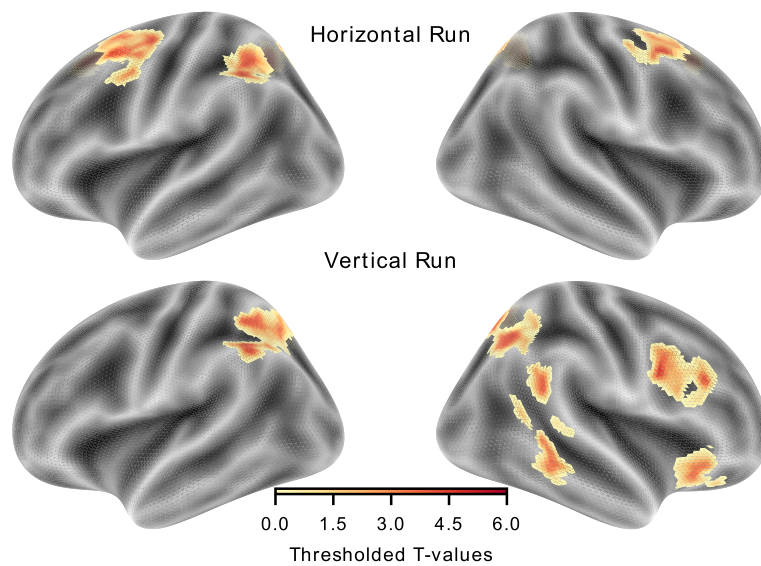
Vertical Run

TABLE 2 Cluster coordinates for reorienting-related activity in horizontal and vertical runs

Global maximum	Side	MNI coordinates			Peak statistic (T)	Cluster size (mm)
		X	Y	Z		
Invalid > valid horizontal						
Angular gyrus	R	10	−60	51	5.23	2,578
Parietal cortex	L	−43	−51	47	5.12	4,737
FEF	L	−24	9	57	4.94	6,413
FEF	R	29	6	51	4.89	2,835
SMA	L	−5	21	51	4.55	2,964
Precuneus	L	−12	−60	51	4.53	2062
Invalid > valid vertical						
Precentral	R	45	6	31	5.7	4,382
TPJ	R	60	−51	21	5.36	1,869
Insula	R	29	27	−12	5.03	2,352
Temporal	R	63	−35	−9	4.89	2,159
Parietal cortex	L	−49	−51	41	4.65	8,153
Parietal cortex	R	20	−73	54	4.56	9,700
Precuneus	L	−8	−73	47	4.22	1,353
Lingual gyrus	L	−2	−76	54	3.48	32

Note: Only the coordinates of the global maxima in the main clusters are reported.

Abbreviations: FEF, frontal eye fields; SMA, supplementary motor area; TPJ, temporoparietal junction.

- target right
- target left
- target lower
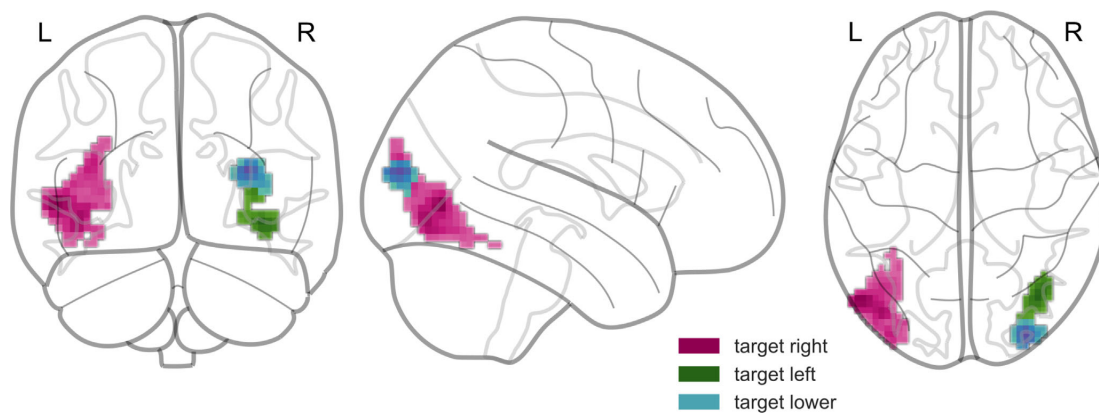
FIGURE 6 Attentional modulation by the direction of attention in valid trials (i.e., targets appearing in the left, right, upper, and lower visual fields)

applied a hierarchical familywise model selection. The family with modulations in both hemispheres was slightly superior (exceedance probability [*ep*] = .54) when compared to the other two families (left lateralization *ep* = .46, right lateralization *ep* = .00). This family was then further subdivided into three families consisting of models describing the direction of the interhemispheric IPS connections. The model family with a modulation from right IPS to left IPS had the highest evidence with an *ep* of .76 (*ep* IPS right to IPS left = .00; *ep* bidirectional modulation = .24). Finally, the models in this winning family were subjected to BMA. The participant-specific DCM models with averaged parameter estimates had a good to moderate fit to the data, with a mean coefficient of determination (R^2) of 33.74 (*SD* = 10.39, range 16.65 to 63.33).

The parameters for invalid horizontal (B^1) and invalid vertical (B^3) trials were compared using Bayesian paired t-tests. Most modulations provided positive evidence for an absence of differences between both runs (Table 4). For the connections from left TPJ to left FEF, left FEF to left TPJ, and right FEF to right TPJ, there was only anecdotal
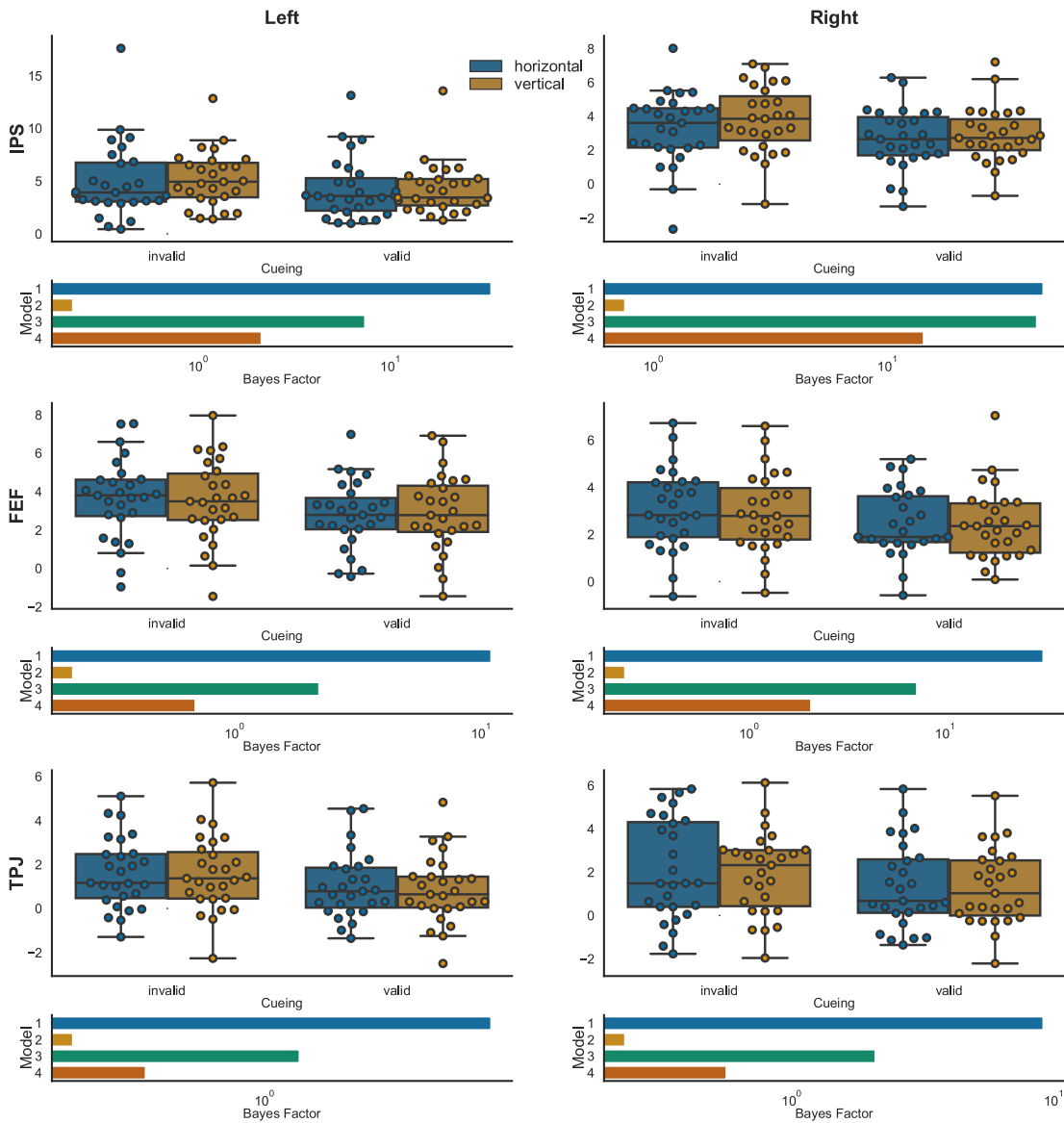
FIGURE 7　Results of the VOI based analysis. For each of the six VOIs, boxplots show the distribution of the data (the median, 25th, and 75th percentile, whiskers indicate minimum and maximum, outliers are determined using the 1.5 * IQR criterion). Swarm plots were used to show individual data points in the sample. The bar graphs below the box plots indicate the Bayes factor (in logarithmic scale) against an intercept model. VOIs are displayed separately for left- and right-hemispheric regions and in the order IPS, FEF, TPJ. Model1—cueing only; Model 2—direction only; Model 3—cueing + direction; Model 4—cueing + direction + cueing × direction. FEF, frontal eye-fields; IPS, intraparietal sulcus; TPJ, temporoparietal junction

evidence against a difference in parameters ($M = 0.12$, $SD = 0.49$, $BF_{10} = 0.44$; $M = 0.13$, $SD = 0.47$, $BF_{10} = 0.48$; $M = -0.3$, $SD = 0.84$, $BF_{10} = 0.90$).

Further interrogating the DCMs for each participant revealed that DCMs based on the BMA (RMSE: $M = 0.35$, $SD = 0.08$) performed in general better than the random models (RMSE: $M = 0.41$, $SD = 4.00$,

all $p < .001$, except for one with $p = .006$). Swapping the vertical and horizontal inputs (iH (u_1) ↔ iV (u_3), vH (u_2) ↔ vV (u_4)) led to slightly worse performance in each model (R^2: $M = 33.09$, $SD = 10.42$), when compared to the original data. Still, the swapped model was superior to a random input model for most participants (RMSE: $M = 0.37$, $SD = 0.09$). Using a cutoff of $p < .05$ (i.e., 5% of random models had a

TABLE 3 Summary statistics VOI-based BF_ANOVA on the regression (beta) weights

| | Invalid | | Valid | | BF_ANOVA | | |
| | | | | | Model 1 versus | | |
VOI	Horizontal M ± *SD*	Vertical M ± *SD*	Horizontal M ± *SD*	Vertical M ± *SD*	Model 2	Model 3	Model 4
IPS L	4.97 ± 3.60	5.19 ± 2.64	4.24 ± 2.93	4.22 ± 2.44	150.60	4.54	15.73
IPS R	3.27 ± 2.13	3.80 ± 1.96	2.69 ± 1.79	2.91 ± 1.63	61.47	1.07	3.24
FEF L	3.64 ± 2.10	3.53 ± 2.11	2.80 ± 1.77	2.90 ± 2.02	48.62	4.98	15.78
FEF R	3.07 ± 1.71	2.92 ± 1.67	2.47 ± 1.41	2.43 ± 1.51	135.10	4.42	15.35
TPJ L	1.60 ± 1.61	1.56 ± 1.66	1.02 ± 1.49	0.85 ± 1.54	26.72	4.51	15.31
TPJ R	2.10 ± 2.33	1.93 ± 1.86	1.35 ± 1.95	1.31 ± 1.74	39.99	4.36	16.10

Note: Each row displays the mean (M) and standard deviation (SD) for each of the six VOIs. The BFs for the comparison of Model 1 versus the three other models are shown. These BF_{10}s indicate how much more likely Model 1 is, compared to the other models. Model 1—cueing only; Model 2—direction only; Model 3—cueing + direction; Model 4—cueing + direction + cueing × direction.

lower RMSE than the swapped model), the model with swapped inputs performed better than the random input model in 18 out of 26 participants (69%).

4 | DISCUSSION

This fMRI study used two versions of a spatial cueing paradigm to compare the behavioral and neural mechanisms underlying attentional reorienting along the horizontal and vertical meridians. Regardless of cueing direction, our experimental procedures induced the well-established reaction time costs in responses following invalid cues when compared to valid cues (Hedge, Powell, & Sumner, 2017). Attentional reorienting behavior was comparable within participants for the vertical and the horizontal direction, suggesting that the costs of reorienting spatial attention are unaffected by directionality. Along the same lines, the analysis of the fMRI data using a GLM, a VOI-based approach, and DCM analyses revealed no evidence for direction-sensitive effects in the higher-level regions of the attentional networks.

To tackle the difficult task of quantifying the absence of an effect of direction or interaction of direction and cueing, we applied, wherever possible, Bayesian inference methods like Bayes factor ANOVAs and Bayesian t-tests to get an estimate of the likelihood of the presence (or absence) of the effects of interest. In the case of Bayes factor ANOVAs, this provided us with the possibility to compare the main effect of cueing against other possible interactions and main effects. For the behavioral measures, this analysis revealed evidence in favor of a model including an effect of attentional reorienting only, without additional interactions. Similar results were observed in the fMRI analyses suggesting a similar neural mechanism of attentional reorienting in different spatial directions.

In addition to statistical analysis, we were also able to show that predictive models trained on BOLD data related to attentional reorienting along one meridian generalized well to the other. In other words, the effect of direction was not only statistically insignificant but also had no impact on the generalizability of statistical models—so that

the cueing condition in one run could be successfully predicted by the model from the respective other run. This novel analysis approach, which does not rely on classical inferential statistics based on *p*-values, strongly suggests that the higher-order neural mechanisms underlying attentional reorienting are insensitive to different spatial directions.

Along the same lines, we also demonstrate that the network dynamics of a DCM between runs were so similar that they could be used to reproduce the BOLD activity patterns induced by attentional reorienting in the respective other spatial direction.

Our results replicate the findings of Macaluso and Patria (2007), who also did not find any significant differences between vertical and horizontal reorienting in a similar experimental set-up using classical inferential statistics. However, our study extends these findings in multiple ways since we considerably increased statistical power by including more than twice the number of participants in our study and employed the Bayesian and predictive approaches described above.

Still, other studies contrasting vertical and horizontal stimulus layouts have shown direction-sensitive effects for behavioral and neuro-imaging data. For example, differential activity in superior parietal and frontal areas was found in fMRI studies using an attentional cueing paradigm (Mao et al., 2007), or vertical and horizontal saccades and anti-saccades (Lemos et al., 2016, 2017).

One reason for these discrepancies might be that horizontal and vertical asymmetries critically depend on the basic perceptual properties of the visual system. For example, it has been argued that horizontal and vertical asymmetries (Rizzolatti, Riggio, Dascola, & Umiltá, 1987) are particularly evident at high visual eccentricities (Abrams, Nizam, & Carrasco, 2012; Carrasco & Chang, 1995), where the different physiological properties of different parts of the retina become perceptually and behaviorally relevant (Carrasco, Talgar, & Cameron, 2001; Jóhannesson, Tagu, & Kristjánsson, 2018). In our current study, the stimuli were presented at relatively small eccentricities so that the stimulus configurations may have minimized the impact of early retinal asymmetries. At the same time, stimuli were located distant enough to allow for a specific attentional modulation in cortical visual areas, as indicated by selective functional modulations in response to valid target stimuli. Our experimental design controlled

TABLE 4 BMA parameter inference

	Left hemisphere				Right hemisphere				Inter-hemispheric
	TPJ to IPS	TPJ to FEF	IPS to TPJ	FEF to TPJ	TPJ to IPS	TPJ to FEF	IPS to TPJ	FEF to TPJ	IPS-R to IPS-L
M ± SD	0.11 ± 0.96	0.12 ± 0.49	0.00 ± 0.43	0.13 ± 0.47	−0.14 ± 0.94	0.04 ± 0.45	0.10 ± 0.61	−0.30 ± 0.84	−0.11 ± 0.98
BF_{10}	0.24	0.44	0.21	0.48	0.27	0.23	0.28	0.90	0.24

Note: Paired BF t-tests were employed to compare the differences in connection strength between invalid horizontal and invalid vertical trials based on the parameters resulting from the BMA. Mean (M) and standard deviations (SD) show the group paired statistics (i.e., horizontal–vertical parameters for each subject combination) and the BF_{10} indicating evidence for a difference between the two runs. Connections are ordered by left-, right-, and inter-hemispheric connections.

for early bottom-up influences and hence allowed determining cortical effects related to top-down control.

However, despite carefully controlling for bottom-up influences and using an attentional cueing task, Mao et al. (2007) reported a horizontal-vertical asymmetry in brain activity and behavior. A critical difference between this and our study concerns the informational value of the cues. In Mao et al.'s study, the cues were always valid. Hence, attentional reorienting could not be investigated. The cues in the present study were probabilistic (i.e., not always valid). This aspect is relevant for the level of uncertainty involved in attentional control since a higher level of uncertainty induces a preparedness for reallocation of visual attention. Eckstein, Shimozaki, and Abbey (2002) showed that perceptual properties of the target stimulus and its attentional enhancement do not modulate reorientation costs. Instead, reorientation costs were rather driven by expectations. This view is in line with other studies manipulating the percentage of cue validity in similar location-cueing paradigms and reporting effects on response times and brain activity in dorsal and ventral attentional networks. For instance, increased uncertainty during invalid trials increases activity in the ventral attention network (Vossel et al., 2012; Vossel, Mathys, Stephan, & Friston, 2015) and decreases activity in the dorsal network (Weissman & Prado, 2012).

Similarly, higher activity in the ventral network correlates with worse behavioral performance in valid trials (Wen, Yao, Liu, & Ding, 2012). It has been suggested that the ventral network, and particularly the right TPJ, seems to be more generally involved in tracking and updating of expectations. Moreover, there are stroke patients with lesions to the right TPJ who display impaired rule changing and belief updating behavior in nonspatial tasks (Danckert, Stottinger, Quehl, & Anderson, 2012; Stöttinger et al., 2014; for a review on different TPJ involvements see Geng & Vossel, 2013). Hence, the processes critically related to attentional reorienting in the current study might not necessarily be location-specific but might represent higher-order functions such as the processing of expectancy violations.

While the previous studies focused on the right TPJ, we observed that invalid cueing heightens TPJ activation in both hemispheres. Similar bilateral involvement of the TPJ has been described previously (Beume et al., 2017; Macaluso & Patria, 2007; Silvetti et al., 2016). However, the exact functional role of left- and right-hemispheric areas in the ventral network might differ (Dugué, Merriam, Heeger, & Carrasco, 2018).

The spatial independence of attention networks observed in the present study seems to contradict clinical data: Patients with ventral parietal lesions to one hemisphere are not able to reorient attention to an invalidly or neutrally cued target in the visual field contralateral to the lesion (Posner, Walker, Friedrich, & Rafal, 1984). Since the ventral network is generally assumed to respond to invalid trials irrespective of the target hemifield, such behavior may reflect functional impairment of the dorsal system or dorsal-ventral interactions (Corbetta, Kincade, Lewis, Snyder, & Sapir, 2005). TMS studies provide strong evidence for spatially selective effects in the dorsal

network. For example, a concurrent TMS-fMRI study, where participants attended to stimuli in the left or right visual field, showed that TMS over posterior parietal cortices could modulate activations in the contralateral extrastriate cortex (Blankenburg et al., 2010). Similarly, TMS over left or right FEF led to top-down modulation of ipsilateral extrastriate areas (Duecker, Formisano, & Sack, 2013; Silvanto, Lavie, & Walsh, 2006). Still, these effects may not be purely symmetric, as right IPS and FEF have been shown to modulate not only the contralateral, but also the ipsilateral visual areas in some studies (Sheremata & Silver, 2015; Silvanto et al., 2006). Please note that we did not explicitly test for hemispheric asymmetries following left or right target displays in the present study. We used bilateral stimulus layouts, which have been shown to yield higher activation in superior parietal areas due to attention competition between the stimuli (Molenberghs, Gillebert, Peeters, & Vandenberghe, 2008). While we can show in this paradigm with a contrast of leftward versus rightward validly cued attention that the stimulus display evoked direction-specific activation in extrastriate areas, there were no signs of asymmetry in superior-parietal areas. Our DCM analysis, however, provides subtle evidence for a more dominant role of right IPS, by favoring a modulation from right to left IPS, over modulations from left to right IPS.

Unilateral lesions to the ventral system may, therefore, lead to dysfunction and imbalance in the reallocation of attention in the dorsal system, resulting in attentional deficits in the horizontal spatial dimension in patients with neglect (Corbetta & Shulman, 2011; Macaluso & Patria, 2007). The allocation and reorientation of attention along the vertical meridian, on the other hand, may be more robust to unilateral lesions, as a central stimulus display would be represented in both hemispheres. Following this line of thought, bilateral lesions should be necessary to cause altitudinal neglect, and this has indeed been observed in a few patients with bilateral lesions to temporal areas (Shelton et al., 1990) and parietal areas (Rapcsak, Cimino, & Heilman, 1988).

Further experiments will be necessary to investigate whether the dorsal and ventral attention network interact in the hypothesized way. Despite extensive work using fMRI, for example on the direction coding in IPS (Molenberghs et al., 2008; Vandenberghe et al., 2005), as well as attention-modulated receptive fields in the dorsal attention network (Sheremata & Silver, 2015), to date it remains to be determined whether directional coding can also be found in ventral parietal areas.

In conclusion, we observed that reorienting visuospatial attention along the horizontal and vertical meridians relies on very similar neural processes in frontoparietal areas of the dorsal and ventral attention network. The absence of direction-specific effects in the ventral attention network, together with the bilateral involvement of the TPJ, corroborates the notion that this network is involved in higher-order cognitive processes such as violations of prior expectations, rather than being dependent on stimulus properties, such as its spatial location (Geng & Vossel, 2013).These findings also have important implications for our understanding of the neurobiology underlying impairments of spatial processing after brain damage. In particular,

they suggest that deficits in orienting and reorienting attention along the horizontal meridian as commonly observed in stroke patients with spatial neglect are caused by disrupted interactions between higher-level attention networks and sensory areas, rather than by circumscribed damage of directionally tuned brain regions.

CONFLICT OF INTERESTS
The authors declare no competing financial interests.

DATA AVAILABILITY STATEMENT
The data that support the findings of this study are available on request from the corresponding author. The data are not publicly available due to privacy or ethical restrictions.

ORCID
Simon R. Steinkamp https://orcid.org/0000-0002-6437-0700

REFERENCES
Abraham, A., Pedregosa, F., Eickenberg, M., Gervais, P., Mueller, A., Kossaifi, J., … Varoquaux, G. (2014). Machine learning for neuroimaging with scikit-learn. *Frontiers in Neuroinformatics*, *8*, 1–10. https://doi.org/10.3389/fninf.2014.00014

Abrams, J., Nizam, A., & Carrasco, M. (2012). Isoeccentric locations are not equivalent: The extent of the vertical meridian asymmetry. *Vision Research*, *52*(1), 70–78. https://doi.org/10.1016/j.visres.2011.10.016

Beume, L.-A., Martin, M., Kaller, C. P., Klöppel, S., Schmidt, C. S. M., Urbach, H., … Umarova, R. M. (2017). Visual neglect after left-hemispheric lesions: A voxel-based lesion–symptom mapping study in 121 acute stroke patients. *Experimental Brain Research*, *235*(1), 83–95. https://doi.org/10.1007/s00221-016-4771-9

Blankenburg, F., Ruff, C. C., Bestmann, S., Bjoertomt, O., Josephs, O., Deichmann, R., & Driver, J. (2010). Studying the role of human parietal cortex in visuospatial attention with concurrent TMS-fMRI. *Cerebral Cortex*, *20*(11), 2702–2711. https://doi.org/10.1093/cercor/bhq015

Bressler, S. L., Tang, W., Sylvester, C. M., Shulman, G. L., & Corbetta, M. (2008). Top-down control of human visual cortex by frontal and parietal cortex in anticipatory visual spatial attention. *Journal of Neuroscience*, *28*(40), 10056–10061. https://doi.org/10.1523/JNEUROSCI.1776-08.2008

Cappelletti, M., Freeman, E. D., & Cipolotti, L. (2007). The middle house or the middle floor: Bisecting horizontal and vertical mental number lines in neglect. *Neuropsychologia*, *45*(13), 2989–3000. https://doi.org/10.1016/j.neuropsychologia.2007.05.014

Carrasco, M., & Chang, I. (1995). The interaction of objective and subjective organizations in a localization search task. *Perception & Psychophysics*, *57*(8), 1134–1150.

Carrasco, M., Talgar, C. P., & Cameron, E. L. (2001). Characterizing visual performance fields: Effects of transient covert attention, spatial frequency, eccentricity, task and set size. *Spatial Vision*, *15*(1), 61–75.

Cazzoli, D., Nyffeler, T., Hess, C. W., & Müri, R. M. (2011). Vertical bias in neglect: A question of time? *Neuropsychologia*, *49*(9), 2369–2374. https://doi.org/10.1016/j.neuropsychologia.2011.04.010

Corbetta, M., Kincade, M. J., Lewis, C., Snyder, A. Z., & Sapir, A. (2005). Neural basis and recovery of spatial attention deficits in spatial neglect. *Nature Neuroscience*, *8*(11), 1603–1610. https://doi.org/10.1038/nn1574

Corbetta, M., Patel, G., & Shulman, G. L. (2008). The reorienting system of the human brain: From environment to theory of mind. *Neuron*, *58*(3), 306–324. https://doi.org/10.1016/j.neuron.2008.04.017

Corbetta, M., & Shulman, G. L. (2011). Spatial neglect and attention networks. *Annual Review of Neuroscience*, *34*(1), 569–599. https://doi.org/10.1146/annurev-neuro-061010-113731

Danckert, J., Stottinger, E., Quehl, N., & Anderson, B. (2012). Right hemisphere brain damage impairs strategy updating. *Cerebral Cortex*, *22*(12), 2745–2760. https://doi.org/10.1093/cercor/bhr351

Daunizeau, J., Adam, V., & Rigoux, L. (2014). VBA: A probabilistic treatment of nonlinear models for neurobiological and Behavioural data. *PLoS Computational Biology*, *10*(1), e1003441. https://doi.org/10.1371/journal.pcbi.1003441

Duecker, F., Formisano, E., & Sack, A. T. (2013). Hemispheric differences in the voluntary control of spatial attention: Direct evidence for a right-hemispheric dominance within frontal cortex. *Journal of Cognitive Neuroscience*, *25*(8), 1332–1342. https://doi.org/10.1162/jocn_a_00402

Dugué, L., Merriam, E. P., Heeger, D. J., & Carrasco, M. (2018). Specific visual subregions of TPJ mediate reorienting of spatial attention. *Cerebral Cortex*, *28*(7), 2375–2390. https://doi.org/10.1093/cercor/bhx140

Eckstein, M. P., Shimozaki, S. S., & Abbey, C. K. (2002). The footprints of visual attention in the Posner cueing paradigm revealed by classification images. *Journal of Vision*, *2*(1), 3. https://doi.org/10.1167/2.1.3

Esteban, O., Markiewicz, C. J., Blair, R. W., Moodie, C. A., Isik, A. I., Erramuzpe, A., ... Gorgolewski, K. J. (2019). fMRIPrep: A robust preprocessing pipeline for functional MRI. *Nature Methods*, *16*(1), 111–116. https://doi.org/10.1038/s41592-018-0235-4

Fink, G. R., Marshall, J. C., Weiss, P. H., & Zilles, K. (2001). The neural basis of vertical and horizontal line bisection judgments: An fMRI study of Normal volunteers. *NeuroImage*, *14*(1), S59–S67. https://doi.org/10.1006/nimg.2001.0819

Fonov, V., Evans, A., McKinstry, R., Almli, C., & Collins, D. (2009). Unbiased nonlinear average age-appropriate brain templates from birth to adulthood. *NeuroImage*, *47*, S102. https://doi.org/10.1016/S1053-8119(09)70884-5

Friston, K. J. (Ed.). (2007). *Statistical parametric mapping: The analysis of funtional brain images* (1st ed.). Amsterdam, Boston: Elsevier/Academic Press.

Friston, K. J., Harrison, L., & Penny, W. (2003). Dynamic causal modelling. *NeuroImage*, *19*(4), 1273–1302. https://doi.org/10.1016/S1053-8119(03)00202-7

Geng, J. J., & Vossel, S. (2013). Re-evaluating the role of TPJ in attentional control: Contextual updating? *Neuroscience & Biobehavioral Reviews*, *37*(10), 2608–2620. https://doi.org/10.1016/j.neubiorev.2013.08.010

Gorgolewski, K., Burns, C. D., Madison, C., Clark D., Halchenko, Y. O., Waskom, M. L., & Ghosh, S. S. (2011). Nipype: A Flexible, Lightweight and Extensible Neuroimaging Data Processing Framework in Python. *Frontiers in Neuroinformatics*, *5*, 1–15. http://dx.doi.org/10.3389/fninf.2011.00013.

Halligan, P. W., Fink, G. R., Marshall, J. C., & Vallar, G. (2003). Spatial cognition: Evidence from visual neglect. *Trends in Cognitive Sciences*, *7*(3), 125–133.

Hedge, C., Powell, G., & Sumner, P. (2017). The reliability paradox: Why robust cognitive tasks do not produce reliable individual differences. *Behavior Research Methods.*, *50*, 1166–1186. https://doi.org/10.3758/s13428-017-0935-1

Hung, J., Driver, J., & Walsh, V. (2011). Visual selection and the human frontal eye fields: Effects of frontal transcranial magnetic stimulation on partial report analyzed by Bundesen's theory of visual attention. *Journal of Neuroscience*, *31*(44), 15904–15913. https://doi.org/10.1523/JNEUROSCI.2626-11.2011

Jarosz, A. F., & Wiley, J. (2014). What are the odds? A practical guide to computing and reporting Bayes factors. *The Journal of Problem Solving*, *7*(1), 2–9. https://doi.org/10.7771/1932-6246.1167

Jóhannesson, Ó. I., Tagu, J., & Kristjánsson, Á. (2018). Asymmetries of the visual system and their influence on visual performance and oculomotor dynamics. *European Journal of Neuroscience*, *48*(11), 3426–3445. https://doi.org/10.1111/ejn.14225

Karnath, H.-O., Rennig, J., Johannsen, L., & Rorden, C. (2011). The anatomy underlying acute versus chronic spatial neglect: A longitudinal study. *Brain*, *134*(3), 903–912. https://doi.org/10.1093/brain/awq355

Lemos, J., Pereira, D., Almendra, L., Rebelo, D., Patrício, M., Castelhano, J., ... Castelo-Branco, M. (2016). Distinct functional properties of the vertical and horizontal saccadic network in health and Parkinson's disease: An eye-tracking and fMRI study. *Brain Research*, *1648*, 469–484. https://doi.org/10.1016/j.brainres.2016.07.037

Lemos, J., Pereira, D., Almendra, L., Rebelo, D., Patrício, M., Castelhano, J., ... Castelo-Branco, M. (2017). Cortical control of vertical and horizontal saccades in progressive supranuclear palsy: An exploratory fMRI study. *Journal of the Neurological Sciences*, *373*, 157–166. https://doi.org/10.1016/j.jns.2016.12.049

Macaluso, E., & Patria, F. (2007). Spatial re-orienting of visual attention along the horizontal or the vertical axis. *Experimental Brain Research*, *180*(1), 23–34. https://doi.org/10.1007/s00221-006-0841-8

Mao, L., Zhou, B., Zhou, W., & Han, S. (2007). Neural correlates of covert orienting of visual spatial attention along vertical and horizontal dimensions. *Brain Research*, *1136*, 142–153. https://doi.org/10.1016/j.brainres.2006.12.031

Molenberghs, P., Gillebert, C. R., Peeters, R., & Vandenberghe, R. (2008). Convergence between lesion-symptom mapping and functional magnetic resonance imaging of spatially selective attention in the intact brain. *Journal of Neuroscience*, *28*(13), 3359–3373. https://doi.org/10.1523/JNEUROSCI.5247-07.2008

Morey, R. D., & Rouder, J. N. (2018). *BayesFactor: Computation of Bayes Factors for Common Designs*. Retrieved from https://CRAN.R-project.org/package=BayesFactor

Müri, R. M., Cazzoli, D., Nyffeler, T., & Pflugshaupt, T. (2009). Visual exploration pattern in hemineglect. *Psychological Research*, *73*(2), 147–157. https://doi.org/10.1007/s00426-008-0204-0

Nicholls, M. E. R., Mattingley, J. B., Berberovic, N., Smith, A., & Bradshaw, J. L. (2004). An investigation of the relationship between free-viewing perceptual asymmetries for vertical and horizontal stimuli. *Cognitive Brain Research*, *19*(3), 289–301. https://doi.org/10.1016/j.cogbrainres.2003.12.008

Nichols, T. E., & Holmes, A. P. (2002). Nonparametric permutation tests for functional neuroimaging: A primer with examples. *Human Brain Mapping*, *15*(1), 1–25.

Ojala, M., & Garriga, G. C. (2010). Permutation tests for studying classifier performance. *Journal of Machine Learning Research*, *11*, 1833–1863.

Oldfield, R.C. (1971). The assessment and analysis of handedness: The Edinburgh inventory. *Neuropsychologia*, *9*(1), 97–113. http://dx.doi.org/10.1016/0028-3932(71)90067-4.

Pedregosa, F., Varoquaux, G., Gramfort, A., Michel, V., Thirion, B., Grisel, O., ... others. (2011). Scikit-learn: Machine learning in python. *The Journal of Machine Learning Research*, *12*, 2825–2830.

Peirce, J. W. (2007). PsychoPy—Psychophysics software in python. *Journal of Neuroscience Methods*, *162*(1–2), 8–13. https://doi.org/10.1016/j.jneumeth.2006.11.017

Peirce, J. W. (2008). Generating stimuli for neuroscience using PsychoPy. *Frontiers in Neuroinformatics*, *2*, 1–8. https://doi.org/10.3389/neuro.11.010.2008

Peirce, J. W., Gray, J. R., Simpson, S., MacAskill, M., Höchenberger, R., Sogo, H., ... Lindeløv, J. K. (2019). PsychoPy2: Experiments in behavior made easy. *Behavior Research Methods*, *51*(1), 195–203. https://doi.org/10.3758/s13428-018-01193-y

Pitzalis, S., Spinelli, D., & Zoccolotti, P. (1997). Vertical neglect: Behavioral and electrophysiological data. *Cortex: A Journal Devoted to the Study of the Nervous System and Behavior*, 33(4), 679–688.

Posner, M. I. (1980). Orienting of attention. *The Quarterly Journal of Experimental Psychology*, 32(1), 3–25.

Posner, M. I., Walker, J. A., Friedrich, F. J., & Rafal, R. D. (1984). Effects of parietal injury on covert orienting of attention. *The Journal of Neuroscience: The Official Journal of the Society for Neuroscience*, 4(7), 1863–1874.

Power, J. D., Mitra, A., Laumann, T. O., Snyder, A. Z., Schlaggar, B. L., & Petersen, S. E. (2014). Methods to detect, characterize, and remove motion artifact in resting state fMRI. *NeuroImage*, 84, 320–341. https://doi.org/10.1016/j.neuroimage.2013.08.048

R Core Team. (2018). *R: A Language and Environment for Statistical Computing*. Retrieved from https://www.R-project.org/

Rapcsak, S. Z., Cimino, C. R., & Heilman, K. M. (1988). Altitudinal neglect. *Neurology*, 38(2), 277–277, 281. https://doi.org/10.1212/WNL.38.2.277

Rizzolatti, G., Riggio, L., Dascola, I., & Umiltá, C. (1987). Reorienting attention across the horizontal and vertical meridians: Evidence in favor of a premotor theory of attention. *Neuropsychologia*, 25(1A), 31–40.

Rouder, J. N., Morey, R. D., Speckman, P. L., & Province, J. M. (2012). Default Bayes factors for ANOVA designs. *Journal of Mathematical Psychology*, 56(5), 356–374. https://doi.org/10.1016/j.jmp.2012.08.001

Ruff, C. C., Bestmann, S., Blankenburg, F., Bjoertomt, O., Josephs, O., Weiskopf, N., ... Driver, J. (2008). Distinct causal influences of parietal versus frontal areas on human visual cortex: Evidence from concurrent TMS-fMRI. *Cerebral Cortex*, 18(4), 817–827. https://doi.org/10.1093/cercor/bhm128

Shelton, P. A., Bowers, D., & Heilman, K. M. (1990). PERIPERSONAL AND VERTICAL NEGLECT. *Brain*, 113(1), 191–205. https://doi.org/10.1093/brain/113.1.191

Sheremata, S. L., & Silver, M. A. (2015). Hemisphere-dependent attentional modulation of human parietal visual field representations. *Journal of Neuroscience*, 35(2), 508–517. https://doi.org/10.1523/JNEUROSCI.2378-14.2015

Silvanto, J., Lavie, N., & Walsh, V. (2006). Stimulation of the human frontal eye fields modulates sensitivity of extrastriate visual cortex. *Journal of Neurophysiology*, 96(2), 941–945. https://doi.org/10.1152/jn.00015.2006

Silvetti, M., Lasaponara, S., Lecce, F., Dragone, A., Macaluso, E., & Doricchi, F. (2016). The response of the left ventral attentional system to invalid targets and its implication for the spatial neglect syndrome: A multivariate fMRI investigation. *Cerebral Cortex*, 26(12), 4551–4562. https://doi.org/10.1093/cercor/bhv208

Simons, D. J. (2000). Attentional capture and inattentional blindness. *Trends in Cognitive Sciences*, 4(4), 147–155.

Stöttinger, E., Filipowicz, A., Marandi, E., Quehl, N., Danckert, J., & Anderson, B. (2014). Statistical and perceptual updating: Correlated impairments in right brain injury. *Experimental Brain Research*, 232(6), 1971–1987. https://doi.org/10.1007/s00221-014-3887-z

Vandenberghe, R., Geeraerts, S., Molenberghs, P., Lafosse, C., Vandenbulcke, M., Peeters, K., ... Orban, G. A. (2005). Attentional responses to unattended stimuli in human parietal cortex. *Brain*, 128(12), 2843–2857. https://doi.org/10.1093/brain/awh522

Vossel, S., Geng, J. J., & Fink, G. R. (2014). Dorsal and ventral attention systems: Distinct neural circuits but collaborative roles. *The Neuroscientist*, 20(2), 150–159. https://doi.org/10.1177/1073858413494269

Vossel, S., Mathys, C., Stephan, K. E., & Friston, K. J. (2015). Cortical coupling reflects Bayesian belief updating in the deployment of spatial attention. *The Journal of Neuroscience*, 35(33), 11532–11542. https://doi.org/10.1523/JNEUROSCI.1382-15.2015

Vossel, S., Weidner, R., Driver, J., Friston, K. J., & Fink, G. R. (2012). Deconstructing the architecture of dorsal and ventral attention systems with dynamic causal modeling. *Journal of Neuroscience*, 32(31), 10637–10648. https://doi.org/10.1523/JNEUROSCI.0414-12.2012

Wang, S., Peterson, D. J., Gatenby, J. C., Li, W., Grabowski, T. J., & Madhyastha, T. M. (2017). Evaluation of field map and nonlinear registration methods for correction of susceptibility artifacts in diffusion MRI. *Frontiers in Neuroinformatics*, 11, 1–9. https://doi.org/10.3389/fninf.2017.00017

Weissman, D. H., & Prado, J. (2012). Heightened activity in a key region of the ventral attention network is linked to reduced activity in a key region of the dorsal attention network during unexpected shifts of covert visual spatial attention. *NeuroImage*, 61(4), 798–804. https://doi.org/10.1016/j.neuroimage.2012.03.032

Wen, X., Yao, L., Liu, Y., & Ding, M. (2012). Causal interactions in attention networks predict behavioral performance. *Journal of Neuroscience*, 32(4), 1284–1292. https://doi.org/10.1523/JNEUROSCI.2817-11.2012

SUPPORTING INFORMATION

Additional supporting information may be found online in the Supporting Information section at the end of this article.

MRI – Preprocessing

The following description of the preprocessing was automatically generated (see http://fmriprep.readthedocs.io/en/1.1.1/workflows.html) and minimally adapted.

The preprocessing of functional and anatomical data was performed using FMRIPREP version 1.1.1 (Esteban et al., 2018, 2019, RRID:SCR_016216), a Nipype (RRID:SCR_002502, Gorgolewski et al., 2011, 2017) based tool, run as a docker-image. Each T1-weighted volume (T1w) was corrected for intensity non-uniformity using N4BiasFieldCorrection v2.1.0 (Tustison et al. 2010) and skull-stripped using antsBrainExtraction.sh v2.1.0 (using the OASIS template). Spatial normalization to the ICBM 152 Nonlinear Asymmetrical template version 2009c (Fonov et al. 2009, RRID:SCR_008796) was performed through nonlinear registration with the antsRegistration tool of ANTs v2.1.0 (Avants et al. 2008, RRID:SCR_004757), using brain-extracted versions of both T1w volume and template. Brain tissue segmentation of cerebrospinal fluid (CSF), white-matter (WM), and gray-matter (GM) was performed on the brain-extracted T1w using fast (Zhang, Brady, and Smith 2001, FSL v5.0.9, RRID:SCR_002823).

Functional data were slice-time corrected using 3dTshift from AFNI v16.2.07 (Cox 1996, RRID:SCR_005927) and motion-corrected using mcflirt (FSL v5.0.9, Jenkinson et al. 2002). "Fieldmap-less" distortion correction was performed by co-registering the functional image to the same-subject T1w image with intensity inverted (Wang et al. 2017), constrained with an average fieldmap template (Treiber et al. 2016), implemented with antsRegistration (ANTs). This procedure was followed by co-registration to the corresponding T1w using boundary-based registration (Greve and Fischl 2009) with 9 degrees of freedom, using flirt (FSL). Motion correcting transformations, field distortion correcting warp, BOLD-to-T1w transformation, and T1w-to-template (MNI) warp were concatenated and applied in a single step using antsApplyTransforms (ANTs v2.1.0) using Lanczos interpolation.

Frame-wise displacement (Power et al. 2014) was calculated for each functional run using the implementation of Nipype.

Many internal operations of FMRIPREP use Nilearn (Abraham et al. 2014, RRID:SCR_001362), principally within the BOLD-processing workflow. For more details of the pipeline, see http://fmriprep.readthedocs.io/en/1.1.1/workflows.html.

Eye Tracking Analysis

When performing the online recording of eye movements during the experiment, we suffered from several technical issues and difficulties, so that only a subset of the data could be analyzed.

Methods

We used an EyeLink® 1000 (SR Research) system to record the eye movements of our participants while they performed the spatial cueing task in the MR-scanner. The infrared camera was placed behind the participants, and their eye-movements were monitored via an infrared capable mirror and recorded at a sampling rate of 500 Hz. Because of the difficult recording environment (for example, large shadows close to the participant's eyes due to the head-coil and the use of lenses to correct for the participant's vison), we could not follow a uniform protocol for data collection and calibration.

The collected raw eye-movement data was converted from the EyeLink® data format (.edf) to asci (.asc) files. During the conversion, raw eye-movements were transformed to gaze-coordinates in pixels. The python package cili (Acland and Wallis 2016) was used to extract and load the data for further processing in Python 3.7, utilizing the scipy-stack (Jones et al. 2001).

1

First, we epoched the eye-tracking data into single trials (250 ms before cue-onset until 400 ms after target onset). Each trial was further subdivided into three phases. The "pre-trial" phase, which lasted from 250 ms before cue onset until cue onset, served as baseline fixation period. The second ("cue") phase comprised the time from cue onset until target onset (600 ms to 800 ms duration). The "target" phase was defined from target onset until 400 ms after.

The eye-data were cleaned by removing not-recorded values (i.e., NaN) and gaze coordinates exceeding the screen coordinates (0 > x > 1279, 0 > y > 799). If more than 10% of data for any of the three phases (assuming 600 ms duration for the "Cue" period) were removed, the whole trial was discarded.

We assumed that the participants were focusing on the screen's center in the "Pre-trial" phase. Thus, we used data from this period to re-align the gaze coordinate. The latter was achieved by subtracting the difference between the screen's center coordinates (x = 640, y = 400) and the robust mean of the pre-stimulus phase (mean of the data points between the 10th and 90th percentile).

Before statistical analyses, we discarded all datasets that had less than 100 valid or less than ten invalid trials. Furthermore, the data of a participant was only included if data of both sessions were present.

The final sample included eye-movement data of 17 out of the 27 participants.

Table 1: Number of trials retained in the eye-tracking analyses.

Run	TrialType	Number of trials (included)	
		M	SD
Horizontal	invalid	37.24	2.68
	valid	150.35	8.94
Vertical	invalid	35.29	2.97
	valid	144.35	12.17

Analyzing Saccades

We used two different estimates to analyze saccades. As a first estimate, we defined that the cue- or the target-phase contained a saccade towards the target position if eye movements along the x-axis for horizontal runs (y-axis for vertical runs) exceeded 50% of the distance between the central fixation cross and the middle of the left (lower) or right (upper) target box ("Eye-50"). Additionally, we also used the automatic saccade classification by the EyeLink® software ("EyeLink"). Saccades were determined using three different thresholds for motion (0.1 °), velocity (30 °/s), and acceleration (8000 °/s2), based on the cognitive preset described in the EyeLink® manual (http://sr-research.jp/support/EyeLink 1000 User Manual 1.5.0.pdf). Here we used the "SSACC" (start-saccade) and "ESACC" (end-saccade) messages in the EyeLink® as time-intervals. If any data point of the cue- or target-phase was contained in any of the saccade intervals, we assumed that a saccade was made in the corresponding phase.

We then calculated the proportion of trials containing a saccade for each participant, cueing-condition, and run. The proportion of trials containing saccades was then submitted to a 2 (cueing-condition) x 2 (run) Bayes Factor ANOVA (Morey and Rouder 2018) to test for possible differences between the factors of interest; participant was included as a random factor. We also calculated linear mixed effects models in R (R Core Team 2018) using lmertest (Kuznetsova, Brockhoff, and Christensen 2017) with participant as random intercept,

2

using the same 2 x 2 design. Both analyses were done separately for the cue- and target-phase.

Pearson's correlation coefficient between proportions of saccades between "EyeLink" and "Eye-50" in the cue-phase equaled 0.791 (p < 0.001), and 0.826 (p < 0.001) in the target-phase.

Results

The results (see Table 3) provided no evidence for a significantly different distribution of saccades between the two runs, nor between the different cueing-conditions, nor their interactions. While none of the coefficients of the linear mixed effects model was statistically significant, the BF_ANOVAs often did not provide solid evidence against an effect. Still we are confident that participant's eye-movements are not driving the effects (or the absence thereof) in the main analyses.

Table 2: Descriptive statistics (mean and standard deviation) for the proportion of trials containing a saccade.

Phase	Run	Condition	Eye-50 M ± SD	EyeLinkSaccade M ± SD
Cue	Horizontal	invalid	0.080 ± 0.197	0.310 ± 0.220
		valid	0.077 ± 0.216	0.296 ± 0.219
	Vertical	invalid	0.099 ± 0.206	0.322 ± 0.182
		valid	0.095 ± 0.212	0.308 ± 0.219
Stimulus	Horizontal	invalid	0.098 ± 0.231	0.162 ± 0.210
		valid	0.083 ± 0.228	0.101 ± 0.100
	Vertical	invalid	0.110 ± 0.238	0.163 ± 0.202
		valid	0.098 ± 0.228	0.121 ± 0.107

Table 3: Results of BF_ANOVAs and linear mixed effects models. The values in the first position are the BF_{01} in favor of the baseline model (based on the random intercept). The BF-ANOVA models all included the participant as random factor. P-values are the results for the different coefficients in the linear mixed effects model, where the p-values in the last column only describe the interaction of condition * run.

Phase	Definition	Condition	Run	Condition + Run	Condition + Run + Condition * Run
Cue	Eye-50	3.77 (p = 0.792)	3.25 (p = 0.135)	2.13	0.44 (p = 0.975)
	EyeLink	0.61 (p = 0.626)	3.41 (p = 0.642)	2.16	3.72 (p = 0.988)
Stimulus	Eye-50	2.34 (p = 0.342)	10.82 (p = 0.450)	4.81	1.66 (p = 0.909)
	EyeLink	7.14 (p = 0.059)	32.79 (p = 0.986)	2.32	4.54 (p = 0.663)
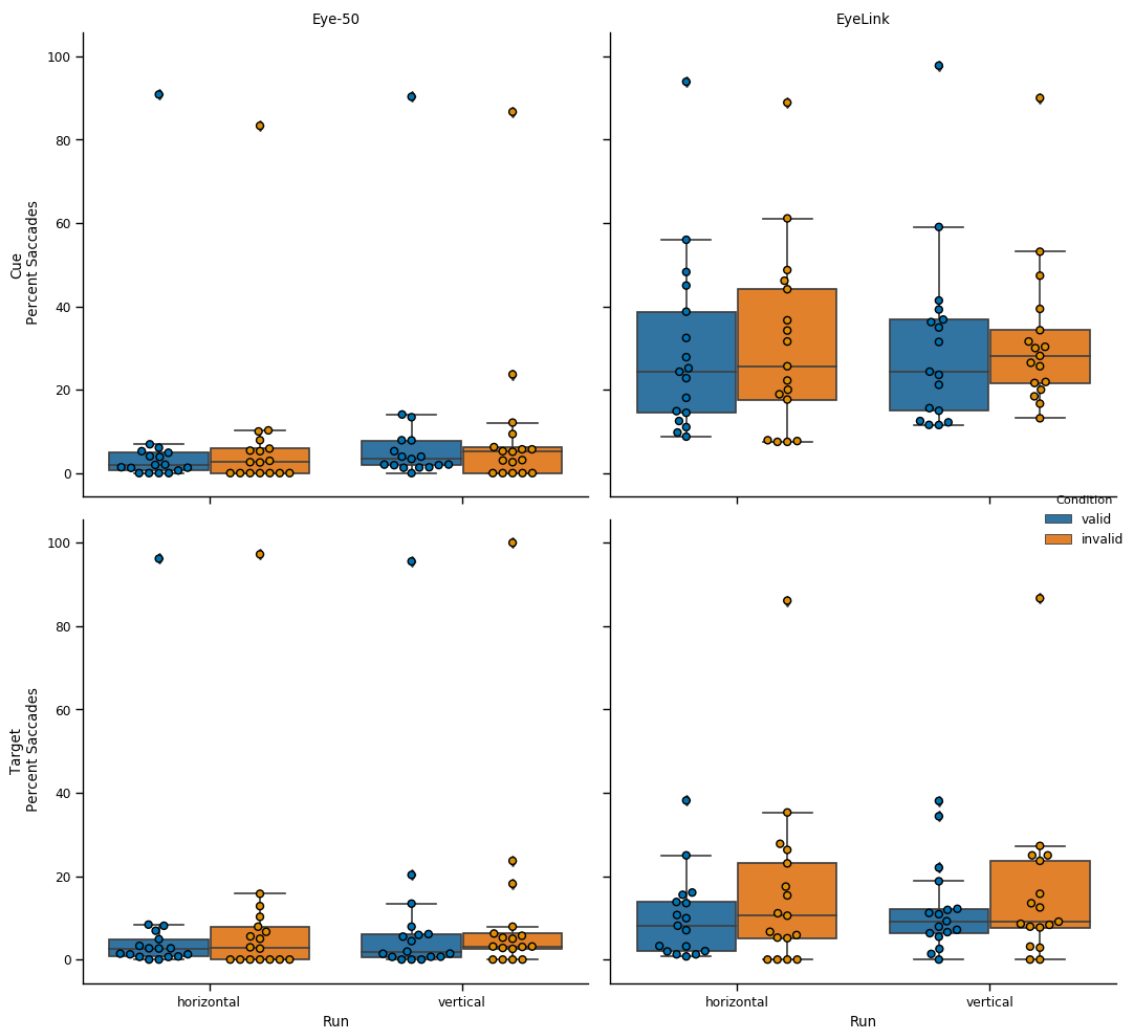
Figure 1: Visualization of the percentage of saccades during the experiment. Classical boxplots displaying the mean and the interquartile range (IQR) are used. Outlier were defined using the 1.5 * IQR criterion.
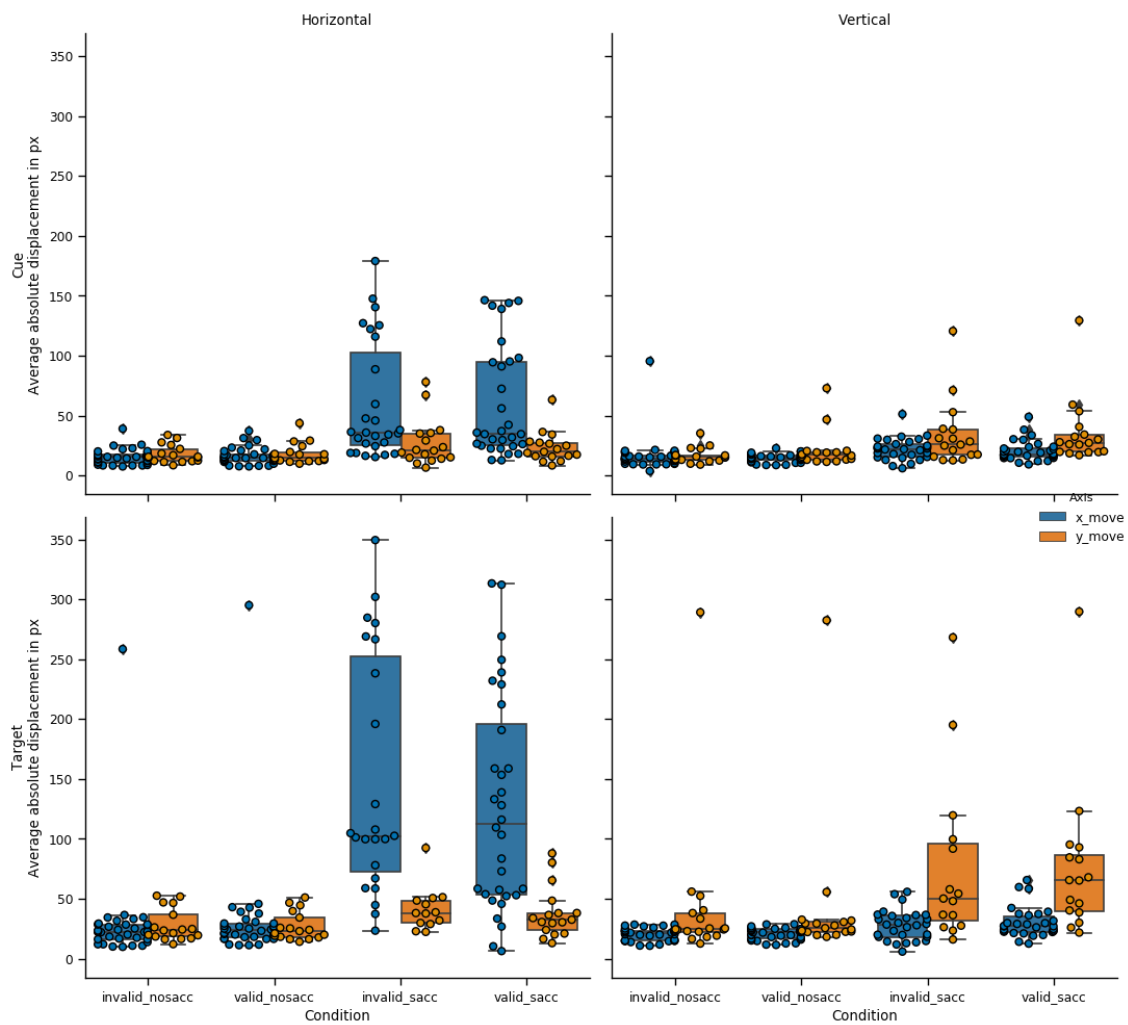
Figure 2: Visualization of the absolute deviations from the midpoint across the experiment. For each participant we calculated the average absolute eye-movement in pixels along the x − and y − axis. Data was split between valid and invalid trials and in each condition split between trials containing a saccade ("_sacc") or not containing a saccade ("_nosacc"). For this purpose of visualization, we used the "EyeLink" saccade classification.
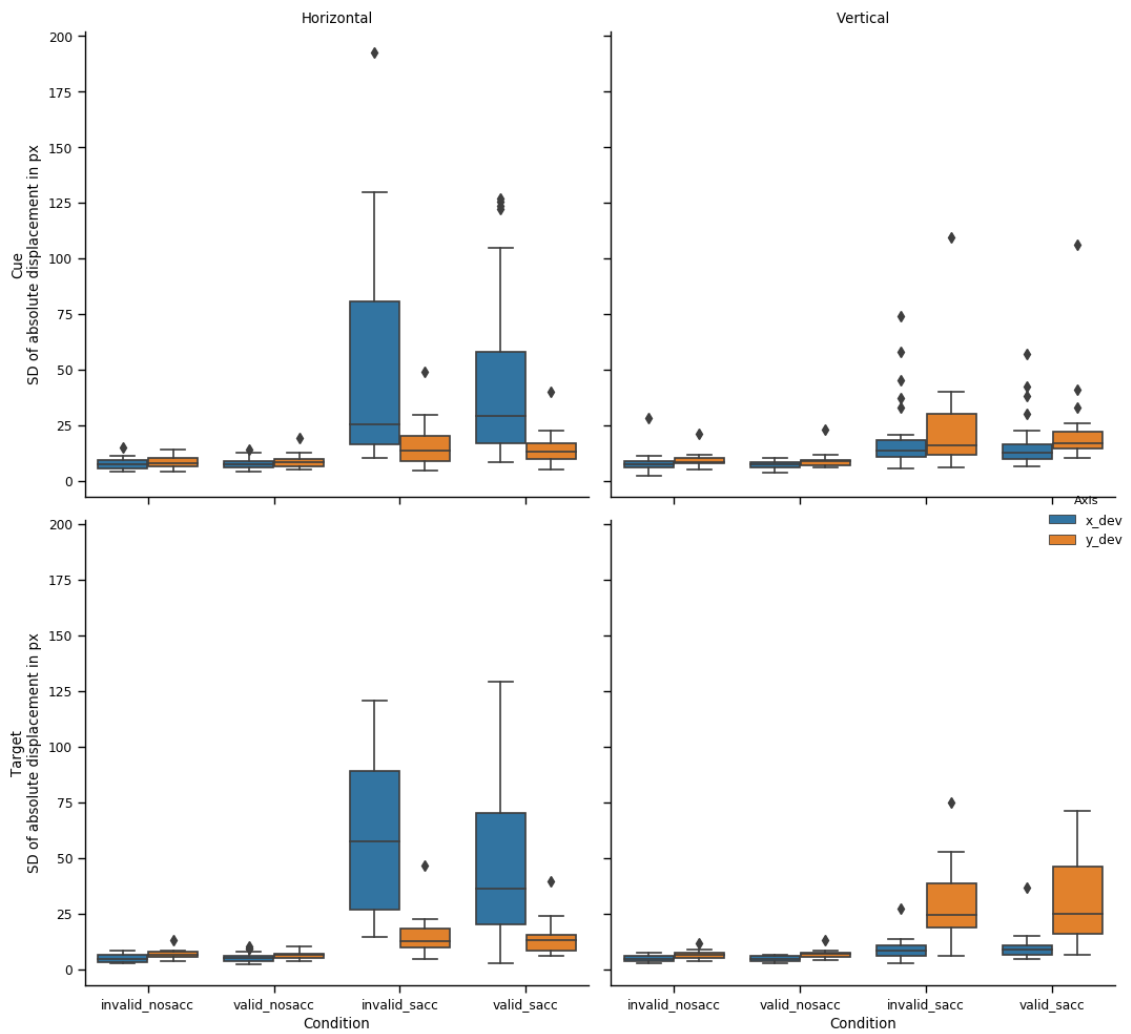
Figure 3: Visualization of the absolute deviations from the midpoint across the experiment. For each participant we calculated the standard deviation of absolute eye-movement in pixels along the x – and y – axis. Data was split between valid and invalid trials and in each condition split between trials containing a saccade ("_sacc") or not containing a saccade ("_nosacc"). For this purpose of visualization, we used the "EyeLink" saccade classification.

References

Abraham, Alexandre, Fabian Pedregosa, Michael Eickenberg, Philippe Gervais, Andreas Mueller, Jean Kossaifi, Alexandre Gramfort, Bertrand Thirion, and Gaël Varoquaux. 2014. "Machine Learning for Neuroimaging with Scikit-Learn." *Frontiers in Neuroinformatics* 8.

Acland, Ben and Tom Wallis. 2016. *Cili: Cili v0.5.4*.

Avants, B., C. Epstein, M. Grossman, and J. Gee. 2008. "Symmetric Diffeomorphic Image Registration with Cross-Correlation: Evaluating Automated Labeling of Elderly and Neurodegenerative Brain." *Medical Image Analysis* 12(1):26–41.

Cox, Robert W. 1996. "AFNI: Software for Analysis and Visualization of Functional Magnetic Resonance Neuroimages." *Computers and Biomedical Research* 29(3):162–73.

Esteban, Oscar, Ross Blair, Christopher J. Markiewicz, Shoshana L. Berleant, Craig Moodie, Feilong Ma, Ayse Ilkay Isik, Asier Erramuzpe, James D. Kent, Mathias Goncalves, Elizabeth DuPre, Kevin R. Sitek, Daniel E. P. Gomez, Daniel J. Lurie, Zhifang Ye, Russell A. Poldrack, and Krzysztof J. Gorgolewski. 2018. "Poldracklab/Fmriprep: 1.1.3."

Esteban, Oscar, Christopher J. Markiewicz, Ross W. Blair, Craig A. Moodie, A. Ilkay Isik, Asier Erramuzpe, James D. Kent, Mathias Goncalves, Elizabeth DuPre, Madeleine Snyder, Hiroyuki Oya, Satrajit S. Ghosh, Jessey Wright, Joke Durnez, Russell A. Poldrack, and Krzysztof J. Gorgolewski. 2019. "FMRIPrep: A Robust Preprocessing Pipeline for Functional MRI." *Nature Methods* 16(1):111–16.

Fonov, Vs, Ac Evans, Rc McKinstry, Cr Almli, and Dl Collins. 2009. "Unbiased Nonlinear Average Age-Appropriate Brain Templates from Birth to Adulthood." *NeuroImage* 47:S102.

Gorgolewski, Krzysztof J., Christopher D. Burns, Cindee Madison, Dav Clark, Yaroslav O. Halchenko, Michael L. Waskom, and Satrajit S. Ghosh. 2011. "Nipype: A Flexible, Lightweight and Extensible Neuroimaging Data Processing Framework in Python." *Frontiers in Neuroinformatics* 5.

Gorgolewski, Krzysztof J., Oscar Esteban, David Gage Ellis, Michael Philipp Notter, Erik Ziegler, Hans Johnson, Carlo Hamalainen, Benjamin Yvernault, Christopher Burns, Alexandre Manhães-Savio, Dorota Jarecka, Christopher J. Markiewicz, Taylor Salo, Daniel Clark, Michael Waskom, Jason Wong, Marc Modat, Blake E. Dewey, Michael G. Clark, Michael Dayan, Fred Loney, Cindee Madison, Alexandre Gramfort, Anisha Keshavan, Shoshana Berleant, Basile Pinsard, Mathias Goncalves, Dav Clark, Ben Cipollini, Gael Varoquaux, Demian Wassermann, Ariel Rokem, Yaroslav O. Halchenko, Jessica Forbes, Brendan Moloney, Ian B. Malone, Michael Hanke, David Mordom, Colin Buchanan, Wolfgang M. Pauli, Julia M. Huntenburg, Christian Horea, Yannick Schwartz, Rosalia Tungaraza, Shariq Iqbal, Jens Kleesiek, Sharad Sikka, Caroline Frohlich, James Kent, Martin Perez-Guevara, Aimi Watanabe, David Welch, Chad Cumba, Daniel Ginsburg, Arman Eshaghi, Erik Kastman, Salma Bougacha, Ross Blair, Benjamin Acland, Ashley Gillman, Alexander Schaefer, B. Nolan Nichols, Steven Giavasis, Drew Erickson, Carlos Correa, Ali Ghayoor, René Küttner, Christian Haselgrove, Dale Zhou, R. Cameron Craddock, Daniel Haehn, Leonie Lampe, Jarrod Millman, Jeff Lai, Mandy Renfro, Siqi Liu, Jörg Stadler, Tristan Glatard, Ari E. Kahn, Xiang-Zhen Kong, William Triplett, Anne Park, Conor McDermottroe, Michael Hallquist, Russell Poldrack, L. Nathan Perkins, Maxime Noel, Stephan Gerhard, John Salvatore, Fred Mertz, William Broderick, Souheil Inati, Oliver Hinds, Matthew Brett, Joke Durnez, Arielle Tambini, Simon Rothmei, Sami Kristian Andberg, Gavin Cooper, Ana Marina, Aaron Mattfeld, Sebastian Urchs, Paul Sharp, K. Matsubara, Daniel Geisler, Brian Cheung, Andrew Floren, Thomas Nickson, Nicolas Pannetier, Alejandro Weinstein, Mathieu Dubois, Jaime Arias, Claire Tarbert, Kai Schlamp, Kesshi Jordan, Franz Liem, Victor Saase, Robbert Harms, Ranjeet Khanuja, Kornelius Podranski, Guillaume Flandin, Dimitri Papadopoulos Orfanos, Isaac Schwabacher, Daniel McNamee, Marcel Falkiewicz, John Pellman, Janosch Linkersdörfer, Jan Varada, Fernando Pérez-García, Andrew Davison, Dmitry Shachnev, and Satrajit Ghosh. 2017. "Nipype: A Flexible, Lightweight And Extensible Neuroimaging Data Processing Framework In Python. 0.13.1."

Greve, Douglas N. and Bruce Fischl. 2009. "Accurate and Robust Brain Image Alignment Using Boundary-Based Registration." *NeuroImage* 48(1):63–72.

Jenkinson, Mark, Peter Bannister, Michael Brady, and Stephen Smith. 2002. "Improved Optimization for the Robust and Accurate Linear Registration and Motion Correction of Brain Images." *NeuroImage* 17(2):825–41.

Jones, Eric, Travis Oliphant, Pearu Peterson, and others. 2001. *SciPy: Open Source Scientific Tools for Python*.

Kuznetsova, Alexandra, Per B. Brockhoff, and Rune H. B. Christensen. 2017. "**LmerTest** Package: Tests in Linear Mixed Effects Models." *Journal of Statistical Software* 82(13).

Morey, Richard D. and Jeffrey N. Rouder. 2018. *BayesFactor: Computation of Bayes Factors for Common Designs*.

Power, Jonathan D., Anish Mitra, Timothy O. Laumann, Abraham Z. Snyder, Bradley L. Schlaggar, and Steven E. Petersen. 2014. "Methods to Detect, Characterize, and Remove Motion Artifact in Resting State FMRI." *NeuroImage* 84:320–41.

R Core Team. 2018. *R: A Language and Environment for Statistical Computing*. Vienna, Austria: R Foundation for Statistical Computing.

Treiber, Jeffrey Mark, Nathan S. White, Tyler Christian Steed, Hauke Bartsch, Dominic Holland, Nikdokht Farid, Carrie R. McDonald, Bob S. Carter, Anders Martin Dale, and Clark C. Chen. 2016. "Characterization and Correction of Geometric Distortions in 814 Diffusion Weighted Images" edited by J. Najbauer. *PLOS ONE* 11(3):e0152472.

Tustison, Nicholas J., Brian B. Avants, Philip A. Cook, Yuanjie Zheng, Alexander Egan, Paul A. Yushkevich, and James C. Gee. 2010. "N4ITK: Improved N3 Bias Correction." *IEEE Transactions on Medical Imaging* 29(6):1310–20.

Wang, Sijia, Daniel J. Peterson, J. C. Gatenby, Wenbin Li, Thomas J. Grabowski, and Tara M. Madhyastha. 2017. "Evaluation of Field Map and Nonlinear Registration Methods for Correction of Susceptibility Artifacts in Diffusion MRI." *Frontiers in Neuroinformatics* 11.

Zhang, Y., M. Brady, and S. Smith. 2001. "Segmentation of Brain MR Images through a Hidden Markov Random Field Model and the Expectation-Maximization Algorithm." *IEEE Transactions on Medical Imaging* 20(1):45–57.

7 | Publication 2

Note: This manuscript is the first version of a pre-publication. Future revised editions and the peer-reviewed version can be found using the URL https://www.biorxiv.org/content/10.1101/2020.11.16.384198v1, or the DOI https://doi.org/10.1101/2020.11.16.384198.

7.1 Author Contributions

S.R.S, S.V., and R.W. conceptualized and designed the research; S.R.S. and R.W. collected the data; S.R.S. wrote software, analyzed and visualized the data; S.V. and R.W. supervised the research project; S.R.S, S.V., G.R.F., and R.W. wrote the manuscript.

Simultaneous modeling of a Spatial Cuing Task

Simultaneous Modeling of Reaction Times and Brain Dynamics in a Spatial Cuing Task

Simon R. Steinkamp[1, *], Gereon R. Fink[1, 2], Simone Vossel[1, 3, †], Ralph Weidner[1, †]

[1] Cognitive Neuroscience, Institute of Neuroscience & Medicine (INM-3), Research Centre Juelich,

52425, Juelich, Germany

[2] Department of Neurology, Faculty of Medicine and University Hospital Cologne, University of

Cologne, 50937, Cologne, Germany

[3] Department of Psychology, Faculty of Human Sciences, University of Cologne, 50923, Cologne,

Germany

[†] both authors contributed equally

[*] **Corresponding author:**

Simon R. Steinkamp

Cognitive Neuroscience, Institute of Neuroscience and Medicine (INM-3)

Forschungszentrum Jülich,

Leo-Brand-Str. 5, 52425 Jülich, Germany

Email: s.steinkamp@fz-juelich.de

Abstract

Understanding how brain activity translates into behavior is a grand challenge in neuroscientific

research. Simultaneous computational modeling of both measures offers to address this

question. The extension of the dynamic causal modeling (DCM) framework for BOLD

responses to behavior (bDCM) constitutes such a modeling approach. However, only very few

studies have employed and evaluated bDCM, and its application has been restricted to binary

behavioral responses, limiting more general statements about its validity.

Simultaneous modeling of a Spatial Cuing Task

This study used bDCM to model reaction times in a spatial attention task, which involved two separate runs with either horizontal or vertical stimulus configurations. We recorded fMRI data and reaction times (n=29) and compared bDCM to classical DCM and a behavioral Rescorla-Wagner model using goodness of fit-statistics and machine learning methods.

Data showed that bDCM performed equally well as classical DCM when modeling BOLD responses and better than the Rescorla Wagner model when modeling reaction times. Notably, only using bDCM's parameters enabled classification of the horizontal and vertical runs suggesting that bDCM seems to be more sensitive than the other models. Although our data also revealed practical limitations of the current bDCM approach that warrant further investigation, we conclude that bDCM constitutes a promising method for investigating the link between brain activity and behavior.

Keywords: spatial attention, fMRI, simultaneous modeling, effective connectivity, dynamic causal modeling, behavioral dynamic causal modeling

Acknowledgements

Conflict of Interest

The authors declare no competing financial interests.

Data Availability Statement

The data that support the findings of this study are available on request from the corresponding author. The data are not publicly available due to privacy or ethical restrictions.

Introduction

Computational modeling can deepen our understanding of how the brain processes information and produces overt behavior. In the field of psychology, computational modeling

Simultaneous modeling of a Spatial Cuing Task

has a long history in describing and explaining behavioral concepts. For example, reinforcement learning algorithms have been used to explain classical conditioning (Rescorla et al., 1972), drift-diffusion models have been used to model reaction times in decision-making tasks (Ratcliff, 1978), and race models have been used as theoretical formulations of visual-spatial attention (Bundesen, 1990). Similarly, different computational modeling approaches have been employed in the fields of neuroscience and neuroimaging. For example, generative graphical models of brain connectivity describing blood oxygenation level-dependent (BOLD) amplitudes in response to experimental inputs can be estimated using dynamic causal modeling (Friston et al., 2003, 2017), and multivariate temporal response functions have been used to model ongoing sensory stimulation, like speech, in electrophysiological recordings (Crosse et al., 2016).

Although computational models are very prominent in the two fields, behavioral and neural responses are mostly treated separately (Turner et al., 2017). However, a combined modeling approach could provide us with deeper insights into the neural processes and the emergence of behavior. Here, different approaches have been proposed: One possibility is to correlate the parameters of neural and behavioral models to describe how the different measures are related across different participants (Vossel et al., 2016). Alternatively, in model-based fMRI, the behavioral computational model's outputs (or hidden states) are used as a factor in a classical GLM analysis. One such factor could be a participant's perceived cue validity in a probabilistic spatial cueing task, which can be recovered from reaction times (e.g., Dombert et al., 2016). Leveraging the theory-driven performance of cognitive models allowed to determine more specific brain activation patterns of cognitive processes than by using non-specific measures such as reaction times (Turner et al., 2017). A third option is a joint modeling approach (Turner et al. 2017). Here, an overarching set of parameters is used to describe both brain activity and behavior. An example is a study by Nunez et al. (2015), where the drift-diffusion model parameters were constrained with task-based brain activity, incorporating the covariation between reaction times and neural-activity on a trial-by-trial basis.

Simultaneous modeling of a Spatial Cuing Task

Although these approaches are tremendously useful, none of them employs an integrative model describing the generation of brain activity and behavior, allowing us to investigate the hidden processes behind the two measurements directly. Rigoux and Daunizeau (2015) have provided such a framework, where DCM is extended by an additional output function to describe behavioral responses (behavioral DCM, bDCM). This simultaneous modeling does have not only high descriptive power but also allows thorough diagnostics of the model. For example, by disabling specific nodes in the network (i.e., artificial lesions), conclusions can be drawn about the contribution or necessity of different brain regions to the emergence of behavioral patterns. So far – to our knowledge – bDCM has been applied to a larger datasets in one study, which modeled binary choices in an economic decision making task (Shaw et al., 2019).

In the current study, we show that bDCM can be extended to continuous measures (i.e., reaction times). Furthermore, we provide a direct comparison between bDCM and classical DCM and between bDCM and an adjusted version of the Rescorla-Wagner model (Rescorla et al., 1972; Vossel, Mathys, et al., 2014).

As a testing ground, we modeled the effects of attentional reorientation along the horizontal and vertical meridians in a spatial cueing-paradigm, where participants had to report the orientation of a pre-cued Gabor patch. In trials in which invalid cues indicated an incorrect location of the target Gabor patch (20 % of the trials), participants had to reorient their attention to the opposite location (Posner, 1980). This paradigm has been found to elicit reliable reaction time differences between invalid and valid trials, both on the individual and the group level (Hedge et al., 2017). Additionally, it has been shown that the internal representation of cue-validity can be modeled using the Rescorla-Wagner model as a generative model of reaction times (Mengotti et al., 2017; Rescorla et al., 1972; Vossel, Mathys, et al., 2014).

Besides the reliable behavioral effects, the cortical networks involved in this task have been characterized by multiple studies. We have previously analyzed the present dataset using classical DCM (Steinkamp et al., 2020), which has also been used in similar cueing paradigms

Simultaneous modeling of a Spatial Cuing Task

(c.f., Vossel et al., 2012). Moreover, studies in patients with stroke-induced lesions have revealed brain regions that are critically involved in spatial cueing-tasks (Corbetta & Shulman, 2011; Malherbe et al., 2018; Posner et al., 1984). It is well established that the orientation of visual-spatial attention is mediated by a dorsal fronto-parietal attention network consisting of the intraparietal sulci (IPS) and the frontal eye fields (FEF). This network interacts with a ventral fronto-parietal attention network of ventral frontal cortex, and the temporoparietal junction (TPJ) when a sudden reorientation of attention is necessary (Corbetta et al., 2005; Corbetta & Shulman, 2011).

In addition to comparing bDCM, which simultaneously models behavior and brain activity, to classical DCM and a purely behavioral model, we also investigated whether bDCM parameters encode additional information about the task that is not comprised in DCM or the Rescorla-Wagner model. For this, we followed the idea of generative embedding (Brodersen, Haiss, et al., 2011; Brodersen, Schofield, et al., 2011) and tested whether we could separate the horizontal and vertical runs of our experiments based on the parameter estimates of our models, which was not possible in previous analyses (Steinkamp et al., 2020).

Methods

Participants

Data were collected from 29 participants (15 female, 21-39 years old, M=25, SD=3) with normal or corrected-to-normal vision (all right-handed, Edinburgh handedness Inventory (Oldfield, 1971), M=0.86, SD=0.14), who provided written informed consent to participate in the study. One participant had to be excluded subsequently because of noncompliance. Another participant was excluded due to excessive head-movement (predefined criteria translation > 3mm, rotation > 3°). Furthermore, we could not extract the time-series for the left-TPJ VOI in one participant. Therefore, the final sample included 26 participants. The ethics board of the German Psychological Association had approved the study. Volunteers were paid 15€ per hour for their participation. The dataset has been used in a previous study (see Steinkamp et al., 2020).

Simultaneous modeling of a Spatial Cuing Task

Task
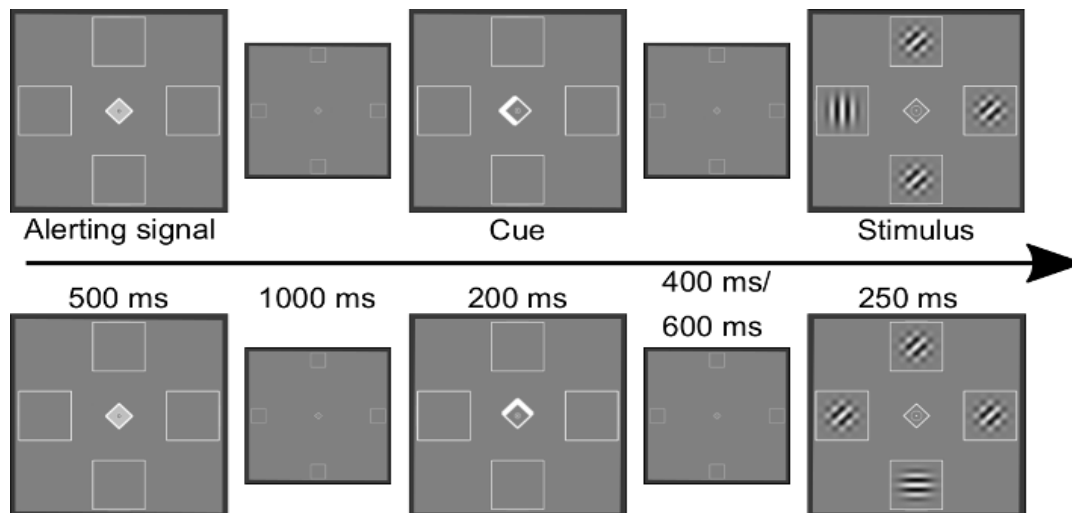
Figure 1 Illustration of the spatial cueing paradigm. In the upper row, a valid trial of the horizontal run is shown. The lower row depicts an example of an invalid trial in the vertical run. Reproduced from Steinkamp et al. (2020).

Participants performed a spatial cueing task while lying in a 3T Trio (Siemens, Erlangen) MRI scanner. Stimuli were displayed on a screen behind the scanner bore, which could be seen via a mirror (mirror to display distance: 245 cm) that was mounted on a 32-channel head coil. The participants' task was to report the orientation (horizontal/vertical) of a target Gabor patch (size 1° visual angle) by button presses of either the left or the right index finger while continuously fixating a diamond in the center of the screen (0.5° visual angle). A brightening of the central diamond (500 ms) indicated the beginning of a trial and was followed by a spatial cue after 1000 ms (brightening of one of the diamond's edges for 200 ms) that indicated the location of the next target stimulus with 80 % probability. Participants were explicitly informed about the percentage of cue validity. The possible target locations were indicated by empty boxes (1° width) located to the left, right, top, and bottom of the fixation diamond (4° visual angle). After 400 ms or 600 ms, the target stimulus appeared for 250 ms at the cued location or in the box opposite to it. Distractor stimuli (constructed from two overlapping Gabor patches that were rotated by -45° and 45°, respectively) appeared simultaneously in the remaining three locations. Participants performed two runs of the spatial cueing-paradigm. In one run,

Simultaneous modeling of a Spatial Cuing Task

targets and cues occurred along the vertical axis, in another along the horizontal axis (see Figure 1).

Each run consisted of five blocks of 40 trials (32 valid, 8 invalid). All possible combinations of target location, target orientation, and inter stimulus interval were presented in random order within each block. The time between the trials was drawn from the set of 2.0 s, 2.7 s, 3.2 s, 3.9s, or 4.5 s with equal probability. Between the blocks, there was a break of 10 to 13 s.

Run order (vertical or horizontal first) and the response mapping (left index finger for vertical orientations/right index finger for horizontal orientations or vice versa) were counterbalanced across participants. Before the experiment, participants performed a rapid detection task to train the mapping of stimulus-response associations. Here, targets appeared rapidly in the middle of the screen, and participants had to press the corresponding button as fast as possible. Immediate feedback and a running score of their accuracy were given. Additionally, there were 20 practice trials with feedback before each run of the main experiment.

Stimulus presentation and response collection were controlled using PsychoPy (version 1.85.3, Peirce, 2007, 2008; Peirce et al., 2019).

Behavioral analysis

The mean reaction time was calculated for each participant and cueing condition and for each target location. Before calculating the mean reaction times, we preprocessed the data for each participant separately. First incorrect, missed, and outlier trials were removed. Outliers were defined as trials with reaction times below 0.2 s and reaction times greater than the 75th percentile + 3 * Inter Quartile Range (IQR). The higher threshold for outlier exclusion was chosen to retain as many trials as possible in the analysis (removed trials, including errors, in the horizontal run: invalid M = 2.54, SD = 2.63; valid M = 6.62, SD = 5.91; in the vertical run: invalid M = 3.12, SD = 1.8; valid M = 6.0 SD = 3.94).

For the analysis of the "validity effect" (i.e., the slowing of reaction times in invalid as compared to valid trials), the data were pooled across the two runs (horizontal/vertical). The mean

Simultaneous modeling of a Spatial Cuing Task

reaction times of the 2 x 4 (cueing x target location) factorial design were then analyzed in a repeated-measures ANOVA. The analysis was conducted in Python 3.7 using pingouin (version 0.3.3, Vallat, 2018).

fMRI analyses

For each participant and each run, we collected 557 T2*-weighted images using an echo planar imaging (EPI) sequence (time of repetition (TR) 2.2 s; echo time (TE) 30 ms; flip angle 90°). Each recorded volume consisted of 36 transverse slices with a slice thickness of 3mm and a field of view of 200mm. The voxel size was 3.1 x 3.1 x 3.3 mm. The first 5 images were discarded to account for T1 equilibrium artifacts. Next to functional images, we also obtained an anatomical T1-weighted image for each participant, which was used in the preprocessing.

We preprocessed the fMRI data using fmriprep (version 1.1.1, Esteban et al., 2019), a robust and standardized pipeline, which applies slice-time correction, realignment, and normalization to MNI space. A detailed preprocessing report can be created automatically (see http://fmriprep.readthedocs.io/en/1.1.1/workflows.html), and has been included in the supplement.

Data was further spatially smoothed using an 8 x 8 x 8 mm FWHM Gaussian kernel. This step was done in Matlab 2018b (The MathWorks, Inc., Natick, Massachusetts, United States), using SPM12 (version 7771, Friston, 2007).

fMRI - GLM

A classical GLM analysis was performed to identify activation peaks during attentional orientation and reorientation, which were later used to extract BOLD time-series data for the DCM analysis. The GLM analysis was conducted using SPM12. First-level models were created with four regressors of interest for each run, representing invalidly cued targets on the left (iL) and on the right (iR), as well as validly cued targets on the left (vL) and the right (vR) for the horizontal run, and invalidly and validly cued targets in the lower (iD, vD) and the upper (iU, vU) part of the screen in the vertical run.

Simultaneous modeling of a Spatial Cuing Task

To account for other physiological noise in the BOLD signal, we added the three rotation and three translation estimates of the rigid body transform, the average white matter signal, and the average cerebral spinal fluid (CSF) signal as nuisance regressors. We further included the squared time-series of the 8 regressors, the time-shifted time-series (t-1), as well as the square of the shifted time-series, resulting in a total of 32 nuisance regressors (Friston et al., 1996). We also applied a high pass filter at 128 s. For each run, four first-level contrasts were calculated: T-contrasts of valid and invalid trials versus baseline, an F-contrast of target onset versus baseline, which were used in the VOI analysis, and a differential contrast of invalid trials greater than valid trials. The latter contrast isolates brain regions involved in the attentional reorientation of attention.

At the group (second)- level, we investigated the differential contrast of invalid > valid trials using two planned one sample permutation t-tests against 0 using SnPM 13 (Nichols & Holmes, 2002), with default settings, 10000 permutations, and no additional variance smoothing. The cluster forming threshold was estimated during the processes with a predefined voxel-level cutoff of p < 0.001.

Modeling Analysis

In the following, we will describe the modeling approaches used in our analysis, followed by a description of our model assessments and further analyses.

Rescorla-Wagner Model

We employed a variant of the Rescorla-Wagner model that we already used previously (Mengotti et al., 2017). While these studies were interested in the α parameter (the learning rate that describes how quickly participants adjust their internal assessment of the cue-validity), we applied this modeling approach to simulate reaction times in a trial-by-trial fashion. For parameter estimation, we defined new functions for the VBA (Variational Bayesian Analysis) toolbox (clone from master, in Jan. 2020, Daunizeau et al., 2014).

We used the following reinforcement learning formula as the evolution function, describing the hidden process governing the generation of reaction times.

Simultaneous modeling of a Spatial Cuing Task

$$v_t = v_{(t-1)} + \alpha * \delta$$

Where $\delta = u_t - v_{(t-1)}$ describes the prediction error at trial t. The external input $u_t \in [0, 1]$

describes whether the cue at time t was either valid (1) or invalid (0), α is the learning rate and

v_t is the participant's perceived cue validity after observation of trial t.

The observation function (i.e., the mapping from perceived cue validity to reaction times) was

defined as:

$$g_t = u_t * (\zeta_v + \zeta_2 * v_{t-1}) + (1 - u_t) * [\zeta_i + \zeta_2 * (1 - v_{t-1})]$$

According to this formulation, the perceived cue-validity of the previous trial governs the

responses, with different bias parameters for valid and invalid trials and a general scaling

parameter of the predictions.

Table 1 depicts the Gaussian priors used in our estimation:

Table 1: Overview of parameters and prior values of the Rescorla-Wagner Model.

Parameters	μ	σ	
α	0.5	0.5	To ensure $0 < \alpha \leq 1$, α was logit and inverse logit transformed during parameter updating
ζ_v	0	1	
ζ_i	0	1	
ζ_2	0	1	
v_0	0.5	1	Initial state of v

Behavioral DCM

In the following, we will provide a short overview of key-concepts of dynamic causal modeling

(DCM). For a full derivation and detailed description of DCM, see (Friston et al., 2003; Rigoux

& Daunizeau, 2015; Stephan et al., 2008). DCM is a fully-Bayesian approach to create a

generative model of brain dynamics and infer effective connectivity between selected brain

regions. In principle, DCM describes how experimental variations (described by the input u)

drive the neural activity (x, the hidden states) in brain regions of interest in a dynamical system.

The evolution function ($\dot{x} = f(x, u)$) describes the temporal dynamics of the hidden states ($\dot{x}$)

Simultaneous modeling of a Spatial Cuing Task

and how they are influenced by external inputs (u). In DCM for fMRI, the evolution function f is

typically described as:

$$f(x, u, \theta) \mathrel{\hat{=}} Ax + \sum_j u_j B^j x + Cu$$

Where j corresponds to the number of inputs and i to the number of brain regions. The neural

evolution parameters in θ correspond to the entries in A (fixed connectivity between brain

regions), B^j (modulation of connection strength by input j), C (direct effects of inputs).

Hemodynamic states z (dependent on the neural states x) are then gated through an

observation function:

$$y = g(z, \phi) + \epsilon$$

This function captures BOLD signal variations based on the hemodynamic states (z) and the

hidden neural activity (x), with hemodynamic parameters ϕ. This mapping allows to observe

and infer the hidden neural dynamics via the BOLD signal.

BDCM augments the described formulation of DCM by an additional evolution ($h(x, u, \psi)$) and

observation functions ($g_r(r) + \epsilon_r$) to map the hidden neural dynamics to behavioral responses.

The evolution function h of the new "behavioral" state follows the same rationale as the function

f in the DCM formulation:

$$h(x, u, \psi) \mathrel{\hat{=}} A_r x + \sum_j u_j B_r^j x + C_r u$$

Here the parameter vector ψ describes the linear (A_r) components of the behavioral state, as

well as the direct (C_r) and modulatory (B_r^j) influences of experimental manipulations. A_r is an

analogy of the weight vector in a regression model. In the original paper, the neural states were

mapped to binary behavioral observations (button press absent or present) via a sigmoidal

function:

$$s(r) = \frac{1}{1 + e^{-100*(\rho+r)}}$$

Simultaneous modeling of a Spatial Cuing Task

Here, ρ is an unknown bias term and r is the response or decision state. In our study, we slightly adjusted the sigmoid mapping, by changing the scale on which it operates. As we are not expecting reaction times slower than 3 s, we used this as an upper bound:

$$s(r) = \frac{3}{1 + e^{-100*(\rho+r)}}$$

Regions

As in our previous study (Steinkamp et al., 2020), we included bilateral IPS and FEF in our DCM model, which correspond to the central nodes of the dorsal fronto-parietal attention network (Vossel, Geng, et al., 2014). Additionally, as part of the ventral attention network, we included the TPJ bilaterally. As additional inclusions (e.g., the inferior/middle frontal gyrus) would have led to increasing model complexity and computational resources (and time), we did not include other brain regions, which may also play a role in attentional reorienting.

Based on our assumptions about the dorsal and ventral attention network's interplay, we created three automatic meta-analysis using Neurosynth (https://www.neurosynth.org/, Yarkoni et al., 2011), to define the seed coordinates for the subsequent VOI analysis (see Table 2). Our regions of interest were bilateral IPS (search term: "intraparietal sulcus"), bilateral FEF (search term: "frontal eye"), and bilateral TPJ (search term: "tpj"). We downloaded the corresponding association maps (associations, p<0.01 FDR corrected) and identified the seed location as the peak voxel in the cluster of interest, using the Anatomy toolbox (v2, Eickhoff et al., 2005). In all three maps, the two largest clusters encompassed our regions of interest in either the left or right hemispheres.

Table 2: Regions and search-terms for automated Neurosynth meta-analyses.

Region	NeuroSynth (accessed 10.10.19)	Z-Statistic	X	Y	Z
IPS – left	"intraparietal sulcus"	14.6	-30	-50	42
IPS – right	"intraparietal sulcus"	13.5	40	-38	44
FEF – left	"frontal eye"	13.9	-30	-4	52
FEF – right	"frontal eye"	14.6	32	-6	52
TPJ – left	"tpj"	8.56	-60	-54	20
TPJ – right	"tpj"	11.4	58	-50	14

Simultaneous modeling of a Spatial Cuing Task

In each run, we used the participant level t-maps (thresholded at p < 0.1 uncorrected) to search for individual local maxima in a 12 mm sphere around the seed coordinates. The first principle component of BOLD time-courses in a 9 mm VOI around the participant's maximum was extracted and adjusted based on the F-contrast defined in the first-level analysis. Task-related activity for the IPS and FEF VOIs was defined by the contrast of valid trials against baseline and for TPJ by the contrast of invalid trials against the baseline.

Preprocessing

We preprocessed the BOLD signal by detrending the signal in each VOI (*spm_detrend*) and scaling the BOLD amplitude across VOIs to a maximum value of 4 (see *spm_dcm_estimate*). Behavioral data were extracted from the event data, and as in the previous analyses, error trials and trials with missed responses, as well as RTs fulfilling the outlier criterion (RT < 0.2s and RT > 3 * IQR + UQ), were excluded.

BOLD data were resampled from a TR of 2.2 s to a sampling rate of 1.1 s (by interspersing "NaN" values). The behavioral observations were set to occur at the corresponding target onset, which was also downsampled to a resolution of 1.1 s. No resampling of BOLD data was performed for the classical DCM analysis. As the Rescorla-Wagner model represents trial-by-trial dynamics, the corresponding preprocessed reaction times were used, excluding error and missed trials.

For our modeling, we assumed homogenous HRF dynamics across the six regions, fixing the initial states of the model to 0 and estimating the shape of the observation noise hyper-prior distributions. For this, we assumed that we would be able to explain 10 – 90% of the variance in both the BOLD and the reaction time data. The prior distributions over the other parameters were set to the defaults of the VBA toolbox. We used the same hyperpriors for the explained variance of the BOLD signal in the classical DCM analysis and the Rescorla-Wagner model's behavioral responses.

Simultaneous modeling of a Spatial Cuing Task

To define the inputs into the DCM models, we created separate SPM-design matrices that were only used to define the input streams. Stream one was defined as the driving input to all six regions, containing an impulse every time a target stimulus appeared (irrespective of the cueing condition or target location). The second stream was used purely for the modulatory effects, containing an impulse only in invalidly cued targets. The input streams were extracted from the SPM design matrix and were centered before entering the model inversion (*spm_detrend*). As mentioned above, the Rescorla-Wagner model is modeling trial-by-trial variations (rather than continuous time), so the input to this model was a vector consisting of ones and zeros, indicating whether the current trial is invalid or valid.

Model definition

We used the same general model structure for behavioral and classical DCM analysis. As in our previous publication, we used IPS, FEF, and TPJ as our brain regions of interest. For our analysis, we inverted a single model. The fixed connectivity structures of our model (i.e., the A-matrix) had full connections in each hemisphere and connections between homologous regions (Figure 2). As we did not include visual areas in our modeling approach, all six regions received driving input (C-matrix). For bidirectional intra- and interhemispheric modulatory connections (B-matrix), we considered the IPS and TPJ. Connections in both hemispheres to the FEF were unidirectional, assuming that there were no feedback modulations from FEF to the other brain regions. In the case of bDCM, we also considered all six nodes as output regions.

Simultaneous modeling of a Spatial Cuing Task

A and C Matrices
- **A:** Intrinsic connectivity
- **C:** Driving input (target present)

B and hA Matrices
- **B:** modulation by invalid targets
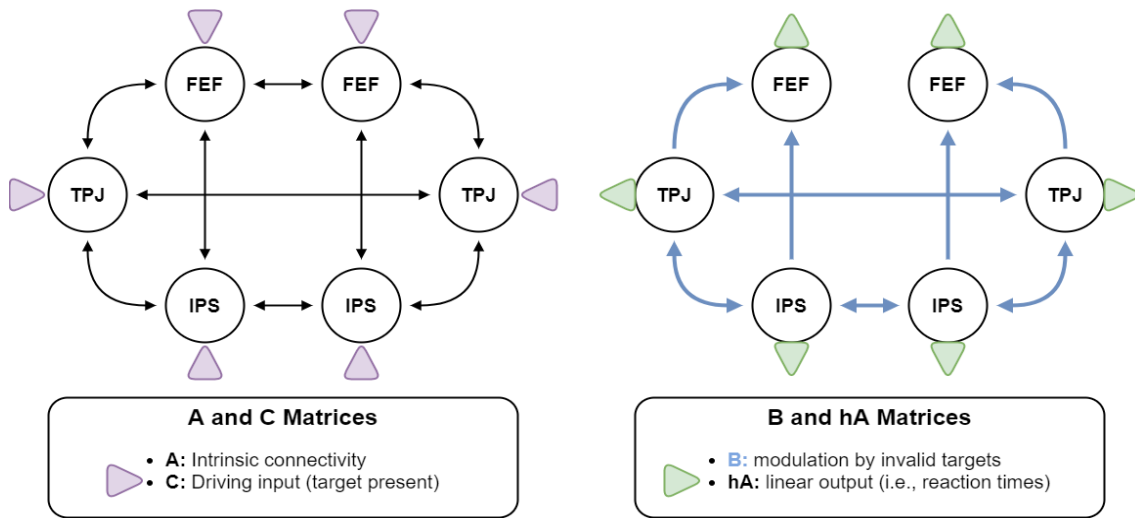- **hA:** linear output (i.e., reaction times)

Figure 2: Basic structure of the DCM model. Regions were fully inter-connected in each hemisphere, and homologous regions were connected. All regions received driving input. We assumed that all connections between the regions were modulated by invalid trials, except for feedback and interhemispheric connections from FEF.

Model evaluation of the Rescorla-Wagner model, classical DCM, and bDCM

As all three models are based on different underlying data at different times scales (i.e., reaction times only, BOLD time-series only, or both), we only compared the models based on their outputs, applying classical goodness of fit-statistics. The R^2-score,

$$SS_{tot} = \sum_{t}^{n}(y_t - \bar{y})^2$$

$$SS_{res} = \sum_{t}^{n}(y_t - \hat{y}_t)^2$$

$$R^2 = 1 - \left(\frac{SS_{res}}{SS_{tot}}\right)$$

where y_t describes the datapoint at t, with n timepoints in total. The average of y is defined as $\bar{y}$, and $\hat{y}$ are predicted values. Similarly, we also calculated the mean absolute error (MAE)

$$MAE = \frac{1}{n}\sum_{t}^{n}|y_t - \hat{y}_t|$$

Simultaneous modeling of a Spatial Cuing Task

Here, we estimated for each subject whether the fit-statistics were different from random for each of the model outputs by permutation testing. The predicted values $\hat{y}$ were shuffled 10000 times (without replacement), and the two statistics were recalculated. The permutation p-value for the models is then reported as the proportion of fits greater than the model's R^2–score (smaller in case of MAE) plus one divided by the number of permutations plus one (Ojala & Garriga, 2010). At the group level, we report the proportion of significant models, based on a permutation p-value < 0.05.

To compare the model performance on reaction times, we used (Bayesian-) paired t-tests to test for differences between the fit-statistics (R^2-score and mean absolute error (MAE)), separately for the two runs. We then investigated how well bDCM and the Rescorla-Wagner model simulate the underlying reaction time distributions. This was achieved by calculating a two-sample Kolmogorov-Smirnov test between the model-derived reaction times of the Rescorla-Wagner model or bDCM and the measured reaction times. Finally, paired t-tests were used on the distance between the distributions (as determined by the KS-test) to test which simulation followed the measured data more closely (i.e., had a smaller distance at the group level).

We applied a mixed-effects linear model for each error term to compare differences in performance to the BOLD data fit between classical DCM and bDCM. The mixed-effects model followed the following formula, where "Score" either depicts the mean absolute error or the R2-score:

$$Score \sim Model + Region + Run + Model * Region + Model * Run$$

and Model has the two factors "DCM" and "bDCM", "Run" describes either the horizontal or vertical run, and "Region" indicates the "Score" for either VOI. Each model also contained a random intercept for each participant.

Simultaneous modeling of a Spatial Cuing Task

Generative Embedding

We also investigated whether bDCM parameters encode additional information, which is not contained in classical DCM or in the Rescorla-Wagner model. Therefore, we tested whether the parameters derived from our computational models could be used to separate the horizontal and vertical run. Note that our previous work using classical DCM did not provide any evidence for distinct behavioral or neural processes (Steinkamp et al., 2020).

To test if a separation is possible and which sets of parameters encode the necessary information, we ran several experiments using different feature sets. Our feature sets for DCM and bDCM were: "AB", the sum of the "A" and "B" matrices (19 parameters); "AB + C", extending the feature set with the "C" matrix parameters (25 parameters); in case of bDCM we additionally tested the feature sets "AB + hA", where the "hA" matrix was also included in the set (25 parameters); "AB + C + hA", including all connectivity parameters of the bDCM (31 parameters); "C + hA", using only the input and outputs connections of bDCM. We then also tested whether we can find any information in the parameters of the Rescorla-Wagner model (see Table 2, "RW", 4 parameters), and whether parameters of DCM and the Rescorla-Wagner model in combination have a beneficial effect ("AB + C + RW", 29 parameters). To be sure that there was no additional information in the BOLD time-series, we also included a feature set based on the correlation of the time-series of the six VOIs in our experiments ("Correlation", 15 parameters) and of the time-lagged correlation with the time-series ("Correlation + $Correlation_{t-1}$", 51 parameters). Correlations were established using nilearn's *ConnectivityMeasure* (Abraham et al., 2014), with no variance scaling.

As we have a minimal sample size for classification approaches (26 participants, 52 instances), we applied an elaborate cross-validation procedure for our results. We applied 5-fold cross-validation to obtain an estimate of the accuracy of each feature set, whose significance was further evaluated by permutation testing (1000 iterations, scikit-learn's, *permutation_test_score*; Pedregosa et al. (2011)). To keep more independence between the train and test-sets, we ensured that a given participant's instances were not distributed across

Simultaneous modeling of a Spatial Cuing Task

training and test-sets. Due to the small sample size and high variance between participants, we repeated the cross-validation procedure 20 times, shuffling the participants order, and creating different train-test splits for each iteration.

To account for a certain amount of algorithmic variance, we performed the procedure above using two classifiers, a logistic regression, and a linear support vector machine (scikit-learn, using default parameters). Input data were normalized using robust-scaling (scikit-learn's *RobustScaler*).

Lesion Analysis

We also applied lesion analysis to the bDCM model, as described in Rigoux and Daunizeau (2015). Here, the afferent connections towards a single brain region were reduced to 0 to simulate the absence of this region (i.e., to create an artificial lesion). The simulated data from such a lesioned model can be used to better understand behavioral changes after damage to certain brain regions.

To alleviate the problem of numerical instabilities, which resulted in values resulting in infinity or minus infinity for the hidden states, we changed the posterior self-inhibitory connection in the DCM model to log(1) (to ensure inhibition, i.e., negativity, self-connections in DCM are exponentiated before subtraction from the diagonal of the A matrix). While increasing the self-inhibition solved the problem of instabilities, it significantly impacted the fit-statistics of the non-lesioned model. Therefore, we only provide a qualitative description of the lesion analysis. In the end, we simulated data for all 26 participants for each lesion and several levels of lesion extent. This means, rather than switching off the afferent connections (i.e., the inputs to the region) altogether, we also simulated data for connections that had 95 %, 75 %, 50 %, 25 %, 5%, and 0 % of the original incoming strength.

Since a few models still were numerically unstable, we then cleaned the simulated data by removing datasets on a per lesion basis where the variance after the 20th trial was close to 0 (i.e., the simulated reaction times flatlined at the maximum/minimum of the sigmoid function) and which returned non-values. In the qualitative analysis, we compared the group-mean

Simultaneous modeling of a Spatial Cuing Task

validity effects for different lesions, extents, and target sides, removing participants who had

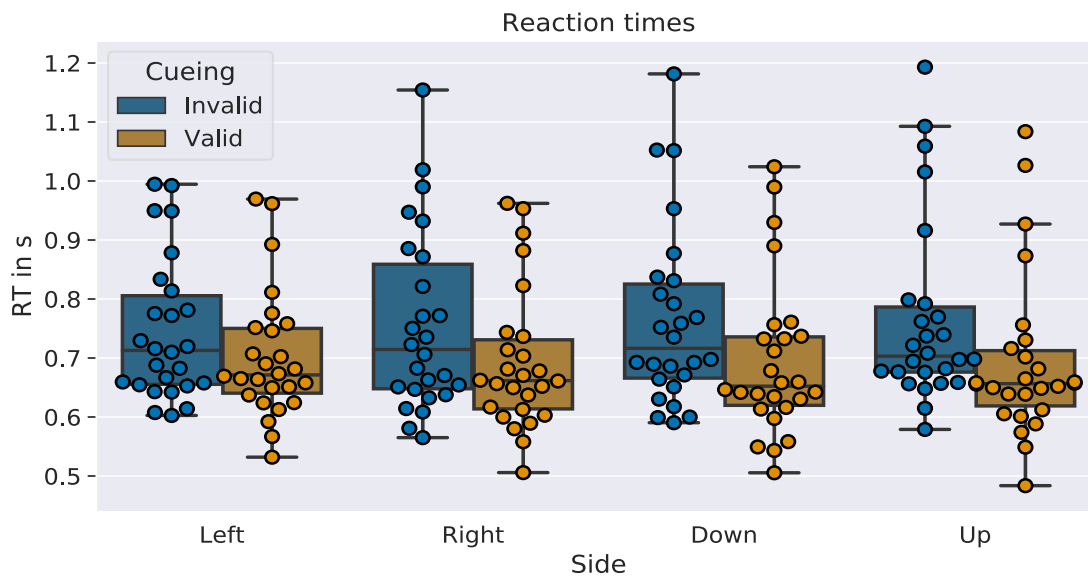an absolute validity difference greater than 2 secs.

Results

Behavior

Figure 3: Box- and swarm plots of mean-reaction time data for each participant in the 8 conditions. The boxes indicate the inter-quartile range (IQR), the line in the middle the median reaction time, whiskers are extended to include the lower and upper quartiles plus 3 times the IQR. Loose points indicate outliers. The ANOVA's results are readily visible, as there are longer reaction times in invalid trials but no apparent effects between the different target-positions.

To test for reaction time effects of cueing (valid or invalid) and target-side (left, right, down, up), as well as their interactions, we applied a 2 x 4 repeated measures ANOVA (see also Figure 3). There was no significant effect of target-side ($F(1.965, 49.125) = 0.1$, $p = 0.902$, $\eta_p^2 = 0.004$, $\varepsilon = 0.655$). However, a significant main effect of cueing ($F(1, 25) = 26.647$, $p < 0.001$, $\eta_p^2 = 0.516$, $\varepsilon = 1.0$) and a weak significant interaction between target-side and cueing ($F(2.88, 72) = 2.866$, $p = 0.045$, $\eta_p^2 = 0.103$, $\varepsilon = 0.96$) were observed. All reported p-values were Greenhouse-Geisser corrected to account for a lack of sphericity.

Simultaneous modeling of a Spatial Cuing Task

FMRI GLM

The contrasts of invalid versus valid trials isolating reorienting-related activity for the two runs are reported in Figure 4 (group t-maps are provided on neurovault:

NV_LINK, (Gorgolewski et al., 2015), the corresponding tables reporting global and local maxima for the different clusters are in supplement S2). We performed a one-sample permutation t-test on the first-level contrast images (invalid > valid), with a predefined cluster-forming threshold of $p < 0.001$, the results are reported family-wise error corrected at $p < 0.05$
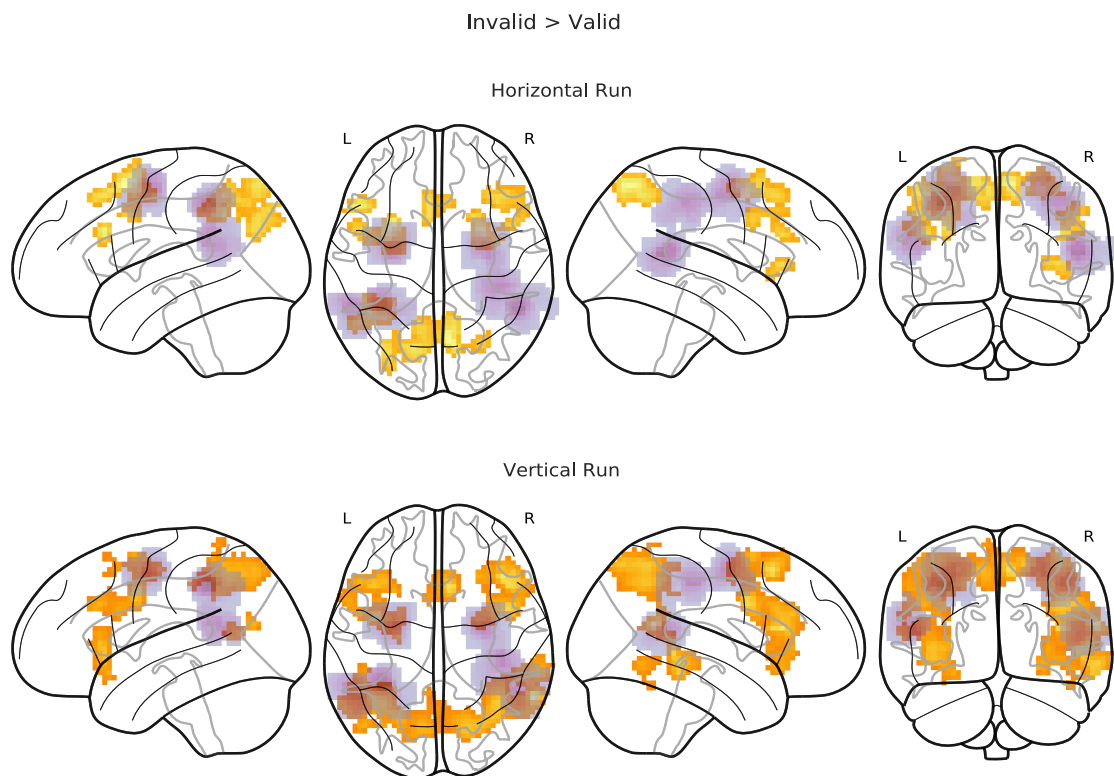

Figure 4: Non-parametric T-maps contrasting invalid > valid trials for the two runs ($p < 0.05$ FWEc). The purple overlay indicates the regions where the 9mm VOIs for the bDCM analysis were extracted (sum of the participant's masks).

(cluster threshold horizontal k = 58 voxels, vertical k = 70 voxels). In both maps, we found areas classically associated with the dorsal and ventral attention networks. For example, in both runs, we observed significant activation in bilateral intraparietal sulci and frontal-eye fields. Activations of the ventral attention networks were less robust. For the horizontal run, for example, the invalid versus valid contrast revealed an involvement of the middle frontal gyrus predominantly in the right hemisphere and no significant activation close to the seed regions

Simultaneous modeling of a Spatial Cuing Task

for the temporoparietal junction at the given threshold. However, the temporoparietal junction was significantly activated in the vertical run.

Model Fit

Reaction Time Data

We calculated the mean absolute error (MAE) and the R^2 statistic for the Rescorla-Wagner and bDCM models and assessed their significance on a per-subject level by calculating permutation tests. In the horizontal run, the bDCM (mean absolute error, M = 0.091, SD = 0.033, percent sig = 96.2 %; R^2 score, M = 0.117, SD = 0.084, percent. sig = 100 %) performed well when compared to the Rescorla-Wagner model (mean absolute error, M = 0.094, SD = 0.033, percent sig. = 53.8 %; R^2 score, M = 0.066, SD = 0.08, percent. sig = 69.2 %). The
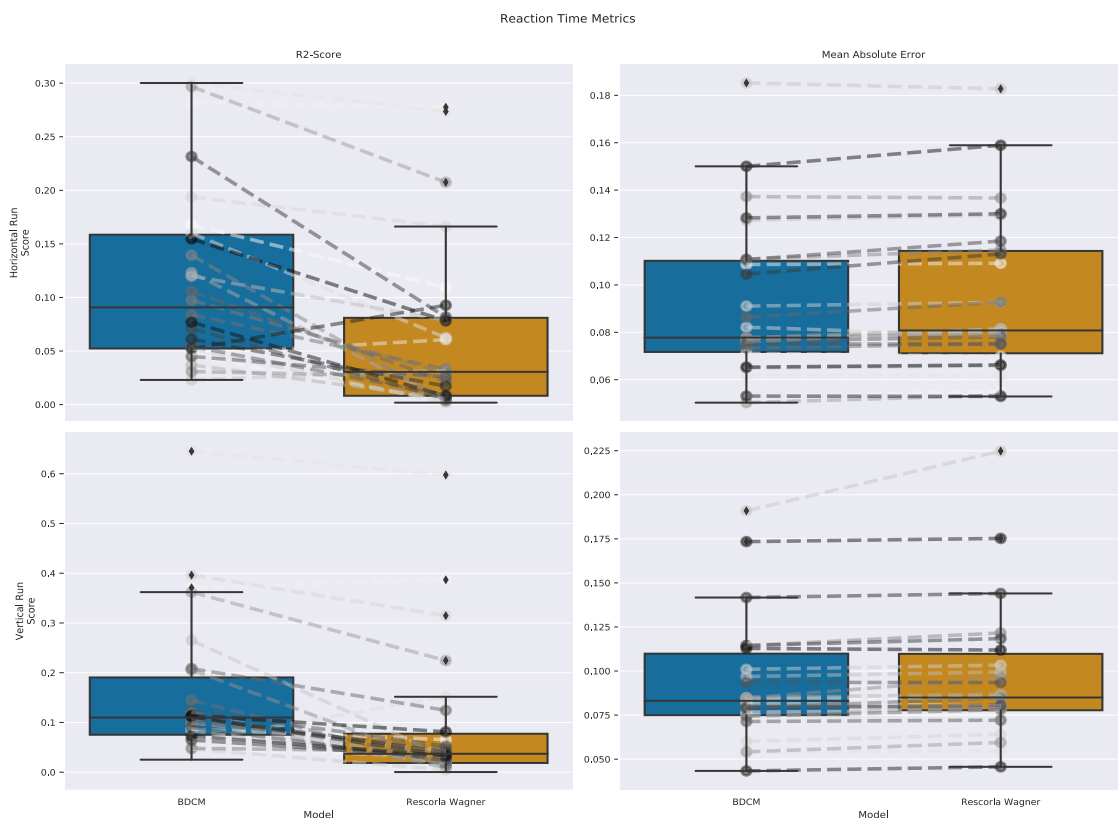
Figure 5: Boxplots comparing the different fit-statistics across models in the horizontal run. Please note that for the R^2-score a higher value is better, while the opposite is true for the mean absolute error. The dashed lines between the boxplots indicate individual participants.

results of the vertical run yielded a very similar picture, where the differences between the

bDCM (mean absolute error, M = 0.093, SD = 0.034, percent sig. = 100 %; R^2 score, M =

Simultaneous modeling of a Spatial Cuing Task

0.158, SD = 0.143, percent. sig = 100 %) and the Rescorla-Wagner model (mean absolute

error, M = 0.096, SD = 0.038, percent sig. = 80.8 %; R^2 score, M = 0.094, SD = 0.141, percent.

sig = 88.5 %) were even more pronounced (see Figure 5). The paired t-tests (Table 3)

confirmed this pattern and revealed a better fit for the vertical run. BDCM had a lower error

and greater fit than the Rescorla-Wagner model.

Table 3: Paired t-tests between the fit-statistics of bDCM and Rescorla-Wagner models. The differences between the fit-statistics favor the bDCM model.

Run	Error	T (df 25)	p-val	CI95%	cohen-d	BF10
Horizontal	MAE	-3.557	0.002	-0.0, -0.0	0.066	23.692
Horizontal	R^2	5.803	< 0.001	0.03, 0.07	0.625	4.249.729
Vertical	MAE	-2.644	0.014	-0.01, -0.0	0.098	3.571
Vertical	R^2	5.204	< 0.001	0.04, 0.09	0.456	1.048.508

Furthermore, we evaluated how well the reaction time distributions of the two models'

simulations matched the real reaction time distribution (Figure 6). We calculated the distance

between the distributions of measured and simulated reaction times for each run, participant,

and cueing-condition using the Kolmogorov-Smirnov test. We then performed paired t-tests in

order to ascertain which simulation better matches the original distribution. In all cases, the

bDCM simulation provided a better match (horizontal run, valid cueing, t(25) = -10.155, p <

0.001, Cohen's d = 2.432, BF_{10} = 4.39 * 10^{10}; horizontal run, invalid cueing, t(25) = -8.121, p <

0.001, Cohen's d = 2.392, BF_{10} = 7.51 * 10^8; vertical run, valid cueing, t(25) = -7.619, p < 0.001,

Cohen's d = 2.049, BF_{10} = 2.56 * 10^8; vertical run, invalid cueing, t(25) = -9.931, p < 0.001,

Cohen's d = 2.475, BF_{10} = 2.87 * 10^{10}). Based on visual inspection of the differences in reaction

time distributions, deviations were especially pronounced at the extreme ends of the

distribution.

Simultaneous modeling of a Spatial Cuing Task
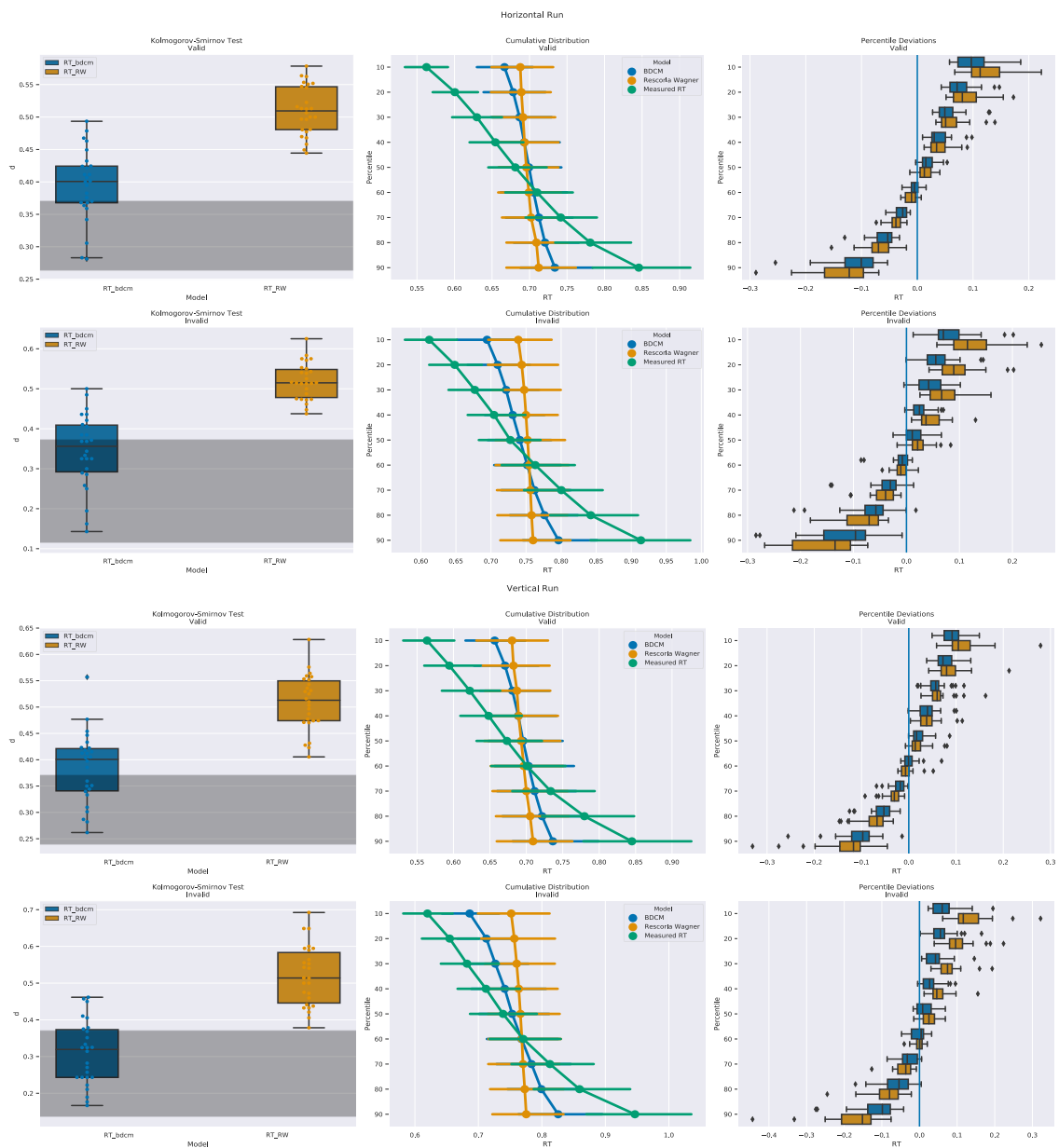
Figure 6: Left column, Kolmogorov-Smirnov distance between the simulated responses between the measured reaction times and bDCM or the Rescorla-Wagner model. The grey shading indicates non-significant differences. BDCM has, in general, a lower distance to the original distribution, and in many cases, the tests were non-significant. Both models also appeared to be better in the prediction of the invalid reaction time distribution. Middle Column: Cumulative reaction time distribution represented by the deciles of each model. The measured reaction times (green) have a more extensive spread than the reaction times from bDCM (blue) and the Rescorla-Wagner model (orange). Right column: The paired difference between the deciles of the Rescorla-Wagner model and bDCM. Differences are especially large in more extreme deciles.

Simultaneous modeling of a Spatial Cuing Task

BOLD Data

In a further step, we investigated whether DCM and bDCM were comparable in their fit to the measured BOLD data. For this, we calculated the fit-statistics (mean absolute error and R^2-score) for the two modeling approaches and the two runs. Since this yields fit-statistics for each brain region, we calculated two linear mixed-effects models (MLM) with participant as a random factor to test for a main-effect or interaction effects of model and fit-statistic, as well as the main effect of run and interactions between model and run (Figure 7). The results of the mixed-effects models are summarized in Table 4. Importantly, we did not find a significant main effect of model. However, there were significant main effects of brain region, these effects did not interact with the choice of model, indicating that the two models performed similarly. A similar conclusion can be drawn when looking at the different runs. Again, there were no significant main effects nor interactions of the factor model.

Table 4: Results of the MLM analysis for BOLD fit-statistics. The table is split for mean absolute error and R^2 score.

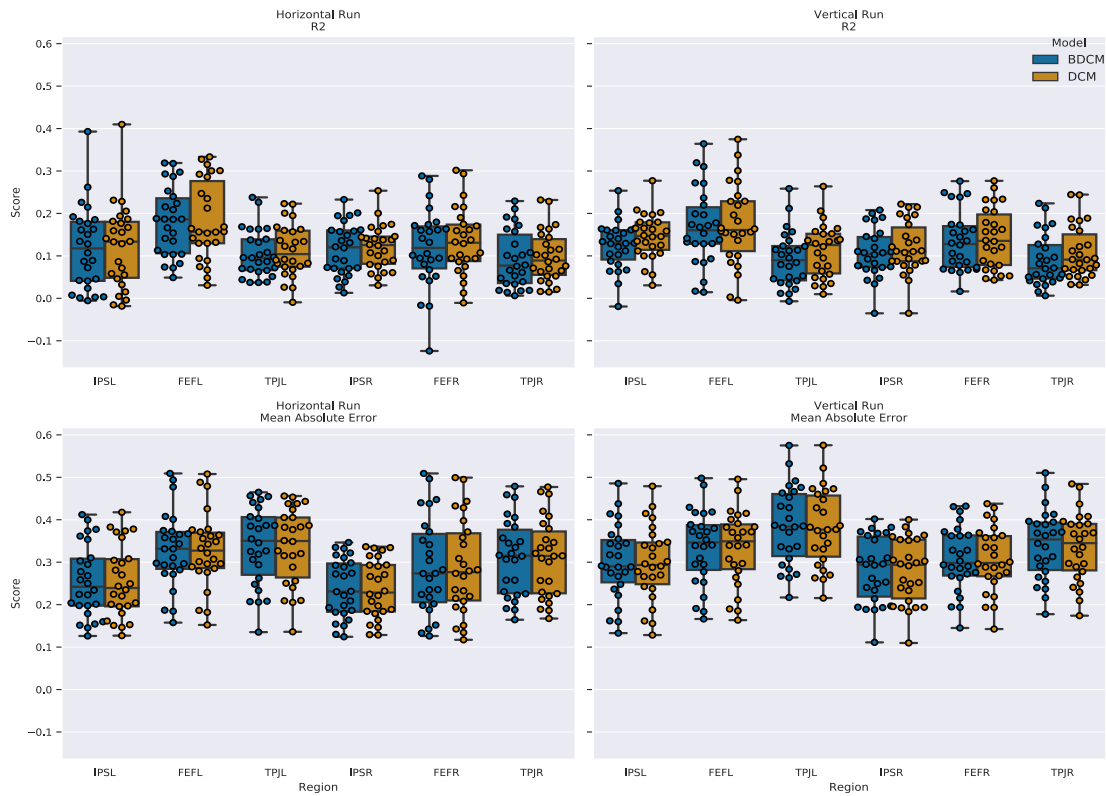|	R^2 Score				Mean Absolute Error			
	Coef.	Std.Err.	z	P>|z|	Coef.	Std.Err.	z	P>|z|
Intercept	0.176	0.012	14.986	< 0.001	0.317	0.014	22.720	< 0.001
DCM	0	0.013	-0.017	0.986	0	0.016	-0.021	0.983
FEF Right	-0.048	0.012	-3.879	< 0.001	-0.033	0.015	-2.189	0.029
IPS Left	-0.053	0.012	-4.268	< 0.001	-0.054	0.015	-3.574	< 0.001
IPS Right	-0.063	0.012	-5.109	< 0.001	-0.072	0.015	-4.764	< 0.001
TPJ Left	-0.075	0.012	-6.074	< 0.001	0.03	0.015	1.946	0.052
TPJ Right	-0.083	0.012	-6.727	< 0.001	-0.007	0.015	-0.436	0.663
Vertical Run	-0.003	0.007	-0.411	0.681	0.031	0.009	3.593	< 0.001
DCM * FEF Right	0.007	0.017	0.428	0.669	0	0.021	0.002	0.999
DCM * IPS Left	0.008	0.017	0.483	0.629	-0.001	0.021	-0.033	0.973
DCM * IPS Right	0.005	0.017	0.301	0.763	-0.001	0.021	-0.044	0.965
DCM * TPJ Left	0.01	0.017	0.552	0.581	-0.002	0.021	-0.087	0.93
DCM * TPJ Right	0.009	0.017	0.501	0.617	-0.001	0.021	-0.059	0.953
Vertical Run * DCM	0.008	0.01	0.801	0.423	-0.002	0.012	-0.137	0.891

Simultaneous modeling of a Spatial Cuing Task

Figure 7: Box plots for the different fit-statistics. Left column shows the data for the horizontal run, the right data for the vertical run. The upper row indicates the R^2 scores and the lower row the mean absolute error.

Simultaneous modeling of a Spatial Cuing Task

Generative Embedding

In this analysis, we tested how well the different models could separate the vertical and
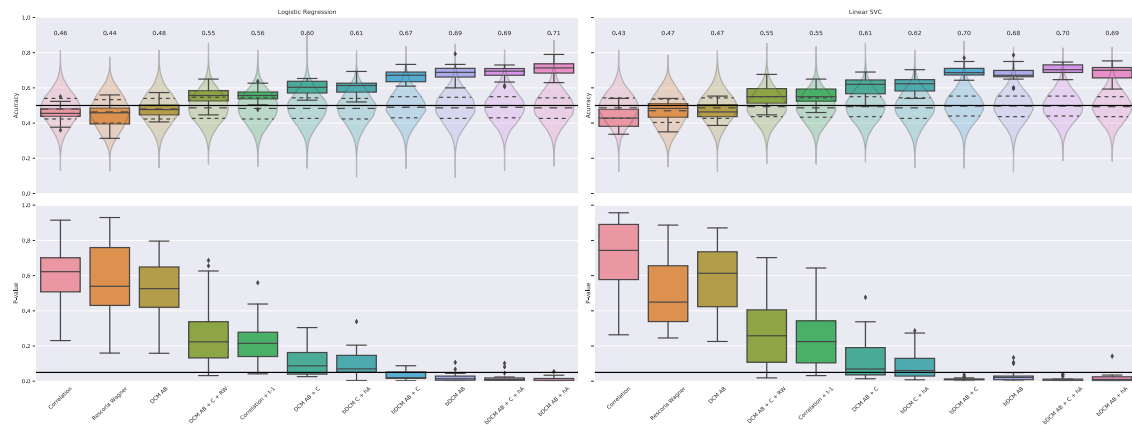
Figure 8: Classifier performance for the 20 shuffles of our dataset, sorted by average performance. In the upper row, the average performance and spread across iterations are shown, and transparent violin-plots indicate the distribution of permutation scores. In the lower panel, the distribution of permutation p-values is indicated, with the black line indicating the p < 0.05 cut-off.

horizontal runs from each other using two different kinds of machine learning algorithms. Due

to the high variability in our data (a very low number of training instances, difficult task), we

decided to shuffle the assignment of train-test folds so that the cross-validation was performed

multiple times. We assessed how often predictions of a classifier were significant (permutation

P-Value < 0.05) and calculated the average predictive accuracy. The horizontal run could not

be separated from the vertical run using combinations of features that were not derived from

bDCM parameters (see Figure 8). This indicated that bDCM provided us with some very minute

differences between the two runs, that were not included in other models or the BOLD signal.

Simultaneous modeling of a Spatial Cuing Task

Lesion Analysis
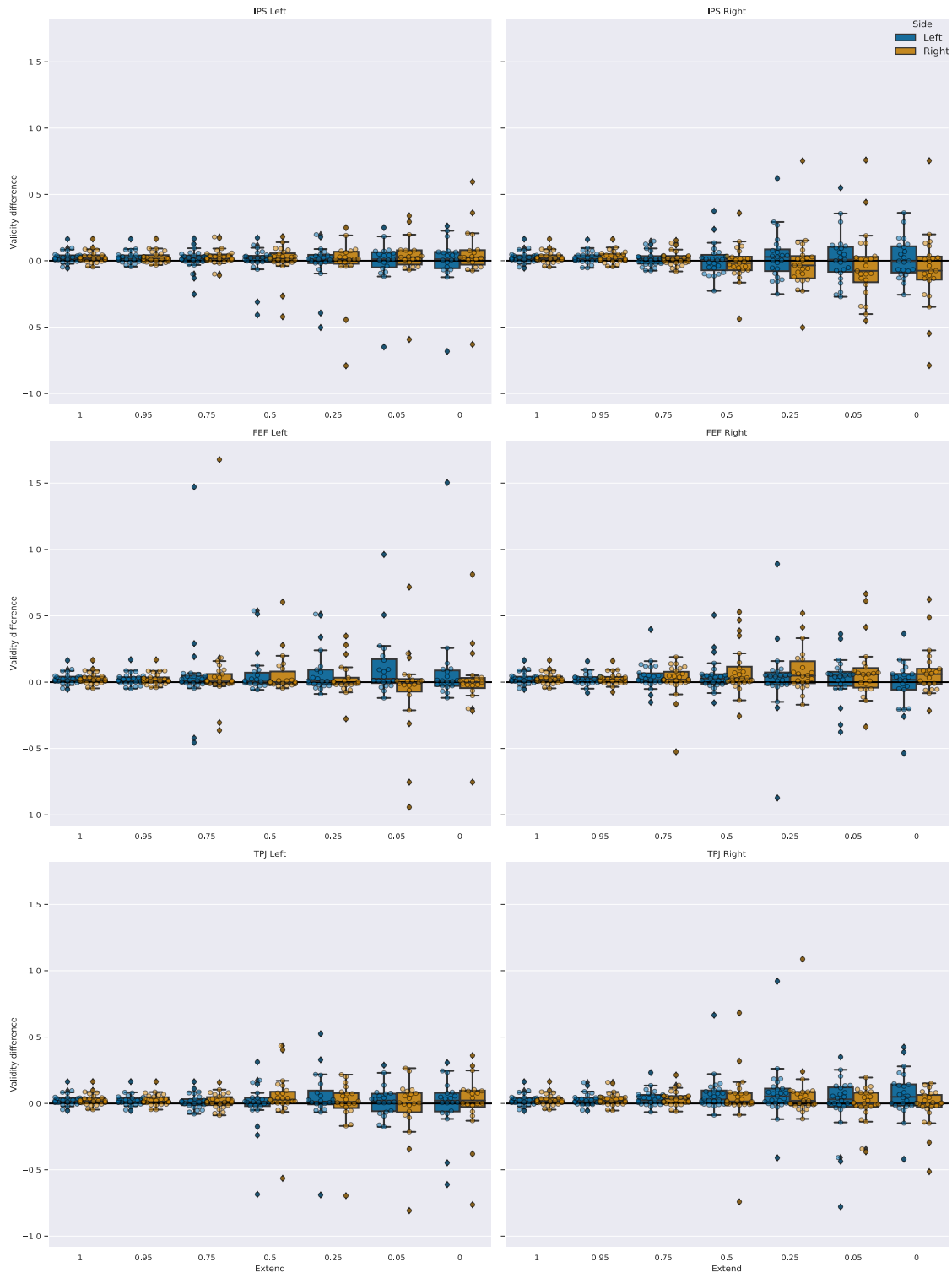
Figure 9: Validity effect for simulated reaction times for the horizontal run, after brain lesions of different extent. An extent of 1 means that no lesion occurred. An extent of 0 indicates that the region was fully disabled. Boxplots indicate the median of the data, the IQR, and the minimum and maximum values. Outliers exceed the 1.5 * IQR criterion.

Simultaneous modeling of a Spatial Cuing Task

Figure 9 depicts the results of the lesion analysis for the horizontal run (the vertical run can be found in the supplement). Constraining the self-connections in the model resulted in significant decreases in model fit of reaction time data in both the horizontal run (paired t-tests; MAE, $t(25) = 5.054$, $p < 0.001$, Cohen's $d = 0.197$; R^2-score, $t(25) = -6.573$, $p < 0.001$, Cohen's $d = 1.260$) and the vertical run (paired t-tests; MAE, $t(25) = 4.159$, $p < 0.001$, Cohen's $d = 0.175$; R^2-score, $t(25) = -7.185$, $p < 0.001$, Cohen's $d = 0.898$). Despite this note of caution, there were some interesting trends in the data. The effect of lesion extent on the validity effect seemed highly specific for the different network nodes with some lesions increasing and other lesion decreasing the validity effect, depending on the extend of the artificial lesion.

From a computational anatomy perspective, lesioning the TPJ yielded plausible effects, with a gradual increase in the contralesional validity effect following larger lesions.

Discussion

We applied bDCM (Rigoux & Daunizeau, 2015) to simultaneously model neural responses and reaction times in a spatial cueing task. We here demonstrated that bDCM could not only be applied to binary responses, but also to continuous read-outs (i.e., reaction times).

After reproducing previously published effects of cue validity at the behavioral and neural level, we modeled behavioral and functional imaging data in three different ways. BDCM, as a novel approach, was compared to both classical DCM and the behavioral Rescorla-Wagner model. As all three models serve different purposes and rely on different data on different timescales, we restricted the model comparison to the models' outputs and fit-statistics.

Although the original paper on bDCM suggested that incorporating behavior also leads to an advantage in representing the BOLD response of bDCM over classical DCM, we did not find significant differences between both modeling approaches. The benefit of including behavioral measures might only be prevalent when BOLD recordings are noisier than behavioral recordings (Rigoux & Daunizeau, 2015).

Simultaneous modeling of a Spatial Cuing Task

Furthermore, we compared simulated reaction times of bDCM and our implementation of the Rescorla-Wagner model (Vossel, Mathys, et al., 2014). BDCM had in general a better fit to reaction time data (reflected in higher R^2-score and lower error) and represented the distribution of reaction times more closely in both valid and invalid trials (reflected in significantly lower distances, which were calculated by the Kolmogorov-Smirnov test). Both the Rescorla-Wagner model and bDCM did not model the extreme ends of the reaction distributions well, however, bDCM deviated less from the measured data.

Note that this comparison was not performed to favor one model over the other. Instead, it was conducted to evaluate bDCM against the performance of a highly specialized, validated, and less complex model in a cueing task. Despite the superior fit of bDCM, the Rescorla-Wagner model performed extremely well, given the small number of parameters. Hence, if we penalized for model complexity, the Rescorla-Wagner model would probably be identified as the preferred model for reaction times. BDCM also incorporates the dynamics of the BOLD response and operates on a timescale of seconds, rather than trials. Thus, having only 8 parameters more than the classical DCM (69 parameters) seems to be an adequate increase in complexity. The resulting more detailed representation of reaction time distributions in bDCM might be useful to uncover relevant aspects for assessing cognitive functions as previously demonstrated for other modeling approaches. For example, parameters of drift-diffusion models of reaction times (Smith & Ratcliff, 2009) were found to be related to general intelligence (van Ravenzwaaij et al., 2011) and working memory (Schmiedek et al., 2007). Furthermore, distributional reaction time analysis may categorize healthy participants and patients suffering from psychiatric disorders (Kaiser et al., 2019; Karalunas et al., 2014; Vinogradov et al., 1998). The Rescorla-Wagner model could also be used for such differentiations, especially in the domain of belief-updating (Mengotti et al., 2017). By modeling a single cognitive process, however, the Rescorla-Wagner model is very dependent on the presence and size of a participant's validity effects (see analysis in S3, showing that the correlation between model fit and cue-validity are higher for Rescorla-Wagner than bDCM).

Simultaneous modeling of a Spatial Cuing Task

BDCM, in contrast, simulated smoother reaction time distributions (larger number of non-significant p-values in KS-test), possibly providing a richer representation of the underlying processes. Although bDCM may reflect a portion of variance in the reaction time data that is not task-related, this variance could reflect the processes of belief-updating in a more complex brain-dynamics-dependent matter. BDCM is a *model of brain dynamics* that can, in principle, be applied to any task, while the Rescorla-Wagner model represents a specialized *model of a cognitive process*.

As bDCM can be applied to model different behavioral read-outs in various tasks, it can enhance our understanding of how DCM's connectivity parameters relate to behavior. So far, this link could only be established using indirect methods, such as correlations between DCM parameters and behavioral measures across participants. For example, DCM's task connectivity parameters have been related to symptoms of depression and schizophrenia (Desseilles et al., 2011; Schlösser et al., 2008; Wu et al., 2014), and have been correlated with behavioral measures before and after interventions using non-invasive neurostimulation (Grefkes et al., 2010). Although the investigation of such associations does not allow causal interpretations, bDCM enables more firm conclusions how brain dynamics in selected brain regions impact behavior.

Furthermore, brain and behavioral dynamics both regularize bDCM, so that the model parameters encode the most reliable set of information from both sources (Rigoux & Daunizeau, 2015). This procedure could yield more robust and stable connectivity estimates but also encode more specific information. This may be particularly relevant for so-called "generative embedding" approaches, where a generative model and its estimated parameters are used as a form of dimensionality reduction (Brodersen, Haiss, et al., 2011; Brodersen, Schofield, et al., 2011). In fact, this was confirmed by our findings, where it was possible to differentiate the horizontal from the vertical run only when using the bDCM model's connectivity parameters. This makes bDCM a unique approach for the identification of biomarkers that are relevant for certain behaviors – provided that they are stable across participants and sessions (Elliott et al., 2020).

Simultaneous modeling of a Spatial Cuing Task

Since bDCM is a generative model, it can also be used to simulate how alterations to the underlying brain network might change behavior (Rigoux & Daunizeau, 2015). This allows simulating the behavioral effects of neuromodulatory interventions and the generation of new hypotheses and experiments. The guidance and information of computational models will eventually lead to a better understanding of the neural mechanisms underlying behavioral outcomes (Kriegeskorte & Douglas, 2018; Turner et al., 2017).

Unfortunately, applying artificial lesions to the network model in our study revealed technical problems of this approach. More specifically, the estimated models lacked numerical stability and required manual intervention, which substantially changed the model's output. Even though some of the resulting patterns were consistent with the literature (e.g., an increase of the contralesional validity effect after a lesion to right TPJ and to a lesser extent in left TPJ (Malherbe et al., 2018; Posner et al., 1984)), other simulations were highly variable. Hence, the relatively novel bDCM approach's potential problems, such as over-fitting and non-generalizability, need to be considered in future studies.

Conclusion

bDCM was applied for the first time to reaction time data of a larger sample of participants. Our findings provided evidence for a considerable additional value of the method compared to a purely behavioral model and classical DCM and identified practical use issues. Data suggest that bDCM is indeed a promising tool to enhance our understanding of how brain dynamics generate specific behavioral patterns.

References

Abraham, A., Pedregosa, F., Eickenberg, M., Gervais, P., Mueller, A., Kossaifi, J., Gramfort,
A., Thirion, B., & Varoquaux, G. (2014). Machine learning for neuroimaging with
scikit-learn. *Frontiers in Neuroinformatics*, *8*. https://doi.org/10.3389/fninf.2014.00014

Brodersen, K. H., Haiss, F., Ong, C. S., Jung, F., Tittgemeyer, M., Buhmann, J. M., Weber,
B., & Stephan, K. E. (2011). Model-based feature construction for multivariate

Simultaneous modeling of a Spatial Cuing Task

decoding. *NeuroImage*, *56*(2), 601–615.

https://doi.org/10.1016/j.neuroimage.2010.04.036

Brodersen, K. H., Schofield, T. M., Leff, A. P., Ong, C. S., Lomakina, E. I., Buhmann, J. M., &

Stephan, K. E. (2011). Generative Embedding for Model-Based Classification of fMRI

Data. *PLoS Computational Biology*, *7*(6), e1002079.

https://doi.org/10.1371/journal.pcbi.1002079

Bundesen, C. (1990). A theory of visual attention. *Psychological Review*, *97*(4), 523–547.

https://doi.org/10.1037/0033-295x.97.4.523

Corbetta, M., Kincade, M. J., Lewis, C., Snyder, A. Z., & Sapir, A. (2005). Neural basis and

recovery of spatial attention deficits in spatial neglect. *Nature Neuroscience, 8*(11),

1603–1610. https://doi.org/10.1038/nn1574

Corbetta, M., & Shulman, G. L. (2011). Spatial Neglect and Attention Networks. *Annual

Review of Neuroscience*, *34*(1), 569–599. https://doi.org/10.1146/annurev-neuro-

061010-113731

Crosse, M. J., Di Liberto, G. M., Bednar, A., & Lalor, E. C. (2016). The Multivariate Temporal

Response Function (mTRF) Toolbox: A MATLAB Toolbox for Relating Neural Signals

to Continuous Stimuli. *Frontiers in Human Neuroscience*, *10*.

https://doi.org/10.3389/fnhum.2016.00604

Daunizeau, J., Adam, V., & Rigoux, L. (2014). VBA: A Probabilistic Treatment of Nonlinear

Models for Neurobiological and Behavioural Data. *PLoS Computational Biology*,

10(1), e1003441. https://doi.org/10.1371/journal.pcbi.1003441

Desseilles, M., Schwartz, S., Dang-Vu, T. T., Sterpenich, V., Ansseau, M., Maquet, P., &

Phillips, C. (2011). Depression alters "top-down" visual attention: A dynamic causal

modeling comparison between depressed and healthy subjects. *NeuroImage*, *54*(2),

1662–1668. https://doi.org/10.1016/j.neuroimage.2010.08.061

Dombert, P. L., Kuhns, A., Mengotti, P., Fink, G. R., & Vossel, S. (2016). Functional

mechanisms of probabilistic inference in feature- and space-based attentional

Simultaneous modeling of a Spatial Cuing Task

systems. *NeuroImage*, *142*, 553–564.

https://doi.org/10.1016/j.neuroimage.2016.08.010

Eickhoff, S. B., Stephan, K. E., Mohlberg, H., Grefkes, C., Fink, G. R., Amunts, K., & Zilles,

K. (2005). A new SPM toolbox for combining probabilistic cytoarchitectonic maps and

functional imaging data. *NeuroImage*, *25*(4), 1325–1335.

https://doi.org/10.1016/j.neuroimage.2004.12.034

Elliott, M. L., Knodt, A. R., Ireland, D., Morris, M. L., Poulton, R., Ramrakha, S., Sison, M. L.,

Moffitt, T. E., Caspi, A., & Hariri, A. R. (2020). What Is the Test-Retest Reliability of

Common Task-Functional MRI Measures? New Empirical Evidence and a Meta-

Analysis. *Psychological Science*, 095679762091678.

https://doi.org/10.1177/0956797620916786

Esteban, O., Markiewicz, C. J., Blair, R. W., Moodie, C. A., Isik, A. I., Erramuzpe, A., Kent, J.

D., Goncalves, M., DuPre, E., Snyder, M., Oya, H., Ghosh, S. S., Wright, J., Durnez,

J., Poldrack, R. A., & Gorgolewski, K. J. (2019). fMRIPrep: A robust preprocessing

pipeline for functional MRI. *Nature Methods*, *16*(1), 111–116.

https://doi.org/10.1038/s41592-018-0235-4

Friston, K. J. (Ed.). (2007). *Statistical parametric mapping: The analysis of funtional brain*

images (1st ed). Elsevier/Academic Press.

Friston, K. J., Harrison, L., & Penny, W. (2003). Dynamic causal modelling. *NeuroImage*,

19(4), 1273–1302. https://doi.org/10.1016/S1053-8119(03)00202-7

Friston, K. J., Preller, K. H., Mathys, C., Cagnan, H., Heinzle, J., Razi, A., & Zeidman, P.

(2017). Dynamic causal modelling revisited. *NeuroImage*.

https://doi.org/10.1016/j.neuroimage.2017.02.045

Friston, K. J., Williams, S., Howard, R., Frackowiak, R. S. J., & Turner, R. (1996). Movement-

Related effects in fMRI time-series. *Magnetic Resonance in Medicine*, *35*(3), 346–

355. https://doi.org/10.1002/mrm.1910350312

Gorgolewski, K. J., Varoquaux, G., Rivera, G., Schwarz, Y., Ghosh, S. S., Maumet, C.,

Sochat, V. V., Nichols, T. E., Poldrack, R. A., Poline, J.-B., Yarkoni, T., & Margulies,

Simultaneous modeling of a Spatial Cuing Task

D. S. (2015). NeuroVault.org: A web-based repository for collecting and sharing unthresholded statistical maps of the human brain. *Frontiers in Neuroinformatics*, *9*. https://doi.org/10.3389/fninf.2015.00008

Grefkes, C., Nowak, D. A., Wang, L. E., Dafotakis, M., Eickhoff, S. B., & Fink, G. R. (2010). Modulating cortical connectivity in stroke patients by rTMS assessed with fMRI and dynamic causal modeling. *NeuroImage*, *50*(1), 233–242. https://doi.org/10.1016/j.neuroimage.2009.12.029

Hedge, C., Powell, G., & Sumner, P. (2017). The reliability paradox: Why robust cognitive tasks do not produce reliable individual differences. *Behavior Research Methods*. https://doi.org/10.3758/s13428-017-0935-1

Kaiser, D., Haeberle, G., & Cichy, R. M. (2019). *Cortical sensitivity to natural scene structure* [Preprint]. Neuroscience. https://doi.org/10.1101/613885

Karalunas, S. L., Geurts, H. M., Konrad, K., Bender, S., & Nigg, J. T. (2014). Annual Research Review: Reaction time variability in ADHD and autism spectrum disorders: measurement and mechanisms of a proposed trans-diagnostic phenotype. *Journal of Child Psychology and Psychiatry*, *55*(6), 685–710. https://doi.org/10.1111/jcpp.12217

Kriegeskorte, N., & Douglas, P. K. (2018). Cognitive computational neuroscience. *Nature Neuroscience*. https://doi.org/10.1038/s41593-018-0210-5

Malherbe, C., Umarova, R. M., Zavaglia, M., Kaller, C. P., Beume, L., Thomalla, G., Weiller, C., & Hilgetag, C. C. (2018). Neural correlates of visuospatial bias in patients with left hemisphere stroke: A causal functional contribution analysis based on game theory. *Neuropsychologia*, *115*, 142–153. https://doi.org/10.1016/j.neuropsychologia.2017.10.013

Mengotti, P., Dombert, P. L., Fink, G. R., & Vossel, S. (2017). Disruption of the Right Temporoparietal Junction Impairs Probabilistic Belief Updating. *The Journal of Neuroscience*, *37*(22), 5419–5428. https://doi.org/10.1523/JNEUROSCI.3683-16.2017

Simultaneous modeling of a Spatial Cuing Task

Nichols, T. E., & Holmes, A. P. (2002). Nonparametric permutation tests for functional

 neuroimaging: A primer with examples. *Human Brain Mapping*, *15*(1), 1–25.

Nunez, M. D. (2015). Individual differences in attention influence perceptual decision making.

 Frontiers in Psychology, *6.* https://doi.org/10.3389/fpsyg.2015.00018

Ojala, M., & Garriga, G. C. (2010). Permutation Tests for Studying Classifier Performance. *J.*

 Mach. Learn. Res., *11*, 1833–1863.

Oldfield, R. C. (1971). The assessment and analysis of handedness: The Edinburgh

 inventory. *Neuropsychologia*, *9*(1), 97–113. https://doi.org/10.1016/0028-

 3932(71)90067-4

Pedregosa, F., Varoquaux, G., Gramfort, A., Michel, V., Thirion, B., Grisel, O., Blondel, M.,

 Prettenhofer, P., Weiss, R., Dubourg, V., & others. (2011). Scikit-learn: Machine

 learning in Python. *The Journal of Machine Learning Research*, *12*, 2825–2830.

Peirce, J. W. (2007). PsychoPy—Psychophysics software in Python. *Journal of*

 Neuroscience Methods, *162*(1–2), 8–13.

 https://doi.org/10.1016/j.jneumeth.2006.11.017

Peirce, J. W. (2008). Generating stimuli for neuroscience using PsychoPy. *Frontiers in*

 Neuroinformatics, *2.* https://doi.org/10.3389/neuro.11.010.2008

Peirce, J. W., Gray, J. R., Simpson, S., MacAskill, M., Höchenberger, R., Sogo, H., Kastman,

 E., & Lindeløv, J. K. (2019). PsychoPy2: Experiments in behavior made easy.

 Behavior Research Methods, *51*(1), 195–203. https://doi.org/10.3758/s13428-018-

 01193-y

Posner, M. I. (1980). Orienting of attention. *The Quarterly Journal of Experimental*

 Psychology, *32*(1), 3–25.

Posner, M. I., Walker, J. A., Friedrich, F. J., & Rafal, R. D. (1984). Effects of parietal injury on

 covert orienting of attention. *The Journal of Neuroscience: The Official Journal of the*

 Society for Neuroscience, *4*(7), 1863–1874.

Ratcliff, R. (1978). A theory of memory retrieval. *Psychological Review*, *85*(2), 59–108.

 https://doi.org/10.1037/0033-295X.85.2.59

Simultaneous modeling of a Spatial Cuing Task

Rescorla, R. A., Wagner, A. R., & others. (1972). A theory of Pavlovian conditioning: Variations in the effectiveness of reinforcement and nonreinforcement. *Classical Conditioning II: Current Research and Theory*, *2*, 64–99.

Rigoux, L., & Daunizeau, J. (2015). Dynamic causal modelling of brain–behaviour relationships. *NeuroImage*, *117*, 202–221. https://doi.org/10.1016/j.neuroimage.2015.05.041

Schlösser, R. G. M., Wagner, G., Koch, K., Dahnke, R., Reichenbach, J. R., & Sauer, H. (2008). Fronto-cingulate effective connectivity in major depression: A study with fMRI and dynamic causal modeling. *NeuroImage*, *43*(3), 645–655. https://doi.org/10.1016/j.neuroimage.2008.08.002

Schmiedek, F., Oberauer, K., Wilhelm, O., Süß, H.-M., & Wittmann, W. W. (2007). Individual differences in components of reaction time distributions and their relations to working memory and intelligence. *Journal of Experimental Psychology: General*, *136*(3), 414–429. https://doi.org/10.1037/0096-3445.136.3.414

Shaw, D., Czekóová, K., Gajdoš, M., Staněk, R., Špalek, J., & Brázdil, M. (2019). Social decision-making in the brain: Input-state-output modelling reveals patterns of effective connectivity underlying reciprocal choices. *Human Brain Mapping*, *40*(2), 699–712. https://doi.org/10.1002/hbm.24446

Smith, P. L., & Ratcliff, R. (2009). An integrated theory of attention and decision making in visual signal detection. *Psychological Review*, *116*(2), 283–317. https://doi.org/10.1037/a0015156

Steinkamp, S. R., Vossel, S., Fink, G. R., & Weidner, R. (2020). Attentional reorientation along the meridians of the visual field: Are there different neural mechanisms at play? *Human Brain Mapping*, hbm.25086. https://doi.org/10.1002/hbm.25086

Stephan, K. E., Kasper, L., Harrison, L. M., Daunizeau, J., den Ouden, H. E. M., Breakspear, M., & Friston, K. J. (2008). Nonlinear dynamic causal models for fMRI. *NeuroImage*, *42*(2), 649–662. https://doi.org/10.1016/j.neuroimage.2008.04.262

Simultaneous modeling of a Spatial Cuing Task

Turner, B. M., Forstmann, B. U., Love, B. C., Palmeri, T. J., & Van Maanen, L. (2017).

Approaches to analysis in model-based cognitive neuroscience. *Journal of*

Mathematical Psychology, *76*, 65–79. https://doi.org/10.1016/j.jmp.2016.01.001

Vallat, R. (2018). Pingouin: Statistics in Python. *Journal of Open Source Software*, *3*(31),

1026. https://doi.org/10.21105/joss.01026

van Ravenzwaaij, D., Brown, S., & Wagenmakers, E.-J. (2011). An integrated perspective on

the relation between response speed and intelligence. *Cognition*, *119*(3), 381–393.

https://doi.org/10.1016/j.cognition.2011.02.002

Vinogradov, S., Poole, J. H., Willis-Shore, J., Ober, B. A., & Shenaut, G. K. (1998). Slower

and more variable reaction times in schizophrenia: What do they signify?

Schizophrenia Research, *32*(3), 183–190. https://doi.org/10.1016/S0920-

9964(98)00043-7

Vossel, S., Geng, J. J., & Fink, G. R. (2014). Dorsal and Ventral Attention Systems: Distinct

Neural Circuits but Collaborative Roles. *The Neuroscientist*, *20*(2), 150–159.

https://doi.org/10.1177/1073858413494269

Vossel, S., Mathys, C., Daunizeau, J., Bauer, M., Driver, J., Friston, K. J., & Stephan, K. E.

(2014). Spatial Attention, Precision, and Bayesian Inference: A Study of Saccadic

Response Speed. *Cerebral Cortex*, *24*(6), 1436–1450.

https://doi.org/10.1093/cercor/bhs418

Vossel, S., Weidner, R., Driver, J., Friston, K. J., & Fink, G. R. (2012). Deconstructing the

Architecture of Dorsal and Ventral Attention Systems with Dynamic Causal Modeling.

Journal of Neuroscience, *32*(31), 10637–10648.

https://doi.org/10.1523/JNEUROSCI.0414-12.2012

Vossel, S., Weidner, R., Moos, K., & Fink, G. R. (2016). Individual attentional selection

capacities are reflected in interhemispheric connectivity of the parietal cortex.

NeuroImage, *129*, 148–158. https://doi.org/10.1016/j.neuroimage.2016.01.054

Wu, G., Wang, Y., Mwansisya, T. E., Pu, W., Zhang, H., Liu, C., Yang, Q., Chen, E. Y. H.,

Xue, Z., Liu, Z., & Shan, B. (2014). Effective connectivity of the posterior cingulate

Simultaneous modeling of a Spatial Cuing Task

and medial prefrontal cortices relates to working memory impairment in schizophrenic

and bipolar patients. *Schizophrenia Research*, *158*(1–3), 85–90.

https://doi.org/10.1016/j.schres.2014.06.033

Yarkoni, T., Poldrack, R. A., Nichols, T. E., Van Essen, D. C., & Wager, T. D. (2011). Large-

scale automated synthesis of human functional neuroimaging data. *Nature Methods*,

8(8), 665–670. https://doi.org/10.1038/nmeth.1635

S1 Details for fMRIprep

The preprocessing of functional and anatomical data was performed using FMRIPREP version 1.1.1 (Esteban et al., 2018, 2019, RRID:SCR_016216), a Nipype (RRID:SCR_002502, Gorgolewski et al., 2011, 2017) based tool, run as a docker-image. Each T1-weighted volume (T1w) was corrected for intensity non-uniformity using N4BiasFieldCorrection v2.1.0 (Tustison et al., 2010) and skull-stripped using antsBrainExtraction.sh v2.1.0 (using the OASIS template). Spatial normalization to the ICBM 152 Nonlinear Asymmetrical template version 2009c (Fonov, Evans, McKinstry, Almli, & Collins, 2009, RRID:SCR_008796) was performed through nonlinear registration with the antsRegistration tool of ANTs v2.1.0 (Avants, Epstein, Grossman, & Gee, 2008, RRID:SCR_004757), using brain-extracted versions of both T1w volume and template. Brain tissue segmentation of cerebrospinal fluid (CSF), white matter (WM) and gray matter (GM) was performed on the brain-extracted T1w using fast (Zhang, Brady, & Smith, 2001, FSL v5.0.9, RRID:SCR_002823).

Functional data were slice-time corrected using 3dTshift from AFNI v16.2.07 (Cox, 1996, RRID:SCR_005927) and motion-corrected using mcflirt (FSL v5.0.9, Jenkinson, Bannister, Brady, & Smith, 2002). "Fieldmap-less" distortion correction was performed by co-registering the functional image to the same-subject T1w image with intensity inverted (Wang et al., 2017) constrained with an average fieldmap template (Treiber et al., 2016), implemented with antsRegistration (ANTs). This was followed by co-registration to the corresponding T1w using boundary-based registration (Greve & Fischl, 2009) with 9 degrees of freedom, using flirt (FSL). Motion correcting transformations, field distortion correcting warp, BOLD-to-T1w transformation, and T1w-to-template (MNI) warp were concatenated and applied in a single step using antsApplyTransforms (ANTs v2.1.0) using Lanczos interpolation.

Frame-wise displacement (Power et al., 2014) was calculated for each functional run using the implementation of Nipype.

Many internal operations of FMRIPREP use Nilearn (Abraham et al., 2014, RRID:SCR_001362), principally within the BOLD-processing workflow. For more details of the pipeline see http://fmriprep.readthedocs.io/en/1.1.1/workflows.html.

S2 fMRI – GLM analysis coordinates

Table 1 and Table 2 for the peak coordinates shown in Figure 4 of the main manuscript. The contrast invalid > valid is shown for each run of the fMRI experiment separately. To label the regions, we used the Harvard-Oxford atlas and reported the region with maximum probability.

Table S1: Peak statistics and clusters sizes for the horizontal T-map. Labels were automatically extracted from the Harvard-Oxford atlas, reporting the region with the highest probability from the coordinates.

Horizontal Run

Cluster ID	X	Y	Z	Peak Stat (T)	Cluster Size (mm3)	Label
1	-27.25	8.62	57.3	5.57	8056	Superior Frontal Gyrus
1a	-46	5.5	37.5	4.43		Inferior Frontal Gyrus, pars opercularis
1b	-24.12	2.38	73.8	3.85		Insular Cortex
1c	-39.75	-3.88	47.4	3.68		Inferior Frontal Gyrus, pars opercularis
2	29	2.38	54	5.56	4350	Superior Frontal Gyrus
2a	22.75	14.88	54	4.51		Insular Cortex

Cluster ID	X	Y	Z	Peak Stat (T)	Cluster Size (mm3)	Label
3	7.12	-69.5	57.3	5.4	15565	Cingulate Gyrus, posterior division
3a	-14.75	-75.75	57.3	4.77		Angular Gyrus
3b	-33.5	-75.75	34.2	4.57		Angular Gyrus
3c	-8.5	-60.12	47.4	4.41		Cingulate Gyrus, posterior division
4	-49.12	21.12	27.6	5.11	1998	Inferior Frontal Gyrus, pars triangularis
5	-33.5	-53.88	37.5	5.08	6123	Postcentral Gyrus, Supramarginal Gyrus, posterior division
5a	-42.88	-50.75	47.4	5.07		Supramarginal Gyrus, posterior division
5b	-30.38	-44.5	37.5	4.07		Supramarginal Gyrus, anterior division
6	-5.38	14.88	54	4.73	3222	Subcallosal Cortex
6a	7.12	24.25	54	4.11		Insular Cortex
7	41.5	27.38	24.3	4.5	3609	Superior Frontal Gyrus
7a	44.62	8.62	34.2	4.26		Inferior Frontal Gyrus, pars opercularis
7b	50.88	24.25	40.8	3.93		Superior Frontal Gyrus

Table S2: Peak statistics and clusters sizes for the vertical T-map. Labels were automatically extracted from the Harvard-Oxford atlas, reporting the region with the highest probability from the coordinates.

Vertical Run

Cluster ID	X	Y	Z	Peak Stat (T)	Cluster Size (mm3)	Label
1	60.25	-53.88	17.7	7.18	7927	Supramarginal Gyrus, posterior division
1a	54	-41.38	-2.1	5.62		Middle Temporal Gyrus, posterior division
1b	63.38	-38.25	-8.7	5.5		Middle Temporal Gyrus, posterior division
2	41.5	27.38	14.4	6.29	21269	Middle Frontal Gyrus
2a	44.62	5.5	30.9	5.81		Inferior Frontal Gyrus, pars opercularis
2b	41.5	33.62	24.3	5.01		Superior Frontal Gyrus
2c	29	-0.75	54	5		Superior Frontal Gyrus
3	7.12	21.12	54	6.09	4898	Insular Cortex
3a	-5.38	11.75	57.3	4.02		Insular Cortex
4	-36.62	-0.75	40.8	6	11053	Inferior Frontal Gyrus, pars opercularis
4a	-24.12	-13.25	54	5.02		Inferior Frontal Gyrus, pars opercularis
4b	-33.5	-3.88	57.3	4.84		Superior Frontal Gyrus
4c	-49.12	24.25	30.9	4.75		Superior Frontal Gyrus
5	38.38	-57	57.3	5.39	33612	Angular Gyrus
5a	-36.62	-53.88	47.4	5.23		Postcentral Gyrus
5b	19.62	-72.62	57.3	5.19		Angular Gyrus
5c	35.25	-60.12	44.1	5.19		Angular Gyrus
6	-39.75	21.12	-5.4	5.18	4382	Frontal Pole
6a	-33.5	24.25	1.2	4.89		Frontal Pole
6b	-27.25	18	-15.3	4.57		Cuneal Cortex

| 6c | -42.88 | 24.25 | 11.1 | 4.29 | Middle Frontal Gyrus |

S3 Correlation between fit-statistic and validity differences

To test whether the size of the validity effect influenced the resulting fit-statistic, we correlated (using Pearson's correlation) each permutation of error (R^2, mean absolute error), model (Rescorla-Wagner), and run with the validity difference (mean RT invalid – mean RT valid). The R^2-score was highly correlated with the validity difference, where the effect appeared to be stronger for the Rescorla-Wagner model than for the behavioral DCM. There was, however, no correlation with the mean absolute error (MAE).

Table S3: Pearson's Correlations between the validity difference and the different fit-statistics.

Model	Score	Run	r	adj_r2	p-value	BF$_{10}$
Rescorla Wagner	MAE	Horizontal	0.214	-0.037	0.294	0.410
		Vertical	0.112	-0.073	0.586	0.28
	R^2	Horizontal	0.817	0.639	< 0.001	$5.06 * 10^7$
		Vertical	0.854	0.706	< 0.001	$4.86 * 10^8$
BDCM	MAE	Horizontal	0.232	-0.028	0.253	0.452
		Vertical	0.108	-0.074	0.600	0.277
	R^2	Horizontal	0.719	0.475	< 0.001	795.149
		Vertical	0.789	0.589	< 0.001	$1.22 * 10^7$
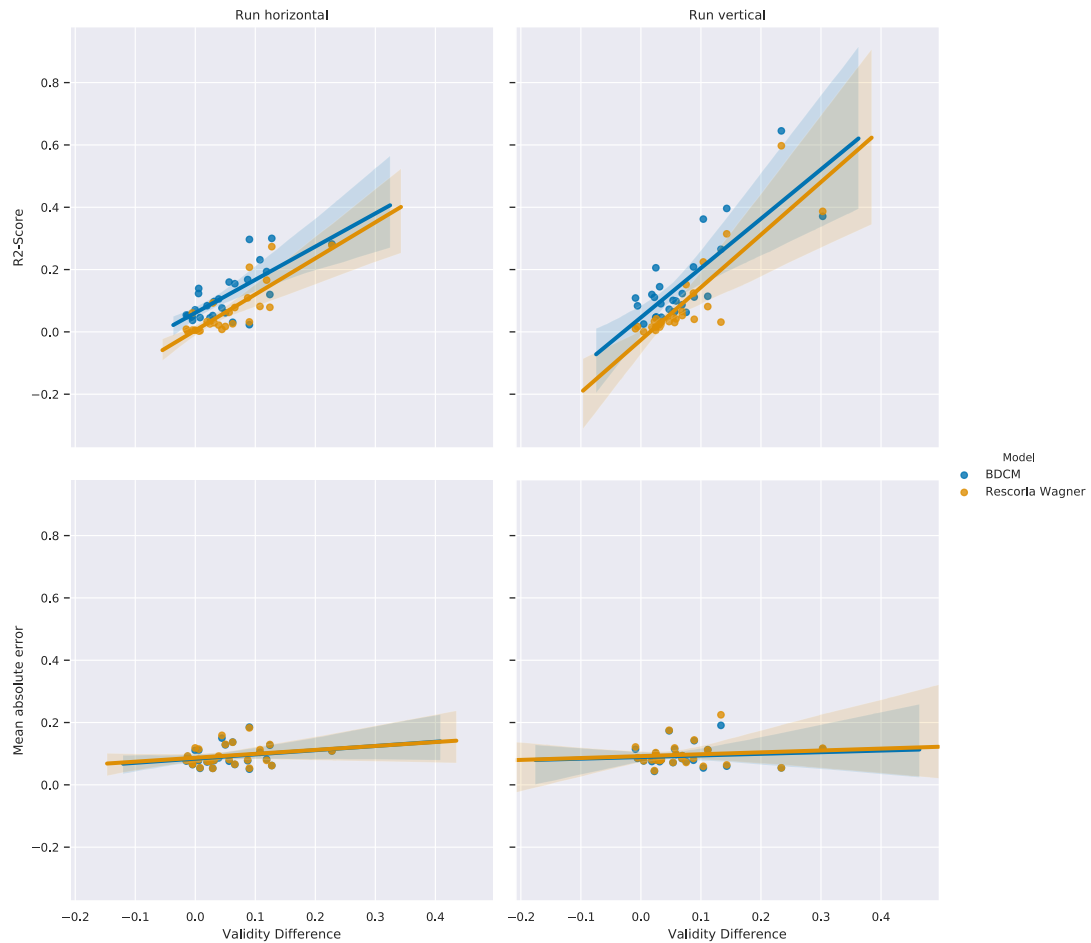
Figure S1: Pearson correlation between the validity difference (y-axis) and the fit-statisti axis) for the two models, the different metrics (rows), and the two runs (columns).

S4 Lesion analysis additional reporting

We used a similar approach as before to compare the fit-statistics between the data with an increased self-inhibition and the regular models. The dampened model performed significantly worse than the original models, with the R2-score being particularly affected, while the mean absolute error remained relatively stable. This analysis showed why we ought to be cautious in the analysis of the lesion data results.

Figure S2 is the analog to Figure 9 in the main manuscript, for lesions simulated for up-wards and down-wards orienting.
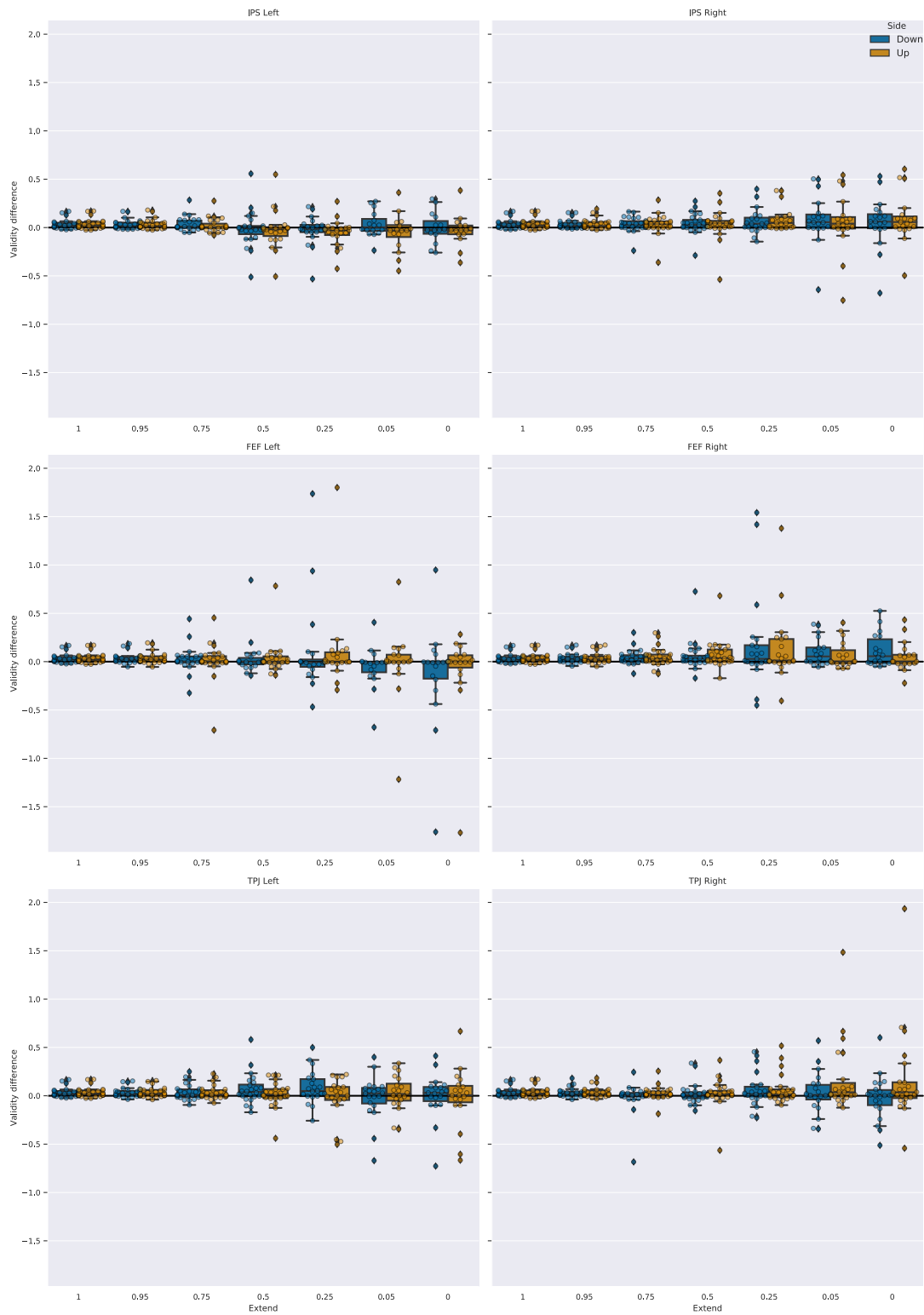
Figure S2: Validity effect for simulated reaction times for the vertical run, after brain lesions of di extent. An extent of 1 means that no lesion occurred, an extent of 0 indicates that the region w disabled. Boxplots indicate the median of the data, the IQR, and the minimum and maximum Outliers exceeded the 1.5 * IQR criterion.

S5 Connectivity matrices

Figures S3-S6 displays the average connectivity strength of the (behavioral) dynamic causal modeling analysis. Connectivity parameters were averaged across participants. Inhibitory connections (A matrix diagonal) were exponentiated before averaging.
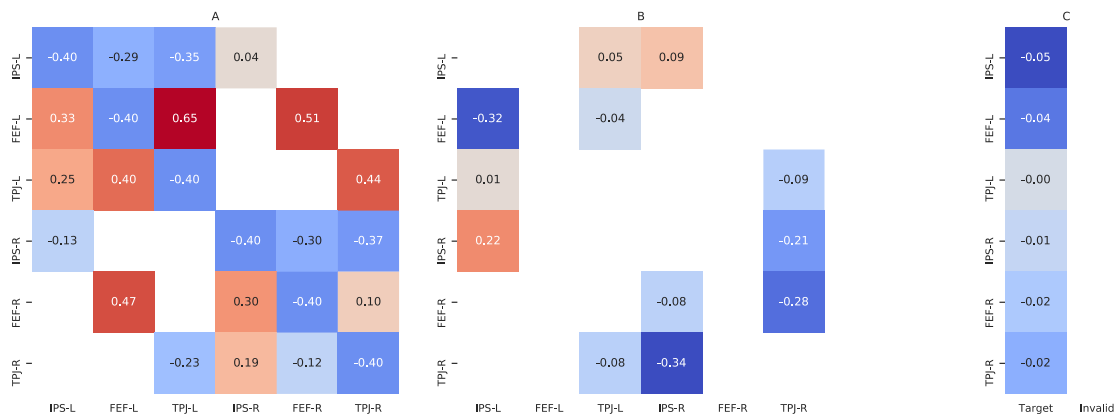
Figure S3: The average strength of the DCM connectivity parameters of the horizontal run.
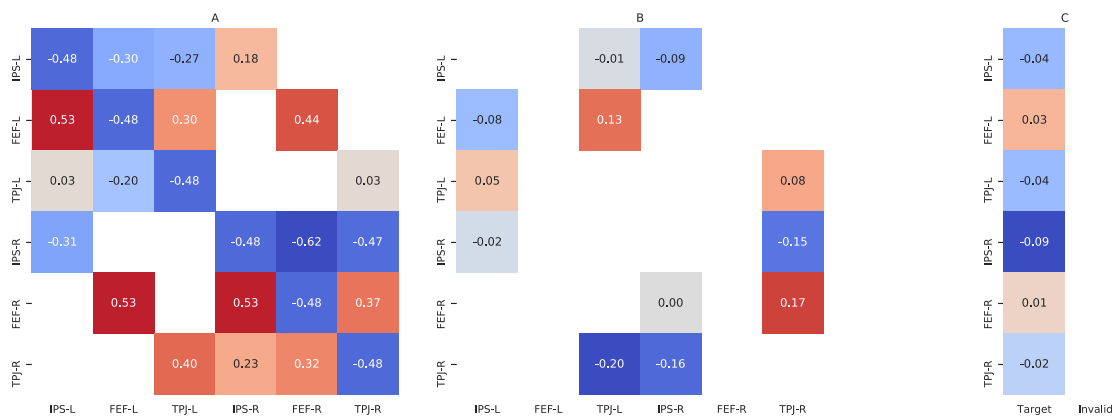
Figure S4: The average strength of the DCM connectivity parameters of the vertical run.
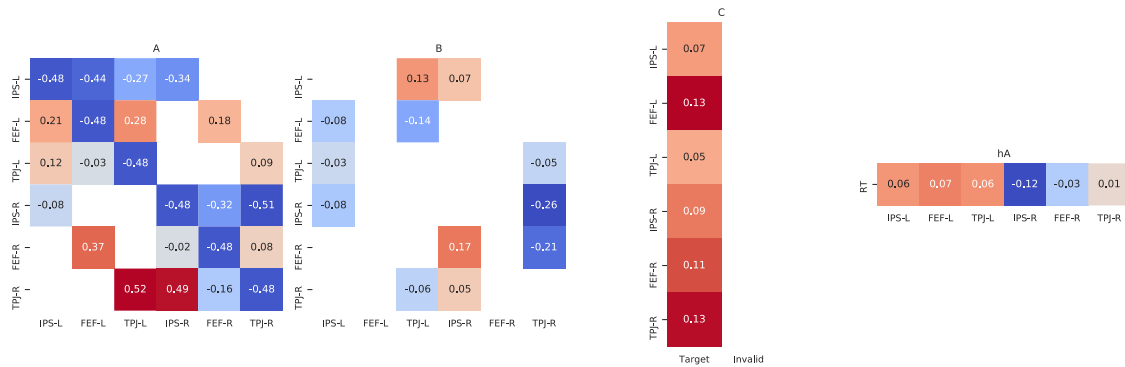
Figure S5: The average strength of the bDCM connectivity parameters of the horizontal run
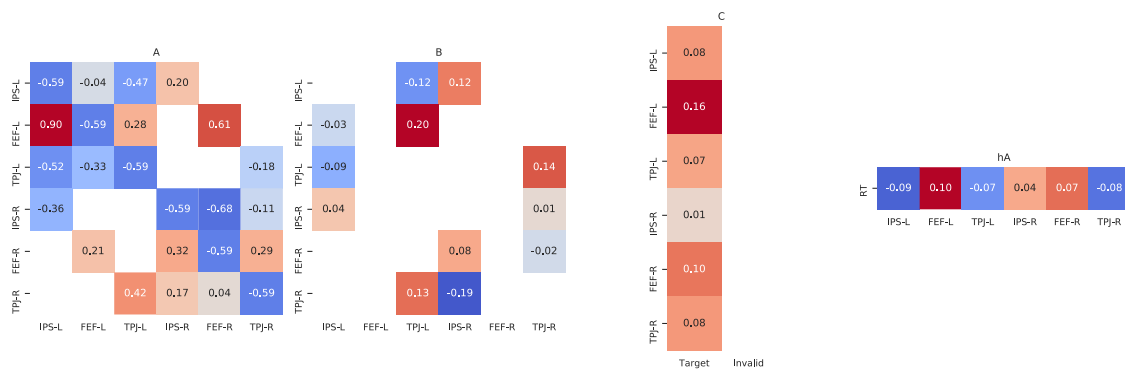
Figure S6: The average strength of the bDCM connectivity parameters of the vertical run.

References

Abraham, A., Pedregosa, F., Eickenberg, M., Gervais, P., Mueller, A., Kossaifi, J., … Varoquaux, G. (2014). Machine learning for neuroimaging with scikit-learn. *Frontiers in Neuroinformatics*, *8*. doi: 10.3389/fninf.2014.00014

Avants, B., Epstein, C., Grossman, M., & Gee, J. (2008). Symmetric diffeomorphic image registration with cross-correlation: Evaluating automated labeling of elderly and neurodegenerative brain. *Medical Image Analysis*, *12*(1), 26–41. doi: 10.1016/j.media.2007.06.004

Cox, R. W. (1996). AFNI: Software for Analysis and Visualization of Functional Magnetic Resonance Neuroimages. *Computers and Biomedical Research*, *29*(3), 162–173. doi: 10.1006/cbmr.1996.0014

Esteban, O., Blair, R., Markiewicz, C. J., Berleant, S. L., Moodie, C., Ma, F., … Gorgolewski, K. J. (2018, July 31). *Poldracklab/Fmriprep: 1.1.3*. Zenodo. doi: 10.5281/zenodo.1323934

Esteban, O., Markiewicz, C. J., Blair, R. W., Moodie, C. A., Isik, A. I., Erramuzpe, A., … Gorgolewski, K. J. (2019). fMRIPrep: A robust preprocessing pipeline for functional MRI. *Nature Methods*, *16*(1), 111–116. doi: 10.1038/s41592-018-0235-4

Fonov, V., Evans, A., McKinstry, R., Almli, C., & Collins, D. (2009). Unbiased nonlinear average age-appropriate brain templates from birth to adulthood. *NeuroImage*, *47*, S102. doi: 10.1016/S1053-8119(09)70884-5

Gorgolewski, K. J., Burns, C. D., Madison, C., Clark, D., Halchenko, Y. O., Waskom, M. L., & Ghosh, S. S. (2011). Nipype: A Flexible, Lightweight and Extensible Neuroimaging Data Processing Framework in Python. *Frontiers in Neuroinformatics*, *5*. doi: 10.3389/fninf.2011.00013

Gorgolewski, K. J., Esteban, O., Ellis, D. G., Notter, M. P., Ziegler, E., Johnson, H., … Ghosh, S. (2017, May 21). *Nipype: A Flexible, Lightweight And Extensible Neuroimaging Data Processing Framework In Python. 0.13.1*. Zenodo. doi: 10.5281/zenodo.581704

Greve, D. N., & Fischl, B. (2009). Accurate and robust brain image alignment using boundary-based registration. *NeuroImage*, *48*(1), 63–72. doi: 10.1016/j.neuroimage.2009.06.060

Jenkinson, M., Bannister, P., Brady, M., & Smith, S. (2002). Improved Optimization for the Robust and Accurate Linear Registration and Motion Correction of Brain Images. *NeuroImage*, *17*(2), 825–841. doi: 10.1006/nimg.2002.1132

Power, J. D., Mitra, A., Laumann, T. O., Snyder, A. Z., Schlaggar, B. L., & Petersen, S. E. (2014). Methods to detect, characterize, and remove motion artifact in resting state fMRI. *NeuroImage*, *84*, 320–341. doi: 10.1016/j.neuroimage.2013.08.048

Treiber, J. M., White, N. S., Steed, T. C., Bartsch, H., Holland, D., Farid, N., … Chen, C. C. (2016). Characterization and Correction of Geometric Distortions in 814 Diffusion Weighted Images. *PLOS ONE*, *11*(3), e0152472. doi: 10.1371/journal.pone.0152472

Tustison, N. J., Avants, B. B., Cook, P. A., Yuanjie Zheng, Egan, A., Yushkevich, P. A., & Gee, J. C. (2010). N4ITK: Improved N3 Bias Correction. *IEEE Transactions on Medical Imaging*, *29*(6), 1310–1320. doi: 10.1109/TMI.2010.2046908

Wang, S., Peterson, D. J., Gatenby, J. C., Li, W., Grabowski, T. J., & Madhyastha, T. M. (2017). Evaluation of Field Map and Nonlinear Registration Methods for Correction of Susceptibility Artifacts in Diffusion MRI. *Frontiers in Neuroinformatics*, *11*. doi: 10.3389/fninf.2017.00017

Zhang, Y., Brady, M., & Smith, S. (2001). Segmentation of brain MR images through a hidden Markov random field model and the expectation-maximization algorithm. *IEEE Transactions on Medical Imaging*, *20*(1), 45–57. doi: 10.1109/42.906424

8 | Behavioral DCM Additional Analysis

One of the interesting results in *"Simultaneous Modeling of Reaction Times and Brain Dynamics in a Spatial Cuing Task"*, is that I could separate vertical and horizontal runs using behavioral dynamic causal modeling (bDCM) parameters, which was not possible in previous analyses (Steinkamp, Vossel, et al., 2020). In this chapter I will further explore which of bDCM's parameters are important for the classification and further interrogate bDCM and Rescorla-models.

8.1 Features Differentiating Horizontal and Vertical Orienting

In Figure 7.8 of Steinkamp, Fink, et al. (2020), I found that the sum of intrinsic (A matrix) and modulatory (B matrix) effective connectivity parameters of bDCM encode necessary information to separate vertical and horizontal runs. The addition of parameters mapping to the behavioral response (hA) further improved classification performance and a smaller additional performance boost can be gained by including parameters representing input encoding (C).
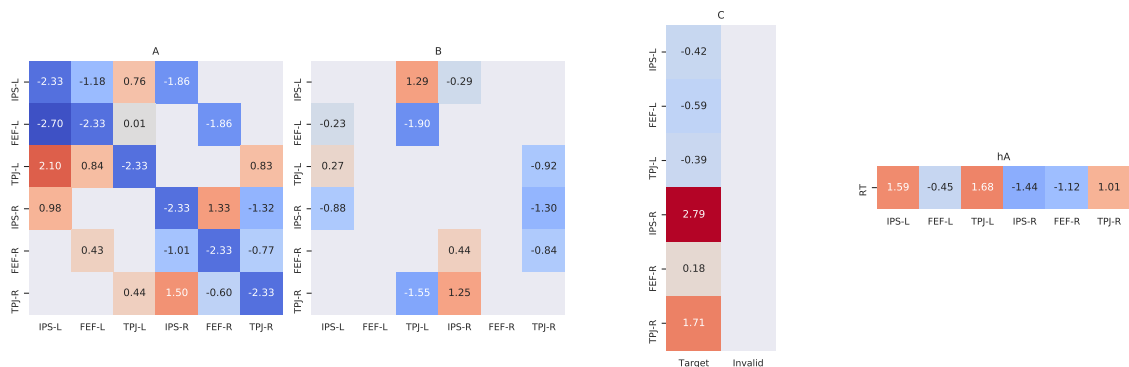
Figure 8.1: T-values of paired t-tests between bDCM parameters in the vertical and horizontal run. Where $t(25) = 2.787$ is the cut-off for $p < 0.01$ (two-tailed) uncorrected.

The first analyses should elucidate, how effective connectivity of brain regions differs between bDCM and DCM. In Figure 8.1, we see a paired t-test between the bDCM parameters of horizontal and vertical runs. Interestingly, there is only one significant difference in parameters of the C matrix, indicating that right intraparietal sulcus (IPS) receives a larger input in the horizontal run when compared to the vertical run — please note, that the sum of A and B matrices entered the classification analysis and not the separate matrices investigated here.

In the DCM analysis alone, we find a significant difference in the C matrix, related to input in the left frontal eye-fields (FEF) (Figure 8.2), indicating that in the horizontal run, there is less direct modulation when targets are presented. Especially, the relatively low t-values in the B-matrices seem to represent the results of Steinkamp, Vossel, et al. (2020), where no differences in effective connectivity between the two runs could be found.
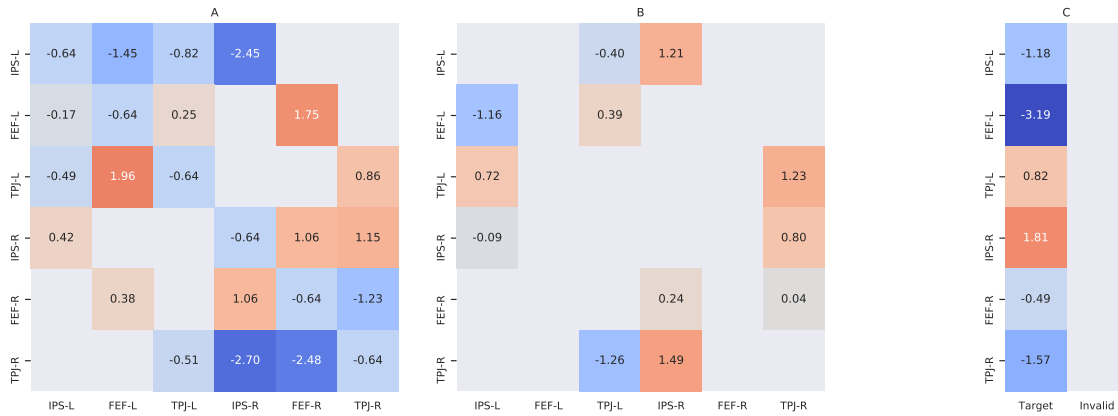
Figure 8.2: T-values of paired t-tests between DCM parameters in the vertical and horizontal run. Where $t(25) = 2.787$ is the cut-off for $p < 0.01$ (two-tailed) uncorrected.

Table 8.1: The top five important features. For the training set (left) and for the hold-out set (right). Edge connections (like "IPS-R to TPJ-R") indicate important features in the $A + B$ matrix, for other features the corresponding matrix name is used as a prefix (e.g. "hA_TPJ-R).

Features	Importance	Std	Features	Importance	Std
TPJ-R to IPS-R	0.108	0.039	IPS-R to TPJ-R	0.020	0.080
IPS-R to TPJ-R	0.100	0.043	hA_IPS-L	0.018	0.080
hA_IPS-L	0.081	0.032	IPS-L to TPJ-L	0.012	0.066
IPS-R to IPS-L	0.074	0.039	IPS-R to IPS-L	0.010	0.068
hA_TPJ-L	0.073	0.031	hA_TPJ-R	0.010	0.052

   Based on the previous inference approaches, namely the paired t-test and the classification analysis in Steinkamp, Fink, et al. (2020), we still cannot conclude, which connections are important for the separation of the two runs (Bzdok et al., 2020).
   One way to estimate the contribution of each feature to the classification result is called permutation importance, which is implemented in scikit-learn (Pedregosa et al., 2011). Each feature's contribution is estimated by shuffling (permuting) the feature and calculating the performance difference between the unperturbed and shuffled inputs (Breiman, 2001). Model fitting and calculation of feature importance followed the same rational as in Steinkamp, Fink, et al. (2020), where I aggregated results over twenty different five-fold cross-validation sets. Note in Table 8.1 that performance differences between the training and test sets differ by an order of magnitude and that the standard deviations are very large in the test-sets. This is most likely due to a larger variance in the small test sets of 5 participants. Still, the generalization importance on the right side is more important for our interpretation.

8.2   Generalization

In Chapter 4, I discussed some requirements for a good computational model. Similarly to machine learning models, computational models should generalize to unseen data, and in the best case should be applicable to new conditions (Bzdok et al., 2018; Kriegeskorte & Douglas, 2018).
   Testing how the computational performance in new situations, additionally provides us with a great tool to derive new hypothesis and guide new experiments through in silico

simulations (Navarro, 2020; Smaldino, 2020).

Although applying Bayesian methods as a form of regularization and being a generative model, the DCM framework is more of a scaffolding to allow for interindividual differences of participants. Thus, even though the network architecture might be the same for the modeled task, parameters can differ widely, leading to poor generalization. We see this in Figure 8.3, where bDCM does not generalize well from the horizontal to the vertical run and vice versa. The models' fit of the blood oxygen level-dependent (BOLD) response, appears to have a higher confidence than the behavioral run, which might be another sign for a large trial-to-trial variance in reaction times, which were discussed in the second publication.
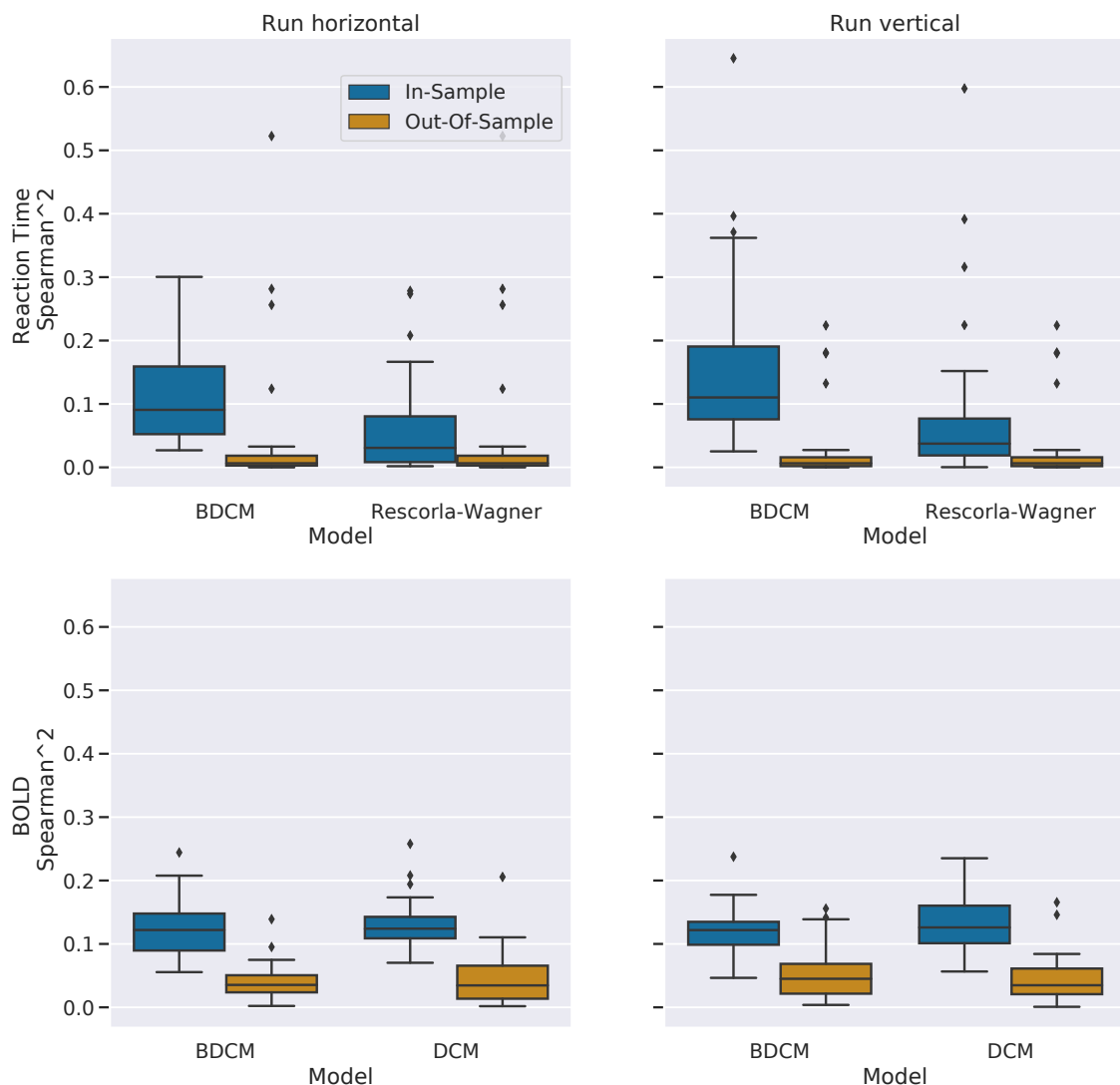
Figure 8.3: Out-of-sample predictions of bDCM, DCM, and the Rescorla-Wagner model. Pearson's squared correlation coefficient is provided as an estimate of how well each of the models generalizes to the other run (Out-of-Sample), when compared to the model fitted on the same data (In-Sample). The squared Pearson correlation coefficient was used over the R^2 score, as we care more about the general dynamics of the prediction, rather than the prediction of actual values. Why the R^2 is generally preferred is discussed in Poldrack et al. (2019).

8.3   New Situations

A more interesting question, is how bDCM can be used in new situations, which means stepping on the intervention rung of Pearl's causal ladder. A straightforward new situation is to change the cue-validity. Based on studies performed by Dombert et al. (2016) and Vossel et al. (2006), we would predict, that the validity effect increases with higher cue-validity, as it induces larger prediction errors. Again, the Rescorla-Wagner model can be used in direct comparison, as it explicitly models how participants update their internal state of the cue-validity through the learning rate (α) — which might be stable across runs. Indeed, the Rescorla-Wagner performs as predicted, showing monotonic increase in the validity difference with increasing cue-validity (Figure 8.4). bDCM, however, predicts a clear improvement in average reaction times with higher cue-validity, but does not show the predicted increase in the validity difference.
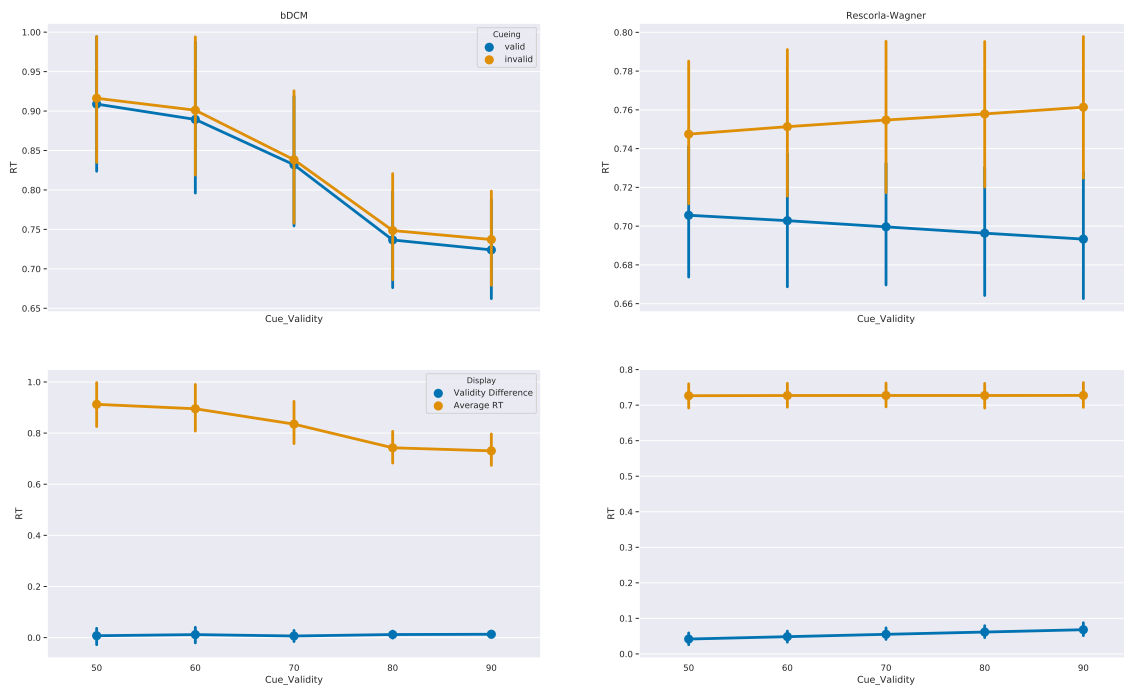
Figure 8.4: Simulations for bDCM and the Rescorla-Wagner model when varying the cue-validity of the inputs. In case of bDCM the input was again centered. Data is pooled across the vertical and horizontal run. The upper row shows how the general reaction times develop along the different cuing levels, the lower row shows the averaged reaction time (across cuing levels) and the validity differences. Note, that each sub-plot has a different y-axis!

9 | Summaries

9.1 Attentional Orienting Along the Horizontal and Vertical Meridian

In *"Attentional reorientation along the meridians of the visual field: Are there different neural mechanisms at play?"*, Steinkamp, Vossel, et al. (2020), I investigated how horizontal and vertical orienting and reorienting is represented in the dorsal and ventral attention networks when participants perform Posner's cuing task. For this, I designed an experiment where participants oriented their attention in two runs either only along the vertical or horizontal meridian. Distractor stimuli, however, always appeared in all non-target positions at the four cardinalities, ensuring that perceptual qualities were the same between the two runs. Initially, I expected differences in blood oxygen level-dependent (BOLD) amplitude levels, as clinical conditions like neglect, which are more prevalent along the horizontal meridian, indicate that there are differences between stimulus processing along the two meridians. Not seeing these results, however, I used Bayesian inference and machine learning methods on the volume of interest (VOI) level, to establish, whether there truly is no effect. Additionally, I relied on dynamic causal modeling (DCM) for the analysis of connectivity differences in reorienting during the vertical and horizontal run. Even based on these more advanced analysis, I could not establish, differential activity between the two tasks.

Based on these findings, I concluded that a horizontal-vertical anisotropy (HVA), often observed in visual perception task, is probably due to intricacies of the visual system and do not play a major role in spatial cuing tasks. Furthermore, I discussed the possibility that attentional reorienting is not governed by spatial, but by higher order cognitive processes.

9.2 Simultaneous Modeling of Brain and Behavior

In *"Simultaneous Modeling of Reaction Times and Brain Dynamics in a Spatial Cuing Task"*, I used the same data as in the study before, to create an *integrative* model (B. M. Turner et al., 2017) of brain and behavioral responses (behavioral dynamic causal modeling (bDCM)), which I compared to single modality models (DCM, Rescorla-Wagner model). In a first step, I was able to show that bDCM could model responses at least as well as the single modality models. Because DCM and bDCM have the same conceptual basis, I did not further investigate the modeling of functional magnetic resonance imaging (fMRI) data, but focused instead on the modeling of reaction time data, which was the novel aspect of the study. I found that when compared to the Rescorla-Wagner model, bDCM provides a better representation of the reaction time distribution. As bDCM is a network model of brain dynamics and behavior, we can use the framework to see how interference with the underlying brain network changes behavioral outputs. Unfortunately, the insertion of artificial lesions proved more difficult than expected. On the other hand, I could show that bDCM encodes more information than the other modalities, allowing the differentiation of vertical from horizontal orienting.

10 | Discussion

In my first study I used an adapted version of Posner's cuing task to investigate whether attentional processes differ along the visual field's meridians. In the second study I used the same data to explore a new computational modeling framework. Although both studies share the same underlying data, their approaches and goals are very different, so I decided to split the discussion into a *Visual Attention* and a *Computational Modeling* part. However, in the first study I also applied dynamic causal modeling (DCM) in a novel way, whereas in the second study I investigated horizontal and vertical orienting further, so I will try to discuss both studies in each part of the discussion.

10.1 Visual Attention

The first project's main finding is a null-result: There are no significant differences between vertical and horizontal attentional orienting and reorienting regarding behavioral and neural data, replicating results of previous studies investigating endogenous cuing along the meridians (Macaluso & Patria, 2007; Rizzolatti et al., 1987).

10.1.1 Horizontal-vertical anisotropy

This null-finding can be surprising at a first glance, due to observations of pseudo-neglect (Jewell & McCourt, 2000; Nicholls et al., 2004) and other studies reporting a strong horizontal-vertical anisotropy (HVA) and visual field asymmetries (Carrasco et al., 2001; Lemos et al., 2016; Mao et al., 2007). Furthermore, as altitudinal neglect appears to be rare in comparison to hemispatial neglect (Beume et al., 2017; Heilman et al., 2000; Karnath et al., 2011), I assumed there would be special components to horizontal versus vertical reorienting of attention. While this is true, these differences are likely caused by our visual system and are not due to attentional differences. This was elegantly shown by Carrasco et al. (2001), who conducted multiple experiments using orientation discrimination, detection, and localization tasks with Gabor stimuli (which were also used in my experiment) at cardinal and oblique positions. They found that exogenous cuing leads to a better performance overall, but did not interact with location, or other visual manipulations. The HVA, however, could be manipulated by changing a stimulus' perceptual qualities (spatial frequency, eccentricity). As the HVA's extend is correlated with the distribution of retinal Ganglion cells and photoreceptors, they concluded that asymmetrical performance patterns along horizontal and vertical meridians is due to properties of our visual system (Carrasco et al., 2001).

10.1.2 Perceptual asymmetries

Carrasco et al. (2001) also describe a vertical meridian asymmetry, where acuity is better in the lower visual field when compared to the upper visual field. This non-uniform distribution of visual acuity, was referred to as visual performance fields (see left of Figure 10.1, after Barbot et al., 2020).

Next to upper-lower visual field asymmetries, left-right asymmetries have also been reported. Mao et al. (2007) for example describe faster reaction times to targets in the left visual field in a cued detection task. Since I pooled data across the meridians, it might
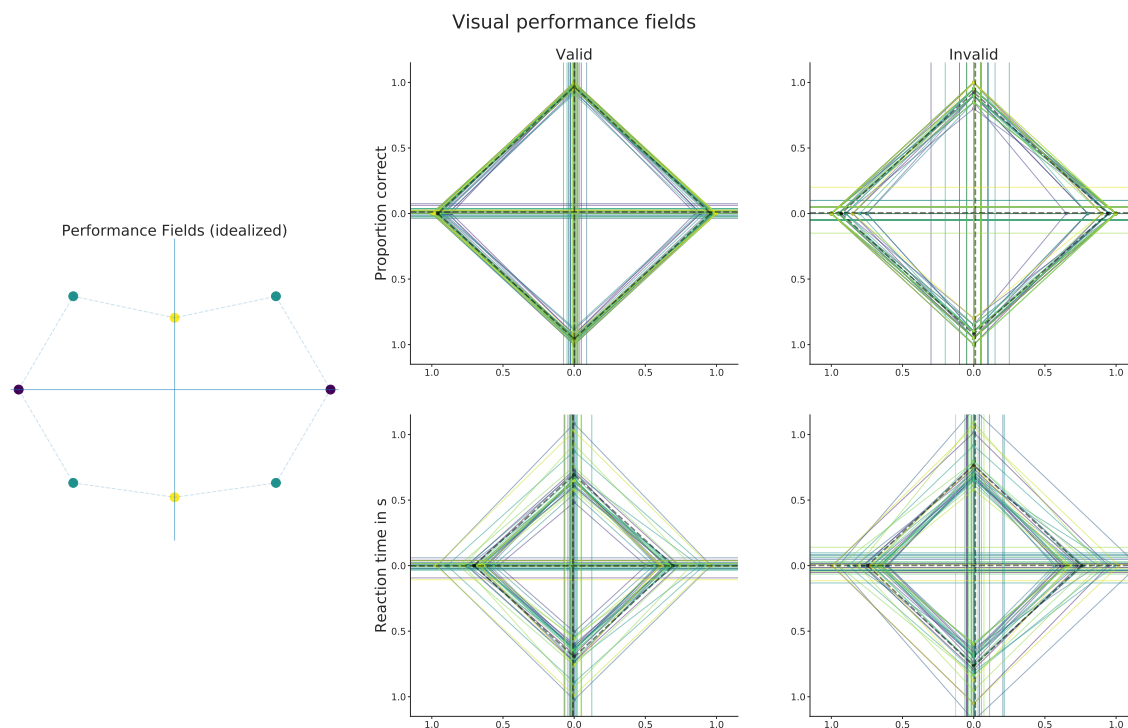
Figure 10.1: Visual performance fields in Steinkamp, Fink, et al. (2020). On the left are idealized visual performance fields for detection tasks, inspired by Barbot et al. (2020): Performance is best along the horizontal meridian, and worst along the vertical meridian, especially in the upper visual field. On the right data from my studies is shown. In the upper row proportions of correct trials are provided, the lower row describes reaction times in seconds. The left column displays valid and the right invalid trials. Diamonds describe the averaged performance of individual participants to targets at the given cardinality. Vertical lines describe the left-right asymmetries, whereas horizontal lines indicate the upper-lower asymmetry. Black dashed lines are the group-average. Albeit large individual differences and asymmetries, there appears to be no overall asymmetry on the group level.

be possible that I averaged out within meridian asymmetries. To test for these effects, I analyzed our data regarding location specific effect in my first and second project. Using frequentist mixed effects models, I found a weak interaction between stimulus location and attentional cuing in Steinkamp, Fink, et al. (2020), a main effect of cuing, but no main effect of spatial location. In a previous analysis (not reported) in the first study, I however, only found a main effect of cuing. As the latter analysis included two more participants and used Bayesian methods, the observed interaction in the second study might not be as reliable. See also Figure 10.1, which shows large individual differences in within meridian asymmetries, but no group effect.

Although I have not found behavioral evidence for attentional asymmetries in the spatial cuing task, it is useful for our further discussion to elucidate visual field asymmetries along the vertical and horizontal meridians. As alluded to, Carrasco et al. (2001) attribute lower and upper visual field asymmetries to physiological restrictions of the visual system. The extent of these performance fields, can be probed by increasing a stimulus' eccentricity. Visual acuity decreases more slowly along the horizontal than along the vertical meridian. While acuity decreases almost uniformly in the left and right peripheries, it decreases faster in the upper visual field, when compared to the lower visual field (Barbot

et al., 2020; Kupers et al., 2019). Interestingly, HVA is most pronounced in the visual field's center (Abrams et al., 2012) and less pronounced at oblique positions (Abrams et al., 2012; Barbot et al., 2020). Lower and upper visual field asymmetries, also exist for stimulus properties. Participants are better in discriminating sets of stimuli regarding color, hue, motion, contrast (Levine & McAnany, 2005), and spatial frequency (Carrasco et al., 2001) when they are presented in the lower visual field. Depth and shape discrimination, however, is better in the upper visual field (Levine & McAnany, 2005; Zito et al., 2016). There appear to be no differences for orientation discrimination, which I have used for my studies (Zito et al., 2016).

As there is neither behavioral evidence for a HVA, nor vertical asymmetries in my experiments, this might be a sign that there were no perceptual differences between the conditions. As stimuli were placed at relatively low eccentricities and an orientation discrimination task was used, perceptual asymmetries were becoming even less likely (Carrasco et al., 1995; Zito et al., 2016). This means, that if I had found location specific effects they would have been likely due to attentional (re)orienting and task processing, which I was interested in, but not due to perceptual influences.

One has to note, however, that perceptual asymmetries can propagate to higher cognitive domains. For example, vertical asymmetries can be found in short-term memory tasks, that require the sampling of visual information (Montaser-Kouhsari & Carrasco, 2009). In contrast to Carrasco et al. (2001), it has also been shown that vertical asymmetries can be modulated by exogenous attention, for example in apparent contrasts (Fuller et al., 2008).

These observations indicate that factors other than perceptual properties of the visual system could also play a role in vertical meridian asymmetries and HVA. For example a computational modeling study concluded that only about 10 % of the variance in vertical acuity can be explained by retinal cell distributions (Kupers et al., 2019). The authors note, however, that they did not model later processing stages in the visual system (Kupers et al., 2019), which might further exacerbate perceptual asymmetries (Barbot et al., 2020).

Task asymmetries

Horizontal asymmetries, on the other hand, are highly unlikely due to asymmetries in visual acuity (Kupers et al., 2019). In fact, some studies investigating visual performance fields average behavioral responses to left and right stimuli, due to their high similarity (Barbot et al., 2020). Thus, there has to be a different cause for horizontal asymmetries.

In a large replication study Brederoo et al. (2019) show horizontal asymmetries for a multitude of tasks. For example, participants detect a face's emotion quicker when the stimulus is presented in the right as opposed to the left visual field. The opposite is true when face similarity is judged. Other than vertical asymmetries, horizontal asymmetries are often attributed to hemispheric lateralization of cognitive processes. We already introduced, that spatial processing has a right hemispheric dominance (Mengotti et al., 2020), so that we would expect faster processing of stimuli in the left visual field. We can see this for example in line-bisection tasks and other examples of pseudo-neglect, where the right visual field is less attended to (Jewell & McCourt, 2000; Klatt et al., 2020). Faster reaction times to stimuli in the left visual field in the study by Mao et al. (2007), might also be attributed to hemispheric lateralization.

Box 10.1: A future study

A very interesting observation has been made in hierarchical letter tasks. In such a task stimuli consist of many small letters (for example "S") which make up a

larger letter (for example an "H"). These stimuli are also known as Navon figures (Navon, 1977). Participants respond faster to the small letters (local processing) when they are presented in the right visual field, compared to the left visual field. When responding to large letters (global processing), however, they now respond faster to stimuli in the left visual field (Brederoo et al., 2019). But there also appears to be vertical asymmetry, so that local processing is better in the lower, and global processing is better in the upper visual field (Christman, 1993).

While vertical asymmetries are explained with functional specialization of the upper and lower visual fields (Christman, 1993), it is also possible that the asymmetry is due to perceptual factors: small letters might interfere less with global processing due to the lower visual acuity in the upper visual field.

In a further study, one might want to investigate the effect of exogenous and endogenous cuing in combination with probabilistic cues, to investigate which factors cause vertical and horizontal asymmetries. Here the focus would be on investigating how within meridian asymmetries change when using trials without a cue, with 100 % valid cues, predictive cues (70 %) and non-predictive cues (50 %). If asymmetries disappear with predictive cues, it might be possible, that prediction and control processes are becoming more dominant than perceptual processes, speaking for a non-spatially restricted allocation of attention.

10.1.3   Reorienting

Furthermore, there is also no sign of horizontal asymmetries in my behavioral data. Which indicates, that attention is deployed globally and not influenced by spatial constraints. But it is possible, that, although there is no behavioral evidence, cortical representations could still code for spatial location differently (Brederoo et al., 2019). I tested for visual field effects in the first study's functional magnetic resonance imaging (fMRI) data (Figure 6.6, Steinkamp, Vossel, et al., 2020), where I only found evidence for location effects in valid trials, which was restricted to extrastriate visual areas. Notably, I did not find significant activations for upper visual field stimuli, which could be explained by a generally weaker representation of the upper visual field in early visual areas, when compared to the lower visual field (Hagler, 2014; Pitzalis et al., 1997)

   While these results investigated visual field asymmetries, my main question in the first project was about horizontal and vertical asymmetries in Posner's cuing task. Neither whole brain analysis nor a closer inspection on the volume of interest (VOI) level yielded evidence of a between meridian effect for attentional orienting or reorienting (Steinkamp, Vossel, et al., 2020). As non-significant results in statistical analysis can also be due to a lack of statistical power, I further strengthened my conclusions by using machine learning and computational modeling. Thus, I could show that activation patterns of intraparietal sulcus (IPS), frontal eye-fields (FEF), and temporoparietal junction (TPJ) are so similar, that a classifier of valid and invalid trials trained on one run can be applied to the other.

   In a not further expanded side analysis, I also applied the classifier to an openly available data (see https://openneuro.org/datasets/ds000102/) provided by Kelly et al. (2008), who recorded fMRI and behavioral data of participants who performed an Eriksen Flanker task (Eriksen & Eriksen, 1974). The logistic regression model trained to separate valid and invalid trials in my spatial-cuing data, could also be used to differentiate incongruent from congruent trials in the Flanker task. This finding suggest that Eriksen and Posner tasks tap into similar aspects of visual spatial attention (Chajut et al., 2009) and that neural responses in invalid and valid trials possibly also code for conflict monitoring.

   Conflict monitoring in Posner's cuing task has been related to the right TPJ before

(Corbetta et al., 2008). My analysis, however, shows that also nodes of the dorsal attention network, as well as left TPJ might play a role. Next to my classification results, my DCM analysis also shows that if swapped, modulations by invalid trials of either vertical and horizontal runs, do not alter neural dynamics dramatically (Steinkamp, Vossel, et al., 2020).

My conclusion, that attentional reorienting is likely not affected by perceptual influences, has been shared by another fMRI study (Macaluso & Patria, 2007). As fMRI has a few limitations (see Box 10.2), it is important that other studies reach similar conclusions. Eckstein et al. (2002) provided evidence using computational modeling, that the validity effect in a Posner task is not influenced by the target's perceptual properties. To underline this point: The Rescorla-Wagner model and similar models can describe reaction time dynamics in a spatial cuing task very well, without including any spatial information (Steinkamp, Fink, et al., 2020; Vossel, Mathys, et al., 2014). These models, however, track the participants' expectation of valid and invalid trials, indicating that higher level cognitive processes are at play in attentional reorienting. Furthermore, the cuing or validity effect is not restricted to the visual domain. As mentioned in Chapter 2, several studies have shown that expectations of cue validity can interact between modalities (Chambers et al., 2007; Mengotti et al., 2018), so that this form of attention might not be restricted to the visual domain (Treisman & Gelade, 1980).

As previously described, expectation monitoring is associated with the ventral attention network, especially right TPJ. A recent transcranial magnetic stimulation (TMS) study also showed that right TPJ further plays a crucial role in updating and adjusting these expectations with new information (Mengotti et al., 2017). This believe updating is not limited to spatial attention, as lesions to right TPJ have also been shown to impair rule updating behavior in other tasks (Danckert et al., 2012; Stöttinger et al., 2014).

Put together, my results support the notion that the ventral attention network's role, be it believe updating or expectation monitoring, is non-spatial, as I do not find difference between vertical and horizontal reorienting and are able to show that activity patterns coding for valid and invalid trials, as well as blood oxygen level-dependent (BOLD) dynamics of attentional reorienting are very similar between the two runs. My studies further soften the view of a strictly right hemispheric dominant ventral attention network, as I have found that left TPJ is consistently activated by attentional reorienting and appears to be an important node in the network models (Corbetta et al., 2008; Corbetta & Shulman, 2011). Although, left hemispheric lesions to the ventral attention network lead to less severe neglect symptoms, they are still present (Beume et al., 2017; Malherbe et al., 2018). However, left TPJ might not only be involved in the monitoring of expectancy violations, but could also track the occurrence of expected events (Mengotti et al., 2020; Silvetti et al., 2016).

> **Box 10.2: Limitations: fMRI**
>
> Although, fMRI is ubiquitous in human neuroscience, the field is still maturing. There are three major problem groups identified for fMRI studies.
> **Statistics:** The majority of fMRI studies uses mass-univariate analyses, that is calculating statistical tests for each voxel. As there are several thousands of voxels in a fMRI-volume, controlling for false-positives is paramount (recall the dead salmon, Lyon, 2017) but also very difficult. For example, many fMRI studies might have reported false positive results, because the default settings of a commonly used software package were overly liberal (Eklund et al., 2016). Additionally, certain preprocessing decisions might inflate the false-positive rate in mass-univariate analyses (Mueller et al., 2017). To alleviate these issues I used a standardized

preprocessing pipeline (Esteban et al., 2019) and used permutation tests, which appear to be more robust against false positives (Nichols & Holmes, 2002).

Sample Size: Small sample sizes are a common issue in psychology and neuroscience research (c.f., B. O. Turner et al., 2018; Yarkoni, 2019). Although, warnings against underpowered studies are widespread, sample sizes have only been slowly increasing over the years, so that the sample size in my projects, is still above the median (Szucs & Ioannidis, 2020). Still, the sample size is not ideal, so that I might have missed differences between vertical and horizontal orienting due to low statistical power.

Researchers' degrees of freedom: The final issue with fMRI as a method is the large amount of degrees of freedom a researcher faces. Using different software packages, software versions or even operating systems can have large effects on a study's results (Bowring et al., 2019). Although, some evidence indicates that the software's influence is not too large, interpretation of results also varies dramatically between researchers. This was shown in a large study, in which seventy teams (including myself) analyzed the same dataset, but could not agree on whether certain brain areas were activated or not. More strikingly, the participating teams had no stakes in the outcomes and were answering a priori hypotheses (Botvinik-Nezer et al., 2020).

Orienting

As attentional reorienting has previously been discussed as a non-spatial process, the previous results are not too surprising. Due to the functional specialization of the right hemisphere in spatial attention tasks (Mengotti et al., 2020), I would have expected visual field effects in the nodes of the dorsal attention network, even though I did not specifically investigate hemispheric asymmetries. But, there were also no signs of such effects for attentional orienting (left versus right contrast, Figure 6.6, Steinkamp, Vossel, et al., 2020).

Such results, however, are not necessarily at odds with current theories of neglect (Macaluso & Patria, 2007). Next to Corbetta et al. (2008)'s ventral attention network model, other theories describe neglect in terms of imbalanced functions of the dorsal attention network. Heilman's hemispatial theory (1979) proposes that the right hemisphere does not only process the contralateral (left) but also the ipsilateral (right) visual field, where the left hemisphere is constricted to the contralateral field. Thus, right hemispheric lesions would lead to larger impairments (Duecker & Sack, 2015). Kinsbourne's opponent process model (1977), however, puts left and right hemispheres in competition of directing attention. Lesions on either side would therefore lead to imbalances (Duecker & Sack, 2015). In a hybrid model, FEF might follow the hemispatial theory and IPS the opponent process model (Duecker & Sack, 2015).

Although a hybrid model seems to be likely, the attribution of functions to IPS and FEF, is debatable. For example, right IPS appears to extend attentional modulation to the left visual field, whereas left IPS is restricted to the right visual field (Sheremata & Silver, 2015). Results of my DCM analysis in the first study appear to corroborate this idea (Figure 6.2), as I found that the connection between right and left IPS is more likely to be modulated by invalid cuing, when compared to modulations in the opposite or both directions, hinting at a dominant role of right IPS in attentional (re)orienting.

10.1.4   Picking horizontal and vertical apart

The study by Sheremata and Silver (2015) also indicates, that we likely would need more specialized methods to investigate modulations by visual fields in dorsal, or even ventral attention networks (Dugué et al., 2018). On the other hand, my results also show that the larger dynamics in the two networks are not affected by spatial locations. Except for a rather unsuspected finding in Steinkamp, Fink, et al. (2020): Using features derived from behavioral dynamic causal modeling (bDCM), I was able to differentiate whether a participant's model was used to model the vertical or horizontal run (Figure 7.8). As this was not possible using features derived from other sources, these findings are not directly at odds with the first project, but show that incorporating behavioral responses in DCM appears to increase sensitivity to subtle task manipulations. In my additional analysis see Table 8.1, page 112, I further found that connections between IPS and TPJ appear to be most important to separate the two runs, as well as their output connections relating the model's dynamics to behavioral observations.

Unfortunately, this further analysis only tells us which features are important for classification, but does not provide more detail. However, I already found that right IPS in the first study has been more strongly activated in vertical when compared to horizontal trials. According to Fink et al. (2001), it is possible that the vertical direction of attention is more difficult, thus leading to higher parietal activation in general. Furthermore, the bDCM used in my study had twice the sampling rate than DCM, possibly being more sensitive to small temporal variations in the BOLD response that differentiate horizontal and vertical orienting runs. Variations, that might not become visible in more conventional analyses like general linear model (GLM) contrasts of the BOLD response.

As can be seen in Chapter 8, Figure 8.3, bDCM is very prone to overfit to the training data, so that also variations between the visual fields are included in the dynamics, without being explicitly modeled. We can see this qualitatively in the artificial lesion analysis in Steinkamp, Fink, et al. (2020). Changes to the validity effect in the horizontal run appear to more closely follow the hemispheric asymmetries expected, whereas lesions in the vertical run appear to lead to less visual field dependent asymmetries (see Figures 7.9 and 7.S2).

10.1.5   Horizontal and vertical neglect

The latter observation appears to be in line with the idea, that upper and lower visual fields are more distributed across hemispheres, so that bilateral lesions are necessary to inflict vertical neglect (Rapcsak et al., 1988; Shelton et al., 1990). However, there are also interactions between the vertical meridian and hemispatial neglect. For example, the lower left visual field is often more affected by neglect than the upper left visual field after right hemispheric lesions (Pitzalis et al., 1997). A combination of left hemispatial neglect and upper visual field neglect has also been reported after a lesion to the right temporal cortex (Morris et al., 2020).

The unclear extent and locations of vertical neglect underline how diverse and distributed hemispatial neglect can be, typically affecting a wide range of cognitive processes (Halligan et al., 2003; Heilman et al., 2000) and different aspects of spatial attention (Karnath, 2015). To complicate things, lesions might not only affect attention systems, but also visual pathways. Although, damage to the visual pathways comes with distinct symptoms (Milner, 2017; Sheth & Young, 2016), it is possible that there are some interactions. For example, damage to the visual pathways could explain why vertical asymmetries can diminish over time, if patients are given more time for exploration (Cazzoli et al., 2011; Müri et al., 2009), horizontal asymmetries, however, persist. Because the disconnection of brain areas through damage to white-matter tracts can explain a lot of different behavioral

observations (Thiebaut de Schotten et al., 2020), it might be necessary for our understanding of neglect, to incorporate white matter connections more into the description of cortical functional networks in future studies. For example, by combining functional and anatomical data, it was possible to show that object and egocentric processing recruits dorsal frontal areas differently, as distinct white matter tracts are involved (Szczepanski et al., 2013). Paying attention to the anatomical networks as well might thus be able to answer some of the many open questions regarding vertical neglect.

10.1.6   Attention conclusion

In my thesis I have worked out, that endogenous attention in a variant of Posner's spatial cuing task is likely uniformly distributed across the visual field. I found neither behavioral nor neural evidence for differences between vertical and horizontal (re)orientation and only very specialized analysis could tell the two runs apart. Thus, it is very likely that neglect symptoms as observed by Posner et al. (1984) are caused by a hemispheric imbalance of the left and right dorsal and ventral attention networks. Although there are still many open questions regarding the origins of vertical neglect, I would assume that interactions of vertical and horizontal neglect, as in free-viewing, would not extend to our form of Posner's spatial cuing task. I am furthermore confident in this assumption, as my computational modeling analyses show that behavioral and neural dynamics of attentional (re)orienting can be modeled without including stimulus locations, which is further evidence that attentional reorienting is not a spatial process.

Still, it would be interesting to investigate vertical and horizontal extent in endogenous, predictive cuing tasks in neglect patients. See Boxes 10.1 and 10.3 for further considerations in future studies.

Box 10.3: Future directions

Larger networks: In my thesis I only included TPJ as part of the ventral attention network (see more in Box 10.6), however, also inferior frontal gyrus (IFG) and middle frontal gyrus (MFG) play important roles in attentional reorienting (Vossel et al., 2012). While my whole brain analyses did not reveal any differences between vertical and horizontal orienting, I might have missed important network dynamics in DCM and especially bDCM networks. In case of bDCM, it is possible that larger and more realistic network models might provide more realistic results in the artificial lesion analysis. Furthermore, it might be interesting to increase the biological validity of these network models by incorporating anatomical information, for example by using tractography based priors for network connections (Stephan et al., 2009). Paying closer attention to the white-matter connections between brain regions and in the study of functional data, might also help us to better understand what impact brain lesions have (Thiebaut de Schotten et al., 2020). On the other hand, all brain regions included in my analyses are distributed along the superior longitudinal fasciculus (SLF), the white matter tract commonly associated in neglect (Thiebaut de Schotten et al., 2014), see Figure 2.4.

A question of time? A limiting factor in my work has been the low temporal resolution of fMRI. Especially, as there is more and more evidence of a rhythmic sampling of spatial attention (Fiebelkorn & Kastner, 2019). Methods like magnetoencephalography, have been shown to have a relatively high spatial and very precise temporal resolution. Applying such methods, could tell us about recurrenct and hierachical interaction between the attentional networks, which are further important to understand the role and function of specific brain areas. An inspiration might be

found in studies by Gwilliams and King (2020) on visual processing and by Gordon et al. (2019) on predictive coding in early visual areas.

Ecological validity: Since many laboratory experiments are stark abstractions of real life situations, we cannot necessarily extend experimental conclusions to daily life (Yarkoni, 2019). For example, we seldom orient attention covertly as it feels more natural to move our eyes or heads, if we want to focus on something. Furthermore, studies have shown that head position affects spatial reference frames, which might be problematic for fMRI studies (Nicholls et al., 2006). Examples of experiments with higher ecological validity come from sport-psychology, for example investigating pseudo-neglect with large screens and tasks which are close to soccer situations (Klatt et al., 2020). Furthermore, virtual reality can be used for more ecologically valid situations, while having full control over the environment. Which has for example been shown for a variant of Posner's cuing task (Soret et al., 2019). Finally, new computational techniques could help us to make sense of large scale data-sets of neural and behavioral data in naturalistic settings (Musall et al., 2019).

10.2   Computational Modeling

In my investigation of horizontal and vertical orienting, I often relied on creative applications of new methods and later investigated the unique insights bDCM can provide. In this section, I will discuss how my work contributes to the advancement of neuroscientific methods. To begin with a major motivation for this chapter, let me reiterate some key concepts of computational modeling.

Ideally, computational modeling can help formulate our implicit theories in testable and falsifiable mathematical frameworks (Guest & Martin, 2020). In turn, writing down and developing research using frameworks will also help us to come up with clearly formulated theories of how we understand the world (Navarro, 2020). But in the last decades, a lack of theory has been complained about in psychology and cognitive neuroscience (Fried, 2020; Lykken, 1991; Muthukrishna & Henrich, 2019). Psychophysics and visual attention in psychology might be one exception, as multiple computational models have been proposed for describing sensory decision processes (Ratcliff, 1978; Ratcliff & McKoon, 2008), visual search (Wolfe, 2007), and even visual attention in general (Bundesen, 1990). As our understanding of the brain is ever increasing, it might now be time to also integrate neural observation into these behavioral theories (Buzsáki, 2020).

Although such an overarching theory for attentional orienting and reorienting in spatial cuing paradigms is out of my work's scope, I show that currently available analysis tools can be used to develop and test theories of brain and behavior (see also Palminteri et al., 2017). But let us start in more general terms with the DCM framework.

10.2.1   DCM framework

Most of my work is centered around the DCM framework and its extension bDCM. As described in Chapter 5, the framework is commonly used to select a "winning" model (architecture) from a set of candidate models and to infer effective connectivity parameters about how brain areas are connected (Friston et al., 2017).

The conventional DCM analysis, however, has not been without its criticisms. For example, model spaces in DCM are vast — growing exponentially with each additional node — and results of Bayesian model selection can easily change depending on the

number of models included in the selection procedure (Lohmann et al., 2012). Furthermore, Bayesian model selection can become overconfident if very diverse sets of models are used (Oelrich et al., 2020). Although some criticism has been heavily refuted (Friston et al., 2013), recent developments in the DCM framework try to alleviate these problems, for example by very efficiently estimating large model spaces (Frässle et al., 2017; Friston et al., 2016; Friston et al., 2018; Friston & Penny, 2011).

Still in my analysis, I experienced some problems with the conventional approach. I found that Bayesian model selection was not very robust to changes in the input data and did not converge on a single model (or model families). This might be caused by very similar model architectures possibly causing an underconfidence, which is in contrast to the aforementioned overconfidence (Oelrich et al., 2020). In the first project I solved this issue by hierarchically selecting model families in multiple stages and finally averaging the parameters in the winning family (Penny et al., 2010). While this approach can lead to zero estimates in individual connectivity estimates, thus making group analysis more difficult, it resulted in a stable and robust model selection, which I used to draw conclusions about hemispheric asymmetry in attentional reorienting, discussed previously (Steinkamp, Vossel, et al., 2020).
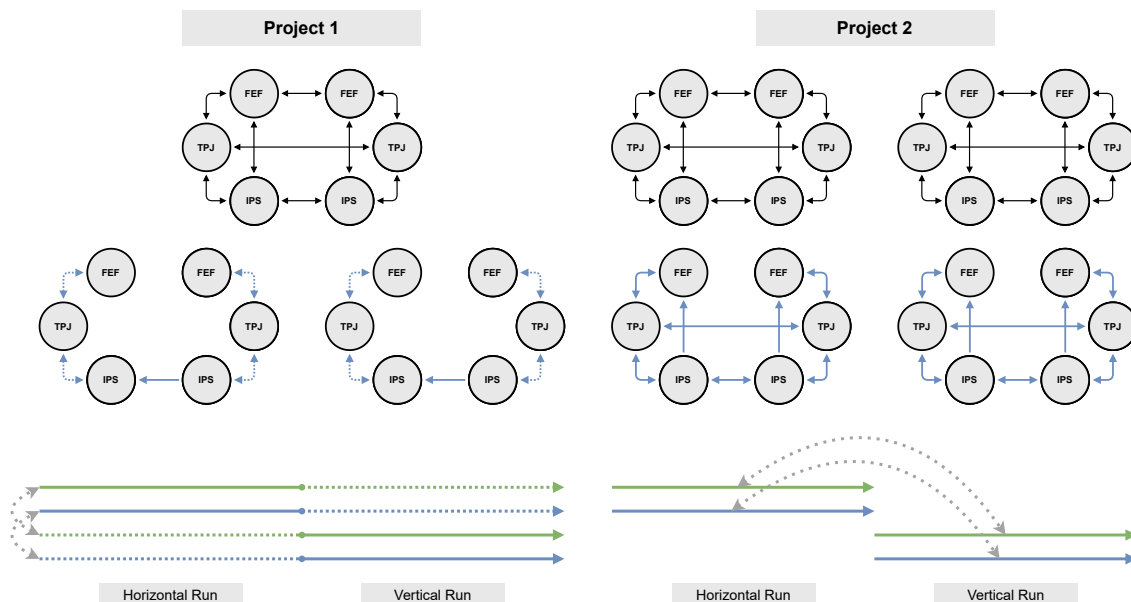
Figure 10.2: Left the DCM architecture used in the first project, right the one used for DCM and bDCM in the second project. The architecture on the left has been determined through Bayesian model selection. Note the important difference between the two projects. In the first project, both runs were included in one model, whereas in the second project, each run got its own. The arrows in the lower part of the figure stress, what this means in terms of my generalization analysis. The dotted arrows on the left indicate that the input was present without any entries.

10.2.2   DCM as a computational model

Bayesian averaging of connectivity parameters possibly improved DCM's generalizability, by introducing another level of regularization. We see this in the fact, that I could swap parameters coding for invalid trials of horizontal and vertical runs, without a significant increase in prediction error (Steinkamp, Vossel, et al., 2020). Let us dwell on this analysis for a bit.

Here I incorporated two things often overlooked in DCM analysis. The first thing is to test whether the DCM model is actually modeling the underlying data (Lohmann et al., 2012). This is crucial, as we need to know whether the model does capture the BOLD dynamics it was fitted to, otherwise the model would not be of much use (Palminteri et al., 2017). A rule of thumb is that DCM should capture around 10 % of the variability in the data ($R^2 > 0.1$ criterion, Friston et al., 2013), which almost all models did in both of my projects.

The second part of this analysis taps into a strength of DCM that tends to be over-looked. As DCM is a generative modeling framework, it does not only learn an input-output mapping, as many machine learning and statistical models do, but it also contains knowl-edge about the underlying distributions of the input data, which in part explains DCM's computational costs (Bishop, 2006, p. 43). Having a generative model, also means that we can generate data for situations not previously observed.

In Steinkamp, Vossel, et al. (2020), I did this by swapping input-streams, so that BOLD dynamics in invalid trials are generated by parameters originally fitted to the respective other run (see Figure 10.2). Because the data simulated in the swapped condition provided results better than random, I concluded, that attentional reorienting in horizontal and vertical runs are very similar.

> **Box 10.4: Limitations: machine learning**
>
> Albeit careful considerations in the use of machine learning models, in the first and especially in the second study, there are a number of caveats. The most glaring one being sample size. Even with well devised cross-validation schemes, it is pos-sible that scores like a model's accuracy are overestimated (Varoquaux, 2017). In general it is advised to use a sample of more than 200 participants in prediction studies (Poldrack et al., 2019). Moreover, a separate test dataset would have been useful to substantiate our claims, especially as the test-retest reliability of predictive neuroimaging models (in a clinical context) has been very low (Elliott et al., 2020). But as stated in the first part of the discussion, in an analysis which was not further developed, I was able to show that the prediction of valid and invalid trials in the Posner cuing task, could also be applied to classify congruent from incongruent trials of an Eriksen Flanker paradigm (Eriksen & Eriksen, 1974; Kelly et al., 2008).

10.2.3 Interventions

This analysis was originally inspired by the predictive framework of machine learning, where generalization across different conditions is the primary objective (Bzdok et al., 2018; Efron, 2020). But it is important to stress a small difference between the general-ization of the DCM model and the generalization of the logistic regression model used in the first publication.

I used machine learning to strengthen statistical claims in the VOI analysis. In addition to Bayesian inference, which only provided convincing evidence for an effect of cuing condition, I further showed that the patterns of BOLD amplitudes in the six VOIs of one run can not only predict the trial type (valid/invalid) with above chance performance for data in the same run, but also that the model could be applied to the other run's data. Indicating that also multivariate patterns are equivalent between the two conditions (see Box 10.4 for a word of caution). Using machine learning inspired analysis to provide evidence for equivalence between two conditions, is an interesting approach, when one deals with null results, that could be used to support other Bayesian or frequentist analysis, aiming to show an effect's absence (c.f., Keysers et al., 2020; Lakens, 2017).

The generalizability of regression models between runs, however, is different from the generalizability shown by DCM. The regression models tests whether the underlying data of the two conditions is similar, but DCM tests whether the same data generation process is applicable to the two conditions. Referring to Box 4.1, this means that we stepped up one rung of Pearl's causal ladder (Pearl & Mackenzie, 2018), moving from inference to intervention. I conducted an *intervention* onto our model, asking: What happens, if participants did the horizontal and vertical run in a different order? And found that changing the run's order *caused* only a small decrease in model fit, indicating that neural dynamics in both runs are very similar!

10.2.4 Counterfactuals

In my first study, evaluating the effect of our intervention was only possible, as we had data for both runs. But if we have a general idea, about how observations change after an intervention, we can simulate data for unseen conditions. Because changes in BOLD dynamics can be difficult to interpret on their own, bDCM is a powerful tool, as it relates interventions on the brain network level directly to behavior (Rigoux & Daunizeau, 2015).

Using interventions and knowing how behavior could change helps us to understand the scope and limitations of a computational model (Palminteri et al., 2017). As the second publication (Steinkamp, Fink, et al., 2020) was already very complex, I provided further analysis for this in Chapter 8.

One intervention I was interested in, was about whether bDCM incorporates cue-validity in a similar manner as the Rescorla-Wagner model. To do this, I simulated data for both bDCM and the Rescorla-Wagner, with different proportions of invalid and valid cues (from 50 % to 90 % cue-validity). Dombert et al. (2016) have shown, that the validity effect increases with more predictable cues. If bDCM does model some form of internal cue-validity and creates predictions of surprise, we should see a similar pattern in the simulated reaction time data. The results of this analysis can be seen in Figure 8.4 on page 114. While the Rescorla-Wagner model is showing the expected pattern, that the validity effect increases, but the average reaction time remains stable (Dombert et al., 2016), average reaction times In bDCM appear to decrease with higher cue-validity, while the validity differences remain constant.

Although bDCM describes reaction time distributions generally better than the Rescorla-Wagner model, it does not appear to be modeling participants' probabilistic assumptions. This analysis reveals a possible weakness of the DCM and bDCM framework in terms of theoretical underpinning, when comparing the DCM framework to classical computational models like the Rescorla-Wagner model. The latter has a strong background in behavioral observations and studies (Niv, 2020; Rescorla & Wagner, 1972), explicitly describing the relationship between basic stimulus(cue)-response(target) mappings. In terms of Marr's levels (Box 4.1), the Rescorla-Wagner model thus comprises both the first and second levels. It is a clear description of why and what the process of classical conditioning contains (which is applicable to Posner's cuing task as well) and describes how the learning process could be implemented algorithmically (Marr, 2010). DCM and bDCM, on the other hand, is a modeling approach of the second and third level, as it describes the algorithm of how hidden states can be related to measurable responses and is a model of how the algorithm might be implemented in terms of connectivity between brain regions. It is a generalistic framework which can be applied easily to a wide variety of situations, but does not necessarily describe the "why" of a cognitive process. In the ideal case, one would be able to implement the computational theory behind behavioral models into DCM as well. For example, by incorporating another hidden state which tracks the participants' believes about cue-validity.

10.2.5 Lesion analysis

What sets bDCM apart from pure cognitive models is the possibility to introduce artificial lesions into the network dynamics (Rigoux & Daunizeau, 2015). Another second to third order intervention according Pearl's causal ladder, allowing us to ask: How would the participant perform, if a brain region was damaged? In their original publication Rigoux and Daunizeau (2015) presented convincing results that introducing artificial lesions into the network model, leads to behavioral patterns that are congruent with the literature.

In our analysis, however, a few practical issues had to be overcome. While Rigoux and Daunizeau (2015) and also Shaw et al. (2019) used binary behavioral responses, the goal for my analysis was to apply bDCM to continuous data (i.e., reaction times). Modeling continuous data, however, requires changes to the output function and the noise model. After some experimentation, I decided to adapt the sigmoid function used for binary classification. The sigmoid has exponential components and is non-negative, but also restricts the output, thus being a good approximation of how we expect DCM's hidden states are related to reaction times. This also means that simulated reaction times are limited to 0 s (unrealistically fast) and 3 s (a trial's maximal duration). As artificial lesions in our study introduced very large fluctuations in hidden states, several simulations oscillated between these extreme values.

Reaching extreme values is not as problematic for binary responses, as it indicates extremely confident decisions in either direction (as in Rigoux & Daunizeau, 2015). In continuous predictions, however, it becomes increasingly difficult to interpret such values.

Thus, I applied a few strategies to introduce more numerical stability into the bDCM model, which was necessary, as artificial lesions lead to large oscillations in hidden states, sometimes approaching positive and negative infinity. To enforce higher numerical stability, I therefore increased the self-inhibitory connections, after the model was already estimated. This step, however, lead to a significant reduction in model fit: Although lesion analysis is now possible, the more stable model might have changed dramatically from the model we wanted to interrogate.

A second step was to introduce gradual lesions instead of using absolute lesions to investigate how decreases in a brain region's function are related to behavior (see Equation 5.10). Together these interventions enabled me to draw a few qualitative conclusions about how horizontal and vertical runs differ in terms of how the validity difference changes in response to lesion location and lesion extent.

Box 10.5: Limitations: DCM

It is necessary, to discuss additional limitations of my modeling approaches, possibly affecting the claims' validity, which have not been mentioned in the discussion.
(Under-)Complexity: By making an effort to keep dynamics in the model as stable as possible (especially for bDCM), I refrained from incorporating non-linear dynamics (Rigoux & Daunizeau, 2015; Stephan et al., 2008), although they were found to have high model evidences during previous experimentation. On the other hand, I used almost the full bilinear model (i.e. including all possible connections) in the second project to investigate how invalid trials were modulating connections between brain regions. So it is possible, that the model space investigated here was either too complex or not complex enough (c.f. Lohmann et al., 2012).
Stability: A second problem I observed, was that connectivity parameters and Bayesian model selection were not robust to minimal changes to the model's architecture, different sets of nuisance regressors, voxel inclusion criterion, or VOI size. One reason might be related to the software I used. In one study investi-

gating the test-retest reliability of (resting-state) DCM, newer versions of the DCM software implemented in SPM (Friston, 2007) lead to less reliable parameter estimates and model selection (Frässle et al., 2015). It was further made clear, that the prior distribution over the parameters can have dramatic effects on reliability (Frässle et al., 2015). This newer version of DCM has been used in the first study, with default settings. In the second study, however, I relied on a different software package (VBA-Toolbox Daunizeau et al., 2014). As the VBA-toolbox closely follows SPM's implementation, it is possible that the prior distributions are similarly leading to models prone to over-fitting (i.e., less reliable models). Additionally, the VBA-toolbox exposes many more options for the modeling and model inversion, that SPM hides, posing another threat for overfitting (Cawley & Talbot, 2010).

Experimental design: One final issues is my experimental design, more specifically the time between individual trials. As the hemodynamic response function (HRF) of the BOLD signal is up to 12 s long, responses to different conditions might be overlapping. In block designs the overlapping signals are less of a problem, which is why blocked designs are preferred for the use of DCM (Daunizeau et al., 2011). Unfortunately, blocked designs are sub-optimal for Posner's cuing task. Although I tried to make the interval between trials as long as possible, we had to find a balance, as participants grew tired when long intervals were used, leading to a deterioration in performance. Thus, I had to use not ideally separable conditions in our model, which possibly had a negative effect on our DCM analysis (see Figure 3.1, page 19).

10.2.6   DCM and overfitting

In Chapter 8, I swapped — similarly to the first project — the horizontal and vertical run's input streams to simulated how DCM, bDCM, and Rescorla-Wagner models generalize across runs. As one can see in Figure 8.3, generalization performance is very low. In general, low generalization across runs would be a clear sign of overfitting, i.e. the model is very good at representing the training data, but is not applicable to new settings (Bishop, 2006, p. 6ff).

Overfitting might indeed be an issue for bDCM and DCM due to their large amounts of parameters. Even though DCM applies a Bayesian framework, which is claimed to be more robust against overfitting than other optimization approaches (Bishop, 2006, chapter 1), in practice, no modeling approach is immune to it (Cawley & Talbot, 2010).

One factor, driving the overfitting in the second study, when compared to my first project, might, be the underlying data. In Figure 8.3 it also becomes clear that BOLD responses generalize slightly better to the opposite run than behavioral data. We might thus conclude that the BOLD modeling was in general more robust between the two runs. For behavioral responses, however, the Rescorla-Wagner model — which only has 4 as opposed to 82 parameter — also does not generalize well.

A possible explanation is that reaction time data is highly variable. Arguably, the Posner cuing task is creating reliable effects on the group and individual level (Haines et al., 2020; Hedge et al., 2017), however, trial by trial variability is high. I stress this observation in Steinkamp, Fink, et al. (2020)'s supplement. Figure 7.S1 shows that the size of the validity effect is highly correlated with the R^2 score, the error on the other hand is not. In a sense, this means, if the participant is showing the expected dynamics, i.e., larger reaction times in invalid trials, my models do represent these dynamics. This figure, however, also shows that bDCM with its higher complexity possibly models other dynamics not included in the Rescorla-Wagner model, as the correlation with the validity effect is not as

strong. During the modeling I experimented with different strategies to normalize reaction times, to no avail. For future studies, this also means that one has to pay attention to reduce noise in the behavioral signal or try to incorporate noise sources in the model.

10.2.7 Generative embedding

Although the strong variations in reaction times might have a negative influence on the computational modeling and bDCM's generalizability, it could also provide unique opportunities. Because bDCM can be used to simulate artificial lesions, it was proposed to be used to better understand and predict individual clinical outcomes (Price et al., 2017). In the previous section, however, I have shown that there are a few practical hurdles, especially, if one wants to use bDCM in combination with reaction times.

But, modeling subtle variations might put bDCM into a unique role for personalized psychiatry (Stephan et al., 2017). Deriving a single model from a large group study might allow us to create predictive models based on connectivity parameter to differentiate healthy from patient groups. This approach is in contrast to the more common analysis of using Bayesian model selection to identify differential model structures between patient and control groups (Wu et al., 2014). Inverting the single model is therefore another form of dimensionality reduction, which is particularly needed in neuroimaging research due to the large amount of features and often small sample sizes (Mwangi et al., 2014). Generative modeling as a form of feature reduction has been termed generative embedding and has been used to classify stroke patients and healthy controls (Brodersen, Haiss, et al., 2011; Brodersen, Schofield, et al., 2011).

I used generative embedding in the second project as a proof of principle to differentiate between vertical and horizontal runs. Interestingly, only parameters derived from bDCM contained enough information to do so. Classification based on parameters of DCM, the Rescorla-Wagner model, and cross-correlations of the BOLD timeseries did not achieve above chance performance. Although machine learning approaches are often seen as "black-box", especially, as in many cases prediction and generalizability are the main goal (Efron, 2020), there are approaches to investigate which features are contributing the most to a prediction (Breiman, 2001). Interestingly, this is a different statement than one of statistical significance, where the "most" significant parameters in a regression model are not necessarily the parameters contributing most to a prediction (Bzdok et al., 2020). Using such models, I could then not only show that bDCM is allowing us to differentiate between horizontal and vertical runs, but also that parameters related to IPS and TPJ contribute the most.

10.2.8 Modeling: differences between the first and second project

The DCM approaches differed between the two projects. I here want to shortly discuss the reasons for this.

In Steinkamp, Vossel, et al. (2020), the goal was to investigate horizontal and vertical orienting, also in terms of a more conventional DCM analysis. Thus, I performed model selection and classical inference on connectivity parameters. As I was especially interested how modulations by invalid trials differed in this study, I decided to combine horizontal and vertical runs (see Figure 10.2, left). In DCM terms this means, that the same A matrix was used, and I could directly compare modulations by invalid trials in each run's B matrix. Setting up the model this way, also increases the generalizability of the model, as only B matrices differed between runs and all dynamics shared the same A matrix.

In my second project the goal was mainly to test bDCM on a spatial cuing task. To be able to compare dynamics and parameters of DCM and bDCM, I decided to use a single

"full" model of brain connectivity, leaving the pruning of non-necessary connections to Bayesian self-regularization. This also circumvented the issue that each run and modality had different winning models in Bayesian model selection. The test for generalizability here is thus more difficult, as each run has its own ("full") set of parameters (see Figure 10.2, right). This way, however, I could also apply generative embedding, to investigate differences in parameter estimates.

Another notable difference between my projects is the software used. In the first project, I used DCM implemented in SPM — the standard implementation — , whereas I used the VBA-toolbox for my second project. Due to difference in the prior and hyperprior distributions in the two studies, results are not necessarily comparable (see Box 10.5 for a discussion on the effects of priors on model estimations). The biggest difference between the two toolboxes, however, is the amount of control the user has on the model estimation.

10.2.9   Modeling conclusion

> *All models are wrong but some are more wrong than others.*
> *(pastiche based on: Box, 1976; Orwell, 1945)*
>
> Guest and Martin, 2020

In conclusion, I extended and validated bDCM to the modeling of reaction time data and provided an overview over the possible limitations and issues one faces when incorporating continuous data. Although I show that bDCM and DCM frameworks have certain limitations in modeling details of cognitive processes, it is also good to remember that instead of finding the most correct model, it is sometimes enough to have a working abstraction (Guest & Martin, 2020; Kriegeskorte & Douglas, 2018), as we see in the application for generative embedding.

More importantly, I wanted to show, that the DCM framework has larger potentials than using Bayesian model selection or parameter inference. Instead, I show that inverted DCM models can be used, tested, and falsified like regular computational models (Palminteri et al., 2017). Taking this extra step in the analysis of neuroimaging data could be a first solution to solve theoretical problems that have been identified in cognitive neuroscience research (Buzsáki, 2020; Muthukrishna & Henrich, 2019). By treating DCM models as a computational theory could also entail that DCMs are shared for functional and resting state data, so that other researchers could use them to simulate data and interventions for their experiments, but also to falsify and adjust these models.

BDCM might play a special role here, as it can provide a bridge between computational modeling in neuroscience and psychology, thus helping to understand the interactions between brain and behavior. As bDCM is based on a commonly known framework, it might facilitate the more widespread us of computational modeling in cognitive neuroscience.

> **Box 10.6: Future directions for (b)DCM**
>
> As concluded, bDCM could be a great tool for the development of computational theories of cognitive processes. But, I identified a few issues that might need to be resolved first.
>
> **Numerical Stability:** Both the VBA-Toolbox and SPM-DCM (in recent versions, Frässle et al., 2015), appear to have issues with numerical stability and are prone to overfit. One possible solution could be an empirical study to find a common set of default priors over the connectivity parameters, that prevent models from overfitting. For this I could imagine having a large, atlas based, connectivity matrix

of anatomical (c.f. Stephan et al., 2009) and resting state data (Frässle et al., 2017), where researchers could look up prior distributions for a variety of edges. This approach could also lead to standardized VOIs and thus a higher comparability of results.

Larger Model Spaces or Single Models: An interesting study could also be to investigate, whether DCM should be used to empirically select a winning model architecture, or whether researchers should rely on a few handcrafted hypothesis driven models. In recent years there has been a development towards model reduction and Parametric Bayesian approaches which can be used to efficiently estimate large model spaces, but also lead to more stable inference, as prior distributions are moved towards group estimates (Friston et al., 2018). Other applications also aim at larger model spaces. For example, regression DCM reduces the model inversion process to a linear regression, so that a model's A and C matrices can be quickly evaluated (Frässle et al., 2017). Other implementations try to use specialized hardware and massive parallelization (Aponte et al., 2016). Hand crafted and thoroughly interrogated model's on the other hand might provide better insights into the brain.

Testing and Validation: In the machine learning community and in computational neuroscience more and more effort is put into the validation and testing of established methods (Elliott et al., 2020). Possibly due to the small community, such work is sparse for DCM, but is in my opinion very necessary. As mentioned, small changes in the prior distributions can have huge impacts, so that researchers might not be able to replicate previous results (Frässle et al., 2015). An effort striving for a high validation and testing, is important, as DCM is a straightforward tool to create computational models of brain dynamics and in bDCM also of behavior (Friston et al., 2017; Rigoux & Daunizeau, 2015). Validation is especially important, as such models might play a role in personalized medicine in the future (Price et al., 2017; Stephan et al., 2017).

11 | Conclusion

In my thesis, I used an adapted version of Posner's cuing task to investigate (re)orienting along the vertical and horizontal meridians and used it to create a simultaneous model of brain and behavior.

There was little evidence for neuronal differences between vertical and horizontal (re)orienting, replicating previous work (Fink et al., 2001; Macaluso & Patria, 2007). To be more concrete neither on the behavioral nor on the level of blood oxygen level-dependent (BOLD) amplitudes a differences could be shown. More importantly, by using dynamic causal modeling (DCM) as a computational model, I could also show that dynamics between the two conditions are largely similar.

Thus, my work provides further evidence that endogenous attention can be deployed uniformly across the visual field and that attentional processes are not influenced by perceptual asymmetries, like the horizontal-vertical anisotropy (HVA) (Carrasco et al., 2001). For our understanding of neglect, this also means that impairments observed in Posner's cuing task are due to hemispheric imbalances, that most likely do not interact with the vertical meridian (Macaluso & Patria, 2007).

My results provide the starting points for new investigations. For attention research it might thus be important to investigate whether endogenous cuing reveals visual performance fields just like exogenous cuing (Barbot et al., 2020). For vertical neglect, my work indicates that it might not be due to voluntary attentional processes, but driven by interactions with perceptual processing, opening ventures for new research.

My second study provides a starting point for such research: Connections between intraparietal sulcus (IPS) and temporoparietal junction (TPJ) appear to be predictive of the orienting run. This result, however, is a proof of concept. More importantly, my second project shows that behavioral dynamic causal modeling (bDCM) can be used for reaction time data, extending its application to a wider audience.

I show in my thesis, that bDCM as a generalist framework does not necessarily model the cognitive processes, we expect to be underlying Posner's cuing task — whereas the Rescorla-Wagner does —, I also show using generative embedding that it can be useful for many other applications. For example in computational psychiatry, where incorporating behavioral responses into a model of brain connectivity might further our understanding of psychiatric disorders and might even be used in individual diagnoses (Price et al., 2017; Stephan et al., 2017).

With my work on DCM in both projects I further hope to inspire a more conscious use of the method. Treating DCM as a computational model and theory that generates new data, can be refined, but also be falsified, could be an important step for more theory driven work in cognitive neuroscience and therefore a countermeasure against generalizability and reproducibility crises (Botvinik-Nezer et al., 2020; Buzsáki, 2020; Fried, 2020; Guest & Martin, 2020; Muthukrishna & Henrich, 2019; Yarkoni & Braver, 2010).

Bibliography

Abrams, J., Nizam, A., & Carrasco, M. (2012). Isoeccentric locations are not equivalent: The extent of the vertical meridian asymmetry. *Vision Research*, *52*(1), 70–78. https://doi.org/10.1016/j.visres.2011.10.016

Aponte, E. A., Raman, S., Sengupta, B., Penny, W. D., Stephan, K. E., & Heinzle, J. (2016). Mpdcm: A toolbox for massively parallel dynamic causal modeling. *Journal of Neuroscience Methods*, *257*, 7–16. https://doi.org/10.1016/j.jneumeth.2015.09.009

Bandettini, P. A. (2012). Twenty years of functional MRI: The science and the stories. *NeuroImage*, *62*(2), 575–588. https://doi.org/10.1016/j.neuroimage.2012.04.026

Barbot, A., Xue, S., & Carrasco, M. (2020). *Asymmetries in visual acuity around the visual field* (Preprint). PsyArXiv. https://doi.org/10.31234/osf.io/ruwp9

Benjamin, D. J., Berger, J. O., Johannesson, M., Nosek, B. A., Wagenmakers, E.-J., Berk, R., Bollen, K. A., Brembs, B., Brown, L., Camerer, C., Cesarini, D., Chambers, C. D., Clyde, M., Cook, T. D., De Boeck, P., Dienes, Z., Dreber, A., Easwaran, K., Efferson, C., … Johnson, V. E. (2018). Redefine statistical significance. *Nature Human Behaviour*, *2*(1), 6–10. https://doi.org/10.1038/s41562-017-0189-z

Beume, L.-A., Martin, M., Kaller, C. P., Klöppel, S., Schmidt, C. S. M., Urbach, H., Egger, K., Rijntjes, M., Weiller, C., & Umarova, R. M. (2017). Visual neglect after left-hemispheric lesions: A voxel-based lesion–symptom mapping study in 121 acute stroke patients. *Experimental Brain Research*, *235*(1), 83–95. https://doi.org/10.1007/s00221-016-4771-9

Bishop, C. M. (2006). *Pattern recognition and machine learning*. New York, Springer.

Bisley, J. W. (2011). The neural basis of visual attention. *The Journal of Physiology*, *589*(1), 49–57. https://doi.org/10.1113/jphysiol.2010.192666

Botvinik-Nezer, R., Holzmeister, F., Camerer, C. F., Dreber, A., Huber, J., Johannesson, M., Kirchler, M., Iwanir, R., Mumford, J. A., Adcock, R. A., Avesani, P., Baczkowski, B. M., Bajracharya, A., Bakst, L., Ball, S., Barilari, M., Bault, N., Beaton, D., Beitner, J., … Schonberg, T. (2020). Variability in the analysis of a single neuroimaging dataset by many teams. *Nature*, *582*(7810), 84–88. https://doi.org/10.1038/s41586-020-2314-9

Bowring, A., Maumet, C., & Nichols, T. E. (2019). Exploring the impact of analysis software on task fMRI results. *Human Brain Mapping*, *40*(11), 3362–3384. https://doi.org/10.1002/hbm.24603

Brederoo, S. G., Nieuwenstein, M. R., Cornelissen, F. W., & Lorist, M. M. (2019). Reproducibility of visual-field asymmetries: Nine replication studies investigating lateralization of visual information processing. *Cortex*, *111*, 100–126. https://doi.org/10.1016/j.cortex.2018.10.021

Breiman, L. (2001). Random Forests. *Machine Learning*, *45*(1), 5–32. https://doi.org/10.1023/A:1010933404324

Broadbent, D. E. (1958). *Perception and communication.* Elmsford, Pergamon Press. https://doi.org/10.1037/10037-000

Brodersen, K. H., Haiss, F., Ong, C. S., Jung, F., Tittgemeyer, M., Buhmann, J. M., Weber, B., & Stephan, K. E. (2011). Model-based feature construction for multivariate decoding. *NeuroImage*, *56*(2), 601–615. https://doi.org/10.1016/j.neuroimage.2010.04.036

Brodersen, K. H., Schofield, T. M., Leff, A. P., Ong, C. S., Lomakina, E. I., Buhmann, J. M., & Stephan, K. E. (2011). Generative Embedding for Model-Based Classification of fMRI Data (O. Sporns, Ed.). *PLoS Computational Biology*, *7*(6), e1002079. https://doi.org/10.1371/journal.pcbi.1002079

Bundesen, C. (1990). A theory of visual attention. *Psychological Review*, *97*(4), 523–547. https://doi.org/10.1037/0033-295x.97.4.523

Bundesen, C. (1998). Visual Selective Attention: Outlines of a Choice Model, a Race Model and a Computational Theory. *Visual Cognition*, *5*(1-2), 287–309. https://doi.org/10.1080/713756774

Bundesen, C., Habekost, T., & Kyllingsbæk, S. (2005). A Neural Theory of Visual Attention: Bridging Cognition and Neurophysiology. *Psychological Review*, *112*(2), 291–328. https://doi.org/10.1037/0033-295X.112.2.291

Buzsáki, G. (2020). The Brain–Cognitive Behavior Problem: A Retrospective. *eneuro*, *7*(4), ENEURO.0069–20.2020. https://doi.org/10.1523/ENEURO.0069-20.2020

Bzdok, D., Altman, N., & Krzywinski, M. (2018). Statistics versus machine learning. *Nature Methods*, *15*(4), 233–234. https://doi.org/10.1038/nmeth.4642

Bzdok, D., Engemann, D., & Thirion, B. (2020). Inference and Prediction Diverge in Biomedicine. *Patterns*, *1*(8), 100119. https://doi.org/10.1016/j.patter.2020.100119

Carrasco, M., Talgar, C. P., & Cameron, E. L. (2001). Characterizing visual performance fields: Effects of transient covert attention, spatial frequency, eccentricity, task and set size. *Spatial Vision*, *15*(1), 61–75. https://doi.org/10.1163/15685680152692015

Carrasco, M. (2011). Visual attention: The past 25 years. *Vision Research*, *51*(13), 1484–1525. https://doi.org/10.1016/j.visres.2011.04.012

Carrasco, M., & Barbot, A. (2014). How Attention Affects Spatial Resolution. *Cold Spring Harbor Symposia on Quantitative Biology*, *79*, 149–160. https://doi.org/10.1101/sqb.2014.79.024687

Carrasco, M., Evert, D. L., Chang, I., & Katz, S. M. (1995). The eccentricity effect: Target eccentricity affects performance on conjunction searches. *Perception & Psychophysics*, *57*(8), 1241–1261. https://doi.org/10.3758/BF03208380

Cawley, G., & Talbot, N. (2010). On over-fitting in model selection and subsequent selection bias in performance evaluation. *Journal of Machine Learning Research*, *11*, 2079–2107.

Cazzoli, D., Nyffeler, T., Hess, C. W., & Müri, R. M. (2011). Vertical bias in neglect: A question of time? *Neuropsychologia*, *49*(9), 2369–2374. https://doi.org/10.1016/j.neuropsychologia.2011.04.010

Chajut, E., Schupak, A., & Algom, D. (2009). Are spatial and dimensional attention separate? Evidence from Posner, Stroop, and Eriksen tasks. *Memory & Cognition*, *37*(6), 924–934. https://doi.org/10.3758/MC.37.6.924

Chambers, C. D., Payne, J. M., & Mattingley, J. B. (2007). Parietal disruption impairs reflexive spatial attention within and between sensory modalities. *Neuropsychologia*, *45*(8), 1715–1724. https://doi.org/10.1016/j.neuropsychologia.2007.01.001

Chambers, C. D., Stokes, M. G., & Mattingley, J. B. (2004). Modality-Specific Control of Strategic Spatial Attention in Parietal Cortex. *Neuron*, *44*(6), 925–930. https://doi.org/10.1016/j.neuron.2004.12.009

Cherry, E. C. (1953). Some Experiments on the Recognition of Speech, with One and with Two Ears. *The Journal of the Acoustical Society of America*, *25*(5), 975. https://doi.org/10.1121/1.1907229

Chica, A. B., Martín-Arévalo, E., Botta, F., & Lupiáñez, J. (2014). The Spatial Orienting paradigm: How to design and interpret spatial attention experiments. *Neuro-*

science & Biobehavioral Reviews, 40, 35–51. https://doi.org/10.1016/j.neubiorev. 2014.01.002

Christman, S. D. (1993). Local-global processing in the upper versus lower visual fields. Bulletin of the Psychonomic Society, 31(4), 275–278. https://doi.org/10.3758/BF03334927

Cole, J. H., Marioni, R. E., Harris, S. E., & Deary, I. J. (2019). Brain age and other bodily 'ages': Implications for neuropsychiatry. Molecular Psychiatry, 24(2), 266–281. https://doi.org/10.1038/s41380-018-0098-1

Corbetta, M., Akbudak, E., Conturo, T. E., Snyder, A. Z., Ollinger, J. M., Drury, H. A., Linenweber, M. R., Petersen, S. E., Raichle, M. E., Van Essen, D. C., & Shulman, G. L. (1998). A Common Network of Functional Areas for Attention and Eye Movements. Neuron, 21(4), 761–773. https://doi.org/10.1016/S0896-6273(00)80593-0

Corbetta, M., Kincade, J. M., Ollinger, J. M., McAvoy, M. P., & Shulman, G. L. (2000). Voluntary orienting is dissociated from target detection in human posterior parietal cortex. Nature neuroscience, 3(3), 292–297.

Corbetta, M., Patel, G., & Shulman, G. L. (2008). The Reorienting System of the Human Brain: From Environment to Theory of Mind. Neuron, 58(3), 306–324. https://doi.org/10.1016/j.neuron.2008.04.017

Corbetta, M., & Shulman, G. L. (2011). Spatial Neglect and Attention Networks. Annual Review of Neuroscience, 34(1), 569–599. https://doi.org/10.1146/annurev-neuro-061010-113731

Danckert, J., Stottinger, E., Quehl, N., & Anderson, B. (2012). Right Hemisphere Brain Damage Impairs Strategy Updating. Cerebral Cortex, 22(12), 2745–2760. https://doi.org/10.1093/cercor/bhr351

Daunizeau, J., Adam, V., & Rigoux, L. (2014). VBA: A Probabilistic Treatment of Nonlinear Models for Neurobiological and Behavioural Data (A. Prlic, Ed.). PLoS Computational Biology, 10(1), e1003441. https://doi.org/10.1371/journal.pcbi.1003441

Daunizeau, J., Preuschoff, K., Friston, K., & Stephan, K. (2011). Optimizing Experimental Design for Comparing Models of Brain Function (O. Sporns, Ed.). PLoS Computational Biology, 7(11), e1002280. https://doi.org/10.1371/journal.pcbi.1002280

Deutsch, J. A., & Deutsch, D. (1963). Attention: Some theoretical considerations. Psychological Review, 70(1), 80–90. https://doi.org/10.1037/h0039515

Dombert, P. L., Kuhns, A., Mengotti, P., Fink, G. R., & Vossel, S. (2016). Functional mechanisms of probabilistic inference in feature- and space-based attentional systems. NeuroImage, 142, 553–564. https://doi.org/10.1016/j.neuroimage.2016.08.010

Domingos, P. (2012). A few useful things to know about machine learning. Communications of the ACM, 55(10), 78. https://doi.org/10.1145/2347736.2347755

Duecker, F., & Sack, A. T. (2015). The hybrid model of attentional control: New insights into hemispheric asymmetries inferred from TMS research. Neuropsychologia, 74, 21–29. https://doi.org/10.1016/j.neuropsychologia.2014.11.023

Dugué, L., Merriam, E. P., Heeger, D. J., & Carrasco, M. (2018). Specific Visual Subregions of TPJ Mediate Reorienting of Spatial Attention. Cerebral Cortex, 28(7), 2375–2390. https://doi.org/10.1093/cercor/bhx140

Eckstein, M. P., Shimozaki, S. S., & Abbey, C. K. (2002). The footprints of visual attention in the Posner cueing paradigm revealed by classification images. Journal of Vision, 2(1), 3. https://doi.org/10.1167/2.1.3

Efron, B. (2020). Prediction, Estimation, and Attribution. Journal of the American Statistical Association, 115(530), 636–655. https://doi.org/10.1080/01621459.2020.1762613

Eklund, A., Nichols, T. E., & Knutsson, H. (2016). Cluster failure: Why fMRI inferences for spatial extent have inflated false-positive rates. Proceedings of the National

Academy of Sciences, *113*(28), 7900–7905. https://doi.org/10.1073/pnas.1602413113

Elliott, M. L., Knodt, A. R., Ireland, D., Morris, M. L., Poulton, R., Ramrakha, S., Sison, M. L., Moffitt, T. E., Caspi, A., & Hariri, A. R. (2020). What Is the Test-Retest Reliability of Common Task-Functional MRI Measures? New Empirical Evidence and a Meta-Analysis. *Psychological Science*, *31*(7), 792–806. https://doi.org/10.1177/0956797620916786

Eriksen, B. A., & Eriksen, C. W. (1974). Effects of noise letters upon the identification of a target letter in a nonsearch task. *Perception & Psychophysics*, *16*(1), 143–149. https://doi.org/10.3758/BF03203267

Esteban, O., Markiewicz, C. J., Blair, R. W., Moodie, C. A., Isik, A. I., Erramuzpe, A., Kent, J. D., Goncalves, M., DuPre, E., Snyder, M., Oya, H., Ghosh, S. S., Wright, J., Durnez, J., Poldrack, R. A., & Gorgolewski, K. J. (2019). fMRIPrep: A robust preprocessing pipeline for functional MRI. *Nature Methods*, *16*(1), 111–116. https://doi.org/10.1038/s41592-018-0235-4

Fernandez-Duque, D., & Johnson, M. L. (1999). Attention Metaphors: How Metaphors Guide the Cognitive Psychology of Attention. *Cognitive Science*, *23*(1), 83–116. https://doi.org/10.1207/s15516709cog2301_4

Fiebelkorn, I. C., & Kastner, S. (2019). A Rhythmic Theory of Attention. *Trends in Cognitive Sciences*, *23*(2), 87–101. https://doi.org/10.1016/j.tics.2018.11.009

Fiebelkorn, I. C., & Kastner, S. (2020). Functional Specialization in the Attention Network. *Annual Review of Psychology*, *71*(1), 221–249. https://doi.org/10.1146/annurev-psych-010418-103429

Fink, G. R., Marshall, J. C., Weiss, P. H., & Zilles, K. (2001). The Neural Basis of Vertical and Horizontal Line Bisection Judgments: An fMRI Study of Normal Volunteers. *NeuroImage*, *14*(1), S59–S67. https://doi.org/10.1006/nimg.2001.0819

Fox, P. T. (2012). The coupling controversy. *NeuroImage*, *62*(2), 594–601. https://doi.org/10.1016/j.neuroimage.2012.01.103

Frässle, S., Lomakina, E. I., Razi, A., Friston, K. J., Buhmann, J. M., & Stephan, K. E. (2017). Regression DCM for fMRI. *NeuroImage*, *155*, 406–421. https://doi.org/10.1016/j.neuroimage.2017.02.090

Frässle, S., Stephan, K. E., Friston, K. J., Steup, M., Krach, S., Paulus, F. M., & Jansen, A. (2015). Test-retest reliability of dynamic causal modeling for fMRI. *NeuroImage*, *117*, 56–66. https://doi.org/10.1016/j.neuroimage.2015.05.040

Fried, E. I. (2020). *Lack of theory building and testing impedes progress in the factor and network literature* (Preprint). PsyArXiv. https://doi.org/10.31234/osf.io/zg84s

Friston, K. J., Litvak, V., Oswal, A., Razi, A., Stephan, K. E., van Wijk, B. C., Ziegler, G., & Zeidman, P. (2016). Bayesian model reduction and empirical Bayes for group (DCM) studies. *NeuroImage*, *128*, 413–431. https://doi.org/10.1016/j.neuroimage.2015.11.015

Friston, K. J., Parr, T., Zeidman, P., Razi, A., Flandin, G., Daunizeau, J., Hulme, O. J., Billig, A. J., Litvak, V., Moran, R. J., Price, C. J., & Lambert, C. (2020). Dynamic causal modelling of COVID-19. *Wellcome Open Research*, *5*, 89. https://doi.org/10.12688/wellcomeopenres.15881.2

Friston, K. J. (Ed.). (2007). *Statistical parametric mapping: The analysis of funtional brain images* (1st ed). Amsterdam ; Boston, Elsevier/Academic Press.

Friston, K. J., Daunizeau, J., & Stephan, K. E. (2013). Model selection and gobbledygook: Response to Lohmann et al. *NeuroImage*, *75*, 275–278. https://doi.org/10.1016/j.neuroimage.2011.11.064

Friston, K. J., Harrison, L., & Penny, W. D. (2003). Dynamic causal modelling. *NeuroImage*, *19*(4), 1273–1302. https://doi.org/10.1016/S1053-8119(03)00202-7

Friston, K. J., Parr, T., & Zeidman, P. (2018). Bayesian model reduction. *arXiv*arxiv 1805.07092.

Friston, K. J., & Penny, W. D. (2011). Post hoc Bayesian model selection. *NeuroImage*, *56*(4), 2089–2099. https://doi.org/10.1016/j.neuroimage.2011.03.062

Friston, K. J., Preller, K. H., Mathys, C., Cagnan, H., Heinzle, J., Razi, A., & Zeidman, P. (2017). Dynamic causal modelling revisited. *NeuroImage*, *199*, 730–744. https://doi.org/10.1016/j.neuroimage.2017.02.045

Friston, K. J., Williams, S., Howard, R., Frackowiak, R. S. J., & Turner, R. (1996). Movement-Related effects in fMRI time-series. *Magnetic Resonance in Medicine*, *35*(3), 346–355. https://doi.org/10.1002/mrm.1910350312

Fuller, S., Rodriguez, R. Z., & Carrasco, M. (2008). Apparent contrast differs across the vertical meridian: Visual and attentional factors. *Journal of Vision*, *8*(1), 16. https://doi.org/10.1167/8.1.16

Gillebert, C. R., Mantini, D., Thijs, V., Sunaert, S., Dupont, P., & Vandenberghe, R. (2011). Lesion evidence for the critical role of the intraparietal sulcus in spatial attention. *Brain*, *134*(6), 1694–1709. https://doi.org/10.1093/brain/awr085

Glover, G. H. (2011). Overview of Functional Magnetic Resonance Imaging. *Neurosurgery Clinics of North America*, *22*(2), 133–139. https://doi.org/10.1016/j.nec.2010.11.001

Golomb, J. D., & Kanwisher, N. (2012). Higher Level Visual Cortex Represents Retinotopic, Not Spatiotopic, Object Location. *Cerebral Cortex*, *22*(12), 2794–2810. https://doi.org/10.1093/cercor/bhr357

Gordon, N., Tsuchiya, N., Koenig-Robert, R., & Hohwy, J. (2019). Expectation and attention increase the integration of top-down and bottom-up signals in perception through different pathways (M. Posner, Ed.). *PLOS Biology*, *17*(4), e3000233. https://doi.org/10.1371/journal.pbio.3000233

Green, J. J., Boehler, C. N., Roberts, K. C., Chen, L.-C., Krebs, R. M., Song, A. W., & Woldorff, M. G. (2017). Cortical and Subcortical Coordination of Visual Spatial Attention Revealed by Simultaneous EEG–fMRI Recording. *The Journal of Neuroscience*, *37*(33), 7803–7810. https://doi.org/10.1523/JNEUROSCI.0326-17.2017

Grosenick, L., Klingenberg, B., Katovich, K., Knutson, B., & Taylor, J. E. (2013). Interpretable whole-brain prediction analysis with GraphNet. *NeuroImage*, *72*, 304–321. https://doi.org/10.1016/j.neuroimage.2012.12.062

Guest, O., & Martin, A. E. (2020). *How computational modeling can force theory building in psychological science* (Preprint). PsyArXiv. https://doi.org/10.31234/osf.io/rybh9

Gwilliams, L., & King, J.-R. (2020). Recurrent processes support a cascade of hierarchical decisions. *eLife*, *9*, e56603. https://doi.org/10.7554/eLife.56603

Hagler, D. J. (2014). Visual field asymmetries in visual evoked responses. *Journal of Vision*, *14*(14), 13–13. https://doi.org/10.1167/14.14.13

Haines, N., Kvam, P. D., Irving, L. H., Smith, C., Beauchaine, T. P., Pitt, M. A., Ahn, W.-Y., & Turner, B. (2020). *Learning from the Reliability Paradox: How Theoretically Informed Generative Models Can Advance the Social, Behavioral, and Brain Sciences* (Preprint). PsyArXiv. https://doi.org/10.31234/osf.io/xr7y3

Halligan, P. W., Fink, G. R., Marshall, J. C., & Vallar, G. (2003). Spatial cognition: Evidence from visual neglect. *Trends in Cognitive Sciences*, *7*(3), 125–133.

Hedge, C., Powell, G., & Sumner, P. (2017). The reliability paradox: Why robust cognitive tasks do not produce reliable individual differences. *Behavior Research Methods*, *50*, 1166–1186. https://doi.org/10.3758/s13428-017-0935-1

Heilman, K. M., & Valenstein, E. (1979). Mechanisms underlying hemispatial neglect. *Annals of Neurology*, *5*(2), 166–170. https://doi.org/10.1002/ana.410050210

Heilman, K. M., Valenstein, E., & Watson, R. T. (2000). Neglect and Related Disorders. *Seminars in Neurology*, *20*(04), 463–470. https://doi.org/10.1055/s-2000-13179

Hommel, B., Chapman, C. S., Cisek, P., Neyedli, H. F., Song, J.-H., & Welsh, T. N. (2019). No one knows what attention is. *Attention, Perception, & Psychophysics*, *81*, 2288–2303. https://doi.org/10.3758/s13414-019-01846-w

Huettel, S. A., Song, A. W., & McCarthy, G. (2008). *Functional magnetic resonance imaging* (2nd ed). Sunderland, Mass, Sinauer Associates.

James, W. (1890). *The Principles of Psychology* (Vol. 1). Cambridge, Mass., Harvard Univ. Press.

Jarosz, A. F., & Wiley, J. (2014). What Are the Odds? A Practical Guide to Computing and Reporting Bayes Factors. *The Journal of Problem Solving*, *7*(1). https://doi.org/10.7771/1932-6246.1167

Jewell, G., & McCourt, M. E. (2000). Pseudoneglect: A review and meta-analysis of performance factors in line bisection tasks. *Neuropsychologia*, *38*(1), 93–110. https://doi.org/10.1016/S0028-3932(99)00045-7

Jóhannesson, Ó. I., Tagu, J., & Kristjánsson, Á. (2018). Asymmetries of the visual system and their influence on visual performance and oculomotor dynamics. *European Journal of Neuroscience*, *48*(11), 3426–3445. https://doi.org/10.1111/ejn.14225

Karnath, H.-O. (2015). Spatial attention systems in spatial neglect. *Neuropsychologia*, *75*, 61–73. https://doi.org/10.1016/j.neuropsychologia.2015.05.019

Karnath, H.-O., Rennig, J., Johannsen, L., & Rorden, C. (2011). The anatomy underlying acute versus chronic spatial neglect: A longitudinal study. *Brain*, *134*(3), 903–912. https://doi.org/10.1093/brain/awq355

Kastner, S., & Ungerleider, L. G. (2001). The neural basis of biased competition in human visual cortex. *Neuropsychologia*, *39*(12), 1263–1276. https://doi.org/10.1016/S0028-3932(01)00116-6

Kelly, A. C., Uddin, L. Q., Biswal, B. B., Castellanos, F. X., & Milham, M. P. (2008). Competition between functional brain networks mediates behavioral variability. *NeuroImage*, *39*(1), 527–537. https://doi.org/10.1016/j.neuroimage.2007.08.008

Keysers, C., Gazzola, V., & Wagenmakers, E.-J. (2020). Using Bayes factor hypothesis testing in neuroscience to establish evidence of absence. *Nature Neuroscience*, *23*(7), 788–799. https://doi.org/10.1038/s41593-020-0660-4

Kinsbourne, M. (1977). Hemi-neglect and hemisphere rivalry. *Advances in Neurology*, *18*, 41–49.

Klatt, S., Ford, P. R., & Smeeton, N. J. (2020). Attentional and perceptual asymmetries in an immersive decision-making task. *Attention, Perception, & Psychophysics*, *82*(4), 1847–1857. https://doi.org/10.3758/s13414-019-01935-w

Klein, R. M. (2000). Inhibition of return. *Trends in Cognitive Sciences*, *4*(4), 138–147. https://doi.org/10.1016/S1364-6613(00)01452-2

Konnikova, M. (2020). *The biggest bluff: How I learned to pay attention, master the odds, and win*. New York, Penguin Press.

Kording, K., Blohm, G., Schrater, P., & Kay, K. (2018). *Appreciating diversity of goals in computational neuroscience* (Preprint). Open Science Framework. https://doi.org/10.31219/osf.io/3vy69

Krauzlis, R. J., Lovejoy, L. P., & Zénon, A. (2013). Superior Colliculus and Visual Spatial Attention. *Annual Review of Neuroscience*, *36*(1), 165–182. https://doi.org/10.1146/annurev-neuro-062012-170249

Kriegeskorte, N., & Douglas, P. K. (2018). Cognitive computational neuroscience. *Nature Neuroscience*, *21*(9), 1148–1160. https://doi.org/10.1038/s41593-018-0210-5

Kupers, E. R., Carrasco, M., & Winawer, J. (2019). Modeling visual performance differences 'around' the visual field: A computational observer approach (W. Einhäuser,

Ed.). *PLOS Computational Biology*, *15*(5), e1007063. https://doi.org/10.1371/journal.pcbi.1007063

Kyllingsbæk, S. (2006). Modeling visual attention. *Behavior Research Methods*, *38*(1), 123–133. https://doi.org/10.3758/BF03192757

Lakens, D. (2017). Equivalence Tests: A Practical Primer for *t* Tests, Correlations, and Meta-Analyses. *Social Psychological and Personality Science*, *8*(4), 355–362. https://doi.org/10.1177/1948550617697177

Lavie, N., & Tsal, Y. (1994). Perceptual load as a major determinant of the locus of selection in visual attention. *Perception & Psychophysics*, *56*(2), 183–197. https://doi.org/10.3758/BF03213897

Lemos, J., Pereira, D., Almendra, L., Rebelo, D., Patrício, M., Castelhano, J., Cunha, G., Januário, C., Cunha, L., Freire, A., & Castelo-Branco, M. (2016). Distinct functional properties of the vertical and horizontal saccadic network in Health and Parkinson's disease: An eye-tracking and fMRI study. *Brain Research*, *1648*, 469–484. https://doi.org/10.1016/j.brainres.2016.07.037

Lemos, J., Pereira, D., Almendra, L., Rebelo, D., Patrício, M., Castelhano, J., Cunha, G., Januário, C., Cunha, L., Freire, A., & Castelo-Branco, M. (2017). Cortical control of vertical and horizontal saccades in progressive supranuclear palsy: An exploratory fMRI study. *Journal of the Neurological Sciences*, *373*, 157–166. https://doi.org/10.1016/j.jns.2016.12.049

Levine, M. W., & McAnany, J. J. (2005). The relative capabilities of the upper and lower visual hemifields. *Vision Research*, *45*(21), 2820–2830. https://doi.org/10.1016/j.visres.2005.04.001

Liu, T. T. (2017). Reprint of 'Noise contributions to the fMRI signal: An Overview'. *NeuroImage*, *154*, 4–14. https://doi.org/10.1016/j.neuroimage.2017.05.031

Logothetis, N. K., Pauls, J., Augath, M., Trinath, T., & Oeltermann, A. (2001). Neurophysiological investigation of the basis of the fMRI signal. *Nature*, *412*(6843), 150–157. https://doi.org/10.1038/35084005

Lohmann, G., Erfurth, K., Müller, K., & Turner, R. (2012). Critical comments on dynamic causal modelling. *NeuroImage*, *59*(3), 2322–2329. https://doi.org/10.1016/j.neuroimage.2011.09.025

Lunven, M., & Bartolomeo, P. (2017). Attention and spatial cognition: Neural and anatomical substrates of visual neglect. *Annals of Physical and Rehabilitation Medicine*, *60*(3), 124–129. https://doi.org/10.1016/j.rehab.2016.01.004

Lunven, M., Thiebaut De Schotten, M., Bourlon, C., Duret, C., Migliaccio, R., Rode, G., & Bartolomeo, P. (2015). White matter lesional predictors of chronic visual neglect: A longitudinal study. *Brain*, *138*(3), 746–760. https://doi.org/10.1093/brain/awu389

Lykken, D. T. (1991). What's wrong with psychology, anyway? In *Thinking clearly about psychology, vol. 1* (pp. 3–39). University of Minnesota Press.

Lyon, L. (2017). Dead salmon and voodoo correlations: Should we be sceptical about functional MRI? *Brain*, *140*(8), e53–e53. https://doi.org/10.1093/brain/awx180

Macaluso, E., & Patria, F. (2007). Spatial re-orienting of visual attention along the horizontal or the vertical axis. *Experimental Brain Research*, *180*(1), 23–34. https://doi.org/10.1007/s00221-006-0841-8

Malherbe, C., Umarova, R., Zavaglia, M., Kaller, C., Beume, L., Thomalla, G., Weiller, C., & Hilgetag, C. (2018). Neural correlates of visuospatial bias in patients with left hemisphere stroke: A causal functional contribution analysis based on game theory. *Neuropsychologia*, *115*, 142–153. https://doi.org/10.1016/j.neuropsychologia.2017.10.013

Mao, L., Zhou, B., Zhou, W., & Han, S. (2007). Neural correlates of covert orienting of visual spatial attention along vertical and horizontal dimensions. *Brain Research*, *1136*, 142–153. https://doi.org/10.1016/j.brainres.2006.12.031

Marr, D. (2010). *Vision: A computational investigation into the human representation and processing of visual information*. Cambridge, Mass, MIT Press OCLC: ocn472791457.

Mathys, C. (2011). A Bayesian foundation for individual learning under uncertainty. *Frontiers in Human Neuroscience*, *5*. https://doi.org/10.3389/fnhum.2011.00039

Meister, I., Wienemann, M., Buelte, D., Grünewald, C., Sparing, R., Dambeck, N., & Boroojerdi, B. (2006). Hemiextinction induced by transcranial magnetic stimulation over the right temporo-parietal junction. *Neuroscience*, *142*(1), 119–123. https://doi.org/10.1016/j.neuroscience.2006.06.023

Mengotti, P., Boers, F., Dombert, P. L., Fink, G. R., & Vossel, S. (2018). Integrating modality-specific expectancies for the deployment of spatial attention. *Scientific Reports*, *8*(1). https://doi.org/10.1038/s41598-018-19593-7

Mengotti, P., Dombert, P. L., Fink, G. R., & Vossel, S. (2017). Disruption of the Right Temporoparietal Junction Impairs Probabilistic Belief Updating. *The Journal of Neuroscience*, *37*(22), 5419–5428. https://doi.org/10.1523/JNEUROSCI.3683-16.2017

Mengotti, P., Käsbauer, A.-S., Fink, G. R., & Vossel, S. (2020). Lateralization, functional specialization, and dysfunction of attentional networks. *Cortex*, *132*, 206–222. https://doi.org/10.1016/j.cortex.2020.08.022

Merel, J., Aldarondo, D., Marshall, J., Tassa, Y., Wayne, G., & Ölveczky, B. (2019). Deep neuroethology of a virtual rodent. *arXiv:1911.09451 [q-bio]*arxiv 1911.09451.

Milner, A. D. (2017). How do the two visual streams interact with each other? *Experimental Brain Research*, *235*(5), 1297–1308. https://doi.org/10.1007/s00221-017-4917-4

Mirman, D., Landrigan, J.-F., Kokolis, S., Verillo, S., Ferrara, C., & Pustina, D. (2018). Corrections for multiple comparisons in voxel-based lesion-symptom mapping. *Neuropsychologia*, *115*, 112–123. https://doi.org/10.1016/j.neuropsychologia.2017.08.025

Misaki, M., Kim, Y., Bandettini, P. A., & Kriegeskorte, N. (2010). Comparison of multivariate classifiers and response normalizations for pattern-information fMRI. *NeuroImage*, *53*(1), 103–118. https://doi.org/10.1016/j.neuroimage.2010.05.051

Miyawaki, Y., Uchida, H., Yamashita, O., Sato, M.-a., Morito, Y., Tanabe, H. C., Sadato, N., & Kamitani, Y. (2008). Visual Image Reconstruction from Human Brain Activity using a Combination of Multiscale Local Image Decoders. *Neuron*, *60*(5), 915–929. https://doi.org/10.1016/j.neuron.2008.11.004

Montaser-Kouhsari, L., & Carrasco, M. (2009). Perceptual asymmetries are preserved in short-term memory tasks. *Attention, Perception & Psychophysics*, *71*(8), 1782–1792. https://doi.org/10.3758/APP.71.8.1782

Moray, N. (1959). Attention in dichotic listening: Affective cues and the influence of instructions. *Quarterly Journal of Experimental Psychology*, *11*(1), 56–60. https://doi.org/10.1080/17470215908416289

Morey, R. D., Romeijn, J.-W., & Rouder, J. N. (2016). The philosophy of Bayes factors and the quantification of statistical evidence. *Journal of Mathematical Psychology*, *72*, 6–18. https://doi.org/10.1016/j.jmp.2015.11.001

Morris, M., Mańkowska, A., & Heilman, K. M. (2020). Upper Vertical Spatial Neglect With A Right Temporal Lobe Stroke: *Cognitive and Behavioral Neurology*, *33*(1), 63–66. https://doi.org/10.1097/WNN.0000000000000221

Mueller, K., Lepsien, J., Möller, H. E., & Lohmann, G. (2017). Commentary: Cluster failure: Why fMRI inferences for spatial extent have inflated false-positive rates. *Frontiers in Human Neuroscience*, *11*. https://doi.org/10.3389/fnhum.2017.00345

Müri, R. M., Cazzoli, D., Nyffeler, T., & Pflugshaupt, T. (2009). Visual exploration pattern in hemineglect. *Psychological Research*, *73*(2), 147–157. https://doi.org/10.1007/s00426-008-0204-0

Murphy, G., Groeger, J. A., & Greene, C. M. (2016). Twenty years of load theory—Where are we now, and where should we go next? *Psychonomic Bulletin & Review*, *23*(5), 1316–1340. https://doi.org/10.3758/s13423-015-0982-5

Musall, S., Urai, A. E., Sussillo, D., & Churchland, A. K. (2019). Harnessing behavioral diversity to understand neural computations for cognition. *Current Opinion in Neurobiology*, *58*, 229–238. https://doi.org/10.1016/j.conb.2019.09.011

Muthukrishna, M., & Henrich, J. (2019). A problem in theory. *Nature Human Behaviour*, *3*(3), 221–229. https://doi.org/10.1038/s41562-018-0522-1

Mwangi, B., Tian, T. S., & Soares, J. C. (2014). A Review of Feature Reduction Techniques in Neuroimaging. *Neuroinformatics*, *12*(2), 229–244. https://doi.org/10.1007/s12021-013-9204-3

Navarro, D. (2020). *If mathematical psychology did not exist we would need to invent it: A case study in cumulative theoretical development* (Preprint). PsyArXiv. https://doi.org/10.31234/osf.io/ygbjp

Navon, D. (1977). Forest before trees: The precedence of global features in visual perception. *Cognitive Psychology*, *9*(3), 353–383. https://doi.org/10.1016/0010-0285(77)90012-3

Nicholls, M. E. R., Mattingley, J. B., Berberovic, N., Smith, A., & Bradshaw, J. L. (2004). An investigation of the relationship between free-viewing perceptual asymmetries for vertical and horizontal stimuli. *Cognitive Brain Research*, *19*(3), 289–301. https://doi.org/10.1016/j.cogbrainres.2003.12.008

Nicholls, M. E. R., Smith, A., Mattingley, J. B., & Bradshaw, J. L. (2006). The effect of body and environment-centred coordinates on free-viewing perceptual asymmetries for vertical and horizontal stimuli. *Cortex; a Journal Devoted to the Study of the Nervous System and Behavior*, *42*(3), 336–346.

Nichols, T. E., Das, S., Eickhoff, S. B., Evans, A. C., Glatard, T., Hanke, M., Kriegeskorte, N., Milham, M. P., Poldrack, R. A., Poline, J.-B., Proal, E., Thirion, B., Van Essen, D. C., White, T., & Yeo, B. T. T. (2017). Best practices in data analysis and sharing in neuroimaging using MRI. *Nature Neuroscience*, *20*(3), 299–303. https://doi.org/10.1038/nn.4500

Nichols, T. E., & Holmes, A. P. (2002). Nonparametric permutation tests for functional neuroimaging: A primer with examples. *Human Brain Mapping*, *15*(1), 1–25.

Niv, Y. (2020). *The primacy of behavioral research for understanding the brain* (Preprint). PsyArXiv. https://doi.org/10.31234/osf.io/y8mxe

Norman, D. A. (2013). *The design of everyday things* (Revised and expanded edition). New York, New York, Basic Books.

Norman, K. A., Polyn, S. M., Detre, G. J., & Haxby, J. V. (2006). Beyond mind-reading: Multi-voxel pattern analysis of fMRI data. *Trends in Cognitive Sciences*, *10*(9), 424–430. https://doi.org/10.1016/j.tics.2006.07.005

Noudoost, B., Chang, M. H., Steinmetz, N. A., & Moore, T. (2010). Top-down control of visual attention. *Current Opinion in Neurobiology*, *20*(2), 183–190. https://doi.org/10.1016/j.conb.2010.02.003

Oelrich, O., Ding, S., Magnusson, M., Vehtari, A., & Villani, M. (2020). When are Bayesian model probabilities overconfident? *arXiv:2003.04026 [math, stat]*arxiv 2003.04026.

Ogawa, S., Lee, T. M., Kay, A. R., & Tank, D. W. (1990). Brain magnetic resonance imaging with contrast dependent on blood oxygenation. *Proceedings of the National*

Academy of Sciences of the United States of America, *87*(24), 9868–9872. https://doi.org/10.1073/pnas.87.24.9868

Ojala, M., & Garriga, G. C. (2010). Permutation Tests for Studying Classifier Performance. *J. Mach. Learn. Res.*, *11*, 1833–1863.

O'Sullivan, J. A., Power, A. J., Mesgarani, N., Rajaram, S., Foxe, J. J., Shinn-Cunningham, B. G., Slaney, M., Shamma, S. A., & Lalor, E. C. (2014). Attentional Selection in a Cocktail Party Environment Can Be Decoded from Single-Trial EEG. *Cerebral Cortex*, *25*(7), 1697–1706. https://doi.org/10.1093/cercor/bht355

Palminteri, S., Wyart, V., & Koechlin, E. (2017). The Importance of Falsification in Computational Cognitive Modeling. *Trends in Cognitive Sciences*, *21*(6), 425–433. https://doi.org/10.1016/j.tics.2017.03.011

Parr, T., & Friston, K. J. (2018). The Computational Anatomy of Visual Neglect. *Cerebral Cortex*, *28*(2), 777–790. https://doi.org/10.1093/cercor/bhx316

Pearl, J. (2018). Remark: Both Harvard's #causalinference group and Rubin's potential outcome framework do not distinguish Rung-2 from Rung-3. (cont.) https://twitter.com/yudapearl/status/1069533953223155713.

Pearl, J., & Mackenzie, D. (2018). *The book of why: The new science of cause and effect*. New York, Basic Books.

Pedregosa, F., Varoquaux, G., Gramfort, A., Michel, V., Thirion, B., Grisel, O., Blondel, M., Prettenhofer, P., Weiss, R., Dubourg, V., Et al. (2011). Scikit-learn: Machine learning in Python. *The Journal of Machine Learning Research*, *12*, 2825–2830.

Penny, W. D. (2012). Comparing Dynamic Causal Models using AIC, BIC and Free Energy. *NeuroImage*, *59*(1), 319–330. https://doi.org/10.1016/j.neuroimage.2011.07.039

Penny, W. D., Stephan, K. E., Daunizeau, J., Rosa, M. J., Friston, K. J., Schofield, T. M., & Leff, A. P. (2010). Comparing families of dynamic causal models. *PLoS computational biology*, *6*(3), e1000709. https://doi.org/10.1371/journal.pcbi.1000709

Petersen, S. E., & Posner, M. I. (2012). The Attention System of the Human Brain: 20 Years After. *Annual Review of Neuroscience*, *35*(1), 73–89. https://doi.org/10.1146/annurev-neuro-062111-150525

Pitzalis, S., Spinelli, D., & Zoccolotti, P. (1997). Vertical neglect: Behavioral and electrophysiological data. *Cortex; a Journal Devoted to the Study of the Nervous System and Behavior*, *33*(4), 679–688.

Poldrack, R. A., Huckins, G., & Varoquaux, G. (2019). Establishment of Best Practices for Evidence for Prediction: A Review. *JAMA Psychiatry*, *77*(5), 534–540. https://doi.org/10.1001/jamapsychiatry.2019.3671

Poline, J.-B., & Brett, M. (2012). The general linear model and fMRI: Does love last forever? *NeuroImage*, *62*(2), 871–880. https://doi.org/10.1016/j.neuroimage.2012.01.133

Posner, M. I. (1980). Orienting of attention. *The Quarterly Journal of Experimental Psychology*, *32*(1), 3–25. https://doi.org/10.1080/00335558008248231

Posner, M. I., Walker, J. A., Friedrich, F. J., & Rafal, R. D. (1984). Effects of parietal injury on covert orienting of attention. *The Journal of Neuroscience: 4*(7), 1863–1874. https://doi.org/10.1523/jneurosci.04-07-01863.1984

Posner, M. I. (2016). Orienting of Attention: Then and Now. *Quarterly Journal of Experimental Psychology*, *69*(10), 1864–1875. https://doi.org/10.1080/17470218.2014.937446

Posner, M. I., Nissen, M. J., & Ogden, W. C. (1978). Attended and unattended processing modes: The role of set for spatial location. *Modes of perceiving and processing information*, *137*(158), 137–157.

Price, C. J., Hope, T. M., & Seghier, M. L. (2017). Ten problems and solutions when predicting individual outcome from lesion site after stroke. *NeuroImage*, *145*, 200–208. https://doi.org/10.1016/j.neuroimage.2016.08.006

Raichle, M. E. (1998). Behind the scenes of functional brain imaging: A historical and physiological perspective. *Proceedings of the National Academy of Sciences*, *95*(3), 765–772. https://doi.org/10.1073/pnas.95.3.765

Rapcsak, S. Z., Cimino, C. R., & Heilman, K. M. (1988). Altitudinal neglect. *Neurology*, *38*(2), 277–277. https://doi.org/10.1212/WNL.38.2.277

Ratcliff, R. (1978). A theory of memory retrieval. *Psychological Review*, *85*(2), 59–108. https://doi.org/10.1037/0033-295X.85.2.59

Ratcliff, R., & McKoon, G. (2008). The Diffusion Decision Model: Theory and Data for Two-Choice Decision Tasks. *Neural Computation*, *20*(4), 873–922. https://doi.org/10.1162/neco.2008.12-06-420

Rescorla, R. A., & Wagner, A. R. (1972). A theory of Pavlovian conditioning: Variations in the effectiveness of reinforcement and nonreinforcement. In *Classical conditioning II: Current research and theory* (pp. 64–99). New-York.

Rigoux, L., & Daunizeau, J. (2015). Dynamic causal modelling of brain–behaviour relationships. *NeuroImage*, *117*, 202–221. https://doi.org/10.1016/j.neuroimage.2015.05.041

Rizzolatti, G., Riggio, L., Dascola, I., & Umiltá, C. (1987). Reorienting attention across the horizontal and vertical meridians: Evidence in favor of a premotor theory of attention. *Neuropsychologia*, *25*(1A), 31–40. https://doi.org/10.1016/0028-3932(87)90041-8

Rosenblueth, A., & Wiener, N. (1945). The Role of Models in Science. *Philosophy of Science*, *12*(4), 316–321.

Rouder, J. N., Speckman, P. L., Sun, D., Morey, R. D., & Iverson, G. (2009). Bayesian t tests for accepting and rejecting the null hypothesis. *Psychonomic Bulletin & Review*, *16*(2), 225–237. https://doi.org/10.3758/PBR.16.2.225

Ruff, C. C., Bestmann, S., Blankenburg, F., Bjoertomt, O., Josephs, O., Weiskopf, N., Deichmann, R., & Driver, J. (2008). Distinct Causal Influences of Parietal Versus Frontal Areas on Human Visual Cortex: Evidence from Concurrent TMS-fMRI. *Cerebral Cortex*, *18*(4), 817–827. https://doi.org/10.1093/cercor/bhm128

Ruff, C. C., Blankenburg, F., Bjoertomt, O., Bestmann, S., Weiskopf, N., & Driver, J. (2009). Hemispheric Differences in Frontal and Parietal Influences on Human Occipital Cortex: Direct Confirmation with Concurrent TMS–fMRI. *Journal of Cognitive Neuroscience*, *21*(6), 1146–1161. https://doi.org/10.1162/jocn.2009.21097

Shaw, D., Czekóová, K., Gajdoš, M., Staněk, R., Špalek, J., & Brázdil, M. (2019). Social decision-making in the brain: Input-state-output modelling reveals patterns of effective connectivity underlying reciprocal choices. *Human Brain Mapping*, *40*(2), 699–712. https://doi.org/10.1002/hbm.24446

Shelton, P. A., Bowers, D., & Heilman, K. M. (1990). PERIPERSONAL AND VERTICAL NEGLECT. *Brain*, *113*(1), 191–205. https://doi.org/10.1093/brain/113.1.191

Sheremata, S. L., & Silver, M. A. (2015). Hemisphere-Dependent Attentional Modulation of Human Parietal Visual Field Representations. *Journal of Neuroscience*, *35*(2), 508–517. https://doi.org/10.1523/JNEUROSCI.2378-14.2015

Sheth, B. R., & Young, R. (2016). Two Visual Pathways in Primates Based on Sampling of Space: Exploitation and Exploration of Visual Information. *Frontiers in Integrative Neuroscience*, *10*. https://doi.org/10.3389/fnint.2016.00037

Silvetti, M., Lasaponara, S., Lecce, F., Dragone, A., Macaluso, E., & Doricchi, F. (2016). The Response of the Left Ventral Attentional System to Invalid Targets and its

Implication for the Spatial Neglect Syndrome: A Multivariate fMRI Investigation. *Cerebral Cortex*, *26*(12), 4551–4562. https://doi.org/10.1093/cercor/bhv208

Simons, D. J., & Chabris, C. F. (1999). Gorillas in our midst: Sustained inattentional blindness for dynamic events. *Perception*, *28*(9), 1059–1074. https://doi.org/10.1068/p281059

Smaldino, P. E. (2020). How to Translate a Verbal Theory Into a Formal Model. *Social Psychology*, *51*(4), 207–218. https://doi.org/10.1027/1864-9335/a000425

Soares, J. M., Magalhães, R., Moreira, P. S., Sousa, A., Ganz, E., Sampaio, A., Alves, V., Marques, P., & Sousa, N. (2016). A Hitchhiker's Guide to Functional Magnetic Resonance Imaging. *Frontiers in Neuroscience*, *10*. https://doi.org/10.3389/fnins.2016.00515

Soret, R., Charras, P., Hurter, C., & Peysakhovich, V. (2019). Attentional orienting in virtual reality using endogenous and exogenous cues in auditory and visual modalities, In *Proceedings of the 11th ACM Symposium on Eye Tracking Research & Applications - ETRA '19*, Denver, Colorado, ACM Press. https://doi.org/10.1145/3314111.3321490

Steinkamp, S. R., Fink, G. R., Vossel, S., & Weidner, R. (2020). *Simultaneous Modeling of Reaction Times and Brain Dynamics in a Spatial Cuing Task* (Preprint). bioRxiv. https://doi.org/10.1101/2020.11.16.384198

Steinkamp, S. R., Vossel, S., Fink, G. R., & Weidner, R. (2020). Attentional reorientation along the meridians of the visual field: Are there different neural mechanisms at play? *Human Brain Mapping*, *41*(13), 3765–3780. https://doi.org/10.1002/hbm.25086

Stephan, K. E., Kasper, L., Harrison, L. M., Daunizeau, J., den Ouden, H. E. M., Breakspear, M., & Friston, K. J. (2008). Nonlinear dynamic causal models for fMRI. *NeuroImage*, *42*(2), 649–662. https://doi.org/10.1016/j.neuroimage.2008.04.262

Stephan, K. E., Schlagenhauf, F., Huys, Q., Raman, S., Aponte, E., Brodersen, K., Rigoux, L., Moran, R., Daunizeau, J., Dolan, R., Friston, K. J., & Heinz, A. (2017). Computational neuroimaging strategies for single patient predictions. *NeuroImage*, *145*, 180–199. https://doi.org/10.1016/j.neuroimage.2016.06.038

Stephan, K. E., Weiskopf, N., Drysdale, P. M., Robinson, P. A., & Friston, K. J. (2007). Comparing hemodynamic models with DCM. *NeuroImage*, *38*(3), 387–401. https://doi.org/10.1016/j.neuroimage.2007.07.040

Stephan, K. E., Tittgemeyer, M., Knösche, T. R., Moran, R. J., & Friston, K. J. (2009). Tractography-based priors for dynamic causal models. *NeuroImage*, *47*(4), 1628–1638. https://doi.org/10.1016/j.neuroimage.2009.05.096

Stöttinger, E., Filipowicz, A., Marandi, E., Quehl, N., Danckert, J., & Anderson, B. (2014). Statistical and perceptual updating: Correlated impairments in right brain injury. *Experimental Brain Research*, *232*(6), 1971–1987. https://doi.org/10.1007/s00221-014-3887-z

Szczepanski, S. M., Pinsk, M. A., Douglas, M. M., Kastner, S., & Saalmann, Y. B. (2013). Functional and structural architecture of the human dorsal frontoparietal attention network. *Proceedings of the National Academy of Sciences*, *110*(39), 15806–15811. https://doi.org/10.1073/pnas.1313903110

Szucs, D., & Ioannidis, J. P. (2020). Sample size evolution in neuroimaging research: An evaluation of highly-cited studies (1990–2012) and of latest practices (2017–2018) in high-impact journals. *NeuroImage*, *221*, 117164. https://doi.org/10.1016/j.neuroimage.2020.117164

Thiebaut de Schotten, M., Dell'Acqua, F., Ratiu, P., Leslie, A., Howells, H., Cabanis, E., Iba-Zizen, M. T., Plaisant, O., Simmons, A., Dronkers, N. F., Corkin, S., & Catani, M. (2015). From Phineas Gage and Monsieur Leborgne to H.M.: Revisiting Dis-

connection Syndromes. *Cerebral Cortex*, *25*(12), 4812–4827. https://doi.org/10.1093/cercor/bhv173

Thiebaut de Schotten, M., Tomaiuolo, F., Aiello, M., Merola, S., Silvetti, M., Lecce, F., Bartolomeo, P., & Doricchi, F. (2014). Damage to White Matter Pathways in Subacute and Chronic Spatial Neglect: A Group Study and 2 Single-Case Studies with Complete Virtual "In Vivo" Tractography Dissection. *Cerebral Cortex*, *24*(3), 691–706. https://doi.org/10.1093/cercor/bhs351

Thiebaut de Schotten, M., Foulon, C., & Nachev, P. (2020). Brain disconnections link structural connectivity with function and behaviour. *Nature Communications*, *11*(1), 5094. https://doi.org/10.1038/s41467-020-18920-9

Thompson, K. G. (2005). Neuronal Basis of Covert Spatial Attention in the Frontal Eye Field. *Journal of Neuroscience*, *25*(41), 9479–9487. https://doi.org/10.1523/JNEUROSCI.0741-05.2005

Treisman, A. M. (1960). Contextual cues in selective listening. *Quarterly Journal of Experimental Psychology*, *12*(4), 242–248. https://doi.org/10.1080/17470216008416732

Treisman, A. M., & Gelade, G. (1980). A feature-integration theory of attention. *Cognitive Psychology*, *12*(1), 97–136. https://doi.org/10.1016/0010-0285(80)90005-5

Turner, B. O., Paul, E. J., Miller, M. B., & Barbey, A. K. (2018). Small sample sizes reduce the replicability of task-based fMRI studies. *Communications Biology*, *1*(1). https://doi.org/10.1038/s42003-018-0073-z

Turner, B. M., Forstmann, B. U., Love, B. C., Palmeri, T. J., & Van Maanen, L. (2017). Approaches to analysis in model-based cognitive neuroscience. *Journal of Mathematical Psychology*, *76*, 65–79. https://doi.org/10.1016/j.jmp.2016.01.001

Turner, B. M., & Van Zandt, T. (2012). A tutorial on approximate Bayesian computation. *Journal of Mathematical Psychology*, *56*(2), 69–85. https://doi.org/10.1016/j.jmp.2012.02.005

Valero-Cabré, A., Amengual, J. L., Stengel, C., Pascual-Leone, A., & Coubard, O. A. (2017). Transcranial magnetic stimulation in basic and clinical neuroscience: A comprehensive review of fundamental principles and novel insights. *Neuroscience & Biobehavioral Reviews*, *83*, 381–404. https://doi.org/10.1016/j.neubiorev.2017.10.006

Varoquaux, G. (2017). Cross-validation failure: Small sample sizes lead to large error bars. *NeuroImage*, *180*, 68–77. https://doi.org/10.1016/j.neuroimage.2017.06.061

Verdon, V., Schwartz, S., Lovblad, K.-O., Hauert, C.-A., & Vuilleumier, P. (2010). Neuroanatomy of hemispatial neglect and its functional components: A study using voxel-based lesion-symptom mapping. *Brain*, *133*(3), 880–894. https://doi.org/10.1093/brain/awp305

Vossel, S., Geng, J. J., & Fink, G. R. (2014). Dorsal and Ventral Attention Systems: Distinct Neural Circuits but Collaborative Roles. *The Neuroscientist*, *20*(2), 150–159. https://doi.org/10.1177/1073858413494269

Vossel, S., Mathys, C., Daunizeau, J., Bauer, M., Driver, J., Friston, K. J., & Stephan, K. E. (2014). Spatial Attention, Precision, and Bayesian Inference: A Study of Saccadic Response Speed. *Cerebral Cortex*, *24*(6), 1436–1450. https://doi.org/10.1093/cercor/bhs418

Vossel, S., Thiel, C. M., & Fink, G. R. (2006). Cue validity modulates the neural correlates of covert endogenous orienting of attention in parietal and frontal cortex. *NeuroImage*, *32*(3), 1257–1264. https://doi.org/10.1016/j.neuroimage.2006.05.019

Vossel, S., Weidner, R., Driver, J., Friston, K. J., & Fink, G. R. (2012). Deconstructing the Architecture of Dorsal and Ventral Attention Systems with Dynamic Causal Modeling. *Journal of Neuroscience*, *32*(31), 10637–10648. https://doi.org/10.1523/JNEUROSCI.0414-12.2012

Vossel, S., Weidner, R., Moos, K., & Fink, G. R. (2016). Individual attentional selection capacities are reflected in interhemispheric connectivity of the parietal cortex. *NeuroImage*, *129*, 148–158. https://doi.org/10.1016/j.neuroimage.2016.01.054

Wang, S., Peterson, D. J., Gatenby, J. C., Li, W., Grabowski, T. J., & Madhyastha, T. M. (2017). Evaluation of Field Map and Nonlinear Registration Methods for Correction of Susceptibility Artifacts in Diffusion MRI. *Frontiers in Neuroinformatics*, *11*. https://doi.org/10.3389/fninf.2017.00017

Weissman, D. H., & Prado, J. (2012). Heightened activity in a key region of the ventral attention network is linked to reduced activity in a key region of the dorsal attention network during unexpected shifts of covert visual spatial attention. *NeuroImage*, *61*(4), 798–804. https://doi.org/10.1016/j.neuroimage.2012.03.032

Wen, X., Yao, L., Liu, Y., & Ding, M. (2012). Causal Interactions in Attention Networks Predict Behavioral Performance. *Journal of Neuroscience*, *32*(4), 1284–1292. https://doi.org/10.1523/JNEUROSCI.2817-11.2012

Wolfe, J. M. (1994). Guided Search 2.0 A revised model of visual search. *Psychonomic Bulletin & Review*, *1*(2), 202–238. https://doi.org/10.3758/BF03200774

Wolfe, J. M. (2007). Guided Search 4.0. In W. D. Gray (Ed.), *Integrated Models of Cognitive Systems* (pp. 99–119). Oxford University Press. https://doi.org/10.1093/acprof:oso/9780195189193.003.0008

Wu, G., Wang, Y., Mwansisya, T. E., Pu, W., Zhang, H., Liu, C., Yang, Q., Chen, E. Y., Xue, Z., Liu, Z., & Shan, B. (2014). Effective connectivity of the posterior cingulate and medial prefrontal cortices relates to working memory impairment in schizophrenic and bipolar patients. *Schizophrenia Research*, *158*(1-3), 85–90. https://doi.org/10.1016/j.schres.2014.06.033

Yarkoni, T. (2019). *The Generalizability Crisis* (Preprint). PsyArXiv. https://doi.org/10.31234/osf.io/jqw35

Yarkoni, T., & Braver, T. S. (2010). Cognitive Neuroscience Approaches to Individual Differences in Working Memory and Executive Control: Conceptual and Methodological Issues. In A. Gruszka, G. Matthews, & B. Szymura (Eds.), *Handbook of Individual Differences in Cognition* (pp. 87–107). New York, NY, Springer New York. https://doi.org/10.1007/978-1-4419-1210-7_6

Yeh, F.-C., Panesar, S., Fernandes, D., Meola, A., Yoshino, M., Fernandez-Miranda, J. C., Vettel, J. M., & Verstynen, T. (2018). Population-averaged atlas of the macroscale human structural connectome and its network topology. *NeuroImage*, *178*, 57–68. https://doi.org/10.1016/j.neuroimage.2018.05.027

Zito, G. A., Cazzoli, D., Müri, R. M., Mosimann, U. P., & Nef, T. (2016). Behavioral Differences in the Upper and Lower Visual Hemifields in Shape and Motion Perception. *Frontiers in Behavioral Neuroscience*, *10*. https://doi.org/10.3389/fnbeh.2016.00128